ANALYSIS AND CLASSIFICATION OF BREAST ABNORMALITIES USING ULTRASOUND IMAGES

A THESIS

Submitted in partial fulfilment of the requirements for the award of the degree

of

DOCTOR OF PHILOSOPHY

in

ELECTRICAL AND INSTRUMENTATION ENGINEERING DEPARTMENT

by

KRITI (901504013)

Under the Supervision of

Dr. Jitendra Virmani
(CSIR-CSIO, Chandigarh)

Dr. Ravinder Agarwal
(TIET, Patiala)

Department of Electrical and Instrumentation Engineering
THAPAR INSTITUTE OF ENGINEERING AND TECHNOLOGY, PATIALA
(Declared as Deemed-to-be-University u/s 3 of the UGC Act, 1956)
Punjab (India)–147001

September 2020

Candidate's Declaration

I hereby certify that the work which is being presented in this thesis entitled **"ANALYSIS AND CLASSIFICATION OF BREAST ABNORMALITIES USING ULTRASOUND IMAGES"** in partial fulfilment of the requirements for the award of the degree of Doctor of Philosophy and submitted in Electrical and Instrumentation Engineering Department of Thapar Institute of Engineering and Technology, Patiala, is an authentic record of my own work carried out during a period from January 2016 to January 2020 under the guidance of Dr. Jitendra Virmani, CSIR-CSIO, Chandigarh and Dr. Ravinder Agarwal, Professor, Electrical and Instrumentation Engineering Department, Thapar Institute of Engineering and Technology, Patiala.

The matter presented in this thesis has not been submitted partially or wholly to any other University or Institute for the award of this or any other degree or diploma.

Kriti

(KRITI)

This is to certify that the above statement made by the candidate is correct to the best of our knowledge.

Jitendra

(Dr. Jitendra Virmani)
Supervisor

Agarwal

(Dr. Ravinder Agarwal)
Supervisor

Date: 11-09-2020

Acknowledgements

It was rightly said by Kalpana Chawla, "*The path from dreams to success does exist. All you need is the vision to find, courage to get on to it and perseverance to follow it*". This thesis work is the most awaited accomplishment of my life by far. However, the happiness of achieving this milestone would be incomplete without the mention of some very special people who have stood by me through these years and helped me in all my endeavors.

I would like extend a sincere and heartfelt gratitude to my supervisor Dr. Jitendra Virmani, CSIR-CSIO, Chandigarh, without whose invaluable support this research work would not have been possible. It was Dr. Virmani who first introduced me to the field of medical image processing when I enrolled myself under him for my M.Tech thesis in 2014. It was his able guidance, unwavering confidence, vision, attention to details, inspiring leadership and inherent talent to create new learning possibilities that motivated me to further my research under him as a Ph.D. candidate at Thapar University, Patiala in Jan 2016. He is the shining example of an ideal supervisor as well as an ideal researcher as he continued to support my research work with the same passion and zeal even after joining CSIR-CSIO in Aug 2016. Over the years that I have been working with Dr. Virmani, he has constantly motivated me to strive to be a better version of myself. He has always helped me to develop my own ideas and learn from my mistakes rather than imposing his ideas and beliefs on me. He has made me understand the importance of logical and critical thinking and broadened my vision of research. It takes a lot of effort on the supervisor's part as well to inculcate the candidate's interest in research and I without a doubt can vouch for the fact that Dr. Virmani is one such person who puts in all his efforts to ensure that his students are working efficiently and are up-to-date in their domain knowledge. I would also like thank him from the bottom of my heart for all the countless hours he has invested in thoroughly refining and strengthening my manuscripts and thesis chapters over and over again to perfection because of which they have taken their present form. I look forward to continuing this journey of research with him.

I would also like to express my gratitude to Dr. Ravinder Agarwal, Professor, Department of Electrical and Instrumentation Engineering, Thapar Institute of Engineering and Technology for his support and guidance he has given me by supervising my Ph.D. thesis. I thank him for his words of encouragement and imperative support. He has helped me overcome the challenges I faced at the administrative front and guided me in my journey through Thapar Institute of Engineering and Technology.

Next, I would like to thank Dr. Shruti Thakur, Department of Radiology, Kamla Nehru Hospital, Shimla, making me understand the different sonographic features which are clinically significant for the grading of despeckled images, marking the tumor contours in original images and validating the results of despeckling and segmentation algorithms. I would also like to thank Dr. Surneet Kaur, radiologist at Modern Scan Centre, Patiala owned by Dr. SPS Narula, for taking the time to explain the various sonographic appearances exhibited by breast tumors.

I would also like to thank the members of my doctoral committee, Dr. Vishal Srivastava, Dr. Saurabh Bhardwaj, Department of Electrical and Instrumentation Engineering, Thapar Institute of Engineering and Technology, Patiala and Dr. Siddharth Sharma, Department of Biotechnology, Thapar Institute of Engineering and Technology, Patiala, for providing their timely suggestions.

I am grateful to the anonymous reviewers for providing invaluable suggestions and constructive criticism that helped in shaping up the quality of the publications derived from this research work.

I would like to sincerely thank my seniors, Dr. Indrajeet Kumar and Dr. Jyoti Rawat (Dr. Virmani's former Ph.D. students) for stimulating discussions related to machine learning. I would also like to thank Mr. Niranjan Yadav (Dr. Virmani's Ph.D. student) for stimulating discussions related to deep learning.

I would also like to thank my fellow lab member Mr. Ashish Agarwal (Dr. Agarwal's PhD student) for introducing Origin software to me which I used for statistical representations.

I would also like to thank my mother Mrs. Geetanjali and grandparents Mr. V.N. Pathak and Mrs. Yagya Pathak for their unconditional love, care and support. I cannot thank them enough for being my pillars of strength and motivating me to work hard towards my goals. I am also thankful to my aunt and uncle Dr. Sonia Gupta and Mr. Monish Gupta for their constant words of encouragement and support and also providing a homely stay during my visits to Chandigarh, never letting me feel homesick. A special mention goes to my baby sister Supriya Gupta who was always around me brightening my days with her angelic smiles and showering me with love at all times whenever I felt exhausted.

A special thanks goes to Dr. Virmani's family, his wife Mrs. Sarika Virmani, Anshul Virmani (elder son) and Aarush Virmani (younger son) for being supportive specifically during the last 06 months of my thesis when Dr. Virmani worked exhaustively for refining my thesis chapters and proof-reading them through successive iterations that took a lot of his personal family time which led to sharing his support between me and the studies of Anshul who is

appearing for his CBSE Board exams for class 10th in February 2020. I wish him good luck in all his endeavours.

A special mention to my childhood friends Dr. Neha Kondal, Ms. Vaishali Kashmiri and Ms. Aaruti Sood who have always motivated me to strive forward with conviction. I feel truly blessed to have them.

One of the major accomplishments of my life during the last semester of my Ph.D. was my engagement to Mr. Rizakdeep Singh Dutt. I thank him for his love, care and support. Also, I am thankful to my in-laws, Mr. Jagjit Singh Dutt and Mrs. Davinder Dutt for all their love and best wishes.

We all have dreams; converting dreams into reality requires a lot of determination, self-discipline, and effort. I dedicate my dissertation work, to my family.

Kriti

List of Abbreviations

Acc.	Accuracy
ACM	Active contour model
AD	Anisotropic diffusion
AE	Autoencoder
ANFC	Adaptive neuro-fuzzy classifier
ANFC-LH	Adaptive neuro-fuzzy classifier using linguistic hedges
ANFIS	Adaptive neuro-fuzzy inference system
ANN	Artificial neural network
AP	Affinity propagation
ARE	Averaged radical error
ATMAV	Asymmetrical triangulation moving average
ATMED	Asymmetrical triangulation median
ATV	Adaptive total variation
Avg	Average
AvgD	Average difference
AUC	Area under the curve
B	Benign class
β	Beta metric
BNN	Bayesian neural net
BPNN	Back propagation neural network
C	Cysts
Ca	Carcinoma
CAD	Computer-aided diagnosis
CC	Complex cyst
CFS	Combined feature set
CLAHE	Contrast limited adaptive histogram equalization
CM	Confusion matrix
CNN	Convolutional neural network
CrC	Correlation coefficient
CrFS	Correlation based feature selection
CT	Computed tomography
D	Despeckled image
DB	Database

DCIS	Ductal carcinoma *in situ*
DDSM	Digital database of screening mammography
DFS	Deep feature set
DPAD	Detail preserving anisotropic diffusion
DT	Decision tree
DWT	Discrete wavelet transform
Ecasort	Linear scaling and sorting
ERI	Edge retrieval index
Err3, Err4	Normalized error summation
F	Fibroadenoma
FB	Fourier Butterworth
FBL	Fast bilateral filter
FCN	Fully convolutional network
FEN	Fuzzy enhancement
FI	Fourier ideal
FLDA	Fischer linear discriminant analysis
FOS	First order statistics
FPS	Fourier power spectrum
FSVM	Fuzzy support vector machine
GA	Genetic algorithm
GAN	Generative adversarial networks
GLCM	Gray level co-occurrence matrix
GLDS	Gray level difference statistics
GLRLM	Gray level run length matrix
GRBF	Gaussian radial basis function
GW	Geometric wiener
GWT	Gabor wavelet transform
HE	Histogram equalization
HFB	Homomorphic Fourier Butterworth
HFI	Homomorphic Fourier ideal
Homo	Homomorphic
Homog	Maximum homogeneity
HyMedian	Hybrid median
HyATMAV	Hybrid asymmetrical triangulation moving average
HyATMED	Hybrid asymmetrical triangulation median

HyTMAV	Hybrid triangulation moving average
HyTMED	Hybrid triangulation median
ICA	Individual class accuracy
IDC	Invasive ductal carcinoma
ILC	Invasive lobular carcinoma
IOU	Intersection over union
IOWT	Inter orthonormal wavelet thresholding
IQI	Image quality index
ISF	Interference based speckle filtering
JI	Jaccard index
kNN	k-nearest neighbour
LBP	Local binary pattern
LDA	Linear discriminant analysis
LFDA	Local Fischer discriminant analysis
LMSE	Laplacian mean square error
LPF	Low pass filter
LR	Logistic regression
LS	Linear scaling
LS_{ratio}	Long axis-to-short axis ratio
Lsminsc	Local statistics minimum speckle index
Lsmv	Local statistics mean variance
M	Malignant class
MAP	Maximum a posteriori
Max	Maximum
MCDE	Modified curvature diffusion equation
MD	Maximum difference
MFS	Morphological feature set
Min	Minimum
MLP	Multilayer perceptron
MMRAD	Median normalized multiresolution anisotropic diffusion
MPT	Multiscale product thresholding
MRA	Multi-resolution analysis
MRI	Magnetic resonance imaging
MRF	Markov random field
mRMR	Minimal redundancy maximal relevance

MSE	Mean square error
NAD	Non-linear anisotropic diffusion
NAE	Normalized average error
NCD	Non-linear coherent diffusion
NCut	Normalized cut
NIQE	Natural image quality estimator
NK	Normalized cross-correlation
NLLR	Non-local low rank
NLM	Non-local mean
NN	Neural network
NSS	NeighShrinkSure
O	Original image
OBNLM	Optimized Bayesian non-local means
ODFS	Optimal deep feature set
OFS	Optimal feature set
PBAC	Phase based active contour
PCA	Principal component analysis
PCs	Principal components
PNN	Probabilistic neural network
PPA	Phase portrait analysis
PPB	Probabilistic patch based
PSNR	Peak signal-to-noise ratio
QDA	Quadratic discriminant analysis
QS	Quick shift
R-CNN	Region based CNNs
RDAU-Net	Residual-dilated-attention-gate-UNet
RDCA	Radius dependent contrast adjustment
RDFS	Reduced deep feature set
RF	Random forest
RFS	Reduced feature set
RGI	Radial gradient index
RMSE	Root mean square error
ROC	Receiver operating curve
ROI	Region of interest
RTFS	Reduced texture feature set

SaDE-ELM	Self adaptive differential evolution-Extreme learning machine
SAE	Stacked autoencoder
SBL	Solid benign lesion
SC	Structural content
SCAE	Sacked convolutional autoencoder
SDAE	Stacked denoising autoencoder
SEPI	Structure and edge preservation index
SFS	Sequential forward search
SGLD	Spatial gray level dependence
SLR	Stepwise logistic regression
SM	Softmax
SNR	Signal-to-noise ratio
SOM	Self organizing map
SPCGAN	Semi-pixel-wise cycle generative adversarial network
SPPA	Sparse phase portrait analysis
SRAD	Speckle reducing anisotropic diffusion
SSIM	Structural similarity index
SVM	Support vector machine
TFS	Texture feature set
TMAV	Triangulation moving average
TMED	Triangulation median
TV	Total variation
UQI	Universal image quality
US	Ultrasound

List of Figures

List of Tables

Abstract

The present research work has been carried out with an aim to enhance the diagnostic potential of B-mode ultrasound imaging modality for the diagnosis of breast abnormalities. To achieve this objective exhaustive experiments have been carried out in the present research work to (*a*) analyse the effect of despeckle filtering algorithms on breast ultrasound images, (*b*) analyse the effect of despeckle filtering algorithms on segmentation of breast tumors, (*c*) analyse the effect of despeckle filtering algorithms on classification of breast tumors, (*d*) design an efficient local binary pattern (LBP) based CAD system for classification of breast tumors, (*e*) design an efficient convolutional neural network based CAD system for classification of breast tumors. For carrying out the experiments a comprehensive dataset of 100 B-mode breast ultrasound images comprising of cysts, fibroadenomas, lipomas in benign category, ductal and lobular carcinomas in malignant category has been taken from a *standard benchmark database*, *ultrasoundcases.info*.

Initially exhaustive experimentations have been carried out to analyze the effect of 42 despeckle filtering algorithms taken from various filter categories namely (*a*) Local statistics based filters, (*b*) Fourier filters, (*c*) Fuzzy filters, (*d*) Multiscale filters, (*e*) Non-local mean filters, (*f*) Non-linear iterative filters, (*g*) Total variation filters and (*h*) Hybrid filters. The resultant despeckled images have been used for objective assessment and subjective assessment. For the objective assessment, an image quality metric named structure and edge preservation index (SEPI) has been proposed. This index quantifies the edge preservation and structure preservation capability of the filtering algorithm. Based on the results of the objective evaluation, out of 42 filters, *06 best performing despeckle filtering algorithms* namely Lee sigma, BayesShrink, Detail preserving anisotropic diffusion (DPAD), Fourier ideal (FI), Fourier Butterworth (FB), and Homomorphic Fourier Butterworth (HFB) filters have been selected that result in controlled despeckling of the images. The images despeckled by these *06 best performing despeckle filtering algorithms* have further been used for the subjective assessment based on the radiologist's grading. On the basis of both objective and subjective assessment, DPAD filter has been selected as an optimal filter for pre-processing the breast ultrasound images. The 100 original breast ultrasound images and 100 despeckled images pre-processed using *06 best performing despeckle filtering algorithms* have been considered for analysing the effect of despeckle filtering algorithms on segmentation of breast tumors.

Effect of despeckle filtering algorithms on segmentation of breast tumors- The original images as well as the images despeckled by the *06 best performing despeckling filtering algorithms have been subjected to the* Chan and Vese active contour method for segmentation of breast tumors. The objective assessment of the segmentation algorithm has been carried out by computing the Jaccard index and subjective assessment has been carried out by the experienced participating radiologist. Based on the results of the study the DPAD has been selected as an optimal despeckle filtering algorithm resulting in efficient segmentation of breast tumors.

Exhaustive experiments were carried out for analysing the effect of best performing despeckle filtering algorithms on classification of breast tumors- Initially four PCA-SVM based CAD systems based on (*a*) texture and morphological features computed from original images (*b*) texture and morphological features computed from despeckled images, (*c*) texture features computed from original images and morphological features computed from despeckled images and (*d*) texture features computed from despeckled images and morphological features computed from original images. It was observed that the PCA-SVM based CAD system design based on texture features computed from original images and morphological features computed from images despeckled using DPAD filter yielded highest classification accuracy of 96.0 % with individual class accuracy values of 95.2 % and 96.6 % respectively.

Four LBP based CAD system designs were implemented using classifiers namely, PCA-SVM, ANFC-LH, GA-SVM and SAE-SM by computing LBP based texture features computed from original images and morphological features computed from images despeckled using DPAD filter- It was observed that the LBP based CAD system with ANFC-LH classifier yielded the highest accuracy of 96.0 % with individual class accuracy values of 90.4 % and 100 % for benign and malignant classes, respectively.

Further to compare the performance of the existing conventional approaches with the state of the art deep learning techniques- Initially four different transfer learning based CNN models with GoogleNet, VGG-19, ResNet-18 and SqueezeNet architecture have been implemented. It was observed that CNN based model based on GoogLeNet architecture yielded highest accuracy. Accordingly an optimal CNN based CAD system design based on deep feature extraction by GoogLeNet architecture and classification by ANFC-LH was designed yielding highest classification accuracy of 98.0 % with ICA values of 100 % and 96.6 % for benign and malignant cases respectively.

Table of Contents

Chapter 1

Introduction

1.1. Motivation

Cancer occurs when cellular changes in the body result in uncontrolled growth of cells, thus forming tissue masses called tumors [76]. These tumors can either be benign or malignant. The benign tumors are considered to be non-cancerous as these tumor cells do not spread to other parts of the body, have a slower growth rate and are more differentiable. The malignant tumors are considered to be cancerous and can invade other healthy tissues in the body. Through the lymph system or blood stream, these cells often travel to other parts of the body resulting in the formation of new tumors. This process is known as metastasis [76]. Breast cancer develops in the breast cells beginning either in the breast lobules or the ducts. It has become a major health concern nowadays and is the most common form of cancer occurring in women [134]. The risk factors associated with the development of breast cancer are: (*a*) Genetic mutations, (*b*) Radiation therapy, (*c*) History of breast cancer, (*d*) Obesity, (*f*) Cosmetic implants and (*g*) Alcohol consumption etc.

It was reported by Indian Council of Medical Research (ICMR) that every year a minimum of one lakh new breast cancer patients are diagnosed in India. For women in U.S.A, it was estimated that in the year 2019, a total of 268,600 new cases of breast cancer would be diagnosed. These facts are alarming and indicate that breast cancer is prevalent not only in India but also globally. It can also be noted that the mortality rate of breast cancer in India is 1.6-1.7 times higher than that of maternal mortality rate. In the year 2017, India had the highest mortality rate for breast cancer globally. Even though high mortality rates have been associated with breast cancer, significant improvement in the chances of survival can be witnessed if detection is made at an early stage [13, 36, 204, 267].

1.2. Imaging Modalities for Breast Cancer Screening

For diagnosing breast diseases, various imaging modalities like mammography, ultrasound (US), computed tomography (CT) and magnetic resonance imaging (MRI) etc. have popularly been used, however CT and MRI are costly modalities and in case of CT the patients are exposed to ionizing radiations therefore, to cater to the need of general population in India, mammography and ultrasound are commonly used as screening tools [16, 18, 28, 36, 80, 118, 204, 271, 272]. Mammography is however not suitable for patients like pregnant women due to the use of ionizing radiations and also sometimes false-negatives are obtained with

mammography due to the effect of high breast density in younger women. The advantages of ultrasound over other modalities are: (*a*) absence of ionizing radiations, (*b*) low cost, (*c*) non-invasive nature, (*d*) ease of availability and (*e*) ability to differentiate between cystic and solid tumors.

1.2.1. Ultrasound imaging

Owing to its various advantages, over the past decade, ultrasound is considered to be a powerful tool used for the diagnosis of breast abnormalities [18, 28, 118, 272]. Ultrasound imaging technique utilizes the high frequency sound waves and their echoes for the formation of a 2D image that can be used for further analysis. High frequency sound waves (> 20 kHz) are transmitted from the ultrasound transducer to the human body using a probe. As these sound waves travel in the body, they get reflected back to the probe after they hit some boundary between the tissues. The probe relays the collected echoes back to the ultrasound machine. The ultrasound machine then computes the distance between the probe and the tissue using the return time of each echo and speed of sound. After this, the echo intensities and the distances are displayed as a 2D image. The formed image is also referred to as brightness mode (B-mode) ultrasound image [172].

The quality of the ultrasound image depends upon its axial and lateral resolution. The axial resolution depends on the wavelength of the ultrasound beam while the lateral resolution depends on the width of the ultrasound beam. Thus for a better quality image, the frequency of the beam and diameter of the transducer should be kept large. The frequencies to be used however depend on the domain of application. Also it should be noted that images having higher resolution are produced by ultrasound beams having lower depth of penetration while ultrasound beams having higher depth of penetration produce lower resolution images. Thus for medical imaging, a tradeoff exists between the image resolution and depth of penetration [172].

Despite of the various advantages, the quality of ultrasound images is sometimes affected by the presence of speckle noise and low contrast. The speckle noise tends to obscure the diagnostically important structures in the image thus resulting in the degradation of spatial resolution of the image. Speckle noise is a locally correlated multiplicative noise that arises in medical ultrasound images at the time of acquisition. Speckle noise appears as a series of light and dark spots on the image, caused by the interference of the back-scattered echoes from multiple targets, that are smaller in size as compared to the wavelength of ultrasound beam or the targets having different impedances lying very close to each other [172, 187, 197]. Mathematically, the speckle noise can be modeled as:

$$y\,(i,j) = x\,(i,j).n\,(i,j) \tag{1.1}$$

Here, $x\ (i, j)$ is the noise-free pixel, $n\ (i, j)$ is the multiplicative noise, $y\ (i, j)$ is the noisy image pixel at the centre of the window, (i, j) represent spatial indices belonging to real numbers. Most of the filters are used to remove the additive noise therefore; the speckle noise can be re-modeled as:

$$\log\big(y\ (i,j)\big) = \log\big(x\ (i,j)\big) + \log\ (n\ (i,j)) \tag{1.2}$$

Due to the presence of speckle noise, the resolution of the ultrasound image is affected resulting in difficulty in detection of small lesions thus making the interpretation difficult. Moreover, it is also believed that the speckle noise contains some diagnostic information therefore, the use of a simple low pass filter to remove high frequency speckle noise may not be adequate. So to remove the speckle noise, efficient adaptive filters need to be designed such that controlled despeckling is achieved. For the despeckling of ultrasound images many attempts have been made by the researchers in the past to efficiently remove speckle from the images without the loss of any diagnostic information [19, 70, 172, 187, 197, 202, 214-216, 255, 299].

1.3. Need for CAD System Designs using Ultrasound Images

With the advent of computer technology, medical image processing techniques and artificial intelligence based algorithms, many opportunities have arisen for the research community to explore the potential of computer-aided diagnosis (CAD) for classification of breast abnormalities using ultrasound images [41, 63, 66, 111, 137, 192, 198, 199, 220, 251, 257, 319]. This tissue classification refers to the quantitative analysis of underlying imaging features of the tissue thus resulting in an accurate distinction between the abnormalities. The computerized tissue classification systems provide additional diagnostic information about the tissue under study, which may not be captured during the subjective analysis of the images.

The tissue specific features need to be computed during characterization of medical images, e.g. for the analysis of breast abnormalities, both texture and shape of the tumor are considered important hence, the CAD systems should be designed based on both texture and morphological features exhibited by the tumors [63, 66, 137, 192, 199, 220, 251, 319]. Thus to enhance the diagnostic potential of B-mode ultrasound imaging modality for classification of soft tissue abnormalities, there is a need to develop efficient CAD systems.

1.4. Breast Tumors on Ultrasound

The breast tumors are broadly classified as either benign or malignant. The benign tumors are considered to be non-cancerous as these tumor cells do not spread to other parts of the body, have a slower growth rate and are more differentiable. The malignant tumors are

considered to be cancerous and can also invade other healthy tissues in the body. A broad categorization of breast tumor types is given in Fig. 1.1.

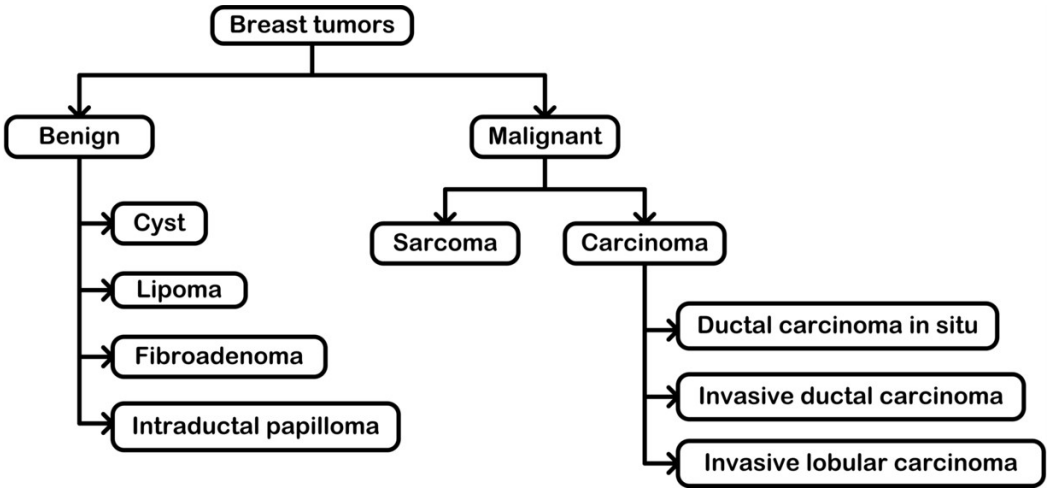

Fig. 1.1 Broad categorization of breast tumor types.

1.4.1. Benign breast tumors

The different benign breast tumors as seen on ultrasound have been described here.

(*a*) Cyst- The cysts are firm and round lumps in the breast that are filled with fluid. They have a regular shape with distinct edges and are usually found in women between the ages 35 to 50. The breast cysts can be *simple* having thin-walls, regular shape, filled with fluid and are anechoic in nature having no solid components. Some cysts contain some debris inside them that results in the formation of echoes, while some cysts have an irregular border with thick walls and contain some solid components within the fluid which result in the formation of echoes [82]. The sample ultrasound images representing different types of cysts are given in Fig. 1.2.

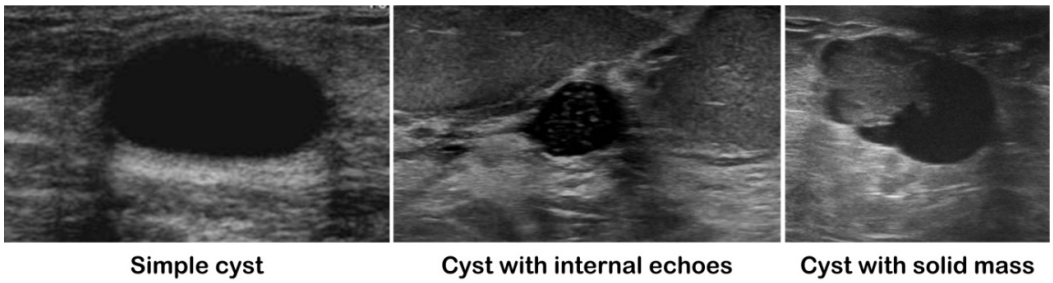

Fig. 1.2 Sample ultrasound images representing different types of cysts.

(*b*) Lipoma- The lipomas are slow growing solid masses having a well-circumscribed margin with fat being the major component. Lipomas commonly occur in women between the ages of 40 and 60 and are benign in nature [82]. Sample ultrasound image representing a lipoma is given in Fig. 1.3.

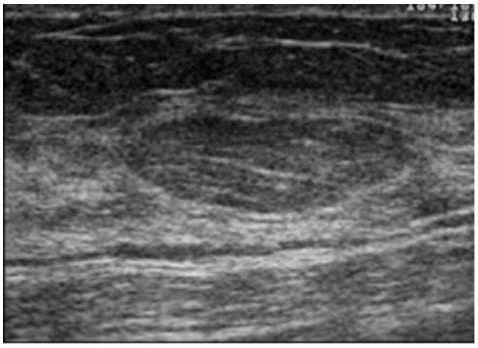

Fig. 1.3 Sample ultrasound image representing a lipoma.

(*c*) Fibroadenoma- The fibroadenomas are the most common solid masses having a well-defined shape. They may vary in size and can shrink or enlarge on their own accordingly these are named as small or large fibroadenomas. They are mostly found in women between the ages 15 to 35. Most of the fibroadenomas are benign in nature [82]. The sample ultrasound images representing fibroadenomas are given in Fig. 1.4.

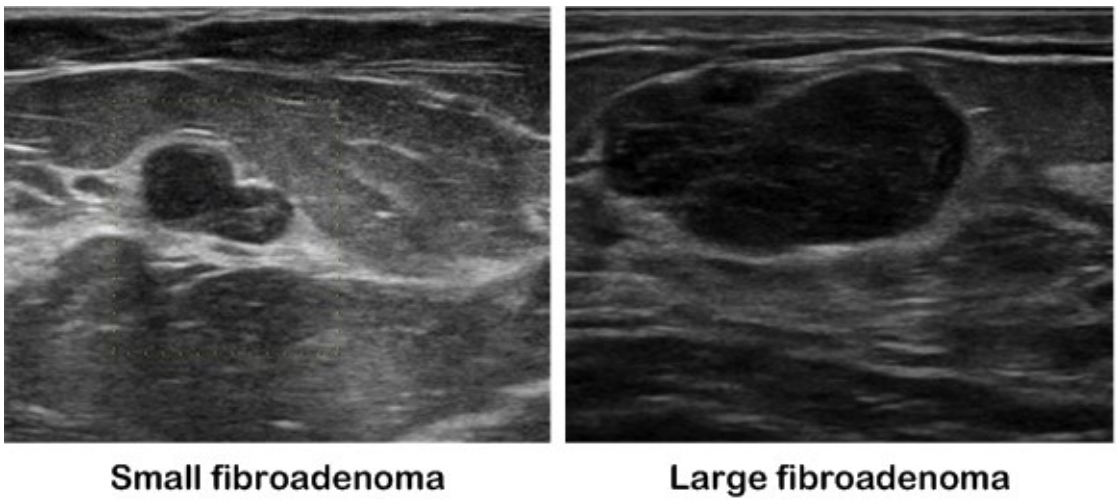

Fig. 1.4 Sample ultrasound images representing different types of fibroadenomas.

(*d*) Intraductal papilloma- The intraductal papillomas are the most common masses that grow inside the breast duct and are found in women between the ages 40 to 45. They appear as well-defined solid nodules within a dilated duct [82]. The sample ultrasound image representing an intraductal papilloma is given in Fig. 1.5.

1.4.2. Malignant breast tumors

The different malignant breast tumors as seen on ultrasound have been described here.

(*a*) Sarcoma: This type of cancer develops in the non-epithelial tissue like bone cartilage, blood vessels, muscles etc. Breast sarcomas start in the connective tissues supporting the ducts and lobules of the breast. However, the incidence rates of breast sarcoma are very low [305].

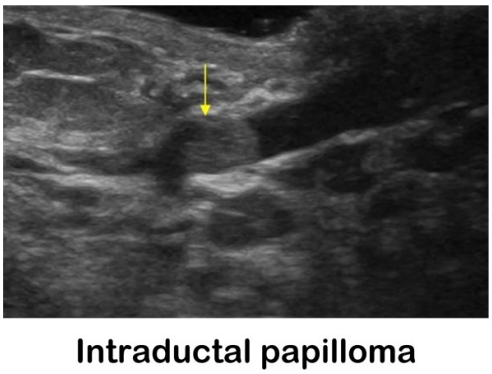

Fig. 1.5 Sample ultrasound image representing an intraductal papilloma.

(*b*) Carcinoma: This type of cancer develops in the epithelial tissue i.e. the cells of the lining of the organ or tissue. The carcinoma developed in the breast tissue is called adenocarcinoma. Carcinomas have a higher rate of incidence than the sarcomas. (*i*) Ductal carcinoma- This is the initial stage of breast cancer and is developed in the inner linings of milk ducts. It can be of two types namely ductal carcinoma in situ (DCIS) and invasive ductal carcinoma (IDC). The DCIS is a non-invasive type of cancer. It does not break through the duct walls to metastasize to other parts of the body [27]. The IDC can metastasize to other organs and body parts by invading the fatty breast tissue [82]. (*ii*) Invasive lobular cancer (ILC)- This is the 2nd most common form of breast cancer found among women. This type of cancer develops inside the lobules that produce milk and then metastasizes beyond the lobules to the breast tissue and other body parts. [82]. The sample ultrasound images representing different carcinomas are given in Fig. 1.6.

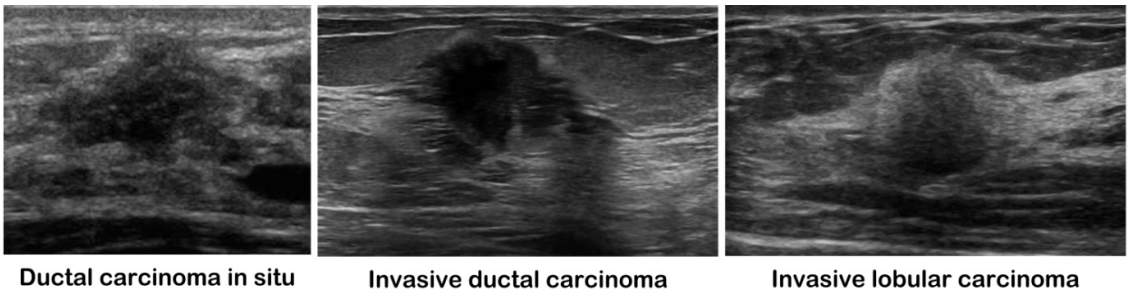

Fig. 1.6 Sample ultrasound images representing different types of carcinomas.

1.4.3. Textural and morphological characteristics of breast tumors as seen on ultrasound

The breast tumors can be identified on the basis of their (*a*) textural characteristics like echo pattern, posterior acoustic features and presence of microcalcifications, (*b*) morphological

characteristics like shape, margin, boundary. The different sonographic characteristics of breast tumors as seen on B-mode ultrasound are described in Fig. 1.7.

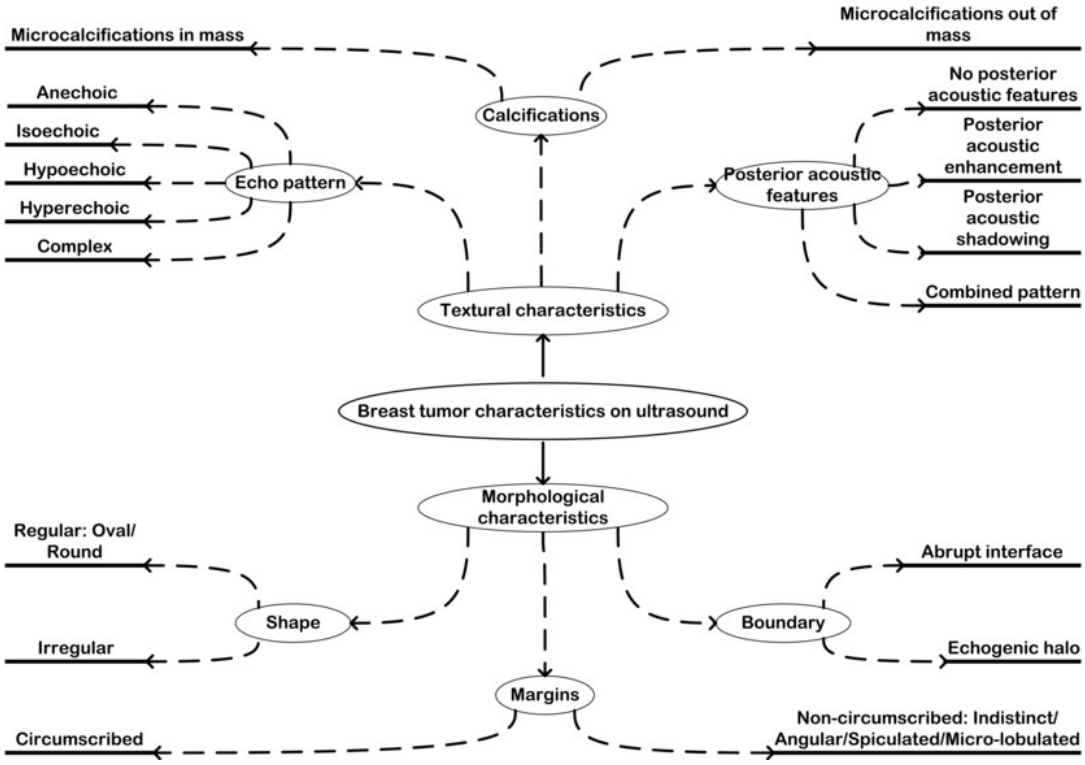

Fig. 1.7 Description of sonographic characteristics (texture and morphological) of breast tumors as seen on B-mode ultrasound.

(*a*) Textural characteristics: The echo pattern exhibited by different tumors can be categorized to be anechoic (without any internal echoes), isoechoic (same echogenicity as the fat), hyperechoic (increased echogenicity relative to the fibro-glandular tissue or fat), hypoechoic (low internal echoes relative to the fat), complex pattern (combination of anechoic and echogenic components). Mostly, benign tumors exhibit a hyperechoic or isoechoic echo pattern whereas a hypoechoic echo pattern is suggestive of malignancy. The presence of calcifications in the mass can also affect the texture of the breast tumor. The calcifications are suggestive of malignancy if they are smaller than 0.5 mm and are clustered in one area. The posterior acoustic features exhibited by the tumors on an ultrasound can either be shadowing, enhancement or complex pattern. The tumors exhibiting posterior acoustic shadowing are indicative of malignancy [82, 83].

(*b*) Morphological characteristics: The shape of the tumor can either be regular or irregular. The regular shape (oval/round) is the characteristic of benign tumor while malignant tumors are characterized by irregular shape. The margins of the tumors can be circumscribed (i.e. well-defined or sharp) or non-circumscribed. Non-circumscribed margin can either be indistinct,

angular, micro-lobulated or spiculated. The tumors having circumscribed margins are often benign while the tumors having non-circumscribed margins are suggestive of malignancy. The boundary of the tumor can have an abrupt interface i.e. a clear demarcation exists between the tumor and the surrounding tissue or the boundary can appear like an echogenic halo with no sharp demarcations between the tumor and surrounding tissue [82, 83].

The sample ultrasound images indicating the sonographic characteristics exhibited by different breast abnormalities are given in Fig. 1.8.

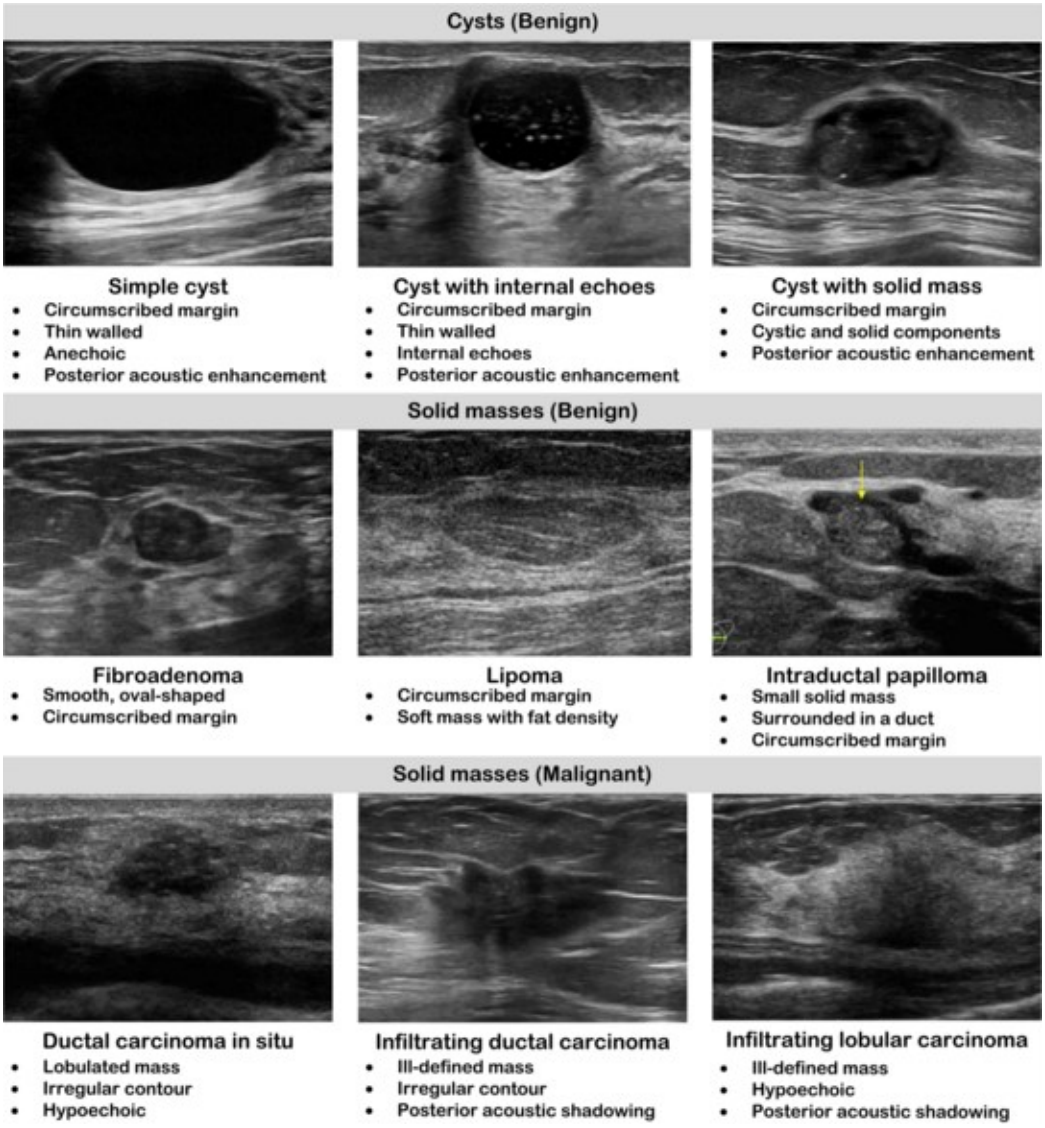

Fig. 1.8 Sample ultrasound images indicating sonographic characteristics exhibited by breast abnormalities.

1.5. Objectives of the Present Work

The present research work has been carried out with an aim to enhance the diagnostic potential of conventional B-mode ultrasound imaging modality for the diagnosis of breast

abnormalities by designing an efficient CAD system using a comprehensive and representative image dataset. To achieve this, different research objectives have been framed. A brief description of these objectives is given here.

(*a*) *Collection of breast ultrasound image database:* For designing an efficient CAD system, it is imperative to train the classifier using representative images from each class. Thus collection of comprehensive image database with representative cases from each class and developing an understanding of the sonographic characteristics exhibited by different benign and malignant breast tumors is taken up as the first objective.

(*b*) *To evaluate the efficacy of different pre-processing methods for segmentation of breast abnormalities*: Presence of speckle noise and low contrast in ultrasound image deteriorates its quality thus making the visual interpretation difficult for the radiologist. The speckle noise sometimes masks the diagnostically important information and the tumor edges, which adversely affects the performance of the computer-assisted algorithms. It is desirable to carefully remove the speckle noise from the homogeneous areas thereby preserving the edge/structure information in the image. Keeping this in view, the second objective has been framed with an aim to (*i*) Evaluate the performance of different despeckle filtering algorithms with respect to their edge/structure preservation capability in order to find an optimal despeckle filtering algorithm for pre-processing the breast ultrasound images, (*ii*) Evaluate the performance of the best performing despeckle filtering algorithms with respect to segmentation of benign and malignant breast tumors.

(*c*) *To evaluate the performance of different classification techniques for differential diagnosis between breast abnormalities:* The textural and morphological characteristics exhibited by breast tumors are considered clinically significant for classification of breast ultrasound images. Therefore, the third objective has been taken up with an aim to evaluate the effect of best performing despeckle filtering algorithms on differential diagnosis between breast tumors using different machine learning and deep learning classification techniques.

(*d*) *To design a CAD system using optimal features extracted from ultrasound images:* To achieve this objective, various texture features based on statistical, signal processing based and transform domain based methods and morphological features would be extracted from both original and pre-processed images. The performance of these hand-crafted features for differential diagnosis between breast tumors would be compared with different deep features extracted using different convolutional neural network (CNN) based architectures.

1.6. Organization of Report

The thesis has been organized into nine chapters. A brief description of the contents and division of the thesis is given here.

Chapter-1 Introduction: This chapter lays the foundation as to why "*Analysis and Classification of Breast Abnormalities Using Ultrasound Images*" is considered to be clinically significant. The chapter begins with documenting the facts about breast abnormalities, recent statistics related to breast cancer among women worldwide, risk factors leading to breast cancer development. The chapter further introduces the advantages of the ultrasound imaging modality for breast cancer diagnosis in comparison to other imaging modalities, highlights the sonographic appearances exhibited by different benign and malignant breast tumors and also explains the effect of speckle noise on the quality of breast ultrasound images. The chapter also discusses the need of developing CAD systems for classification of breast tumors using ultrasound images. This chapter lays a solid foundation about the motivation regarding the design of CAD systems for enhancing the diagnostic potential of ultrasound imaging modality for differential diagnosis between breast tumors.

Chapter-2 Literature Review: An exhaustive review of other related studies carried out for analysis and classification of breast ultrasound images has been presented under different sections i.e., review of (*a*) despeckle filtering algorithms applied to pre-process the breast ultrasound images, (*b*) segmentation algorithms applied to breast ultrasound images, (*c*) machine learning based techniques applied for classification of breast tumors and (*d*) deep learning based techniques applied for classification of breast tumors. The conclusions drawn from the exhaustive literature review of each section have been highlighted and the research gaps corresponding to each section have been identified.

Chapter-3 Effect of despeckle filtering algorithms on breast ultrasound images: This chapter gives a detailed description of the experimental workflow followed for pre-processing the breast ultrasound images using a total of 42 despeckle filtering algorithms. The chapter describes in detail the different filter categories out of which these 42 filters have been selected. The chapter then enlists the different parameters used for the implementation of each filter. Further the chapter also discusses in detail the objective and subjective assessment criteria used for the performance evaluation of despeckle filtering algorithms.

Chapter-4 Effect of despeckle filtering algorithms on segmentation of breast tumors: This chapter describes in detail the experimental workflow followed for evaluating the effect of despeckle filtering algorithms on the segmentation of benign and malignant breast tumors. The

chapter discusses the objective and subjective assessment used for the performance evaluation of the segmentation algorithm.

Chapter-5 Effect of despeckle filtering algorithms on classification of breast tumors: This chapter describes in detail the experimental workflow followed for evaluating the effect of despeckle filtering algorithms on the classification of breast tumors. Four different CAD systems namely (*a*) PCA-SVM based CAD system (RFS_{OO}), (*b*) PCA-SVM based CAD system (RFS_{DD}), (*c*) PCA-SVM based CAD system (RFS_{OD}) and (*d*) PCA-SVM based CAD system (RFS_{DO}) have been designed. The chapter describes the different texture and morphological features computed from the original and despeckled images and also describes the architectural details of the PCA-SVM based CAD system for classification of breast tumors.

Chapter-6 LBP based CAD system designs for classification of breast tumors: This chapter starts with the experimental workflow followed for design of LBP based CAD systems namely (*a*) LBP based CAD system using ANFC-LH ($(OFS_{LBP})_{ANFC\text{-}LH}$), (*b*) LBP based CAD system using GA-SVM ($(OFS_{LBP})_{GA\text{-}SVM}$), (*c*) LBP based CAD system using PCA-SVM ($(OFS_{LBP})_{PCA\text{-}SVM}$), (*d*) LBP based CAD system using SAE-SM ($(OFS_{LBP})_{SAE\text{-}SM}$) for classification of breast tumors. The chapter describes in detail the LBP based texture feature extraction method along with different feature selection and reduction techniques like ANFC-LH, GA-SVM, PCA-SVM and SAE-SM. The chapter also gives a comparative analysis of the results obtained for each CAD system design in order to decide upon an optimal CAD system for classification of breast tumors.

From the design of CAD systems based on machine learning techniques as described in Chapter-5 and Chapter-6, it has been observed that the combined feature set obtained by texture features computed from original images and morphological features computed from images despeckled by DPAD filter yield optimum results for classification of breast ultrasound images. It has been concluded that the tumor mask generated by applying active contour method to images despeckled by DPAD filter, retained optimal morphological characteristics therefore for further experimentation on CNN based CAD system designs, the dataset of segmented tumor images has been generated by superimposing the tumor mask on the original image to retain the optimal texture and optimal morphological characteristics.

Chapter-7 Convolutional neural network based CAD system designs for classification of breast tumors: This chapter describes in detail (*i*) methodology adopted for the generation of dataset for CNN based CAD system designs, (*ii*) experimental workflow followed for design of five CNN based CAD systems, namely (*a*) CNN based CAD system ($DFS_{GoogLeNet}$), (*b*) CNN based CAD system ($DFS_{VGG\text{-}19}$), (*c*) CNN based CAD system ($DFS_{ResNet\text{-}18}$), (*d*) CNN based CAD

system ($DFS_{SqueezeNet}$) and (*e*) CNN-ANFC-LH based CAD system ($ODFS_{GoogLeNet}$) has been described. The chapter further describes the general introduction to CNNs and the basic operations involved in them. Next, the network architectures of the used CNNs have been explained. In the end, the chapter gives a comparative analysis of the results obtained after exhaustive experimentation to find an optimal CAD system design based on CNNs.

Chapter-8 Conclusions and Future Scope: This chapter enlists the main conclusions drawn from various experiments conducted in the present research work for (*a*) effect of despeckle filtering algorithms on breast ultrasound images, (*b*) effect of despeckle filtering algorithms on segmentation of breast tumors, (*c*) effect of despeckle filtering algorithms on classification of breast tumors, (*d*) LBP based CAD system designs for classification of breast tumors, (*e*) convolutional neural network based CAD system designs for classification of breast tumors. The chapter also presents a comparative analysis of the results of CAD systems designed for classification of breast tumors. The chapter also reports the future directions that can be taken up for the extension of the work entitled "*Analysis and Classification of Breast Abnormalities Using Ultrasound Images*".

Chapter 2

Literature Review

2.1. Introduction

The anatomy of the human body is effectively mapped by different imaging modalities. The medical imaging is widely used for disease diagnosis, treatment and follow-up. In the field of healthcare, the effective decisions pertaining to treatment depend on correct diagnosis, which is backed-up by efficient diagnostic services. However, the manual analysis of the medical scans is a laborious task for the radiologists and is highly susceptible to human errors. To reduce the chances of misdiagnosis, recent advances have been made towards computer-assisted medical diagnosis, wherein the computer-assisted algorithms have been used in routine clinical setting for detection and diagnosis of different abnormalities on the basis of the information extracted from the medical images [7, 16, 94, 130, 134, 137, 145, 146, 153, 160, 162]. These algorithms make use of different image processing and artificial intelligence based techniques for the characterization of tissue under study and act as a complimentary tool for the radiologists to gain confidence in their decision by providing additional diagnostic information which cannot be captured during processing of images by human visual system.

In this chapter a review of the published literature on computer-assisted algorithms for (*a*) Despeckling of breast ultrasound images, (*b*) Segmentation of breast tumors, (*c*) Classification of breast tumors using machine learning approaches and (*d*) Classification of breast tumors using deep learning approaches have been discussed.

For carrying out the present literature review, the following protocols have been framed:
(*i*) The studies published between the period 1990-2019 have been considered.

(*ii*) The studies carried out only on B-mode breast ultrasound images have been considered

(*iii*) For classification of breast tumors using machine learning approaches, only those studies have been considered that report the use of both texture and morphological features.

2.2. Review of Literature on Despeckling of Breast Ultrasound Images

For the controlled despeckling of breast ultrasound images different methods have been proposed in the past by researchers [19, 70, 136, 149, 202, 214, 252, 255, 299, 313]. A broad categorization of different despeckle filtering algorithms is given in Fig. 2.1.

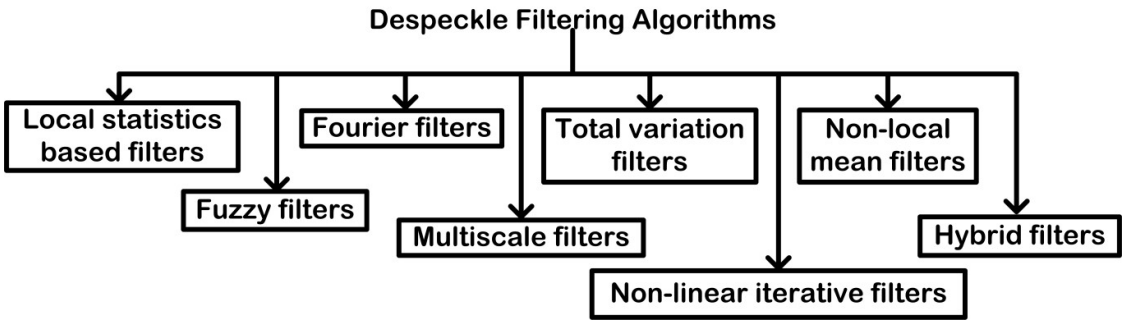

Fig. 2.1 Broad categorization of despeckle filtering algorithms.

A brief description of the studies carried out for the despeckling of breast ultrasound images is given in Table 2.1.

Table 2.1 A brief description of studies carried out for the despeckling of breast ultrasound images.

Investigators	No. of images	No. of filters	Category	Evaluation
Yang et al. (2004) [299]	--	03	Non-linear iterative filters and hybrid filters	Objective
Bhateja et al. (2014) [19]	04	01	Local statistics based filters	Objective
Khusna et al. (2015) [136]	--	04	Local statistics based filters and non-linear iterative filters	Objective
Singh et al. (2015) [252]	28	23	Non-linear iterative filters, Fourier filters, multiscale filters, local statistics based filters	Objective & subjective
Zhang et al. (2016) [313]	400	11	Local statistics based filters, non-linear iterative filters, hybrid filters, multiscale filters, non-local mean filters	Objective & subjective
Lal et al. (2016) [149]	--	01	Hybrid filters	Objective
Nugroho et al. (2016) [202]	--	07	Local statistics based filters and non-linear iterative filters	Objective
Prabhakar et al. (2016) [214]	110	03	Multiscale filters	Objective
Singh et al. (2016) [255]	37	14	Non-linear iterative filters, Fourier filters, multiscale filters	Objective & subjective
Feng et al. (2016) [70]	--	08	Multiscale filters, local statistics based filters, non-linear iterative filters, total variation filters	Objective
Prabhakar et al. (2017) [215]	--	01	Multiscale filters	Objective
Prabusankarlal et al. (2017) [216]	54	01	Non-local mean filters	Objective
Kriti et al. (2019) [141] (Present work)	100	42	Local statistics based filters, fuzzy filters,	Objective & subjective

	Fourier filters, multiscale filters, non-linear iterative filters, total variation filters, non-local mean filters and hybrid filters

From the studies presented in Table 2.1, following points can be observed:

(*i*) Very few attempts have been made for the despeckling of breast ultrasound images. It has been noted that most of the studies have been carried out to compare the performance of various despeckle filtering algorithms for pre-processing the breast ultrasound images [70, 136, 141, 202, 214, 252, 255, 299, 313] while the other studies have made use of a single despeckle filtering algorithm modified for the corresponding problem under study [19, 149, 215, 216]. From the table it can also be observed that the performance of a minimum of 03 filters [299, 214] and a maximum of 42 filters has been compared [141] followed by 23 filters [252].

(*ii*) Most of the studies have used image quality metrics for the evaluation of the quality of despeckled images while very few studies have used both objective as well as subjective evaluation for assessing the despeckled image quality [140, 252, 255, 313].

(*iii*) Most of the studies have carried out the performance analysis of despeckle filtering algorithms on very few images (< 50 images) [46, 252, 255].

(*iv*) Out of the eight different despeckle filtering algorithm categories at most 05 filter categories have been used to select the filters to be used for pre-processing the breast ultrasound images while in the study proposed by authors, filters belonging to all 08 categories have been used [141].

Yang et al. [299] proposed a hybrid filtering technique named median normalized multi-resolution anisotropic diffusion (MMRAD) and compared its performance with adaptive median filter and Gaussian regularized anisotropic diffusion filter on the basis of objective analysis carried out by computing universal image quality (UQI) and peak signal-to-noise ratio (PSNR).

Prabhakar et al. [214] used 03 multiscale filters namely curvelet transform, shearlet transform and tetrolet transform. The performance has been measured on the basis of signal-to-noise ratio (SNR) and PSNR. Based on the results obtained on a set of 110 images it has been observed that the filter based on tetrolet transform gives the best performance in terms of noise suppression.

Singh et al. [255] compared the performance of 14 despeckle filtering algorithms taken from 03 filter categories namely Fourier filters, multiscale filters and non-linear iterative filters.

The performance evaluation of these filters has been carried out on the basis of different image quality metrics like edge retrieval index (ERI) to quantify the edge-retrieval capabilities (objective analysis) as well as subjective analysis by experts. The study has been carried out on 28 breast ultrasound images and on the basis of objective and subjective evaluation, 02 filters namely wavelet filter with 1st level of decomposition, Homomorphic filter with wavelet function outperformed other despeckle filtering algorithms.

In another study, Singh et al. [252] compared the performance of 23 despeckle filtering algorithms taken from 04 different filter categories namely local statistics based filters, Fourier filters, multiscale filters and non-linear iterative filters. The performance evaluation of these filters has been carried out on the basis of different image quality metrics like ERI to quantify the edge-retrieval capabilities (objective analysis) as well as subjective analysis by experts. The study has been carried out on 28 breast ultrasound images and on the basis of objective and subjective evaluation, three filters namely wavelet filter with 1st level of decomposition, Homomorphic filter with wavelet function and AD filter (PM2) achieved comparable performance.

Zhang et al. [313] compared the performance of 11 filters taken from 05 categories of despeckle filtering algorithms namely local statistics based filters, multiscale filters, non-local mean filters, non-linear iterative filters and hybrid filters. The performance has been assessed for 400 breast ultrasound images on the basis of objective as well as subjective evaluation. For the objective assessment, an image quality metric named natural image quality estimator (NIQE) has been used and for the subjective analysis, the grading by 03 experts has been used.

In the present work, an extensive set of despeckle filtering algorithms has been used consisting of 42 despeckle filtering algorithms selected from all the 08 filter categories. The study has been carried out on 100 breast ultrasound images and the performance has been tested on the basis of both objective and subjective assessment [141].

2.3. Review of Literature on Segmentation of Breast Tumors

For the segmentation of breast tumors from ultrasound images many different segmentation algorithms have been employed. A broad categorization of the segmentation algorithms applied to breast ultrasound images is given in Fig. 2.2.

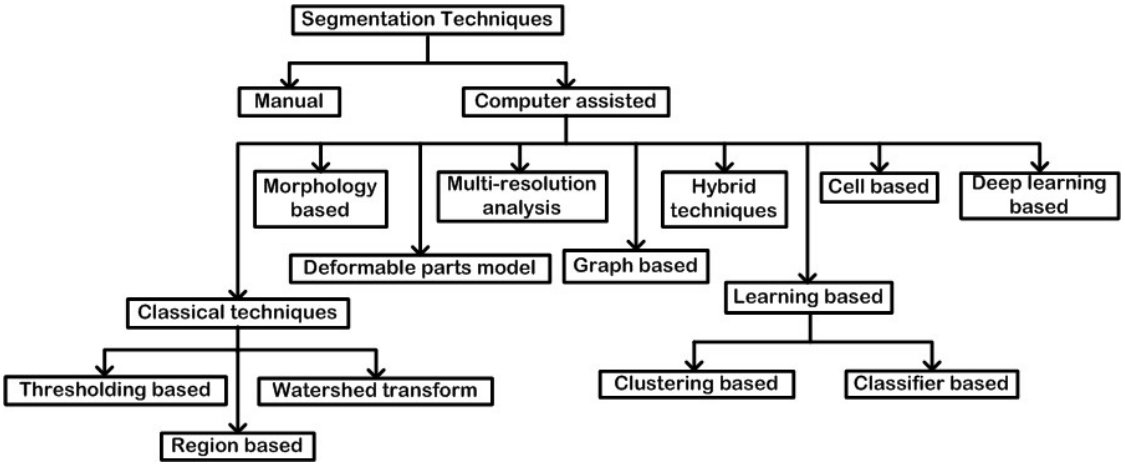

Fig. 2.2 Broad categorization of segmentation techniques.

The various studies conducted by researchers in the past can broadly be categorized as (*a*) Studies carried out for the segmentation of breast tumors using original ultrasound images, (*b*) Studies carried out for the segmentation of breast tumors using pre-processed ultrasound images. A brief description of the related studies for the segmentation of breast tumors is given here.

2.3.1. Studies carried out for the segmentation of breast tumors using original ultrasound images

A brief description of different studies carried out for the segmentation of breast tumors using original ultrasound images is shown in Table 2.2.

Table 2.2 A brief description of studies carried out for the segmentation of breast tumors using original ultrasound images.

Investigators	Images	Segmentation	Evaluation
Boukerroui et al. (1998) [26]	30	Clustering based	Subjective
Xiao et al. (2002) [292]	--	Graph based	Subjective
Cheng et al. (2005) [47]	--	Graph based	Subjective
Liu et al. (2009) [164]	B: 48 M: 55	Deformable parts model	Objective
Xu et al. (2009) [296]	--	Clustering based	Objective
Yeh et al. (2009) [304]	10	Hybrid	Objective
Chiang et al. (2010) [50]	16	Hybrid	Objective
Liu et al. (2010) [165]	B: 33 M: 46	Deformable parts model	Objective
Shi et al. (2010) [247]	35	Hybrid	Objective
Takemura et al. (2010) [263]	C: 50 F: 50 Ca: 300	Hybrid	Objective
Zhang et al. (2010) [318]	90	Classical	Objective
Zhang et al. (2010)[315]	347	Graph based	Objective
Jiao et al. (2011) [121]	18	Hybrid	Objective
Jinyao et al. (2011) [123]	--	Hybrid	Objective
Othman et al. (2011) [206]	20	Classifier based	Objective

Pons et al. (2011) [212]	56	Graph based	Objective
Rodrigues et al. (2011) [228]	250	Classical	--
Gao et al. (2012) [77]	20	Deformable parts model	Objective
Gao et al. (2012) [78]	B: 50 M: 50	Graph based	Objective
Hao et al. (2012) [95]	B: 28 M: 54	Hybrid	Objective
Hao et al. (2012) [96]	480	Graph based	Objective
Jiang et al. (2012) [120]	112	Graph based	Subjective
Liu et al. (2012) [170]	B: 125 M: 80	Cell based	Objective
Xian et al. (2012) [289]	B: 60 M: 71	Graph based	Objective
Cai et al. (2013) [33]	B: 81 M: 87	Deformable parts model	Objective
Lin et al. (2013) [163]	B: 194 M: 114	Deformable parts model	Objective
Liu et al. (2013) [171]	861	Deformable parts model	Objective
Pons et al. (2013) [211]	B: 114 M: 98	Graph based	Objective & subjective
Cho et al. (2014) [52]	B: 300 M: 181	Deformable parts model	Objective
Marcomini et al. (2014) [179]	144	Deformable parts model Hybrid	Objective Objective
Torbati et al. (2014) [268]	30	Classifier based	Objective
Prabusankarlal et al. (2015) [219]	B: 90 M: 60	Clustering based	Objective
Guo et al. (2016) [91]	B: 31 M: 35	Deformable parts model	Objective
Triyani et al. (2016) [269]	--	8 methods with and without morphological operations	Objective
Xi et al. (2016) [287]	B: 135 M: 51	Deformable parts model	Objective
Yap et al. (2016) [303]	120	Deformable parts model	Objective
Kirimasthong et al. (2017) [138]	15	Deformable parts model	Objective
Lestari et al. (2017) [159]	30	Hybrid	Objective
Hu et al. (2018) [104]	570	Hybrid	Objective
Kumar et al. (2018) [147]	--	Deep learning based	Objective
Liu et al. (2018) [169]	B: 120 M: 110	Cell based	Objective
Xian et al. (2018) [291]	562	Graph based, classifier based, based, deformable parts model, clustering based	Objective
Xie et al. (2018) [295]	2600	Deep learning based	Objective
Yap et al. (2018) [302]	469	Deep learning based	Objective
Yu et al. (2018) [308]	187	Deformable parts model	Objective
Chiao et al. (2019) [51]	307	Deep learning based	Objective
Huang et al. (2019) [109]	2238	Hybrid	Objective
Kriti et al. (2019) [141] (Present	100	Chan and Vese active contour	Objective & subjective

work)		model	
Xing et al. (2019) [296]	670	Deep learning based	Objective
Zhuang et al. (2019) [324]	1062	Deep learning based	Objective

Note: B: Benign. M: Malignant, C: Cyst, F: Fibroadenoma, Ca: Carcinoma.

From Table 2.2, it has been observed that many studies have been carried out for the segmentation of breast tumors using original ultrasound images by applying different segmentation algorithms ranging from classical, graph-based, deformable parts model based, learning based to hybrid methods. From the studies presented in Table 2.2, following points can be observed:

(*i*) Most of the methods developed in the past have successfully been applied for the segmentation of original breast ultrasound images ranging from clustering, deformable parts based, classifier based, graph based [26, 47, 123, 141, 228, 292, 296, 315] to new concepts of cellular automata [169], deep learning [51, 147, 295, 296, 302, 324] with some hybrid methods that utilize two or more conventional methods for segmentation purposes [50, 95, 104, 109, 121, 123, 159, 179, 247, 263, 304].

(*ii*) For the assessment of segmentation performance, most of the studies have used objective evaluation by computing different area and boundary based metrics like Jaccard index, dice coefficient, Hausdroff distance etc. while very few studies have evaluated the segmentation performance on the basis of both objective and subjective evaluation [211].

(*iii*) For the evaluation of the segmentation performance it has been observed that almost all the studies have represented the results for the whole dataset while very few studies have represented the results individually for the benign and malignant tumors [91, 287].

(*iv*) Few studies have been carried out using deep learning architectures for the segmentation of breast tumors [51, 147, 295, 296, 302, 324] like variants of fully convolutional networks (FCNs), variants of region based CNNs (R-CNN), generative adversarial networks (GAN), UNet etc. It can also be noted that in two of the studies, active contour models have been used as a post-processing step for refining the tumor contours obtained after the application of deep networks [104, 109].

Cai et al. [33] in their study proposed a phase based active contour (PBAC) model to extract the tumor boundaries from images that are blurry and are marred by low contrast and speckle noise. The study has been carried out on both synthetic and real-time breast ultrasound images for performance comparison on the basis of Jaccard index (JI).

Liu et al. [171] proposed a robust region-based active contour model with point classification in order to segment high-variant breast tumors. The study has been carried out on

a large dataset of 4306 breast ultrasound images and the segmentation performance has been evaluated using JI.

Cho et al. [52] used a region-based active contour model with adaptive parameter estimation in order to segment 481 breast tumors. For the estimation of parameters, different algorithms namely support vector regressor, multivariate linear regression and expectation-maximization have been used. The performance of the segmentation algorithm has been compared on the basis of average JI value.

Marcomini et al. [179] analysed the application of morphological operators as pre-processing step for the segmentation of breast tumors using active contour model. The performance has been tested on 144 images using different quantitative measures.

The study by Pons et al. [211] reported the use of Markov random field-maxim a posteriori (MRF-MAP) based segmentation algorithm for segmenting a total of 212 breast ultrasound images. The performance of segmentation algorithm has been evaluated on the basis of objective as well as subjective assessment.

Guo et al. [91] reported the use of level set method applied to 66 breast ultrasound images for the segmentation of breast tumors based on the neutrosophic score of the image. The performance of the segmentation algorithm has been evaluated objectively on the basis of different metrics like percentage area overlap, Hausdorff distance and average distance. The study also reported the results of the segmentation individually for both benign and malignant cases.

Xi et al. [288] proposed a segmentation method based on prior knowledge and level set method to segment 186 breast ultrasound images. In this approach a learning model has been designed to learn prior knowledge useful for classifying the abnormal tumor regions in the image and then level set method has been employed to segment the classified abnormal regions. The performance of the segmentation algorithm has been tested objectively on the basis of JI individually for the malignant and benign tumors.

Xian et al. [292] compared the performance of five segmentation approaches belonging to 04 different categories of segmentation i.e. graph based, classifier based, cell based and deformable parts model based on the basis of objective evaluation. The study has been carried out on 562 breast ultrasound images

Hu et al. [104] tested the performance of a dilated fully convolutional neural network combined with PBAC model for the segmentation of 570 breast ultrasound images. The active contour model has been used as a post-processing step for refining the tumor contours. The

segmentation performance has been measured on the basis of objective assessment by using different metrics like dice coefficient and Hausdorff distance.

The study proposed by Yap et al. [302] has been carried out on 469 breast ultrasound images to test the performance of different variants of FCN for breast tumor segmentation and the performance has been measured objectively on the basis of dice coefficient individually for benign and malignant tumors.

Xing et al. [296] reported the use of a variant of GAN called semi-pixel-wise cycle generative adversarial network (SPCGAN) for the segmentation of breast tumors using 670 images and the performance of the segmentation algorithm has been measured objectively.

Zhuang et al. [324] proposed a novel method of breast ultrasound image segmentation called residual-dilated-attention-gate-UNet (RDAU-NET) by modifying the U-Net architecture. The model has been tested on a total of 1602 images collected from three different sources and the segmentation performance has been measured objectively.

2.3.2. Studies carried out for the segmentation of breast tumors using pre-processed ultrasound images

A brief description of the studies carried out for the segmentation of breast tumors using pre-processed ultrasound images is shown in Table 2.3.

Table 2.3 A brief description of studies carried out for the segmentation of breast tumors using pre-processed ultrasound images.

Investigators	Images	Pre-processing	Segmentation	Evaluation
Horsch et al. (2001) [101]	CC: 124 B: 182 M: 94	Median filter	Thresholding	Objective
Drukker et al. (2002) [64]	CC: 229 B: 334 M: 194	Median filter	Hybrid	Objective
Madabhushi et al. (2002) [176]	48	2^{nd} order Butterworth filter → HE	Hybrid	Subjective
Madabhushi et al. (2003) [177]	42	2^{nd} order Butterworth filter → HE	Hybrid	Objective
Huang et al. (2004) [110]	B: 21 M: 39	Wiener filter	Hybrid	Objective
Huang et al. (2005) [112]	20	Non-linear medium filter	Hybrid	Objective
Jung et al. (2005) [129]	B: 50 M: 50	Median filter + Thresholding	Morphology based	--
Liu et al. (2005) [168]	B: 25 M: 15	AD → Unsharp masking	Hybrid	Objective
Shen et al. (2006) [244]	45	Butterworth filter → fuzzy logic based	Hybrid	Subjective

		enhancement		
Flores et al. (2007) [73]	32	AD	Deformable parts model	Subjective
Huang et al. (2007) [114]	B: 84 M: 34	MCDE filtering	Deformable parts model	Objective
Yap et al. (2007) [300]	360	HE → hybrid filtering → multifractal analysis	Hybrid	Subjective
Shan et al. (2008) [239]	105	SRAD	Classical	Objective
Shan et al. (2008) [238]	--	SRAD	Classical	Objective
Cui et al. (2009) [59]	250	Gaussian filter	Deformable parts model	Objective
Gomez et al. (2009) [86]	36	Morphological filtering	Classical	Objective
Gomez et al. (2010) [85]	50	CLAHE → AD	Classical	Objective
Gomez et al. (2010) [84]	50	CLAHE→AD	Deformable parts model	Objective
Gomez et al. (2010) [87]	50	CLAHE→AD	Classical	Objective
Jumaat et al. (2010) [127]	80 (phantom) 50 (real-time)	Median filter → Histogram stretching	Deformable parts model	Objective
Jumaat et al. (2010) [126]	45	Median filter → Histogram stretching	Deformable parts model	Objective
Lee et al. (2010) [157]	20	NCD filter	Graph based	Subjective
Massich et al. (2010) [183]	25	Median filter	GCS	Objective
Abdelrahman et al. (2011) [1]	30	HE → 1st order local statistics based filter → median filter	Hybrid	Objective
Bochhi et al. (2011) [25]	60	Filter based on cellular automata	Cell based	Objective
Chucherd et al. (2011) [54]	--	SPPA	Deformable parts model	Objective
Chucherd et al. (2011) [55]	--	PPA + MRA	Deformable parts model	Objective
Jumaat et al. (2011) [128]	50	Median filter → histogram stretching	Deformable parts model	Objective.
Lee et al. (2011) [156]	60	Median filter	Hybrid	Objective
Yu et al. (2011) [306]	B: 539 M: 317	RDCA → Morphological operations → Gaussian LPF	Classical	Subjective
Su et al. (2011) [259]	132	SRAD	Graph based	Objective
Zhang et al. (2011) [316]	--	Mean filter → Fuzzy	Classical	Subjective

		enhancement		
Zhang et al. (2011) [317]	--	Mean filter	Classical	Subjective
Daoud et al. (2012) [61]	10	Decompression + SNR parametric image computation	Deformable parts model	Objective
Huang et al. (2012) [108]	20	NAD	Graph based	Objective
Jia-Wei et al. (2012) [122]	510	Homogeneity histogram → directional average filter	Clustering based	Objective
Marcomini et al. (2012) [181]	50	Wiener filter → image equalization → median filter	Classifier based	Objective
Shan et al. (2012) [241]	120	SRAD	Classical	Objective
Shan et al. (2012) [240]	122	SRAD	Clustering based	Objective
Karimi et al. (2013) [132]	147	Fuzzy-compounding	Classical	Objective
Marcomini et al. (2013) [182]	80 (phantom) 50 (real-time)	Wiener filter → equalization → median filter	Classical, learning based, Deformable parts model	Objective
Rodtook et al. (2013) [231]	48	Local statistics based filter	Deformable parts model	Objective
Huang et al. (2014) [106]	B: 10 M: 10	Bilateral filtering	Graph based	Objective
Moraru et al. (2014) [195]	30	Wiener filter → contrast enhancement	Deformable parts model	Objective
Prabhakar et al. (2014) [213]	B: 2 M: 4	Wavelet based soft thresholding	Deformable parts model	Objective
Prabusankarlal et al. (2014) [217]	B: 18 M: 14	Median filter → stick method	Hybrid	Objective & subjective
Wang et al. (2014) [280]	4	SRAD	Deformable parts model	Objective
Xian et al. (2014) [289]	131	Gaussian filter	Graph based	Objective
Zhou et al. (2014) [323]	B: 38 M: 31	Gaussian filter → HE → pyramid mean shift filter	Graph based	Objective
Huang et al. (2015) [107]	46	TV	Hybrid	Objective
Liu et al. (2015) [167]	--	SRAD	Hybrid	Subjective
Nugroho et al. (2015) [200]	--	Bilateral filter	Deformable parts model	Objective
Rodrigues et al. (2015) [229]	44	AD + bandpass filter	Deformable parts model	Objective
Shao et al. (2015) [242]	450	Gaussian filter + normalization	Graph based	Objective
Xian et al. (2015) [291]	184	Gaussian filter	Hybrid	Objective

Elawady et al. (2016) [69]	20	Frost, DPAD, PPB	Graph based, Quick shift	Objective
Gomez et al. (2016) [89]	100	AD + log Gabor filter	Classifier based	Objective
Marcomini et al. (2016) [180]	DB1: 144 DB2: 123	Wiener filter → contrast enhancement → median filter	Classical, learning based, Deformable parts model	Objective
Prabhakar et al. (2016) [214]	110	Tetrolet	Deformable parts model	Objective
Samundeeswari et al. (2016) [235]	4	Spatial filter	Hybrid	Objective
Cristerna et al. (2017) [58]	1021	5 contrast enhancement → 4 despeckling algorithms	Classical	Objective
Feng et al. (2017) [70]	40	8 despeckling algorithms	Clustering based	Objective
Feng et al. (2017) [71]	30	HE	Hybrid	Objective
Nugroho et al. (2017) [201]	102	SRAD	Hybrid	Subjective
Prabhakar et al. (2017) [215]	--	Wavelet soft thresholding	Deformable parts model	Objective
Shiji et al. (2017) [249]	97	Shearlet transform based filtering → HE	Classical	Objective
Almajalid et al. (2018) [8]	221	SRAD → HE	Deep learning based	Objective
Huang et al. (2018) [105]	325	Histogram normalization	Deep learning based	Objective
Lal et al. (2018) [150]	45	SRAD	Clustering based	Objective
Lal et al. (2018) [151]	DB1: 40 DB2: 20	SRAD	Clustering based	Objective
Liu et al. (2018) [166]	61	NLLR	Deformable parts model	Objective
Lotfollahi et al. (2018) [174]	36	Blockwise non-local means filter	Deformable parts model	Objective
Osman et al. (2018) [205]	306	Altered Phase Preserving Dynamic Range Compression	Classical	Objective
Rodtook et al. (2018) [230]	180	Gaussian filter	Hybrid	Objective
Panigrahi et al. (2019) [208]	127	SRAD	Hybrid	Objective
Kriti et al. (2019) [141] (Present work)	100	DPAD	Deformable parts model	Objective & subjective

Note: CC: Complex cyst, B: Benign, M: Malignant, HE: Histogram equalization, AD: Anisotropic diffusion, MCDE: Modified curvature diffusion equation, SRAD: Speckle reducing anisotropic diffusion, CLAHE: Contrast limited adaptive histogram equalization, NCD: Non-linear coherent diffusion, GCS: Gaussian constraining segmentation, SPPA: Sparse phase portrait analysis, PPA: Phase portrait analysis, MRA: Multi-resolution analysis, RDCA: Radius dependent contrast adjustment, LPF: Low pass filter, SNR: Signal to noise

ratio, NAD: Nonlinear anisotropic diffusion, TV: Total variation, DPAD: Detail preserving anisotropic diffusion, PPB: Probabilistic patch based, DB: Database, NLLR: Non-local low rank.

From Table 2.3, it can be seen that many studies have been carried out for segmentation of breast tumors using pre-processed images. It can be noted that the pre-processing has been carried out either by employing despeckle filtering algorithms, contrast enhancement methods or a combination of the two. It can also be noted from the table that many studies have been carried out on very less number of images (< 50) for the segmentation of breast tumors [1, 61, 69-71, 86, 112, 126, 150, 151, 157, 168, 174, 176, 177, 183, 195, 217, 229, 235, 280, 323]. From the studies presented in Table 2.3, following points can be observed:

(*i*) For the pre-processing of breast ultrasound images prior to segmentation, it has been observed that filtering methods are a popular choice median, SRAD, AD, Wiener and Butterworth filters being used most widely [73, 85, 101, 110, 150, 151, 156, 167, 183, 201, 208, 238-241, 259, 280]. Very few studies have been carried out that use enhancement methods only for the pre-processing of breast ultrasound images [71, 105, 135].

(*ii*) From the studies that have utilized both filtering and enhancement of methods to pre-process breast ultrasound images, it has been observed that Histogram equalization (HE) and contrast enhancement and stick methods are most widely used to improve the image contrast [1, 8, 58, 84, 87, 176, 177, 180, 249, 323].

(*iii*) In most of the studies, variants of deformable parts model based methods of segmentation have been used either as standalone technique [54, 55, 59, 61, 73, 84, 114, 126, 128, 141, 174, 180, 182, 195, 213-215, 280] or as hybrid methods [107, 112, 156, 168, 244, 300].

(*iv*) For the assessment of segmentation performance, most of the studies have utilized objective evaluation i.e. different metrics like Jaccard index, dice coefficient etc. while very few studies have been carried out that assess the performance of segmentation on the basis of subjective evaluation i.e. visual comparison between the tumor contour obtained as a result of segmentation and the ground truth [73, 157, 167, 176, 301, 306].

(*v*) Very few studies have been carried out by using deep learning architectures to segment the breast ultrasounds images [8, 105].

(*vi*) In most of the studies the performance of the segmentation algorithm has been presented for the whole dataset while very few studies have represented the segmentation results individually for both benign and malignant tumors individually [71, 168].

(*vii*) It is also worth noting that very few studies have been carried out that analyse the effect of different pre-processing techniques for the performance evaluation of segmentation of breast tumors in order to find an optimal pre-processing technique for segmentation [58, 69, 70].

Huang et al. [112] used a two-stage segmentation process by applying watershed transform and active contour method (ACM) for segmenting the breast tumors from 20 ultrasound images pre-processed by a non-linear medium filter. The watershed transform has been used to find the initial contour in the tumor images while ACM has been used to refine the obtained initial contour. The segmentation performance has been tested objectively by using the similarity index.

Liu et al. [168] used a hybrid segmentation method employing graph based technique with classical region merging method of segmentation. The study has been carried out on 40 breast ultrasound images pre-processed using AD filter followed by unsharp masking. The segmentation performance has been evaluated objectively for benign and malignant tumors individually.

Shen et al. [244] utilized a 2-stage segmentation procedure by using wavelet transform and ACM. The wavelet transform has been employed to detect the initial boundary of the tumors and then ACM has been used to adjust this initial boundary and obtain an optimal contour. The performance of segmentation algorithm has been evaluated subjectively.

Flores et al. [73] proposed an approach to segment breast tumors pre-processed by anisotropic texture-guided diffusion. The pre-processed images have then been subjected to a front propagation algorithm for obtaining the initial contour of the tumor. To refine the initial contour an adaption of the geodesic ACM has been used. The performance of the segmentation algorithm has been tested objectively on the basis of area and boundary metrics.

Cui et al. [59] utilized a 2-stage ACM for the segmentation of breast tumors using 250 images pre-processed by the Gaussian filter. The preliminary tumor region has been separated using the *k*-means clustering and then been used as the initial contour for the ACM algorithm. The performance of the segmentation algorithm has been tested objectively on the basis of area metrics.

Gomez et al. [84] evaluated the performance of Chan and Vese ACM for the segmentation of 50 breast ultrasound images pre-processed by CLAHE and AD filter. The performance of the segmentation algorithm has been tested objectively on the basis of area and boundary metrics.

Elawady et al. [69] compared the performance of 03 despeckle filtering algorithms and 02 segmentation algorithms for efficient breast tumor segmentation. The authors reported the use of 20 breast ultrasound images pre-processed by frost filter, probabilistic patch based filter (PPB) and detail preserving anisotropic diffusion filter (DPAD). The pre-processed images have been subjected to two segmentation algorithms namely normalized cut and quick shift.

Then performance of the segmentation algorithms has been tested objectively on the dice coefficient, JI and sensitivity. Based on the results it has been concluded by the authors that images despeckled by frost filter and segmented by quick shift method produce optimal segmented tumor images.

Daoud et al. [61] segmented 10 breast ultrasound images by using semi-automated ACM. Prior to segmentation the images have been decompressed and pre-processed to form SNR parametric images. The performance of the segmentation algorithm has been tested objectively on the basis of area metrics.

Cristerna et al. [58] tested the effect of the application of different pre-processing methods on the segmentation performance. A total of 20 pre-processing algorithms have been experimented and formed by the combination of 05 contrast enhancement methods and 04 speckle removing filters. These algorithms have been applied to a total of 1021 breast ultrasound images and the resultant pre-processed images have been subjected to segmentation using watershed transform. The performance of segmentation has been tested objectively on the basis of JI and it has been observed that a combination of fuzzy enhancement followed by interference based speckle filtering, resulted in optimal performance.

Feng et al. [71] used histogram equalization to enhance the breast ultrasound images followed by fuzzy-c means clustering for the segmentation task. The study compared the segmented contour to the contour marked by three expert radiologists. It has been observed that for the benign images, the inter-observer variability values were lower while for malignant images a large inter-observer variation was observed, accounting for the morphological difference between the benign and malignant tumor shapes.

Marcomini et al. [180] compared the performance of different segmentation algorithms namely ACM, fuzzy c-means clustering, *k*-means clustering, region growing and self-organizing map (SOM) for the segmentation of 80 phantom and 50 real time breast ultrasound images pre-processed by using wiener filter, equalization and median filter. The segmentation performance has been evaluated objectively on the basis of different quantitative measures and SOM technique has been proposed to give the best segmentation results.

Huang et al. [107] segmented a total of 46 breast ultrasound images pre-processed by a total variation filter. A robust graph based method has been used to partition the images into sub-regions. This divided image has been fed to an object detection algorithm to automatically detect the tumor regions and lastly ACM has been utilized to refine the initial tumor contour. The performance of this algorithm has been tested objectively on the basis of area metrics.

Wang et al. [280] assessed the segmentation performance of multiscale geodesic ACM for segmenting the breast ultrasound images pre-processed using SRAD filter. The study has been tested on a set of four breast ultrasound images and the performance has been assessed on the basis of JI.

Almajalid et al. [8] used U-Net architecture for the segmentation of 221 breast ultrasound images that have been pre-processed by using SRAD filter and HE. The performance of the segmentation algorithm has been tested objectively by using the dice coefficient and similarity index.

Huang et al. [105] tested the performance of variants of FCN architecture for the segmentation of 325 breast ultrasound images pre-processed using histogram normalization. The segmentation performance has been tested objectively on the basis of intersection over union (IoU).

On the basis of the studies presented in Tables 2.2 and 2.3, it can be observed that for segmentation of breast tumors, either original images have been used or pre-processed images have been used and very few studies have tried to evaluate the effect of pre-processing on the segmentation performance. Therefore, in the present work both original images and images despeckled by different despeckle filtering algorithms have been segmented to analyse the effect of pre-processing on segmentation of breast tumors and hence find an optimal filter that results in efficient segmentation performance.

2.4. Review of Literature on Classification of Breast Tumors using Machine Learning Approaches

The studies conducted for classification of breast tumors using machine learning approaches can use either original images or pre-processed images. It can also be noted that the studies carried out for classification of breast tumors are either based on the computation of texture features only [15, 22, 32, 39, 41, 44-46, 88, 111, 115, 140, 162, 185, 198, 248, 276, 299, 321], morphological features only [10, 11, 17, 40, 113, 124, 125, 179, 257] or both texture and morphological features [12, 21, 43, 62, 90, 158, 192, 194, 209, 233, 264, 301, 310]. For the computation of features the type of regions of interest (ROI) to be used are given in Fig. 2.3.

However, it is worth mentioning that for classification of breast tumors both textural and morphological information exhibited by the breast tumors is considered significant. Therefore, the present review has been conducted on the studies that compute both texture and morphological features from the B-mode breast ultrasound images. The various studies conducted by researchers in the past can broadly be categorized as (*a*) Studies carried out for

classification of breast tumors using original ultrasound images, (*b*) Studies carried out for classification of breast tumors using pre-processed ultrasound images.

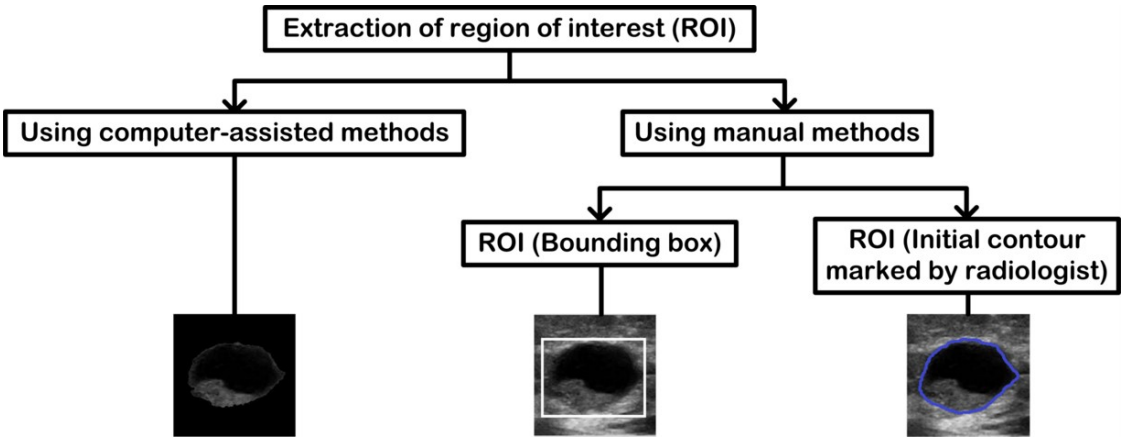

Fig. 2.3 Types of ROIs to be used for breast tumor classification.

A brief summary of the related studies for classification of breast tumors using machine learning approaches is give here.

2.4.1. Machine learning based studies carried out for classification of breast tumors using original ultrasound images

A brief description of various machine learning based CAD systems designed for classification of breast tumors using original ultrasound images is given in Table 2.4.

Table 2.4 A brief description of various machine learning based CAD systems designed for classification of breast tumors using original ultrasound images.

Investigator	Images	ROI extraction	Feature extraction	Feature selection	Classifier (Acc.)
Ruggiero et al. (1998) [233]	C: 41 F: 41 Ca: 41	Multiple manually extracted ROI	GLCM, GLRLM texture + morphological features	--	NN (--)
Lefebvre et al. (2000) [158]	B: 56 M: 19	Lesion contour marked by radiologist	FOS, GLCM, GLRLM + morphological features	--	LDA (--)
Drukker et al. (2004) [63]	CC: 1007 SBL: 544 M: 281	Classical	Autocorrelation texture + morphological features	--	BNN (--)
Piliouras et al. (2004) [209]	154	Lesion contour marked by radiologist	FOS, GLCM, GLRLM + morphological features	Wrapper method	SVM (98.7%)
Shen et al. (2007) [246]	B: 180 M: 85	Lesion contour marked by radiologist	Echo pattern, posterior acoustic features + shape and margin features	Filter method	LR (91.7%)
Shen et al. (2007) [245]	B: 407 M: 219	Lesion contour marked by radiologist	Echo pattern, posterior acoustic features + shape and margin features	--	LR (73.0%)
Gruszauskas et al.	B: 219	Manually	Autocorrelation +	--	Ensemble

(2008) [90]	M: 125	extracted ROI	morphological features		BNN (AUC: 0.87)
Chen et al. (2009) [43]	B: 73 M: 41	Lesion contour marked by radiologist	GLCM + morphological features	Wrapper method	LDA (89.5%) MLP (88.6%)
Yap et al. (2009) [301]	40	Manually extracted ROI	FOS + morphological features	--	SVM (93.0%)
Takemura et al. (2010) [264]	C: 50 F: 50 Ca: 200	Lesion contour marked by radiologist	FOS, GLCM + morphological and margin features	Wrapper method	AdaBoost (100%)
Liao et al. (2011) [161]	B: 113 M: 208	Lesion contour marked by radiologist	GLCM + morphological features	--	SVM (86.9%) kNN (83.8%) NN (86.6%)
Alvarenga et al. (2012) [9]	B: 69 M: 177	Morphology based	GLCM and complexity curve texture + morphological features	Wrapper method	FLDA (85.3%)
Zakeri et al. (2012) [310]	B:47 M: 33	Deformable parts model	Cross correlation + morphological features	--	SVM (95.0%)
Moon et al. (2012) [194]	B: 95 M: 42	Deformable parts model	FOS and GLCM + morphological features	Wrapper method	LR (84.7%)
Moon et al. (2013) [192]	B: 48 M: 21	Deformable parts model	GLCM texture + morphological features	Wrapper method	LR (88.0%)
Lee et al. (2013) [154]	B: 1599 M: 2508	Lesion contour marked by radiologist	GLCM + morphological features based on border irregularity	--	SVM (94.9%)
Zhang et al. (2014) [319]	B: 22 M: 29	--	Echo pattern, Posterior acoustic features + morphological features	Biclustering learning	kNN (94.1%)
Shan et al. (2015) [237]	B: 133 M: 150	--	Echo pattern, Posterior acoustic features + morphological features	Wrapper method	DT (77.7%) NN (78.1%) RF (78.5%) SVM (77.7%)
Verma et al. (2015) [273]	188	Manually extracted ROI	Statistical, Laws' fractal + morphological features	Hybrid method	SVM (86.2%)
Amin et al. (2016) [12]	B: 54 M: 58	Manually extracted ROI	Statistical texture + morphological features in NSS domain	Filter method	SVM (99.1%)
Bhusri et al. (2016) [21]	B: 51 M: 121	Lesion contour marked by radiologist	FOS + morphological features	--	SVM (89.6%)
Daoud et al. (2016) [62]	B: 64 M: 46	Multiple non-overlapping	GLCM + morphological features	Wrapper method	SVM (98.2%)

		ROIs inside lesion			
Kim et al. (2017) [137]	B: 120 M: 72	Boundary generated by S-detect	GLCM, histogram changes based texture + morphological features	--	SVM (70.8%)
Kriti et al. (2019) [142] (Present work)	B: 40 M: 60	ACM	FOS, GLCM, GLRLM, Laws', FPS, Gabor + morphological features	PCA	SVM (94.1%)

Note: ROI: Region of interest, Acc.: Accuracy, C: Cyst, F: Fibroadenoma, Ca: Carcinoma, GLCM: Gray level co-occurrence matrix, GLRLM: Gray level run length matrix, NN: Neural network, B: Benign, M: Malignant, FOS: First order statistics, LDA: Linear discriminant analysis, CC: Complex cyst, SBL: Solid benign lesion, SVM: Support vector machine, BNN: Bayesian neural net, LR: Logistic regression, AUC: Area under the curve, MLP: Multilayer perceptron, kNN: k-nearest neighbour, FLDA: Fischer linear discriminant analysis, DT: Decision tree, RF: Random forest, ACM: Active contour model, FPS: Fourier power spectrum, PCA: Principal component analysis.

From the studies presented in Table 2.4, it can be noted that the studies have been carried out either on ROIs segmented using computer-assisted methods [9, 63, 194, 192, 310] or the ROIs have been extracted manually [12, 21, 43, 62, 90, 137, 154, 158, 161, 209, 233, 245, 246, 264, 273, 301]. It can also be noted that studies carried out in [9, 21, 43, 62, 137, 158, 161, 192, 194, 209, 233, 264, 301] have used statistical methods of texture feature extraction like first order statistics (FOS), gray level co-occurrence matrix (GLCM) and gray level run length matrix (GLRLM) while other studies have been carried out using correlation or covariance based features [63, 90, 310] and BIRADS features [154, 245, 246]. It can also be noted that studies in [158, 301, 310, 319] have been carried out on very few images (< 100). From the studies presented in Table 2.4, following points can be noted:

(*i*) Most of the studies have reported the classification of breast tumors into two classes namely benign and malignant, while the study in [63] has reported the three-class classification of breast tumors into cysts, solid benign lesions and malignant lesions and studies in [233, 264] reported the three-class classification of breast tumors into cysts, fibroadenomas and carcinomas.

(*ii*) For the extraction of texture features from the extracted ROIs, it can be noted that all the studies have made use of statistical methods of feature extraction like FOS, GLCM, correlation, covariance etc. while the study by Verma et al. [273] has reported the use of signal processing based Laws' mask analysis for classification of breast tumors.

(*iii*) Most of the studies have employed feature selection methods in order to find an optimal feature set for classification of breast tumors. It can be noted that wrapper based methods of feature selection have been widely used while very few studies used filter based methods [23, 246].

(*iv*) It can also be noted that support vector machine (SVM) has been used most popularly for classification of breast tumors [12, 21, 62, 137, 142, 161, 209, 237, 273, 301, 310].

For the studies carried out on ROIs extracted by using computer-assisted methods, Zakeri et al. [310] reported the highest classification accuracy of 95.0 % on a set of 80 images using SVM classifier and correlation based texture features combined with morphological features computed from ROI images obtained by using deformable parts model based method of segmentation.

For the studies carried out on manually extracted ROIs (i.e. bounding boxes), two studies have reported comparable accuracies. Amin et al. [12] reported an accuracy of 99.1 % using SVM classifier and a feature set computed from 112 images. The feature set contains pooled statistical texture features and morphological features. The texture features have been computed by transforming the images into the neutrosophic domain. The computed texture features are intensity based and GLCM based, while morphological features like diameter, perimeter, area, eccentricity, etc. have been computed. From the computed feature set, optimal features have been selected on the basis of Chi-square-test.

Daoud et al. [62] implemented a decision fusion based approach for classification of breast tumors using SVM classifier reporting an accuracy of 98.2 %. The study has been carried out on 110 images. For the computation of texture features multiple non-overlapping ROIs have been taken from inside the tumors. The GLCM based texture features have been computed from each ROI while the morphological features have been computed using the whole tumor. Each computed feature set has been subjected to a 2-stage feature selection method employing minimal-redundancy-maximal relevance (mRMR) and backward selection. Based on texture features, the class membership of each ROI has been determined and majority voting has been used to obtain the final tumor class. The study also determined the tumor class based on the computed morphological features and the final tumor class has been obtained by the decision fusion. The study has also experimented the conventional method of combining the computed texture and morphological sets and reported an accuracy of 90.9 %.

In case of the studies carried out on ROIs extracted segmented manually, Takemura et al. [264] reported the highest classification accuracy of 100 % using AdaBoost classifier. The optimal feature set has been obtained by the application of sequential forward search (SFS) on a feature set formed by a combination of FOS, GLCM based texture features and morphological features.

Piliouras et al. [209] reported a classification accuracy of 98.7 % using SVM classifier and a feature set consisting of various texture and morphological features. Texture features

have been computed using different methods like FOS, GLCM, GLRLM. The morphological features have been computed on the basis of radial distance of tumor's centroid from the edges. A wrapper based method of feature selection has been utilized to find out optimal features for classification of breast tumors.

2.4.2. Machine learning based studies carried out for classification of breast tumors using pre-processed ultrasound images

A brief description of various machine learning based CAD systems designed for classification of breast tumors using pre-processed ultrasound images is shown in Table 2.5.

Table 2.5 A brief description of various machine learning based CAD systems designed for classification of breast tumors using pre-processed ultrasound images.

Investigator	Images	Pre-processing	ROI extraction	Feature extraction	Feature selection	Classifier (Acc.)
Horsch et al. (2002) [102]	B: 306 M: 94	Median filter → Gaussian function	Classical	Autocorrelation + morphological features	Wrapper method	LDA (AUC: 0.88)
Drukker et al. (2003) [65]	1740	RGI filtering	Classical	Texture and margin features	Wrapper method	BNN (AUC: 0.81)
Wang et al. (2008) [281]	B: 81 M: 87	2nd order Butterworth filter → contrast enhancement	Deformable parts model based	GLCM , DWT texture + morphological features	--	BPNN (94.1%)
Wu et al. (2008) [286]	B: 120 M: 90	AD filter → stick method→ thresholding method	Deformable parts model based	Autocovariance + morphological features	--	SVM (92.8%)
Drukker et al. (2008) [66]	157	Gray scale inversion, Median filter	Classical	Autocorrelation + morphological features	--	BNN (AUC: 0.9)
Cui et al. (2009) [60]	B: 150 M: 100	Gaussian filter	Deformable parts model	SGLD + morphological features	Wrapper method	LR (AUC:0.83)
Cui et al. (2009) [59]	B: 150 M: 100	Gaussian filter	Deformable parts model	SGLD + morphological features	Wrapper method	LDA (AUC: 0.9)
Drukker et al. (2009) [67]	--	Gray scale inversion, Median filter	Classical	Autocorrelation + morphological features	--	BNN (AUC: 0.8)
Drukker et al. (2009) [68]	341	Gray scale inversion, Median filter	Classical	Autocorrelation + morphological features	Dimensional-ity reduction	BNN (AUC: 0.82) QDA (AUC: 0.76) LDA (AUC: 0.88)

Su et al. (2011) [259]	B: 67 M: 65	SRAD	Hybrid	FOS + morphological features	--	AP clustering (93.1%)
Wu et al. (2012) [284]	B: 120 M: 90	AD filter → stick method→ thresholding method	Deformable parts model based	Autocovariance + morphological features	Wrapper method	SVM (95.2%)
Karimi et al. (2013) [132]	B: 76 M: 71	Fuzzy logic → compounding	Classical	Statistical + morphological features	Wrapper method	Ensemble of FSVM, NN, AdaBoost (98.7%)
Karimi et al. (2014) [133]	240	Fuzzy logic → compounding	Classifier based	Wavelet based + morphological features	Wrapper method	SVM (98.7%)
Flores et al. (2015) [74]	B: 413 M: 228	CLAHE → AD → Gaussian function → Thresholding	Classical	Texture + shape and margin features	Wrapper method	LFDA (AUC: 0.9)
Menon et al. (2015) [186]	--	Median filter → High boost filter → Sobel filter	Deformable parts model	FOS, GLCM + morphological features	Dimensional -ity reduction	SVM (95.7%)
Moon et al. (2013) [193]	B: 166 M: 78	Sigmoid filter → Gradient function	Deformable parts model	GLCM + shape and margin features	Wrapper method	DT (87.0%)
Moon et al. (2015) [191]	B:84 M: 85	Sequential sigmoid and gradient magnitude filter	Deformable parts model	GLCM, Ranklet GLCM + morphological features	Wrapper method	SVM (93.4%)
Prabusankarlal et al. (2015) [218]	B: 70 M: 50	NLM filter	Clustering based	Statistical, MRF, Tamura + morphological features	--	SVM (95.8%)
Singh et al. (2015) [251]	B: 44 M: 45	Wavelet filtering	Manually extracted ROI	Statistical, Laws' texture + morphological features	Wrapper method	NN (84.6%)
Wu et al. (2015) [286]	B: 120 M: 90	AD filter→ stick method→ thresholding method	Deformable parts model based	Autocovariance + morphological features	Wrapper method	SVM (96.6%)
Singh et al. (2016) [253]	B: 88 M: 90	Wavelet filter	Manually extracted ROI	Statistical, Laws' texture + morphological features	Hybrid method	FCNN (94.1 %)
Cristerna et al. (2017) [58]	B: 766 M: 255	FEN → ISF	Classical method	Statistical, Laws', BIRADS + morphological features	--	FLDA (84.0 %)

Prabusankarlal et al. (2017) [220]	B: 80 M: 60	NLM	Hybrid method	GLCM, GLRLM + morphological features	Wrapper method	SaDE-ELM (97.1%)
Raha et al. (2017) [224]	--	Median → high boost → sobel → averaging filters	Classical	GLCM and GLDS + shape and margin features	--	kNN (96.4%)
Singh et al. (2017) [254]	B: 88 M: 90	Wavelet based filter	Manually extracted ROI	Statistical, Laws' texture + shape and moment invariant features	Hybrid method	BPANN (90.0%) SVM (94.4%)
Cristerna et al. (2018) [57]	B: 781 M: 347	CLAHE→ AD	Classical method	Statistical, Ranklet GLCM, + morphological features	--	RF (AUC: 0.87)
Moon et al. (2018) [190]	B: 166 M: 78	Sigmoid filter → gradient magnitude filter → sigmoid filter	Deformable parts based model	GLCM + morphological features	Wrapper method	LR (75.1%)
Nemat et al. (2018) [199]	B: 72 M: 32	CLAHE → AD	Classical	Gabor filter based + shape and margin features	Wrapper method	SLR (97.1%)
Uzunhisarcikli et al. (2018) [270]	B: 64 M: 89	Gaussian filter → CLAHE	Lesion contour marked by radiologist	GLCM texture + morphological features	Filter method	ANFIS (99.3%)
Kriti et al. (2019) [142] (Present work)	B: 40 M: 60	FB	Deformable parts based model	FOS, GLCM, GLRLM, Laws', FPS, Gabor + morphological features	Wrapper method	SVM (66.7 %)

Note: ROI: Region of interest, Acc: Accuracy, B: Benign, M: Malignant, LDA: Linear discriminant analysis, RGI: Radial gradient index, BNN: Bayesian neural network, GLCM: Gray level co-occurrence matrix, DWT: Discrete wavelet transform, BPNN: Back-propagation neural network, AD: Anisotropic diffusion, SVM: Support vector machine, AUC: Area under the curve, SGLD: Spatial gray level dependence, LR: Logistic regression, QDA: Quadratic discriminant analysis, SRAD: Speckle reducing anisotropic diffusion, FOS: First order statistics, AP: Affinity propagation, FSVM: Fuzzy support vector machine, NN: Neural network, FCNN: Fuzzy cluster based neural network, CLAHE: Contrast limited adaptive histogram equalization, LFDA: Local Fischer discriminant analysis, DT: Decision tree, NLM: Non-local mean, RF: Random forest, FEN: Fuzzy enhancement, ISF: Interference based speckle filtering, FLDA: Fischer linear discriminant analysis, GLRLM: Gray level run length matrix, SaDE-ELM: Self adaptive differential evolution-Extreme learning machine, GLDS: Gray level difference statistics, kNN: k-nearest neighbours, BPANN: Back-propagation artificial neural network, SLR: Stepwise logistic regression, ANFIS: Adaptive neuro-fuzzy inference system, FB: Fourier Butterworth.

From Table 2.5, it is noted that all the studies have reported the binary classification of breast tumors into benign and malignant classes. It can also be noted that most of the studies have been carried out on ROIs generated by using computer-assisted methods while very few studies have been carried out on manually extracted ROIs [254, 270]. Based on the studies presented in Table 2.5, following points can be noted:

(*i*) Almost all the segmentation methods ranging from classical, clustering based, classifier based, graph based, deformable parts model based to multi-resolution based have been reported for segmenting the breast tumors from pre-processed images.

(*ii*) Most of the studies make use of different filtering methods for pre-processing the breast ultrasound images, while very few studies have used both filtering and enhancement methods for the pre-processing of breast ultrasound images [67, 57, 58, 74, 199, 284, 286].

(*iii*) It can be noted that most of the studies have been carried out by using statistical methods of texture feature extraction, while only few studies have been reported to use Laws' mask based features and transform domain based methods of feature extraction [57, 58, 133, 195, 203, 229, 255, 286].

(*iv*) Wrapper based methods of feature selection have popularly been used for the selection of optimal features and very few studies have been carried out utilizing filter based methods of feature selection and feature space dimensionality reduction [68, 190, 274].

Menon et al. [190] used a combination of median, high boost and sobel filters to pre-process 78 breast ultrasound images. From the pre-processed images, the tumor regions have been segmented using deformable parts model. From the segmented images a feature set containing texture and morphological features has been computed. The texture features have been computed using FOS, GLCM and covariance based methods. The study reported an accuracy of 95.7 % using SVM classifier and an optimal number of principal components obtained by applying principal component analysis (PCA) to the computed feature set.

Prabusankarlal et al. [222] reported an accuracy of 95.8 % using SVM classifier and a feature set containing different texture and morphological features. The texture features have been computed by using different methods like Histogram, Markov random filed based (MRF), Tamura, GLCM and GLRLM. The performance has been tested on a set of 120 images pre-processed using non-local means filter (NLM) and segmented by clustering based methods. In another study [224] the authors reported an accuracy of 97.1 % achieved using an extreme learning machine based classifier, self adaptive differential evolution-Extreme learning machine (SaDE-ELM). The study has been carried out on a set of 140 images pre-processed using NLM filter and a wavelet transform based segmentation method. From the segmented

tumor images, feature set containing GLCM, GLRLM based texture and morphological features have been computed. The features have been reduced using a rough set method.

Raha et al. [228] reported an accuracy of 96.4 % using kNN classifier and a feature set containing GLCM, gray level difference statistics (GLDS) based texture features and morphological features. The study has been carried out using images pre-processed by median, high boost, sobel and averaging filters and segmented by watershed transform.

Singh et al. [258] used 178 images for classification of breast tumors. The images have been filtered by wavelet based filter and ROIs have been extracted manually. From the extracted ROIs different texture and morphological features have been computed. The texture features have been computed using statistical methods and Laws' mask analysis while the morphological features consist of conventional shape based features and moment invariant features. The study compared the performance of SVM and back propagation artificial neural network (BPANN) classifier using an optimal feature set obtained by using a hybrid feature selection technique.

Uzunhisarcikli et al. [270] reported an accuracy of 99.3 % for classifying 153 breast ultrasound images using a type-2 adaptive neuro-fuzzy inference system (ANFIS) and an optimal feature set containing GLCM based texture features and morphological features. The features have been computed from the ROIs extracted on the basis of lesion contour marked by the radiologist and pre-processed using Gaussian filter and contrast limited adaptive histogram equalization (CLAHE).

Nemat et al. [199] reported an accuracy of 97.1 % using stepwise logistic regression (SLR) classifier. The study has been carried out on 104 breast ultrasound images pre-processed using CLAHE followed by anisotropic diffusion (AD) filter and segmented using watershed transform. From the segmented tumor images a feature set containing texture and morphological features has been computed wherein the texture features have been computed using Gabor based filters.

Wu et al. [286] reported an accuracy of 96.6 % using SVM classifier and optimal feature set obtained using artificial intelligence system. The study has been carried out on 210 breast ultrasound images pre-processed using AD filter followed by stick enhancement. From the segmented tumor images autocovariance texture and morphological features have been computed for classification task.

Karimi et al. [132] used fuzzy enhancement and compounding for pre-processing a total of 147 breast ultrasound images. The images have been segmented using region growing

method. From the segmented tumor images different statistical texture features and morphological features have been computed. The study reported an accuracy of 98.7 % using an ensemble based classifier and optimal feature set computed using wrapper based methods. In another study Karimi et al. [133] proposed a CAD system design using SVM classifier. The study has been carried out on 240 images pre-processed using fuzzy enhancement and compounding technique. The images have been segmented using neural network (NN) classifier. From the segmented images wavelet based texture features and morphological features have been computed and an optimal feature set has been obtained by using a wrapper method. The study reported an accuracy of 98.7 %.

From the machine learning based studies presented in Table 2.4 and 2.5, it has been observed that for classification of breast tumors, either original images have been used or pre-processed images have been used. No study has yet reported the use of both original and pre-processed images for classification of breast tumors. Also most of the studies have employed statistical methods of texture feature extraction like FOS, GLCM and GLRLM. It is also worth mentioning that no study has yet been reported to analyse the effect of despeckle filtering algorithms on the classification performance. Therefore in the present work, to analyse the effect of despeckle filtering algorithms on the classification of breast tumors, both original as well as images despeckled by different despeckle filtering algorithms have been used to design different CAD system designs in order to obtain an optimal CAD system for classification of breast tumors.

2.5. Review of Literature on Classification of Breast Tumors using Deep Learning Approaches

The studies conducted for classification of breast tumors using deep learning based approaches has been conducted by using either generative architectures or discriminative architectures by using convolutional neural networks (CNNs). The various deep learning studies conducted by researchers in the past can broadly be categorized as (*a*) Studies carried out for classification of breast tumors using original ultrasound images, (*b*) Studies carried out for classification of breast tumors using pre-processed ultrasound images. A brief summary of the related studies for classification of breast tumors using deep learning approaches is give here.

2.5.1. Deep learning based studies carried out for classification of breast tumors using original ultrasound images

A brief description of deep learning based studies carried out for classification of breast tumors using original ultrasound images is shown in Table 2.6.

Table 2.6 A brief description of deep learning based studies carried out for classification of breast tumors using original ultrasound images.

Investigator	Images	ROI extraction/ segmentation	Feature extractor	Feature selection /reduction	Classifier (Acc.)
Cheng et al. (2016) [48]	B: 275 M: 245	Full image	--	--	SDAE (82.4%)
Antropova et al. (2017) [14]	C: 1098 SBL: 880 M: 415	Manually extracted ROI	VGG-19	--	SVM (AUC: 0.85)
Han et al. (2017) [92]	B: 4254 M: 3154	Full image	--	--	GoogLeNet (91.0 %)
Byra (2018) [29]	B: 48 M: 52	Full image	VGG-19	--	FLDA (AUC: 0.84)
Xiao et al. (2018) [294]	B: 1370 M: 688	Full image	-- ResNet50 + Xception + InceptionV3	-- --	Self-designed (74.4%) InceptionV3 (85.1%) NN (89.4%)
Xie et al. (2018) [295]	N: 1418 Ca: 1182	Improved Mask R-CNN	--	--	ResNet (--)
Al-Dhabyani et al. (2019) [5]	N: 133 B: 320 M: 490	Full images	--	--	NASNet (99.0 %)
Cao et al. (2019) [34]	B: 577 M: 464	Full image Manually extracted ROI	--	--	DenseNet (85.0 %) DenseNet (87.5 %)
Fujioka et al. (2019) [75]	B: 48 M: 72	Full image	--	--	GoogLeNet (92.0 %)
Han et al. (2019) [93]	B: 4254 M: 3154	Manually extracted ROI	--	--	GoogLeNet (90.4%)
Huang et al. (2019) [109]	B-III: 531 B-IV*a*: 443 B-IV*b*: 376 B-IV*c*: 565 B-V: 323	Multiscale architecture based on FCN-16s	--	--	Self-designed (--)
Kameswari et al. (2019) [131]	B: 250 M: 150	Full image	--	--	Self-designed (98.0 %)
Qi et al. (2019) [221]	N: 5386 M: 2759	Full image	--	--	Mt-Net (94.4%) Sn-Net (90.1%)
Zeimarani et al. (2019) [311]	B: 413 M: 228	Full image	--	--	Self-designed (92.0%)

Note: ROI: Region of interest, Acc.: Accuracy, B: Benign, M: Malignant, SDAE: Stacked denoising autoencoder, C: Cyst, SBL: Solid benign lesion, SVM: Support vector machine, FLDA: Fischer linear discriminant analysis, AUC: Area under the curve, NN: Neural network, N: Normal, Ca: Carcinoma, R-CNN: Region based CNN, B-III: BIRADS category 3, B-IV: BIRADS category 4, B-V: BIRADS category 5, FCN: Fully convolutional network.

From Table 2.6, it has been observed that most of the studies carried out for classification of breast tumors using deep learning approaches have reported the binary classification of tumors into benign and malignant classes. Based on the studies presented in Table 2.6, following points can be noted:

(*i*) The performance of pre-trained networks like GoogLeNet, Inception V3, ResNet, DenseNet and NASNet has been tested. It is worth observing that the GoogLeNet architecture yielded maximum accuracy of 92.0 % and 90.4 %, with full images and manually extracted ROIs respectively [75, 93].

(*ii*) It can also be noted from the table that discriminative deep learning architectures like pre-trained CNNs, self-designed CNNs have widely been used while only one study has been reported to use generative architectures [48].

(*iii*) It can also be seen that for classification purposes, most of the studies have used full images as input to the deep learning architectures, while studies by [109, 295] have reported the use of deep learning based segmentation methods to generate the tumor images. However it is worth noting that the studies utilizing the segmented tumor images gave been carried out for classification of images into classes other than benign and malignant.

The study conducted by Cheng et al. [48] used a total of 520 images for breast tumor classification. The study has been carried out on full images by using a generative architecture stacked denoising autoencoder (SDAE). The study reported an accuracy of 82.4 % with softmax classifier.

By using a self-designed CNN the network architecture proposed by Kameswari et al. [130] yielded the maximum classification accuracy of 98.0 % for classification of benign and malignant breast tumors using 400 full size images.

Xiao et al. [294] experimented three different deep learning architectures viz. pre-trained Inception-V3 network, a self-designed CNN and pre-trained CNNs as feature extractors. The study utilized a combined feature vector using features computed from ResNet50, Xception and InceptionV3 networks for the extraction of features from the ultrasound images. The computed feature vectors were then clubbed together and fed to NN classifier for classification purposes achieving an accuracy of 89.4 % using a dataset containing 2,058 images.

Byra et al. [29] used a set of 100 images for classification of breast tumors using deep features extracted from VGG-19 architecture and classified using Fischer linear discriminant analysis (FLDA) classifier achieving an area under the curve (AUC) value of 0.84.

Fujioka et al. [75] used a set of 120 images for classification of breast tumors using a pre-trained GoogLeNet achieving an accuracy of 92.0 %.

Han et al. reported two studies for classification of breast tumors using pre-trained GoogLeNet architecture on a comprehensive dataset of 7,408 images. In [92], the authors used manually extracted ROIs and reported an accuracy of 91.0 % while in [93], the authors used full images and reported an accuracy of 90.4 %.

In another study Cao et al. [34] experimented the use of different CNN networks like AlexNet, ZFNet, VGG-16, GoogLeNet, ResNet and DenseNet for classification of 1,041 images. The study has also experimented the use of full images as well as manually extracted ROIs for classification of breast tumors. In both cases DenseNet architecture has outperformed other network architectures achieving an accuracy of 85.0 % and 87.5 %, respectively.

2.5.2. Deep learning based studies for classification of breast tumors using pre-processed ultrasound images

A brief description of deep learning based studies carried out for classification of breast tumors using pre-processed ultrasound images is shown in Table 2.7.

Table 2.7 A brief description of deep learning based studies carried out for classification of breast tumors using pre-processed ultrasound images.

Investigator	Images	Pre-processing	ROI extraction/ segmentation	Feature extractor	Feature selection/ reduction	Classifier (Acc.)
Karimi et al. (2013) [132]	B: 76 M: 71	Fuzzy logic → compounding	Region-growing	Self-designed	--	Ensemble of FSVM, NN, AdaBoost (95.0%)
Lee et al. (2018) [153]	B: 100 M: 150	CLAHE	Full image			SDAE (83.0%)
Byra et al. (2019) [30]	B: 678 M: 204	Median filter	Manually extracted ROI	VGG-19	--	SVM (86.0 %)
Ciritsis et al. (2019) [56]	B: 24 M: 19	Median filter	Manually extracted ROI			Self-designed (93.0 %)
Zhang et al. (2019) [312]	B: 107 M: 53 B: 205 M: 90	DTGF	Full image Watershed transform	--	--	SCAE (92.0 %) SCAE (83.9 %)
Kriti et al. (2020) [144] (Present work)	B: 40 M:60	DPAD	Chan-Vese ACM	GoogLeNet	ANFC-LH, CrFS	ANFC (98.0 %)

Note: ROI: Region of interest, Acc.: Accuracy, B: Benign, M: Malignant, FSVM: Fuzzy support vector machine, NN: Neural network, CLAHE: Contrast limited adaptive histogram equalization, SDAE: Stacked denoising autoencoder, SVM: Support vector machine, DTGF: Distance-transformation coupled Gaussian filter, SCAE: Stacked convolutional autoencoder, DPAD: Detail preserving anisotropic diffusion, ACM: Active contour model, ANFC-LH: Adaptive neuro-fuzzy classifier using linguistic hedges, CrFS: Correlation based feature selection.

From Table 2.7, it can be noted that very few deep learning based studies have been carried out for classification breast tumors using pre-processed images. Based on the studies presented in Table 2.7, following points can be noted:

(*i*) Very few studies have been carried out for classification of pre-processed breast ultrasound images using deep learning approaches.
(*ii*) Most of the studies in the literature have made use of both generative and discriminative architectures. In case of discriminative architectures, all the network topologies have been experimented instead of the pre-trained CNNs for classification of breast tumors.

For classification of pre-processed breast ultrasound images using autoencoder and its variants, SDAE and stacked convolutional autoencoder (SCAE) architectures have been used. Lee et al. [153] used SDAE followed by softmax classifier for classification of breast tumors from full size ultrasound images processed by contrast limited adaptive histogram equalization (CLAHE). The study has been carried out on 250 breast ultrasound images and reported an accuracy of 83.0 %.

Zhang et al. [312] used SCAE followed by softmax classifier for classification of breast tumors from ultrasound images pre-processed using distance-transformation coupled Gaussian filter (DTGF). The study has been carried out on 160 full images as well as 295 segmented tumor images obtained by watershed transform achieving an accuracy of 92.0 % and 83.9 %, respectively.

For classification of pre-processed breast ultrasound images using self-designed CNNs, the architecture proposed by Ciritsis et al. [56] achieved an accuracy of 93.0 % using manually extracted ROIs from 43 ultrasound images pre-processed by median filter.

Karimi et al. [132] reported an accuracy of 95.0 % using 147 breast ultrasound images pre-processed using fuzzy logic and compounding and segmented by region growing. A self-designed CNN has been used to extract deep features from the tumor images and an ensemble of FSVM, NN and AdaBoost has been used as classifier.

Byra et al. [30] used 882 breast ultrasound images pre-processed by median filter for classification of breast ultrasound images using VGG-19 as deep feature extractor and SVM as classifier. The study reported an accuracy of 86.0 %.

From the deep learning based studies presented in Table 2.6 and 2.7, it has been observed that for classification of breast tumors, either original images have been used or pre-processed images have been used. No study has yet reported the use of both original and pre-processed images for classification of breast tumors. Also most of the studies have reported to use full images or manually extracted ROIs to be fed as input to the deep network. Very few studies have been conducted that make use of segmented tumor images for classification purposes. Therefore, in the present work an attempt has been made to generate tumor images using both original and despeckled images such that efficient texture and morphological information is

captured by the deep network design [144]. Also the performance of different CNN based CAD system designs has been tested by using these segmented images in order to find an optimal CAD system design based on deep learning approaches.

2.6. Concluding Remarks

The conclusions drawn from the literature review of the related studies are described here.

(*i*) Based on the summary of the different studies it has been noted that a comparative analysis of different despeckle filtering algorithms on the basis of image quality metrics as well as radiologist's opinion to find an optimal filter still needs to be explored further for breast ultrasound images. Therefore, *evaluation of despeckle filtering algorithms for pre-processing of breast ultrasound images* has been taken up as one of the objectives of the present research work.

(*ii*) From the brief summary of literature review available on the problem of segmentation of breast tumors, it can be observed that various successful attempts have been made by the researchers for the segmentation of breast tumors using different techniques like thresholding, region growing methods, watershed transform based methods, active contour methods, clustering methods, hybrid methods and deep learning based methods. The performance evaluation of these methods has been carried out on the basis of different area and boundary based metrics. However it is also worth noting that very few studies have been carried out in the past that analyse the effect of the application of despeckle filtering algorithms on the segmentation of breast tumors therefore, in the present research work, *evaluation of effect of despeckle filtering algorithms on segmentation of breast tumor*s has been taken up as an objective.

(*iii*) From the brief summary of literature review available on the problem of classification of breast tumors using machine learning based approaches, it can be noted that most of the studies have been carried out either on original ultrasound images or pre-processed ultrasound images. No study has been presented in the literature that uses both original and pre-processed images for classification of breast ultrasound images. The potential of both original and despeckled images used for extraction of features needs to be tested for accurate classification of breast ultrasound images. Therefore to *evaluate the effect of despeckle filtering algorithms on the classification of breast tumors* has been taken up as the next objective of the present research work. Also it can be noted that for most of the studies statistical methods of texture feature extraction have been used. However, it is also worth noting that for classification of other soft tissue organs, many studies have made use of local binary pattern (LBP) based texture features

[53, 94, 134, 146, 152, 196, 210, 265, 266] however, the potential of these features combined with morphological features has still not been tested therefore the design of *LBP based CAD systems for classification of breast tumors* has been taken up as the next objective of the present research work.

(*iv*) From the brief summary of literature review available on the problem of classification of breast tumors using deep learning approaches, it can be noted that most of the studies have been carried out either on original ultrasound images or pre-processed ultrasound images. No study has yet been presented in the literature that uses both original and pre-processed images for classification of breast ultrasound images. The potential of both original and despeckled images processed by different deep learning algorithms needs to be tested for accurate classification of breast tumors. Therefore design of efficient *convolutional neural network based CAD systems for classification of breast tumors* has been taken up as the next objective of the present research work.

Chapter 3

Effect of Despeckle Filtering Algorithms on Breast Ultrasound Images

3.1. Introduction

The visual quality of ultrasound image is an important factor to effectively diagnose any abnormality present in the internal body tissues. For an ultrasound image, the visual quality is often hampered by low contrast and sometimes the presence of speckle noise, on this low contrast image presents a daunting challenge for radiologists in their interpretation [27, 193]. Therefore, controlled despeckling of breast ultrasound images (such that important diagnostic information like edges/features/structure is preserved) is important for image interpretation as well as improving the accuracy of computer assisted algorithms for segmentation and classification of these images [58, 69, 70, 138, 149, 173, 205, 214, 216, 249]. Different despeckle filtering algorithms have been widely used for controlled despeckling of breast tissue [19, 58, 69, 70, 135, 148, 149, 202, 205, 208, 214-216, 249, 252, 255, 313].

Prabhakar et al. [214] used 03 transform domain methods of filtering namely curvelet transform, shearlet transform and tetrolet transform taken from multiscale filter category. The objective assessment has been carried out on the basis of two image quality metrics namely signal-to-noise ratio (SNR) and peak signal-to-noise ratio (PSNR).

Nugroho et al. [202] attempted to compare the performance of 07 despeckle filtering algorithms taken from 02 filter categories. Image quality after despeckling was determined on the basis of metrics like SNR, mean square error, speckle index, average difference, contrast to speckle ratio.

Singh et al. [255] compared the performance of 14 despeckle filtering algorithms taken from 03 filter categories namely Fourier filters, multiscale filters and non-linear iterative filters. The performance evaluation of these filters has been carried out on the basis of different image quality metrics like ERI to quantify the edge-retrieval capabilities (objective analysis) as well as subjective analysis by experts. In another study, Singh et al. [252] compared the performance of 23 despeckle filtering algorithms taken from 04 different filter categories namely local statistics based filters, Fourier filters, multiscale filters and non-linear iterative filters. The performance evaluation of these filters has been carried out on the basis of different image quality metrics like ERI to quantify the edge retrieval capabilities (objective analysis) as well as subjective analysis by experts.

Zhang et al. [313] compared the performance of 11 filters taken from 05 categories of despeckle filtering algorithms namely local statistics based filters, multiscale filters, non-local mean filters, non-linear iterative filters and hybrid filters. The study has been carried out on 400 breast ultrasound images and the performance assessment has been carried out on the basis of objective as well as subjective evaluation. For the objective assessment, an image quality metric named natural image quality estimator (NIQE) has been used and for the subjective analysis, the grading by 03 experts has been used.

Based on the observations made by conducting an exhaustive review of literature for despeckling of breast ultrasound images, in the present research work, an exhaustive set of 42 despeckle filtering algorithms taken from the entire 08 filter categories have been chosen for analysis. The performance of these algorithms has been compared on the basis of objective assessment by calculating an image quality metric, structure and edge preservation index (SEPI) to evaluate their structure and edge preservation capability. The best performing filters selected on the basis of SEPI have further been used for subjective analysis by the experienced radiologist to yield an optimal filter for controlled despeckling of breast ultrasound images [141].

3.2. Experimental Workflow : Effect of Despeckle Filtering Algorithms on Breast Ultrasound Images

The experimental workflow followed for analysing the effect of despeckle filtering algorithms on breast ultrasound images is given in Fig. 3.1.

3.2.1. Dataset description

For the researchers working specifically in the area of analysis and classification of breast ultrasound images, collection of a comprehensive dataset representative of all the image subclasses is pre-requisite. Furthermore, only one standard benchmark database containing exhaustive collection of various breast ultrasound images with the representative cases of different types of benign and malignant tumors is available for researchers since the year 2004 namely ultrasoundcases.info [103]. As a result, most of the studies conducted for the analysis and classification of breast ultrasound images have been carried out by using (*a*) image dataset acquired by individual research groups in collaboration with the regional hospitals, (*b*) standard benchmark database ultrasoundcases.info and (*c*) standard benchmark image database ultrasoundcases.info along with image dataset acquired from hospitals. For carrying out the present work, the ultrasound images have been taken from a standard benchmark database of

ultrasound images named ultarsoundcases.info [103]. The website has been developed by Dr. Taco Geertsma in the year 2004.

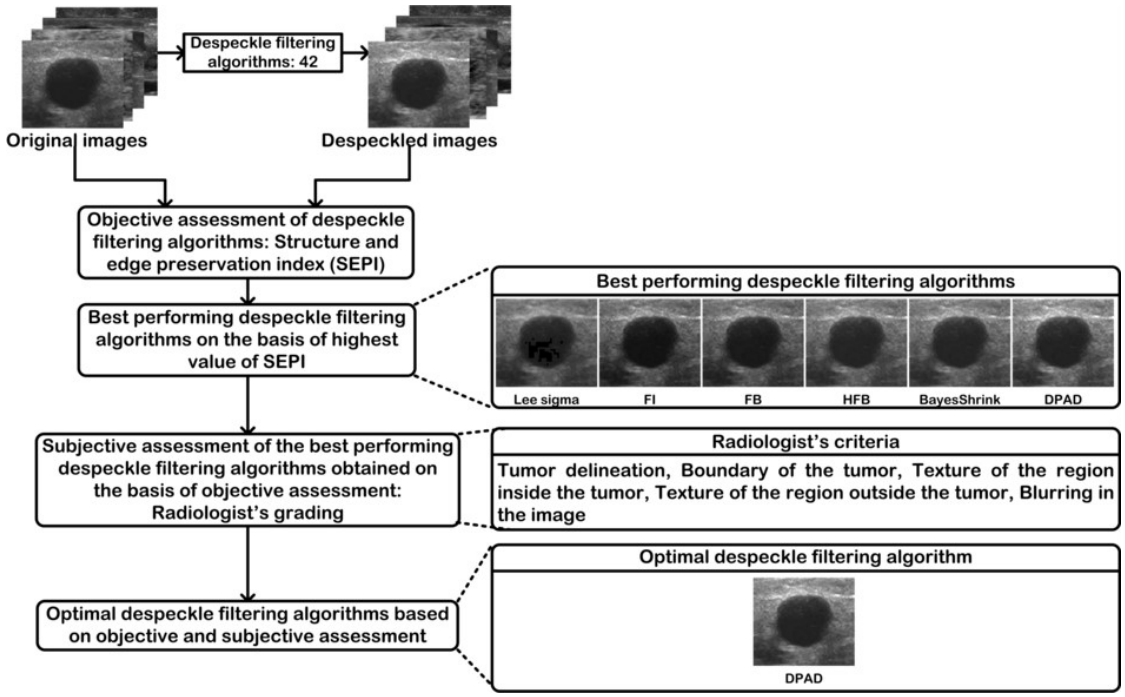

Fig. 3.1 Experimental workflow followed for analysing the effect of despeckle filtering algorithms on breast ultrasound images.
Note: FI: Fourier ideal, FB: Fourier Butterworth, HFB: Homomorphic Fourier Butterworth, DPAD: Detail preserving anisotropic diffusion.

The cases in the dataset have been presented as images having different projections and annotations indicating specific features. These cases have been collected over the years by different radiologists at Gelderse Vallei Hospital, Ede, Netherlands using high-end Hitachi ultrasound equipment [103], where each image consists of 256 gray scale tones and a horizontal and vertical resolution of 96 dpi. Out of the many images present in the dataset, a total of 100 breast ultrasound images consisting of 40 benign and 60 malignant images have been considered for analysis in consultation with the participating radiologist keeping in view the following protocols:

(*i*) Only B-mode ultrasound images have been considered (*i.e.* Color Doppler images and Elastography images have not been included).

(*ii*) From the images with multiple views of the same tumor, only one representative image has been selected.

(*iii*) The size of the tumor region should be at least 800 pixels to provide a good sampling distribution for computing reliable statistics.

(*iv*) The images should be of diagnostic quality and should not contain any artefacts.

(*v*) The images having annotations to point out certain features have not been included.

(*vi*) Due care has been taken to include all the representative cases of various subclasses of benign tumors like simple cysts, cysts with internal echoes, cysts with mass like lesions, fibroadenomas, lipomas etc, as well as subclasses of malignant tumors like invasive ductal carcinoma, invasive lobular carcinoma etc.

The dataset used in the present research work is described in Fig. 3.2.

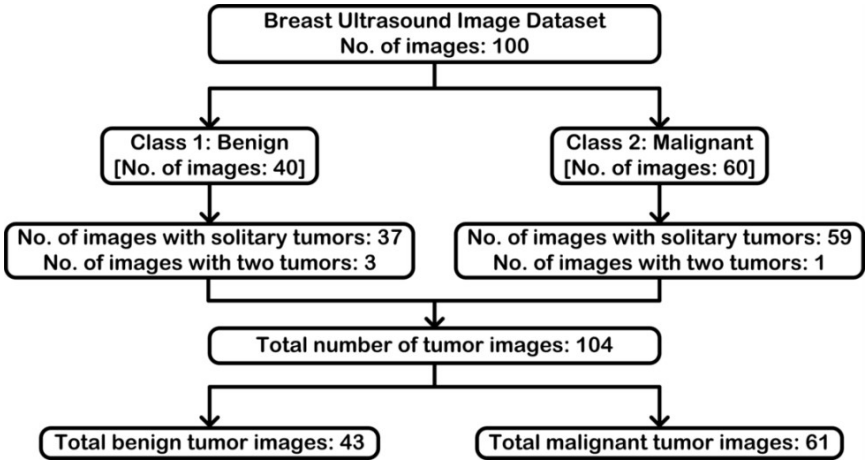

Fig. 3.2 Dataset description.

The entire image dataset was stored on a 64-bit windows 10 PC with Intel (R) Core (TM) i3-5005U, 2.00 GHz processor and 4.00 GB RAM and the experiments have been conducted using MATLABR2015b.

3.2.2. Despeckle filtering algorithms

Speckle noise is a multiplicative noise formed due to the superposition of echoes having random phase and amplitudes. Depending upon the type of interference of the echoes, whether constructive or destructive, speckle noise ranges from zero to maximum. Mathematically, speckle noise can be modelled as:

$$y(i,j) = x(i,j).n(i,j) \tag{3.1}$$

Here, $x(i,j)$ is the noise free image, $n(i,j)$ is the multiplicative noise, $y(i,j)$ is the noisy image.

Some despeckling filters work on the multiplicative noise but for some filters the multiplicative noise needs to be converted to additive noise. This transformation is done using log operation.

$$\log[y(i,j)] = \log[x(i,j).n(i,j)] = \log[x(i,j)] + \log[n(i,j)] \tag{3.2}$$

For the reduction of speckle noise, different techniques have been proposed [23, 24, 171, 173, 184]. A broad characterization of different despeckle filtering algorithms is given in Fig. 3.3.

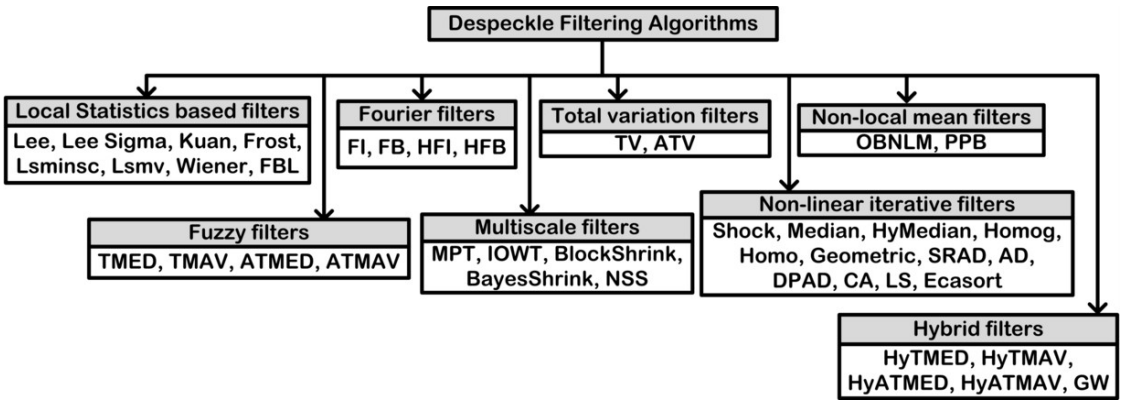

Fig. 3.3 Despeckle filtering algorithms used in the present work.
Note: Lsminsc: local statistics minimum speckle index, Lsmv: Local statistics mean variance, FBL: Fast bilateral, TMED: Triangulation median, TMAV: Triangulation moving average, ATMED: Asymmetrical triangulation median, ATMAV: Asymmetrical triangulation moving average, FI: Fourier ideal, FB: Fourier Butterworth, HFI: Homomorphic Fourier ideal, HFB: Homomorphic Fourier Butterworth, MPT: Multiscale product thresholding, IOWT: Inter orthonormal wavelet thresholding, NSS: NeighShrinkSure, TV: Total variation, ATV: Adaptive total variation, HyMedian: Hybrid median, Homog: Maximum homogeneity, Homo: Homomorphic, SRAD: Speckle reducing anisotropic diffusion, AD: Anisotropic diffusion, DPAD: Detail preserving anisotropic diffusion, CA: Linear scaling of gray-level values, LS: Linear scaling, Ecasort: Linear scaling and sorting, OBNLM: Optimized Bayesian non-local means, PPB: Probabilistic patch based, HyTMED: Hybrid triangulation median, HyTMAV: Hybrid triangulation moving average, HyATMED: Hybrid asymmetrical triangulation median, HyATMAV: Hybrid asymmetrical triangulation moving average, GW: Geometric wiener.

The parameters used in the implementation of each filter are shown in Table 3.1.

Table 3.1 Parameters used for implementation of despeckle filtering algorithms.

Despeckling Filter		**Parameters**
Local statistics based filter	Lee [23, 24, 72, 314]	Neighbourhood size = 5, No. of iterations = 2
	Lee Sigma [154]	Neighbourhood size = 5
	Kuan [23, 24, 72]	No. of iterations = 2
	Frost [23, 24, 72, 314]	Neighbourhood size = 5
	Lsminsc [23, 24, 172, 173]	Neighbourhood size = 5, No. of iterations = 2, Edge = 0
	Lsmv [23, 24, 172, 173]	Neighbourhood size = 5, No. of iterations = 2
	Wiener [23, 24, 171, 172]	Neighbourhood = 5, noise = []
	FBL [23, 24]	Width of spatial Gaussian (sigmaS) = 10, Width of range Gaussian (sigmaR) = 20
Fuzzy filters	TMED [23, 24, 148]	Window size = 3 × 3
	TMAV [23, 24, 148]	Window size = 3 × 3
	ATMED [23, 24, 148]	Window size = 3 × 3
	ATMAV [23, 24, 148]	Window size = 3 × 3
Fourier filters	FI/HFI [23, 24, 184]	Cut off frequency = 500
	FB/HFB [23, 24, 184]	Cut off frequency = 500, Order = 2
Multiscale filters	MPT [23, 24]	Noise variance (v) = 28, Scale number = 2, c = 12
	IOWT [175]	Wavelet type = sym8
	BlockShrink [320]	Low frequency cut off for Shrinkage J_{min} = 5, wavelet filter sym8
	BayesShrink [23, 42]	Wavelet type = haar, levels = 2
	NSS [23, 24]	Decomposition level L = 3, wavelet type = sym8
Total variation	TV [23, 24]	theta = 15, No. of iterations = 5, time step = 0.25

filters	ATV [23]	Regularization parameter *mu* = 20, time step = 0.2, lambda = 1
Non-linear iterative filters	Shock [283]	Mask size = 9, No. of iterations = 30, time step = 0.25
	Median [23, 172]	Neighbourhood size = 5, No. of iterations = 2
	HyMedian [23, 172]	Neighbourhood size = 5, No. of iterations = 3
	Homog [23, 172]	Neighbourhood size = 5, No. of iterations= 3
	Homo [23, 172]	Neighbourhood size =5
	Geometric [23, 72, 172]	Neighbourhood size = 3, No. of iterations = 2
	SRAD [23, 72, 172, 173]	Time step = 0.02, No. of steps = 30
	AD [23, 72, 172, 173]	No. of iterations = 20, diffusion constant *kappa* = 30, rate of diffusion *lambda* = 0.25, option = 1
	DPAD [3, 23, 72, 314]	Step size = 0.02, No. of iterations = 30, Cu noise estimation with *n* = 5
	CA [172, 173]	Neighbourhood size = 5, No. of iterations = 2
	LS [172, 173]	Neighbourhood size = 5, No. of iterations = 3
	Ecasort [172, 173]	Neighbourhood size = 5, No. of iterations = 3
Non-local mean filters	OBNLM [23, 314]	Search area parameter *M* = 11, Block size parameter *alpha* = 7, smoothing parameter *h* =0.4, offset = 100
	PPB [23, 314]	Half size of search window width *hW* = 12, Half size of window width *hD* = 4, alpha = 0.8, T = 2, No. of iterations = 4
Hybrid filters	HyTMED [23, 24, 148] HyTMAV [23, 24, 148] HyATMED [23, 24, 148] HyATMAV [23, 24, 148] GW [23]	Window size for fuzzy and Wiener filters = 3 × 3 Window size for geometric filter = 3 × 3 and No. of iterations = 2

In the present work, controlled despeckling (i.e. despeckling of the homogeneous areas of the image is required while despeckling in the edge pixels is undesired so as to enhance the diagnostic information present in the image). To achieve this objective the speckle noise which is inherently present in the image was controlled in such a manner so as to maximize the structure and edge preservation index. The main idea to maximize structure and edge preservation index (SEPI) for performance evaluation of breast ultrasound images is to preserve the structure and edge information present in the image while despeckling is carried out. To reduce the possible number of combinations, only the key parameter which is common to most of the despeckling filters i.e. window-size has been optimized for the values ϵ {3, 5, 7, and 9} as the window size affects the degree of noise removal in images, while the other parameters have been kept same as given in the base papers.

3.2.2.1. Local statistics based filters

In these filters, the filtering operation is based on the local statistics. Here, a weighted average is computed using sub-region statistics to calculate the statistical measures over different pixel windows with the window size varying from {3, 5, 7, 9}. The basic form of these filters is given as:

$$\hat{y}_{i,j} = \bar{y}_{i,j} + w_{i,j}(y_{i,j} - \bar{y}_{i,j}) \tag{3.3}$$

Here, $\hat{y}_{i,j}$ is pixel value of denoised image in the moving window, $y_{i,j}$ is pixel value of noisy image, $\bar{y}_{i,j}$ is local mean and $w_{i,j}$ is weighing factor and (i, j) are the pixel co-ordinates.

Despeckling filters used under this category are: Lee filter [23, 24, 72, 314], Lee Sigma filter [23, 155], Kuan filter [23, 24, 72, 314], Frost filter [23, 24, 72, 314], local statistics minimum speckle index (Lsminsc) filter [172, 173], local statistics mean variance (Lsmv) filter [173], Wiener filter [27, 172, 173] and fast bilateral (FBL) filter [23, 81]. The sample ultrasound image with benign tumor and corresponding images despeckled by local statistics based filters are given in Fig. 3.4.

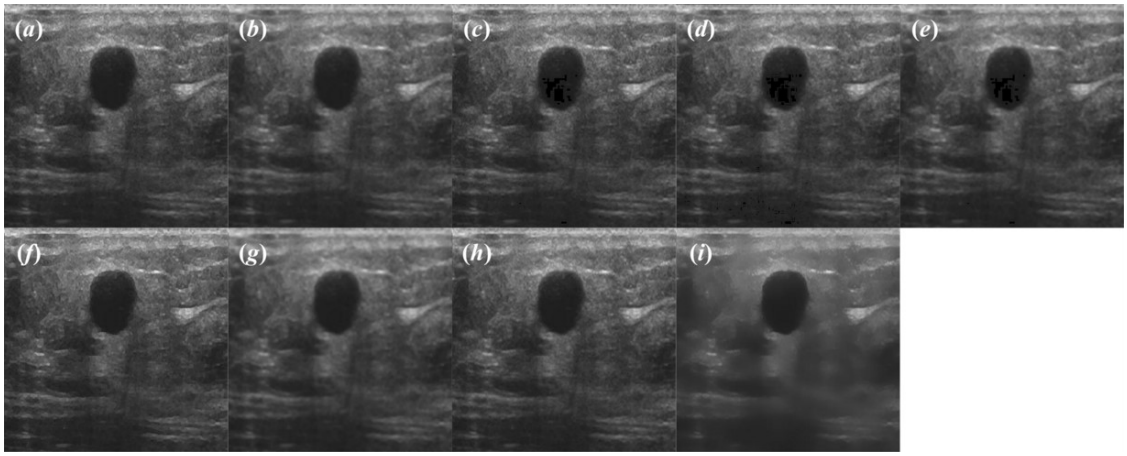

Fig. 3.4 (*a*) Sample ultrasound image of benign tumor and (*b*) - (*i*) corresponding images despeckled by (*b*) Lee filter, (*c*) Lee Sigma filter, (*d*) Kuan filter, (*e*) Frost filter, (*f*) Lsminsc filter, (*g*) Lsmv filter, (*h*) Wiener filter and (*i*) FBL filter.

From Fig. 3.4, it can be noted that the images filtered using Lee Sigma, Kuan filter and Frost filter show a blocky effect inside the tumor region. The images filtered using Lsmv filter are slightly blurred while smoothing is observed in the images after the application of FBL filter.

3.2.2.2. Fuzzy filters

The fuzzy filters are implemented by applying weighted functions of fuzzy membership-type to the image pixels within a moving window. These filters can be used to remove random noise or impulse noise [23, 148]. The general form of fuzzy filters is given as:

$$\hat{y}_{i,j} = \frac{\sum_{(m,n)\in A} Y[y_{i+m,j+n}]y_{i+m,j+n}}{\sum_{(m,n)\in A} Y[y_{i+m,j+n}]} \tag{3.4}$$

Here, $Y[y_{i,j}]$ represents the window function, A is the area, $y_{i,j}$: noisy image, m, n represent the image dimensions.

Different filters used under this category are: triangulation median (TMED) filter [23, 148], triangulation moving average (TMAV) filter [23, 148], asymmetrical triangulation

median (ATMED) filter [23, 148] and asymmetrical triangulation moving average (ATMAV) filter [23, 148]. The sample ultrasound image with benign tumor and corresponding images despeckled by fuzzy filters are given in Fig. 3.5.

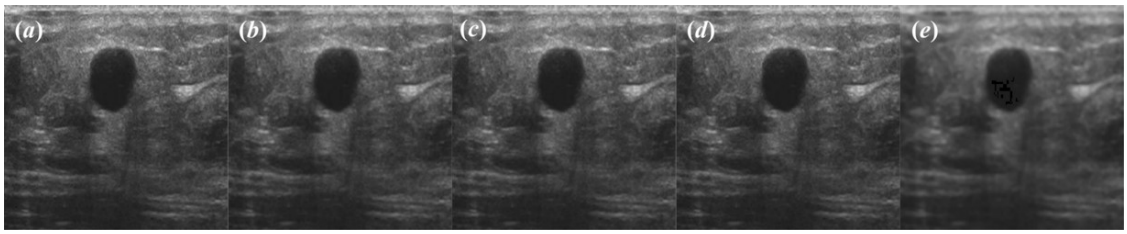

Fig. 3.5 (*a*) Sample original ultrasound image of benign tumor and (*b*)-(*e*) corresponding images despeckled by (*b*) TMED filter, (*c*) TMAV filter, (*d*) ATMED filter and (*e*) ATMAV filter.

From Fig. 3.5, it has been observed that a blocky effect as well as blurring is introduced in the images after the application of ATMAV filter.

3.2.2.3. Fourier filters

These filters are based on the Fourier transform. First, the image is converted to the transform domain using Fourier transform and then the image is filtered using either ideal or Butterworth filters followed by inverse Fourier transform. The same procedure is followed at the time of homomorphic filters except before transforming the image from spatial to transform domain, the image is first projected onto a logarithmic space [180]. The filters that come under this category are: Fourier ideal (FI) filter [23, 184], Fourier Butterworth (FB) filter [180, 23], Homomorphic Fourier ideal (HFI) filter [23, 184] and Homomorphic Fourier Butterworth (HFB) filter [23, 184]. The sample ultrasound image with benign tumor and corresponding images despeckled by Fourier filters are given in Fig. 3.6.

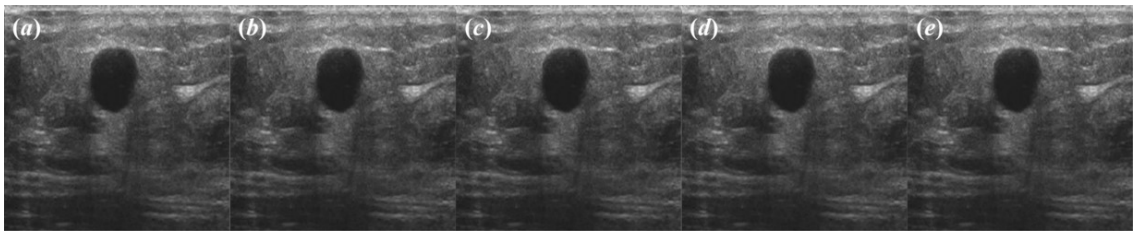

Fig. 3.6 (*a*) Sample original ultrasound image of benign tumor and (*b*)-(*e*) corresponding images despeckled by (*b*) FI filter, (*c*) FB filter, (*d*) HFI filter and (*e*) HFB filter.

3.2.2.4. Multiscale filters

These noise reduction filters are also known as thresholding or wavelet shrinkage filters. These filters are based on the principle of transforming the original image into different scales. The different filters that come under this category are: BayesShrink filter [42], multiscale product thresholding (MPT) filter [23, 24], NeighShrinkSure (NSS) filter [23], BlockShrink

filter [320] and inter orthonormal wavelet thresholding (IOWT) filter [175].The sample ultrasound image with benign tumor and corresponding images despeckled by multiscale filters are given in Fig. 3.7.

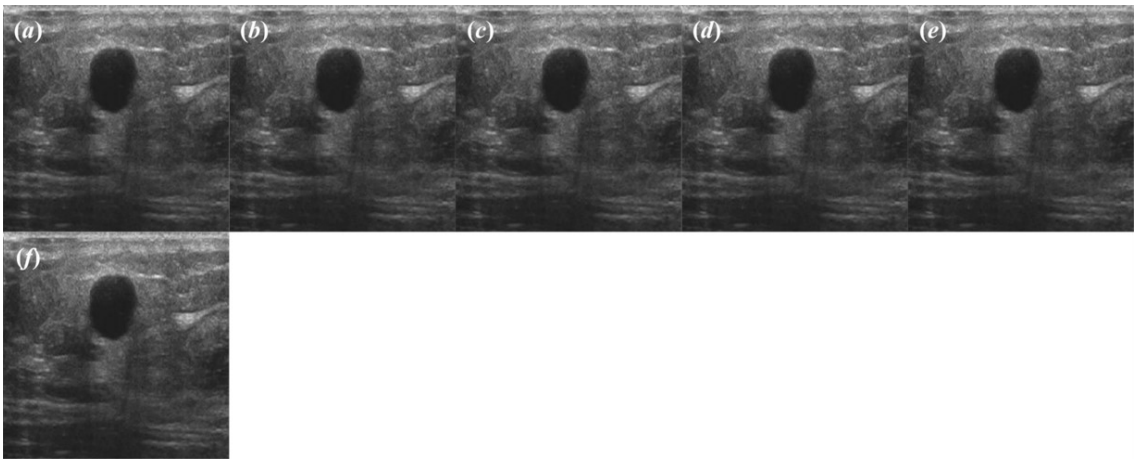

Fig. 3.7 (*a*) Sample original ultrasound image of benign tumor and (*b*),-(*f*) corresponding images despeckled by (*b*) MPT filter, (*c*) IOWT filter, (*d*) BlockShrink filter, (*e*) BayesShrink filter and (*f*) NSS filter.

3.2.2.5. Total variation filters

Total variation denoising reduces the noise in an image while preserving the sharp edges. The basic concept of these filters was coined by Rudin, Osher and Fatemi in 1992 [232]. The denoising by total variation method can be viewed as an optimization problem wherein the filter output can be obtained by minimizing a particular cost function. Different filters used under this category are: Total variation (TV) filter [232] and Anisotropic total variation (ATV) filter [23]. The sample ultrasound image with benign tumor and corresponding images despeckled by total variation filters are given in Fig. 3.8.

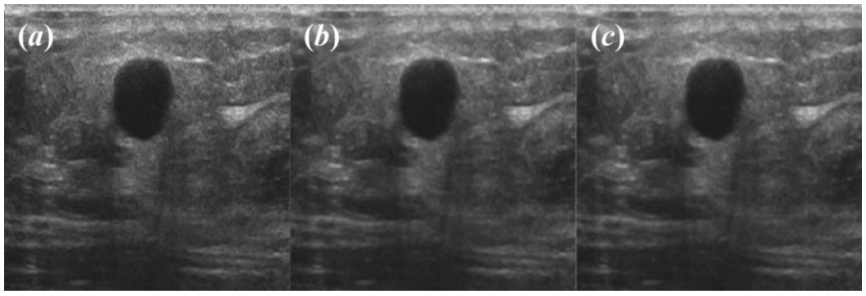

Fig. 3.8 (*a*) Sample original ultrasound image of benign tumor and (*b*), (*c*) corresponding images despeckled by (*b*) TV filter and (*c*) ATV filter.

3.2.2.6. Non-linear iterative filters

The non-linear filtering is based on non-linear operations involving pixels in a neighbourhood. The filters that come under this category are: Geometric filter [172, 173], maximum homogeneity (Homog) filter [23, 172], homomorphic (Homo) filter [23, 172, 184],

anisotropic diffusion (AD) filter [23, 72, 172, 184], speckle reducing anisotropic diffusion (SRAD) filter [23, 172, 173], median filter [23, 172], hybrid median (HyMedian) filter [23, 172], detail preserving anisotropic diffusion (DPAD) filter [3, 23, 314], Linear scaling (LS) filter [172, 173], Linear scaling filter for gray level values (CA) filter [172, 173], Linear scaling and sorting (Ecasort) filter [172, 173] and Shock filter [283]. The sample ultrasound image with benign tumor and corresponding images despeckled by non-linear iterative filters are given in Fig. 3.9.

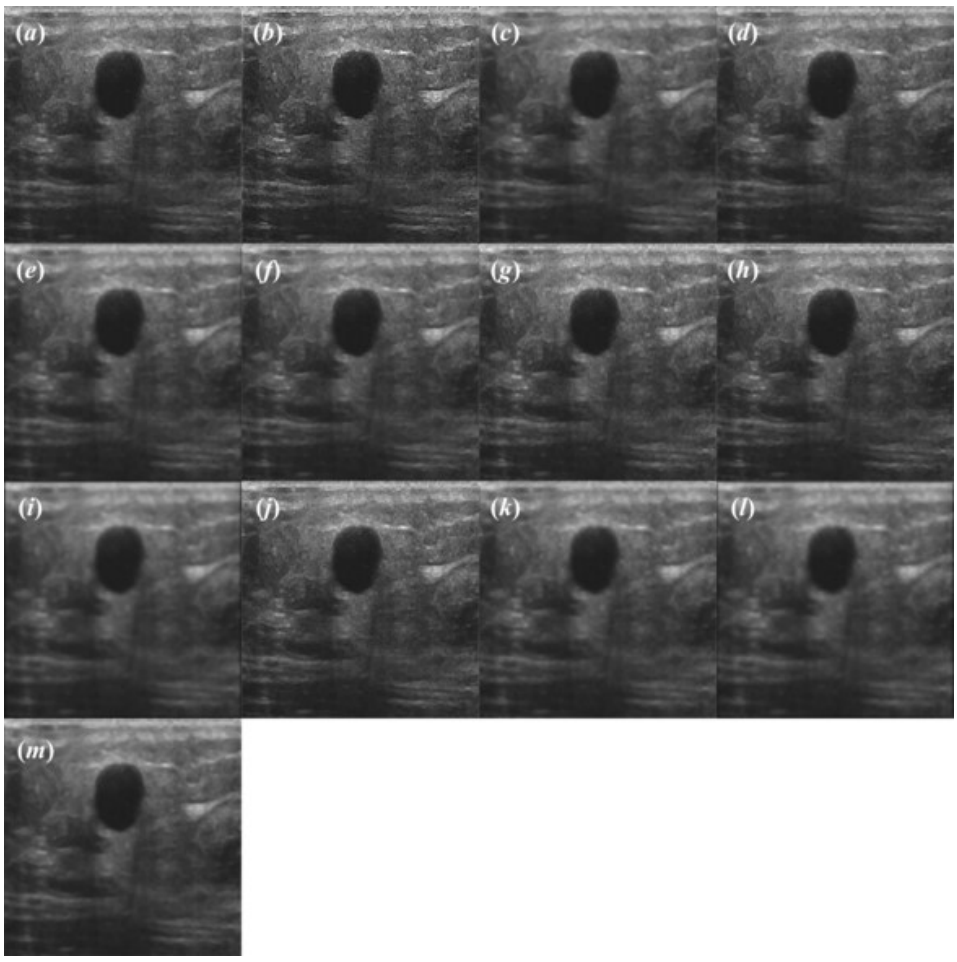

Fig. 3.9 (*a*) Sample original ultrasound image of benign tumor and (*b*)-(*m*) corresponding images despeckled by (*b*) Shock filter, (*c*) Median filter, (*d*) HyMedian filter, (*e*) Homog filter, (*f*) Homo filter, (*g*) Geometric filter, (*h*) SRAD filter, (*i*) AD filter, (*j*) DPAD filter, (*k*) CA filter, (*l*) LS filter and (*m*) Ecasort filter.

From Fig. 3.9, it can be noted that blurring is observed in the images filtered using median filter, AD filter, CA filter, LS filter and Ecasort filter resulting in loss of texture information.

3.2.2.7. Non-local mean filters

These filters work on the concept of patches around each pixel in an image that are used to create the metric for the filters' operation. The performance parameters of these filters are

the size of search window, similarity window and the value of smoothing parameter. The filters considered under this category are: Optimized Bayesian non-local means (OBNLM) based filter [23, 314] and probabilistic patch based (PPB) filter [23]. The sample ultrasound image with benign tumor and corresponding images despeckled by non-local mean filters are given in Fig. 3.10.

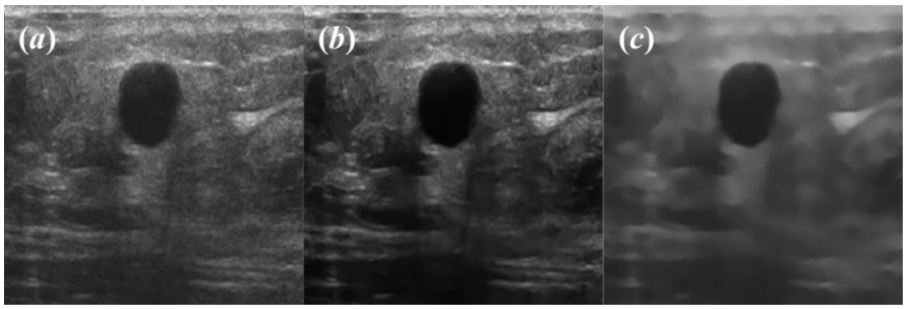

Fig. 3.10 (*a*) Sample original ultrasound image of benign tumor and (*b*), (*c*) corresponding images despeckled by (*b*) OBNLM filter and (*c*) PPB filter.

From Fig. 3.10, it can be noted that images filtered using PPB filter show a smoothening effect resulting in loss of information.

3.2.2.8. Hybrid filters

Different hybrid filters are formed by the combination of fuzzy filters, geometric filter with wiener filter [23, 148]. The filters used under this category are: Hybrid triangulation median (HyTMED) filter [23, 148], Hybrid triangulation moving average (HyTMAV) filter [23, 148], Hybrid asymmetrical triangulation median (HyATMED) filter [23, 148], Hybrid asymmetrical triangulation moving average (HyATMAV) filter [23, 148] and Geometric wiener (GW) filter [23]. The sample original ultrasound image with benign tumor and corresponding images despeckled by hybrid filters are given in Fig. 3.11.

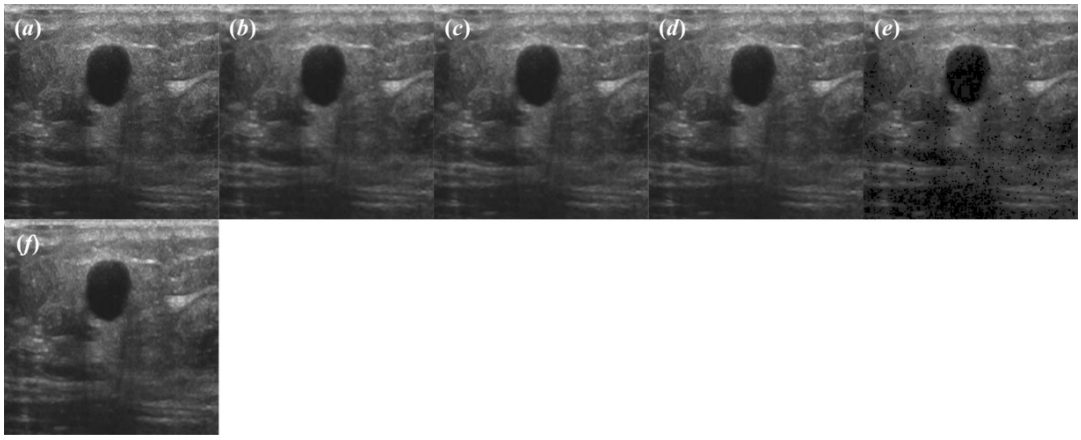

Fig. 3.11 (*a*) Sample original ultrasound image of benign tumor and (*b*)-(*f*) corresponding images despeckled by (*b*) HyTMED filter, (*c*) HyTMAV filter, (*d*) HyATMED filter, (*e*) HyATMAV filter and (*f*) GW filter.

From Fig. 3.11, it can be noted that a blocky effect is observed in images after the application of HyATMAV filter.

3.2.3. Evaluation of despeckle filtering algorithms

The evaluation of despeckle filtering algorithms for noise reduction has been done both on the basis of objective assessment as well as subjective assessment. The objective assessment has been done on the basis of edge and feature/structure preservation capabilities using image quality metrics. The best performing despeckle filtering algorithms based on the objective assessment, are further used for subjective assessment that is carried out by an experienced participating radiologist.

3.2.3.1. Objective assessment of despeckle filtering algorithms

The exhaustive review of literature [23, 24, 172, 173, 314] indicates that a number of metrics/measures i.e. image quality metrics have been used for the objective assessment of despeckle filtering algorithms on medical images. A brief description of these image quality metrics is given in Table 3.2.

Table 3.2 A brief description of image quality metrics used for performance assessment of despeckle filtering algorithms applied to medical images.

Metric Name	Significance
Signal-to-noise ratio (SNR) [23, 172, 173]	Used to find the level of speckle before and after the filtering process.
Peak signal-to-noise ratio (PSNR) [23, 72, 172, 173, 314]	Finds the objective difference between original and despeckled images.
Mean square error (MSE) [23, 72, 172, 173, 314]	Used to estimate the mean difference between original and despeckled images.
Root mean square error (RMSE) [172, 173]	It is the square root of squared average error over a window.
Laplacian mean square error (LMSE) [23, 172, 173]	Used to find the edge features of the image.
Correlation coefficient (CrC) [23, 172, 173]	Used to find the degree of closeness between original and despeckled images.
Average difference (AvgD) [172, 173]	Average of the difference between original and despeckled images.
Maximum difference (MD) [23, 172, 173]	Maximum value of error between original and despeckled images.
Structural content (SC) [23, 172, 173]	Used to find the similarity between original and despeckled images.
Normalized average error (NAE) [23, 172, 173]	Used to measure the error prediction accuracy.
Normalized error summation (Err3, Err4) [23, 172, 173]	Norm of dissimilarity between original and despeckled images.
Normalized cross-correlation (NK) [23, 172, 173]	Measurement of alignment before and after despeckling.
Structural similarity index (SSIM) [23, 172, 173]	Measures similarity between the noisy and denoised images.
Beta metric (β) [23, 173, 187]	Measures the edge preservation capability of the despeckling filter.
Image quality index (IQI) [23, 24, 172, 173]	Used to model the loss of correlation, luminance

From Table 3.2 it can be observed that many quantitative metrics have been computed for assessing the performance of despeckle filtering algorithms [23, 24, 172, 173, 314]. The traditional parameters for image quality evaluation like MSE, PSNR, MD, SNR etc. also sometimes known as full reference image quality metrics, often fail to show the true performance of the despeckling filters due to the absence of a noise free reference input image [24, 314] therefore the true performance of despeckling filters can be evaluated on the basis of edge preservation and feature/structure preservation capabilities.

An ideal despeckling algorithm should retain edges while smoothing the homogeneous areas thereby preserving features/structures of the image. It has been observed from the exhaustive literature review that for the quantification of edge preservation capabilities of the despeckling algorithm, beta metric (β) has been used [23, 173, 184]. The beta metric is given as:

$$\beta = \frac{\sum_{R,C}(\Delta I_0 - \Delta\bar{I_0})(\Delta I_d - \Delta\bar{I_d})}{\sqrt{\sum_{R,C}(\Delta I_0 - \Delta\bar{I_0})^2(\Delta I_d - \Delta\bar{I_d})^2}} \tag{3.5}$$

Here, I_0: Original image, ΔI_0: High pass filtered version of I_0, $\Delta\bar{I_0}$: mean of ΔI_0, I_d: Despeckled image, ΔI_d: High pass filtered version of I_d, $\Delta\bar{I_d}$: mean of ΔI_d, R, C are image dimensions.

The feature/structure preservation can be adequately quantified by evaluating IQI metric [23, 24, 172, 173] given as:

$$IQI = \frac{\sigma_{od}}{\sigma_o\sigma_d} \cdot \frac{2\bar{o}\bar{d}}{(\bar{o})^2 + (\bar{d})^2} \cdot \frac{2\sigma_o\sigma_d}{\sigma_o^2 + \sigma_d^2} \tag{3.6}$$

Here, σ_{od}: covariance between original and despeckled image, σ_o: standard deviation of original image, σ_d: standard deviation of despeckled image, $\bar{o}$: mean of original image, $\bar{d}$: mean of despeckled image.

For the differential diagnosis between benign and malignant breast ultrasound tumors, both the texture and shape of the tumor are important therefore an ideal despeckle filtering algorithm would be the one that yields higher values of both β and IQI. Therefore, in the present study for objective assessment of despeckle filtering algorithms, structure and edge preservation index (SEPI) has been considered [141], given as:

$$SEPI = \frac{\beta + IQI}{2} \tag{3.7}$$

The traditional parameters for image quality evaluation also sometimes known as full reference image quality metrics, often fail to show the true performance of the despeckling

filters due to the absence of a noise free reference input image. In the present context, controlled despeckling is desired as speckle noise also represents the diagnostic information present in the ultrasound image therefore the true performance of despeckling filters in the present work has been evaluated in terms of feature/structure preservation and edge preservation capabilities of a particular filter which is quantified by computing SEPI.

A despeckle filtering algorithm that yields the highest value of SEPI is considered optimal.

These image quality metrics *i.e.* β, IQI and SEPI have been obtained using the original images and the corresponding despeckled images for all the 42 despeckle filtering algorithms and the results are summarized in the form of mean (μ) ± standard deviation (SD).

(*a*) Objective assessment of local statistics based filters

The breast ultrasound images are filtered using eight local statistics based filters yielding 100 pre-processed images for each filter. The performance of each local statistics based filter in terms of SEPI value for the pre-processed images is shown in Table 3.3.

Table 3.3 Image quality metrics (μ ± SD) computed for breast ultrasound images filtered using local statistics based filters.

Quality Metrics	Lee	Lee Sigma	Kuan	Frost	Lsminsc	Lsmv	Wiener	FBL
β	0.79 ± 0.07	0.98 ± 0.04	0.44 ± 0.19	0.73 ± 0.10	0.52 ± 0.09	0.78 ± 0.07	0.92 ± 0.02	0.84 ± 0.05
IQI	0.99 ± 0.00	0.98 ± 0.04	0.98 ± 0.04	0.98 ± 0.04	0.99 ± 0.01	0.99 ± 0.00	0.99 ± 0.00	0.97 ± 0.02
SEPI	0.89 ± 0.11	**0.98 ± 0.04**	0.71 ± 0.30	0.86 ± 0.14	0.76 ± 0.24	0.89 ± 0.11	0.96 ± 0.04	0.91 ± 0.07

Note: β: Beta metric, IQI: Image quality index, SEPI: Structure and edge preservation index, Lsminsc: Local statistics based minimum speckle index, Lsmv: Local statistics minimum variance, FBL: Fast bilateral filter.

From Table 3.3, it has been observed that the filters Lee Sigma and Wiener show good edge preservation capabilities with $\beta > 0.90$ while Lee Sigma shows highest edge preservation with β value 0.98 ± 0.04. The IQI value for each of these filters is above 0.95. However, it is observed that among all the local statistics based filters, highest value of SEPI is obtained for the Lee Sigma filter.

(*b*) Objective assessment of fuzzy filters

The breast ultrasound images are filtered using four fuzzy filters yielding 100 pre-processed images for each filter. The performance of each of these fuzzy filters in terms of SEPI value for the pre-processed images is shown in Table 3.4.

Table 3.4 Image quality metrics (μ ± SD) computed for breast ultrasound images filtered using fuzzy filters.

Quality Metric	TMED	TMAV	ATMED	ATMAV
β	0.54 ± 0.26	0.76 ± 0.15	0.90 ± 0.04	0.58 ± 0.18
IQI	0.99 ± 0.00	0.99 ± 0.00	0.99 ± 0.01	0.98 ± 0.01

SEPI	0.77 ± 0.29	0.88 ± 0.16	**0.95 ± 0.05**	0.78 ± 0.24

Note: β: Beta metric, IQI: Image quality index, SEPI: Structure and edge preservation index, TMED: Triangulation median, TMAV: Triangulation moving average, ATMED: Asymmetrical triangulation median, ATMAV: Asymmetrical triangulation moving average.

From Table 3.4, it has been observed that ATMED filter results in highest edge preservation with β value 0.90 ± 0.04. The IQI value for each of these filters is above 0.95. However, it is observed that among all the fuzzy filters, highest value of SEPI is obtained for ATMED filter.

(*c*) Objective assessment of Fourier filters

The breast ultrasound images are filtered using four Fourier filters yielding 100 pre-processed images for each filter. The performance of each Fourier filter in terms of SEPI value for the pre-processed images is shown in Table 3.5.

Table 3.5 Image quality metrics (μ ± SD) computed for breast ultrasound images filtered using Fourier filters.

Quality Metric	FI	FB	HFI	HFB
β	0.99 ± 0.00	0.98 ± 0.00	0.96 ± 0.05	0.99 ± 0.00
IQI	0.99 ± 0.00	1.00 ± 0.00	0.99 ± 0.00	0.99 ± 0.00
SEPI	**0.99 ± 0.00**	**0.99 ± 0.00**	0.97 ± 0.06	**0.99 ± 0.00**

Note: β: Beta metric, IQI: Image quality index, SEPI: Structure and edge preservation index, FI: Fourier ideal, FB: Fourier Butterworth, HFI: Homomorphic Fourier ideal, HFB: Homomorphic Fourier Butterworth,

From Table 3.5, it has been observed that that all the Fourier filters show good edge preservation capabilities with $\beta \geq 0.95$. The IQI value for each of these filters is above 0.95. However, it is observed that among all the Fourier filters, highest value of SEPI is obtained for FI, FB and HFB filters.

(*d*) Objective assessment of multiscale filters

The breast ultrasound images are filtered using five multiscale filters yielding 100 pre-processed images for each filter. The performance of each multiscale filter in terms of SEPI value for the pre-processed images is shown in Table 3.6.

Table 3.6 Image quality metrics (μ ± SD) computed for breast ultrasound images filtered using multiscale filters.

Quality Metric	MPT	IOWT	BlockShrink	BayesShrink	NSS
β	0.97 ± 0.00	0.98 ± 0.00	0.98 ± 0.00	0.99 ± 0.00	0.97 ± 0.00
IQI	0.99 ± 0.00	0.98 ± 0.00	0.99 ± 0.00	1.00 ± 0.00	0.98 ± 0.00
SEPI	0.98 ± 0.00	0.98 ± 0.00	0.98 ± 0.00	**0.99 ± 0.00**	0.97 ± 0.00

Note: β: Beta metric, IQI: Image quality index, SEPI: Structure and edge preservation index, MPT: Multiscale product thresholding, IOWT: Inter orthonormal wavelet thresholding, NSS: NeighShrinkSure.

From Table 3.6, it has been observed that all the multiscale filters result in good edge preservation with β value above 0.95. The IQI value for each of these filters is also above 0.95. However, it is observed that among all the multiscale filters, highest value of SEPI is obtained for BayesShrink filter.

(*e*) Objective assessment of total variation filters

The breast ultrasound images are filtered using two total variation filters yielding 100 pre-processed images for each filter. The performance of each total variation filter in terms of SEPI value for the pre-processed images is shown in Table 3.7.

Table 3.7 Image quality metrics (μ ± SD) computed for breast ultrasound images filtered using total variation filters.

Quality Metric	TV	ATV
β	0.84 ± 0.05	0.83 ± 0.06
IQI	0.99 ± 0.01	0.99 ± 0.00
SEPI	**0.92 ± 0.08**	0.91 ± 0.09

Note: β: Beta metric, IQI: Image quality index, SEPI: Structure and edge preservation index, TV: Total variation, ATV: Anisotropic total variation.

From Table 3.7, it has been observed that both TV and ATV filters exhibit similar performance with almost same value of SEPI.

(*f*) Objective assessment of non-linear iterative filters

The breast ultrasound images are filtered using twelve non-linear iterative filters yielding 100 pre-processed images for each filter. The performance of each non-linear iterative filter in terms of SEPI value for the pre-processed images is shown in Table 3.8.

Table 3.8 Image quality metrics (μ ± SD) computed for breast ultrasound images filtered using non-linear iterative filters.

Quality Metric	Shock	Median	HyMedian	Homog	Homo	Geometric
β	0.46 ± 0.05	0.70 ± 0.09	0.90 ± 0.03	0.62 ± 0.10	0.72 ± 0.08	0.70 ± 0.15
IQI	0.99 ± 0.01	0.99 ± 0.01	0.99 ± 0.00	0.99 ± 0.03	0.99 ± 0.01	0.98 ± 0.02
SEPI	0.72 ± 0.26	0.84 ± 0.15	0.95 ± 0.05	0.80 ± 0.19	0.85 ± 0.14	0.84 ± 0.17

Quality Metric	SRAD	AD	DPAD	CA	LS	Ecasort
β	0.89 ± 0.05	0.22 ± 0.03	0.99 ± 0.00	0.71 ± 0.12	0.32 ± 0.14	0.71 ± 0.12
IQI	0.99 ± 0.00	0.98 ± 0.02	0.99 ± 0.00	0.99 ± 0.01	0.98 ± 0.01	0.99 ± 0.01
SEPI	0.94 ± 0.06	0.60 ± 0.38	**0.99 ± 0.00**	0.85 ± 0.16	0.65 ± 0.34	0.85 ± 0.16

Note: β: Beta metric, IQI: Image quality index, SEPI: Structure and edge preservation index, HyMedian: Hybrid median, Homog: Maximum homogeneity, Homo: Homomorphic, SRAD: Speckle reducing anisotropic diffusion, AD: Anisotropic diffusion, DPAD: Detail preserving anisotropic diffusion, CA: Linear scaling of gray-level values, LS: Linear scaling, Ecasort: Linear scaling and sorting.

From Table 3.8, it has been observed that all the filters other than SRAD, DPAD and HyMedian result in poor edge preservation with $\beta \leq 0.75$. SRAD and HyMedian filters exhibit moderate edge preservation capabilities while DPAD filter results in highest edge preservation with $\beta \geq 0.95$. The IQI value for each of these filters is above 0.95. However, it is observed that among all the non-linear iterative filters, highest value of SEPI is obtained for the DPAD filter.

(*g*) Objective assessment of non-local mean filters

The breast ultrasound images are filtered using two non-local mean filters yielding 100 pre-processed images for each filter. The performance of each non-local means filter in terms of SEPI value for the pre-processed images is shown in Table 3.9.

Table 3.9 Image quality metrics (μ ± SD) computed for breast ultrasound images filtered using non-local mean filters.

Quality Metric	OBNLM	PPB
β	0.90 ± 0.02	0.71 ± 0.10
IQI	0.94 ± 0.05	0.98 ± 0.01
SEPI	**0.92 ± 0.04**	0.85 ± 0.15

Note: β: Beta metric, IQI: Image quality index, SEPI: Structure and edge preservation index, OBNLM: Optimized Bayesian non-local means, PPB: Probabilistic patch based.

From Table 3.9, it has been observed that OBNLM filter results in better edge preservation than the PPB filter. The IQI value for both these filters is above 0.90. However, it is observed that among all the non-local mean filters, highest value of SEPI is obtained for the OBNLM filter.

(*h*) Objective assessment of hybrid filters

The breast ultrasound images are filtered using five hybrid filters yielding 100 pre-processed images for each filter. The performance of each hybrid filter in terms of SEPI value for the pre-processed images is shown in Table 3.10.

Table 3.10 Image quality metrics (μ ± SD) computed for breast ultrasound images filtered using hybrid filters.

Quality Metric	HyTMED	HyTMAV	HyATMED	HyATMAV	GW
β	0.62 ± 0.27	0.75 ± 0.16	0.84 ± 0.05	0.29 ± 0.11	0.70 ± 0.17
IQI	0.99 ± 0.00	0.99 ± 0.00	0.99 ± 0.00	0.98 ± 0.06	0.98 ± 0.01
SEPI	0.81 ± 0.26	0.87 ± 0.16	**0.92 ± 0.08**	0.64 ± 0.35	0.84 ± 0.18

Note: β: Beta metric, IQI: Image quality index, SEPI: Structure and edge preservation index, HyTMED: Hybrid triangulation median, HyTMAV: Hybrid triangulation moving average, HyATMED: Hybrid asymmetrical triangulation median, HyATMAV: Hybrid asymmetrical triangulation moving average, GW: Geometric wiener.

From Table 3.10, it has been observed that HyATMED filter results in best edge preservation as compared to other filters with β value 0.84 ± 0.05. The IQI value for each of these filters is above 0.95. However, among all the hybrid filters, highest value of SEPI is obtained for HyATMED filter.

3.2.3.2. Best performing despeckle filtering algorithms based on objective assessment

Based on the objective assessment of all the 42 despeckle filtering algorithms, comparative analysis of the filters yielding highest value of SEPI from each filter category is shown in Table 3.11.

Table 3.11 Comparative analysis of despeckle filtering algorithms yielding highest value of SEPI from each filter category.

Filter Category	Filter	Highest value of SEPI
Local statistics based filters	Lee Sigma	0.98 ± 0.04
Fuzzy filters	ATMED	0.95 ± 0.05
Fourier filters	FI	0.99 ± 0.00
	FB	0.99 ± 0.00
	HFB	0.99 ± 0.00
Multiscale filters	BayesShrink	0.99 ± 0.00

Total variation filters	TV	0.92 ± 0.08
Non-linear iterative filters	DPAD	0.99 ± 0.00
Non-local mean filters	OBNLM	0.92 ± 0.04
Hybrid filters	HyATMED	0.92 ± 0.08

Note: SEPI: Structure and edge preservation index, ATMED: Asymmetrical triangulation median, FI: Fourier ideal, FB: Fourier Butterworth, HFB: Homomorphic Fourier Butterworth, TV: Total variation, DPAD: Detail preserving anisotropic diffusion, OBNLM Optimized Bayesian non-local means, HyATMED: Hybrid asymmetrical triangulation median.

From Table 3.11, it has been observed that out of the 42 despeckle filtering algorithms belonging to 08 categories, the 06 despeckle filtering algorithms belonging to 04 categories achieve highest value of SEPI (>0.95) and have been considered optimal for edge, feature/structure preservation. The despeckled images obtained from these *06 best performing despeckle filtering algorithms* have been used for further assessment. The best performing despeckle filtering algorithms are Lee Sigma, FI, FB, HFB, BayesShrink and DPAD.

3.2.3.3. Subjective assessment of despeckle filtering algorithms

The 100 pre-processed breast ultrasound images obtained from the *06 best performing despeckle filtering algorithms* based on the SEPI value as highlighted in Table 3.11 have been considered for further analysis for subjective assessment by the radiologist. The protocols followed by the radiologist for grading the images are (*a*) *Tumor delineation:* The tumor should be clearly distinguishable in the despeckled image, (*b*) *Boundary of the tumor:* The boundary/shape characteristics of the tumor should be clearer after despeckling, (*c*) *Texture of the region inside tumor*: The texture of the region inside tumor should be same after despeckling as in original image i.e. no blocking or echoes should be introduced after despeckling, (*d*) *Blurring in the image*: There should be no blurring of the image as it reduces the visual quality and (*e*) *Texture of the region outside the tumor*: The appearance of the surrounding breast tissue should be nearly same after despeckling as in original image.

Based on the visual assessment of the despeckled image in comparison to the original image in accordance with the above protocols, a grade is assigned to each despeckled image from 1 to 5 (here 1 denotes poor image quality and 5 denotes high image quality). Each factor described above carries a weightage of 1 point. The grades are assigned to an image based on the number of factors being met e.g. if an image has a grade of 1 it means out of the above 5 factors only one factor has been met satisfactorily for majority of the images. Due to the fuzzy nature of images, it might be possible that some of the factors have been fully met while one of the factors has been partially met hence intermediate grading has been assigned to some filters.

3.2.3.4. Optimal despeckle filtering algorithm based on subjective assessment

Based on the grades assigned by the radiologist, the final grade is obtained as the average of the grades given to all the 100 (40 benign and 60 malignant) pre-processed images. The final average grade obtained for each filter is tabulated in Table 3.12.

Table 3.12 Grading obtained for best performing despeckle filtering algorithms.

Despeckle filtering algorithm	Grade assigned
Lee Sigma filter	1
FI filter	3
FB filter	3.5
HFB filter	3
BayesShrink filter	4
DPAD filter	4.5

Note: FI: Fourier ideal, FB: Fourier Butterworth, HFB: Homomorphic Fourier Butterworth, DPAD: Detail preserving anisotropic diffusion

From Table 3.12, it has been observed that despeckled images obtained from the filters BayesShrink and DPAD are clinically acceptable while the images obtained from the Lee Sigma filter are not acceptable in clinical practice.

3.2.3.5. Inter-observer and intra-observer variability

Out of the 42 despeckle filtering algorithms, the 06 *best performing despeckle filtering algorithms* have been selected for grading by radiologist. For grading of the images, the radiologist had to analyse a total of 600 pre-processed images (100 images × 6 despeckling methods = 600 processed images) with respect to 05 parameters (i.e. tumor delineation, boundary of the tumor, texture of region inside the tumor, blurring in the image, texture of the region outside the tumor) in each image with respect to corresponding original images under the same ambient lighting conditions and display settings. So in a way the effect of intra-observer variability has been reduced by keeping the same settings [35]. For inter-observer variability, the opinion of more than one radiologist is required under same settings. Since in the present work the number of processed images as well as the parameters required to be analysed in each image were quite large, only one radiologist has been consulted. Also, the inter-observer variability also depends upon the experience of the participating radiologists. In our case the participating radiologist had rich experience for analysing breast sonographs.

3.3. Concluding Remarks

From the objective and subjective assessment carried out for the performance evaluation of despeckle filtering algorithms it has been observed that on the basis of objective assessment, six despeckle filtering algorithms are considered to be best performing while on the basis of subjective assessment, out of the *06 best despeckle filtering algorithms*, only two despeckle filtering algorithms yield comparable performance.

A comparative analysis of the obtained results for objective and subjective assessment of despeckle filtering algorithms for breast ultrasound images is shown in Table 3.13.

Table 3.13 Comparative analysis of the obtained results for objective and subjective assessment of despeckle filtering algorithms for breast ultrasound images

Despeckle filtering algorithm	Assessment results	
	Objective assessment (Highest value of SEPI)	Subjective assessment (Radiologist's Grading)
Lee Sigma filter	0.98 ± 0.04	1
FI filter	0.99 ± 0.00	3
FB filter	0.99 ± 0.00	3.5
HFB filter	0.99 ± 0.00	3
BayesShrink filter	0.99 ± 0.00	4
DPAD filter	0.99 ± 0.00	4.5

Note: SEPI: Structure and edge preservation index, FI: Fourier ideal, FB: Fourier Butterworth, HFB: Homomorphic Fourier Butterworth, DPAD: Detail preserving anisotropic diffusion.

Based on the results obtained by exhaustive experimentation carried out in the present work for objective and subjective analysis of despeckle filtering algorithms for controlled despeckling of breast ultrasound images, it has been concluded that the DPAD filter produces more clinically acceptable images while reducing noise and simultaneously enhancing the diagnostic information.

For the correct diagnosis of breast tumors, the shape of the tumors is equally important as is the texture. For the correct quantification of shape information, it is necessary that the tumor region should be adequately segmented from the breast ultrasound images. The speckle noise sometimes tends to mask the important diagnostic information in ultrasound images and this might affect the subjective analysis of the radiologist as well as performance of various computer-assisted algorithms. An ideal despeckle filtering algorithm suppress the speckle noise from the homogeneous areas by retaining the edges thereby preserving features/structures of the image. This implies that the shape information of the tumor region should be enhanced after the application of the despeckle filtering algorithms. Therefore, to observe the effect of *06 best performing despeckle filtering algorithms* on the performance of segmentation of breast tumors from ultrasound images is taken up as the next objective in the present work and discussed in detail in Chapter 4.

Chapter 4

Effect of Despeckle Filtering Algorithms on Segmentation of Breast Tumors

4.1. Introduction

Diagnosis of breast cancer at an early stage is very critical for improving the mortality rate among women as this helps in timely treatment options and patient care [13, 36, 267, 204]. For the correct diagnosis of breast tumors, the texture and morphological information exhibited by the tumor is considered clinically significant. For the quantification of morphological characteristics, it is necessary that the tumor region should be efficiently segmented from the breast ultrasound images. It has been observed that speckle noise sometimes masks the diagnostic information of the images thus affecting the performance of various computer-assisted algorithms used for the analysis of breast tumors.

It has also been stated that an ideal despeckle filtering algorithm should retain edges while smoothing the homogeneous areas thereby preserving features/structure of the image, it means that the shape information of the tumor region should be enhanced after the application of despeckle filtering algorithms. Therefore various attempts have been made by the researchers to assess the effect of different filtering algorithms on the segmentation and classification performance and the researchers have also attempted to find suitable despeckle filtering algorithms that could be used for efficient segmentation of the breast ultrasound images [58, 69, 70, 205]

Elawady et al. [69] compared the performance of 03 different filtering methods namely frost, DPAD and PPB taken from 03 filter categories namely local statistics based filter, non-linear iterative filters and non-local mean filter for the segmentation performance of breast ultrasound images using two segmentation techniques, quick shift (QS) and normalized cut (NCut). The segmentation performance has been compared on the basis of dice similarity coefficient, Jaccard index (JI) and sensitivity.

Cristerna et al. [58] evaluated the performance of 20 pre-processing algorithms formed as a combination of 05 contrast enhancement methods and 04 despeckle filtering algorithms taken from the non-linear iterative filter category. The resultant filtered images were then subjected to segmentation by using the watershed transform. The segmentation accuracy was quantified on the basis of JI.

Feng et al. [70] compared the effect of 08 despeckle filtering algorithms taken from 04 filtering categories on the segmentation accuracy of breast tumors using fuzzy C-means algorithm. The performance was measured on the basis of averaged radical error (ARE).

In the present work, the *06 best performing despeckle filtering algorithms* namely Lee sigma, BayesShrink, detail preserving anisotropic diffusion (DPAD), Fourier ideal (FI), Fourier Butterworth (FB) and Homomorphic Fourier Butterwort (HFB) filters chosen on the basis of objective assessment based on highest value of structure and edge preservation index (SEPI) have been considered for analysing the effect of despeckle filtering algorithms on the segmentation of breast tumors [141].

4.2. Experimental Workflow: Effect of Despeckle Filtering Algorithms on Segmentation of Breast Tumors

The experimental workflow followed for analysing the effect of best performing despeckle filtering algorithms on the segmentation of breast tumors is given in Fig. 4.1.

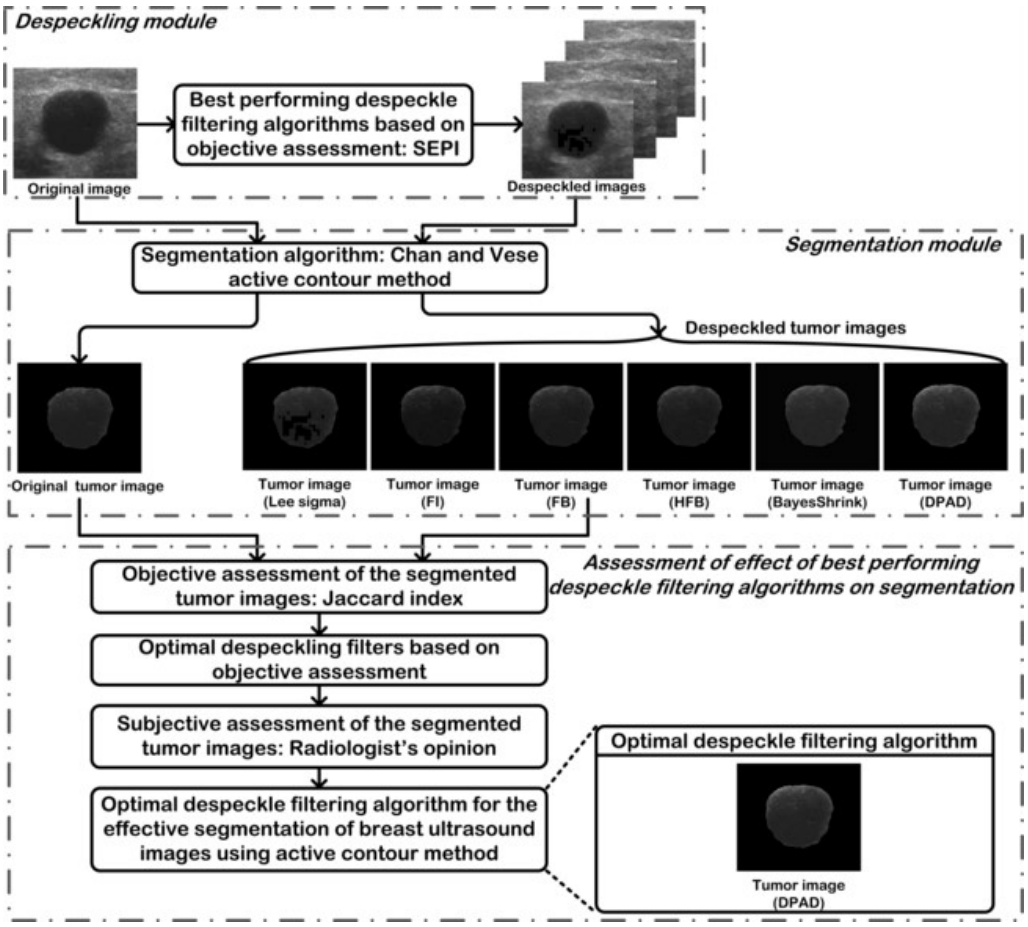

Fig. 4.1 Experimental workflow followed for analysing the effect of best performing despeckle filtering algorithms on the segmentation of breast tumors.
Note: SEPI: Structure and edge preservation index, FI: Fourier ideal, FB: Fourier Butterworth, HFB: Homomorphic Fourier Butterworth, DPAD: Detail preserving anisotropic diffusion.

Both original images and the images despeckled by the *06 best performing despeckle filtering algorithms* have been subjected to Chan and Vese active contour method [37] for delineating the tumor boundary. The segmentation performance has been assessed on the basis of objective evaluation by computing the Jaccard index and subjective evaluation by the participating radiologist. The segmentation performance has been tested individually for benign and malignant tumors.

4.2.1. Dataset Description

For carrying out the present work, dataset described in section 3.2.1 of Chapter 3 has been used as presented in Fig. 3.2. The entire image dataset was stored on a 64-bit windows 10 PC with Intel (R) Core (TM) i3-5005U, 2.00 GHz processor and 4.00 GB RAM and the experiments have been conducted using MATLABR2015b.

4.2.2. Despeckling module

Speckle noise affects the image quality by masking the detailed structures in the image which are diagnostically important thereby affecting the radiologist's visual interpretation. It is important to carefully remove speckle from the medical images so that the image interpretation as well as accuracy of computer assisted algorithms can be improved [69, 58, 70, 139, 172, 205, 249]. In the present research work, the ultrasound images have been despeckled using *06 best performing despeckle filtering algorithms* namely Lee sigma filter [155], BayesShrink filter [320], DPAD filter [3], FI filter [184], FB filter [184], HFB filter [184]. These filters have been selected on the basis of the objective evaluation (highest value of SEPI) as discussed in *Chapter 3.*

4.2.3. Segmentation module

In segmentation, a desired region of interest (ROI) is extracted from an image with the help of an automatic or semi-automatic algorithm. The segmentation techniques have been used in case of breast ultrasound images to alienate the tumors from the background [143].

4.2.3.1.Chan and Vese active contour method

Active contour method and its variants have been a popular choice for segmenting the breast ultrasound images [33, 52, 59, 61, 77, 84, 170, 112, 121, 164, 179, 244]. Accordingly in the present work, Chan and Vese active contour method [37] has been used for segmenting the breast ultrasound images.

The Chan and Vese active contour model was typically used to segment objects that did not have well-defined boundaries and for which the classical active contour model was not applicable. This model is based on level sets that iteratively evolve to minimize an energy function. This energy function is defined by sum of differences in intensity from the average

value outside the segmented region, the sum of differences in intensity from the average value inside the segmented region, and a term which is dependent on the length of the boundary of the segmented region. The model begins with an initial contour that evolves according to the level set method and stops on the desired boundaries of the foreground region.

For an image u_0, let there be a curve C in image space **Ω**, the energy function to be minimized is given as:

$$F(c_1, c_2, C) = \mu L(C) + \nu A\big(in(C)\big) + \lambda_1 \int_{in\,(C)} |u_0(x,y) - c_1|^2\, dxdy + \lambda_2 \int_{out\,(C)} |u_0(x,y) - c_2|^2\, dxdy \quad (4.1)$$

where, c_1, c_2 are average intensity levels inside and outside contour C.

For level set formulation, $C \subset \Omega$ can be represented by zero level set of Lipschitz function ϕ.

$$\begin{aligned} C &= \{(x,y) \in \Omega : \phi(x,y) = 0\} \\ in(C) &= \{(x,y) \in \Omega : \phi(x,y) > 0\} \\ out(C) &= \{(x,y) \in \Omega : \phi(x,y) < 0\} \end{aligned} \quad (4.2)$$

Introducing a Dirac measure and Heaviside function H,

$$\begin{aligned} L\{\phi = 0\} &= \int_{\Omega} \delta\big(\phi(x,y)\big)|\nabla\phi(x,y)|dxdy \\ A\{\phi \geq 0\} &= \int_{\Omega} H(\phi(x,y))dxdy \end{aligned} \quad (4.3)$$

Intensity terms are given as:

$$\begin{aligned} \int_{in\,(C)} |u_0(x,y) - c_1|^2\, dxdy &= \int_{\phi>0} |u_0(x,y) - c_1|^2\, dxdy \\ &= \int_{\Omega} |u_0(x,y) - c_1|^2\, H(\phi(x,y))dxdy \\ \int_{out\,(C)} |u_0(x,y) - c_2|^2\, dxdy &= \int_{\phi<0} |u_0(x,y) - c_2|^2\, dxdy \\ &= \int_{\Omega} |u_0(x,y) - c_2|^2\, (1 - H(\phi(x,y)))dxdy \end{aligned} \quad (4.4)$$

The minimization can be solved by alternately updating c_1, c_2, ϕ. For a fixed vale of ϕ, c_1 and c_2 are given as:

$$\begin{aligned} c_1(\phi) &= \frac{\int_{\Omega} u_0(x,y) H\big(\phi(x,y)\big)dxdy}{\int_{\Omega} H\big(\phi(x,y)\big)dxdy} \\ c_2(\phi) &= \frac{\int_{\Omega} u_0(x,y)\Big(1 - H\big(\phi(x,y)\big)\Big)\, dxdy}{\int_{\Omega}\Big(1 - H\big(\phi(x,y)\big)\Big)\, dxdy} \end{aligned} \quad (4.5)$$

The above terms are combined to form the energy function F in terms of ϕ and this energy function is then minimized using gradient descent method as explained in [37].

For implementation purposes, the user provided parameters are the initial level set function (mask) and the length parameter which is not same in all the images and depends on the size of the tumor to be detected. In the present work the initial rectangular bounding box

(mask) was inputted based on the contour marking by the participating radiologist and the number of iterations (length) was varied from 80 to 250. The stopping criterion for segmentation is to maximize the overlap between the segmented tumor contour and the contour marked by the radiologist.

The true boundary of 104 breast tumors (43 benign, 61 malignant) from 100 breast ultrasound images have been delineated in the presence of experienced radiologist using *Image J* software [117]. The sample benign and malignant images indicating the results of segmentation are given in Fig. 4.2 and Fig. 4.3, respectively.

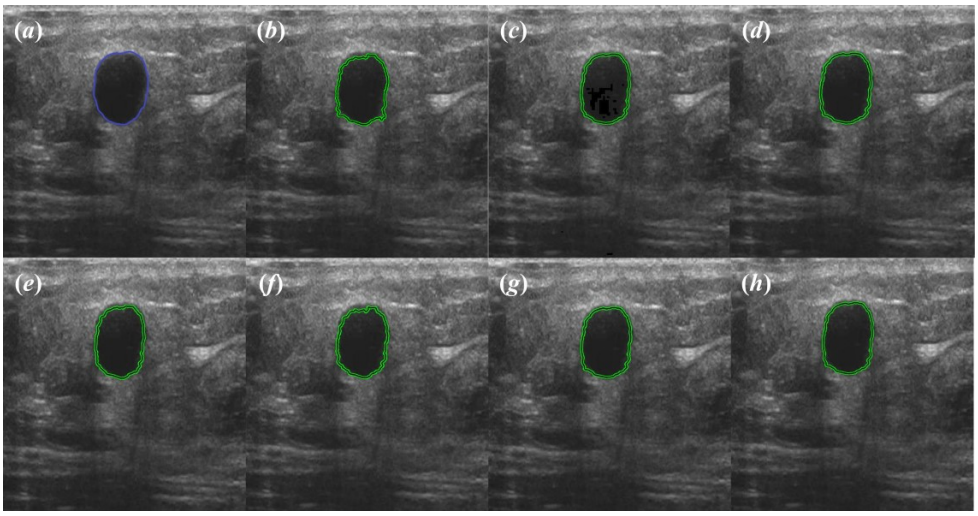

Fig. 4.2 Segmentation of benign tumor from breast ultrasound images (*a*) Original image indicating tumor boundary marked by the radiologist, (*b*) Original image indicating tumor boundary obtained after segmentation, (*c*) Despeckled image using Lee Sigma filter indicating tumor boundary obtained after segmentation, (*d*) Despeckled image using FI filter indicating tumor boundary obtained after segmentation, (*e*) Despeckled image using FB filter indicating tumor boundary obtained after segmentation, (*f*) Despeckled image using HFB filter indicating tumor boundary obtained after segmentation, (*g*) Despeckled image using BayesShrink filter indicating tumor boundary obtained after segmentation, (*h*) Despeckled image using DPAD filter indicating tumor boundary obtained after segmentation.

4.2.4. Evaluating the effect of best despeckle filtering algorithms on segmentation of breast tumors

4.2.4.1. Objective assessment of segmentation of breast tumors

The assessment of the effect of *06 best performing despeckle filtering algorithms* on the segmentation of breast tumors has been carried out objectively and subjectively. The objective assessment has been done on the basis of Jaccard index and the subjective assessment is carried out by the experienced participating radiologist with respect to the clinical acceptability of the tumor images.

The efficacy of the segmentation algorithm has been objectively calculated using the area overlap between the original tumor contour marked by a radiologist and the tumor contour

obtained as a result of applying segmentation algorithm. The area overlap is calculated using Jaccard index (JI) (also referred to as overlap or similarity) [33, 52, 69] given as:

$$Jaccard\ index\ (JI) = \frac{A_G \cap A_S}{A_G \cup A_S} \times 100 \tag{4.6}$$

Here, A_G : Area of the ground truth image (marked by radiologist), A_S : Area of the segmented image

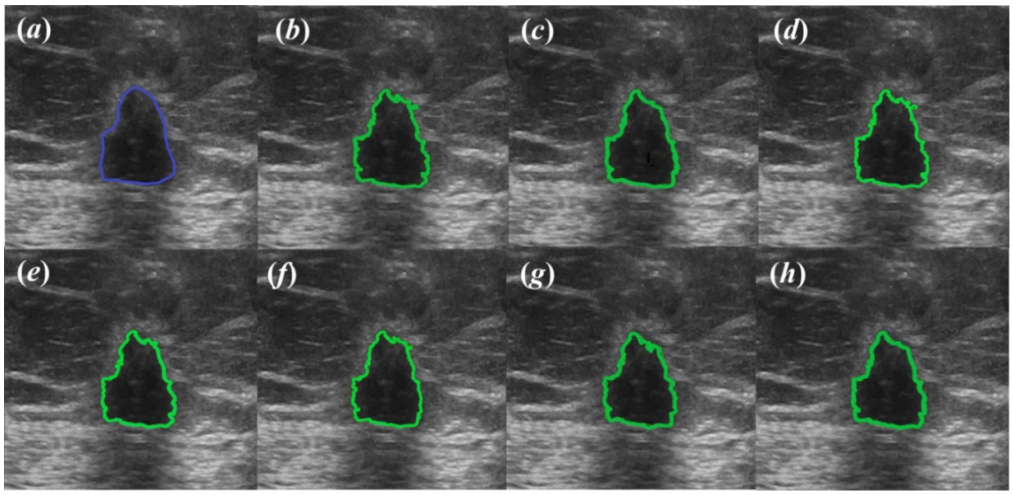

Fig. 4.3 Segmentation of malignant tumor from breast ultrasound images (*a*) Original image indicating tumor boundary marked by the radiologist, (*b*) Original image indicating tumor boundary obtained after segmentation, (*c*) Despeckled image using Lee Sigma filter indicating tumor boundary obtained after segmentation, (*d*) Despeckled image using FI filter indicating tumor boundary obtained after segmentation, (*e*) Despeckled image using FB filter indicating tumor boundary obtained after segmentation, (*f*) Despeckled image using HFB filter indicating tumor boundary obtained after segmentation, (*g*) Despeckled image using BayesShrink filter indicating tumor boundary obtained after segmentation, (*h*) Despeckled image using DPAD filter indicating tumor boundary obtained after segmentation.

The segmentation results in terms of Jaccard index obtained from original tumor images and the tumor images obtained from images despeckled by *06 best performing despeckle filtering algorithms* are shown in Table 4.1.

The Table 4.1 indicates maximum, minimum and average values of Jaccard index for benign and malignant classes for both original tumor images and tumor images obtained from images despeckled by *06 best performing despeckle filtering algorithms*.

Table 4.1 Values of Jaccard index obtained from original tumor images and the tumor images obtained from images despeckled by 06 best performing despeckle filtering algorithms.

Image	**Jaccard Index (%)**			
	Class	**Max. Value**	**Min. Value**	**Avg. Value**
Original images*	Benign	94.17	66.30	84.04
	Malignant	90.42	47.24	75.47
Despeckled images using Lee Sigma filter	Benign	94.02	58.22	84.21
	Malignant	91.28	42.69	76.14
Despeckled images using FI filter	Benign	93.48	59.85	83.99

	Malignant	90.17	42.77	76.04
Despeckled images using FB filter	Benign	93.41	59.36	83.75
	Malignant	89.96	42.77	75.97
Despeckled images using HFB filter	Benign	93.41	58.37	83.25
	Malignant	89.87	43.77	75.98
Despeckled images using BayesShrink filter	Benign	93.82	57.05	84.09
	Malignant	91.17	42.77	76.19
Despeckled images using DPAD filter	Benign	94.17	59.25	84.22
	Malignant	91.74	47.17	76.23

Note: Max.: Maximum value, Min.: Minimum value, Avg.: Average value, FI: Fourier ideal, FB: Fourier Butterworth, HFB: Homomorphic Fourier Butterworth, DPAD: Detail preserving anisotropic diffusion
*Segmentation results obtained using tumor contours marked by radiologist in original images and tumor contours obtained by segmentation process in original images.

However, in malignant cases a marginal increase in average value of Jaccard index has been observed. The reasons of not obtaining nearly 100% Jaccard index value are (*a*) the margins of the lesions are highly spiculated and irregular. (*b*) The speckle noise is inherent in ultrasound imaging due to which sometimes the diagnostic information is buried inside the speckle noise. (*c*) Sometimes the application of despeckle filtering algorithm may adversely affect the texture of the region inside and outside the tumor.

Keeping in view the above points, the subjective analysis also plays a crucial role to analyse the clinical acceptability of segmented tumor images. It has also been observed that even though the Fourier filters obtained higher values of JI in comparison to original images, the performance has degraded in case of benign images while the other three filters have shown improvement in the JI value for both benign and malignant cases. Therefore, the segmented tumor images of the three filters (shaded in gray in Table 4.1) were shown to the participating radiologist for further subjective assessment in terms of the clinical acceptability of the segmented tumor images.

4.2.4.2. Subjective assessment of segmentation of breast tumors (Clinical validation by participating radiologist)

The participating radiologist opined that (*a*) in the images despeckled by DPAD filter the boundary/margins of the tumor have been preserved/sharpened without affecting the texture of the tumor and without introducing any blocking effect, (*b*) as the margin characteristics are more ill-defined in malignant cases so the marginal increase in Jaccard index for malignant cases (as witnessed in images filtered by DPAD, BayesShrink and Lee Sigma filters) is also clinically significant in comparison to benign cases, (*c*) even though Lee Sigma filtered output is also giving higher value of Jaccard index for malignant cases, a blocking effect has been introduced in the images which is undesirable so these segmented tumor images are not clinically acceptable. Sample images belonging to benign and malignant classes indicating

tumor boundary marked by radiologist and obtained after segmentation are given in Fig. 4.4 for original images and despeckled images.

It has been observed from Fig. 4.4, that the value of Jaccard index has improved after the application of despeckle filtering algorithms for both benign and malignant images.

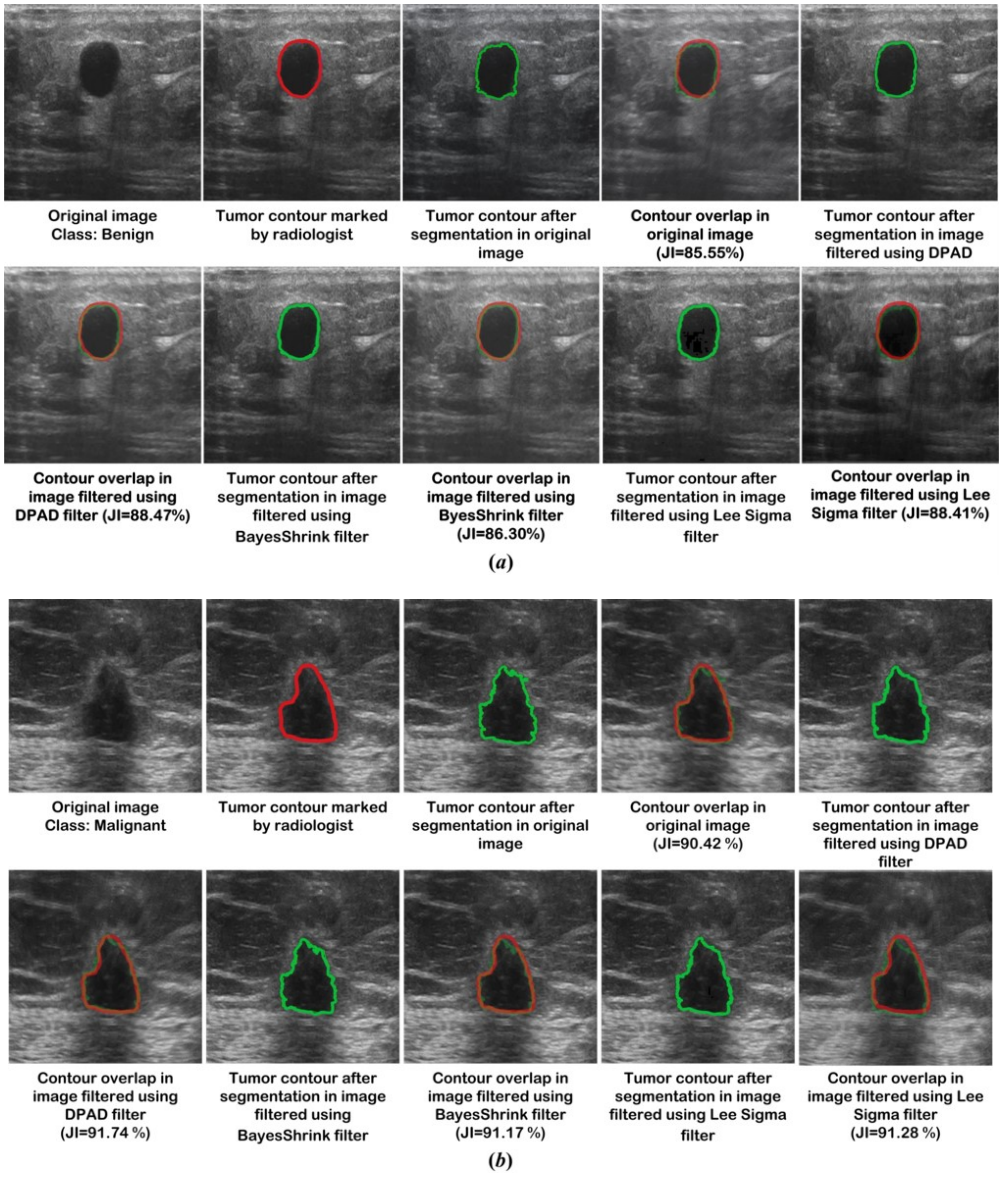

Fig. 4.4 Sample breast ultrasound images indicating tumor boundary marked by radiologist (*red*) and tumor boundary obtained using segmentation algorithm (*green*). (*a*) Benign ultrasound image, (*b*) Malignant ultrasound image.
Note: JI: Jaccard index, DPAD: Detail preserving anisotropic diffusion.

Therefore, according to clinical acceptability criteria as assessed by the participating radiologist, the segmented tumor images yielded by the images despeckled using the DPAD filter are better in terms of clinical acceptability in comparison to other segmented tumor images yielded by BayesShrink and Lee sigma filter.

A comparative analysis of the obtained results for assessment of *06 best performing despeckle filtering algorithms* for breast ultrasound images on the basis of segmentation is shown in Table 4.2.

Table 4.2 Comparative analysis of best performing despeckle filtering algorithms for breast ultrasound images on the basis of segmentation.

Images	Assessment results	
	Objective Assessment (Jaccard Index*)	**Subjective Assessment (Radiologist's Opinion)**
Original images	Benign= 84.04 % Malignant= 75.47 %	The participating radiologist was of the opinion that (*a*) The diagnostic information in US images is masked because of inherent speckle noise and the image despeckled by DPAD filter has been able to sharpen/retain the boundary/margins of the tumor without effecting the texture of the tumor and without introducing any blocking effect. (*b*) As the margin characteristics are more ill-defined in malignant cases so the increase in Jaccard index for malignant cases (as witnessed in images filtered by DPAD, BayesShrink and Lee Sigma filter) is more clinically significant in comparison to benign cases. (*c*) Lee Sigma filtered output is also giving higher value of Jaccard index for malignant cases but introducing blocking effect.
Despeckled images using Lee Sigma filter	Benign= 84.21 % Malignant= 76.14 %	
Despeckled images using FI filter	Benign= 83.99% Malignant= 76.04 %	
Despeckled images using FB filter	Benign= 83.75 % Malignant= 75.97 %	
Despeckled images using HFB filter	Benign= 83.25 % Malignant= 75.98 %	
Despeckled images using BayesShrink filter	Benign= 84.09 % Malignant= 76.19 %	
Despeckled images using DPAD filter	Benign= 84.22 % Malignant= 76.23 %	

Note: *Average value of Jaccard index, FI: Fourier ideal, FB: Fourier Butterworth, HFB: Homomorphic Fourier Butterworth, DPAD: Detail preserving anisotropic diffusion.

The results obtained for both objective and subjective assessment of despeckle filtering algorithms for segmentation of breast tumors from ultrasound images indicate that the ultrasound images filtered using DPAD filter give better segmentation results and are more clinically acceptable.

4.3. Concluding Remarks

Based on the results obtained by exhaustive experimentation carried out in the present work for objective and subjective analysis of despeckle filtering algorithms for the segmentation of breast tumors, it has been noted that the maximum average Jaccard index value has been obtained for images despeckled by DPAD filter. The participating radiologist opined that the DPAD filter retains the tumor boundary/margin without distorting the texture of the tumor region in contrast to the Lee sigma filter that even though attained a similar Jaccard index value for the malignant tumors introduced a blocking effect in the images. Thus based on both objective and subjective assessment, it has been concluded that *DPAD filter yields controlled despeckling of the ultrasound images thus retaining the boundary/margins of the tumor, resulting in better tumor segmentation*.

Due to presence of speckle noise and highly overlapping sonographic appearances of the breast ultrasound tumors the differential diagnosis using conventional gray-scale B-mode ultrasound images is sometimes considerably difficult for experienced radiologists. As discussed earlier, the application of an optimal despeckle filtering algorithm results in the increase in efficiency of the computer-assisted algorithms, therefore the analysis of the effect of *06 best performing despeckle filtering algorithms* on the classification of breast tumors is taken as the next objective of the present research work and is discussed in Chapter 5.

Chapter 5

Effect of Despeckle Filtering Algorithms on Classification of Breast Tumors

5.1. Introduction

The visual quality of ultrasound images is an important factor to effectively diagnose any abnormality present in the body structure. Therefore controlled despeckle filtering i.e. smoothing of homogeneous areas with edge/structure preservation in the images is desired. Accordingly, there is an increasing interest among the research community to design different computer aided diagnostic (CAD) systems using various artificial intelligence based techniques for characterization of breast ultrasound images [58, 62, 90, 162, 218, 253, 264, 273, 285, 298, 310].

It has been noted from the exhaustive survey of literature that the studies conducted for classifying breast tumors have either considered only original images or only pre-processed images for analysis using different features. As both texture and morphological features are considered important for the characterization of breast abnormalities, the studies using both texture and morphological features extracted from either raw or pre-processed images have been exhaustively surveyed in the present research work.

Cristerna et al. [58] analysed the effect of the application of 20 pre-processing algorithms on the classification of breast tumors using Fischer linear discriminant analysis (FLDA) classifier and texture and morphological, features computed from breast tumor ultrasound images segmented by watershed transform. The study reported an accuracy of 84.0 % using images pre-processed by fuzzy enhancement followed by interference based speckle filter.

Verma et al. [273] used different statistical, Laws' and fractal based texture features in combination with morphological features for classification of 188 breast tumor ultrasound images using support vector machine (SVM) classifier. The study reported an accuracy of 86.2 % using an optimal feature set obtained by using majority voting technique on different selected features obtained by applying various filter and wrapper based methods of feature selection.

Daoud et al. [62] reported an accuracy of 98.2 % using SVM classifier and a feature set formed by combining gray level co-occurrence matrix (GLCM) based texture features and morphological features computed from multiple non-overlapping ROIs. The study has been carried out on a set of 110 breast ultrasound images.

Bhusri et al. [21] computed First order statistics (FOS) based texture features and morphological features for classification of 172 breast tumor ultrasound images using SVM classifier and reported an accuracy of 89.6 %.

Zakeri et al. [310] computed correlation based texture features and morphological features from the breast tumor ultrasound images segmented using geodesic active contour method for classification of 80 tumors using SVM classifier and reported an accuracy of 95.0 %.

Wu et al. [285] computed a set of autocovariance based texture features and morphological features from tumor images pre-processed by anisotropic diffusion (AD) filter, stick method and thresholding and segmented by level set method. The study was carried out on 110 images using genetic algorithm (GA) for feature selection and SVM for classification and reported an accuracy of 95.2 %.

Prabusankarlal et al. [218] used non-local means (NLM) filtered breast ultrasound images segmented by Fuzzy C-means clustering for classification of 120 breast tumors images using statistical texture features and Markov random field (MRF) based features along with morphological features. The study reported the classification accuracy of 95.8 % using SVM classifier.

Singh et al. [253] proposed a fuzzy cluster based neural network model, for classification of 178 breast ultrasound images pre-processed using wavelet based despeckle filter. From the extracted regions of interest (ROIs), a set of different texture and morphological features have been computed which has further been reduced by using majority voting applied to features selected by different filter and wrapper based methods of feature selection. The proposed classification system achieved an accuracy of 94.1 %.

The present research work is different from the other related works as a hybrid approach of classification has been tested by utilizing both original and despeckled images [142] while the previous related studies have been carried out either on original images only or on pre-processed images only.

5.2. Experimental Workflow : Effect of Despeckle Filtering Algorithms on Classification of Breast Tumors

The experimental workflow followed for analysing the effect of best performing despeckle filtering algorithms on classification of breast tumors is given in Fig. 5.1.

An attempt has been made to efficiently classify the breast tumors using a combination of texture and morphological features computed from original as well despeckled ultrasound images.

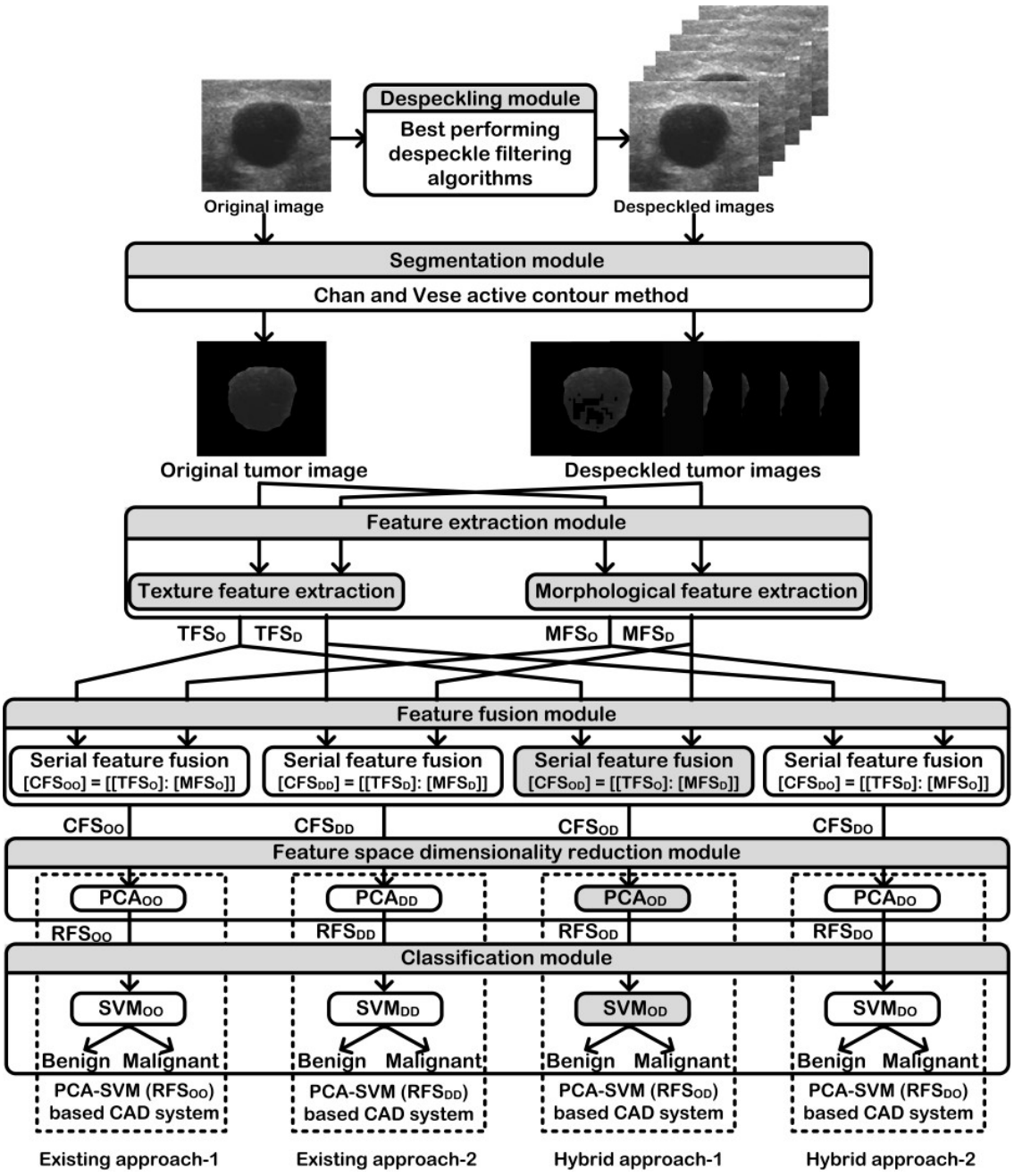

Fig. 5.1 The experimental workflow followed for analysing the effect of best performing despeckle filtering algorithms on classification of breast tumors. ▒ The shaded grey region indicates the optimal CAD system design for classification of breast tumors based on texture features computed from original images and morphological features computed from images despeckled using DPAD filter.

Note: O: Original image, D: Despeckled image, TFS: Texture feature set, MFS: Morphological feature set, CFS: Combined feature set, PCA: Principal component analysis, RFS: Reduced feature set, SVM: Support vector machine.

Four different experiments have been carried out in the present work namely, (*a*) Existing approach-1: Design of PCA-SVM based CAD system using texture and morphological features computed from original images. (*b*) Existing approach-2: Design of PCA-SVM based CAD

system using texture features and morphological features computed from despeckled images. (*c*) Hybrid approach-1: Design of PCA-SVM based CAD system using texture features computed from original images and morphological features computed from despeckled images. (*d*) Hybrid approach-2: Design of PCA-SVM based CAD system using texture features computed from despeckled images and morphological features computed from original images.

5.2.1. Dataset description

For carrying out the experiments in the present work, dataset described in section 3.2.1 of Chapter 3 has been used as presented in Fig. 3.2. The entire image dataset was stored on a 64-bit windows 10 PC with Intel (R) Core (TM) i3-5005U, 2.00 GHz processor and 4.00 GB RAM and the experiments have been conducted using MATLABR2015b.

5.2.2. Despeckling module

In the present work, the ultrasound images have been pre-processed by using *06 best performing despeckle filtering algorithms* obtained in section *3.2.3.2* of *Chapter-3* namely Lee sigma filter, BayesShrink filter, detail preserving anisotropic diffusion (DPAD) filter, Fourier ideal (FI) filter, Fourier Butterworth (FB) filter and Homomorphic Fourier Butterworth (HFB) filter.

5.2.3. Segmentation module

In the present work, to segment the breast tumors from original images and despeckled images, the Chan and Vese active contour method [37] has been used as described in *Chapter-4*.

5.2.4. Feature extraction module

In feature extraction module, visual information in an image is converted into mathematical descriptors. These mathematical descriptors are either based on intensity distribution i.e. texture features or based on shape of the tumor i.e. morphological features or based on the colour information. Based on the type of tissue under examination different features are considered diagnostically important e.g. for analysing the ultrasound images of the breast tissue, radiologists consider both texture as well as shape of the tumors [21, 58, 62, 90, 190, 218, 253, 264, 270, 273, 285, 310] has been used for characterization.

Although different ultrasound machines/settings produce ultrasound images with different resolutions, sufficient evidence is present in the literature highlighting the fact that the size of the region of interest must be at least 800 pixels to provide a good sampling distribution for computing reliable statistics [130].

In the present work, based on the exhaustive literature review and also as opined by the participating radiologist both the texture and morphological features are considered significant for differential diagnosis between benign and malignant tumors [58, 62, 90, 190, 218, 253, 264, 270, 273, 285, 310]. It has been observed that different methods of texture feature extraction like statistical methods, spatial filtering based methods and transform domain based methods combined with conventional morphological features have widely been used [43, 62, 158, 161, 186, 190, 191, 193, 209, 224, 251, 264, 270, 273, 281, 301]. Accordingly in the present work, initially a large feature vector consisting of texture features computed using statistical methods, spatial filtering based methods and transform domain based methods combined with conventional morphological features has been considered for analysis to design an efficient CAD system for classification of breast tumors. The different features computed in the present work are given in Fig. 5.2.

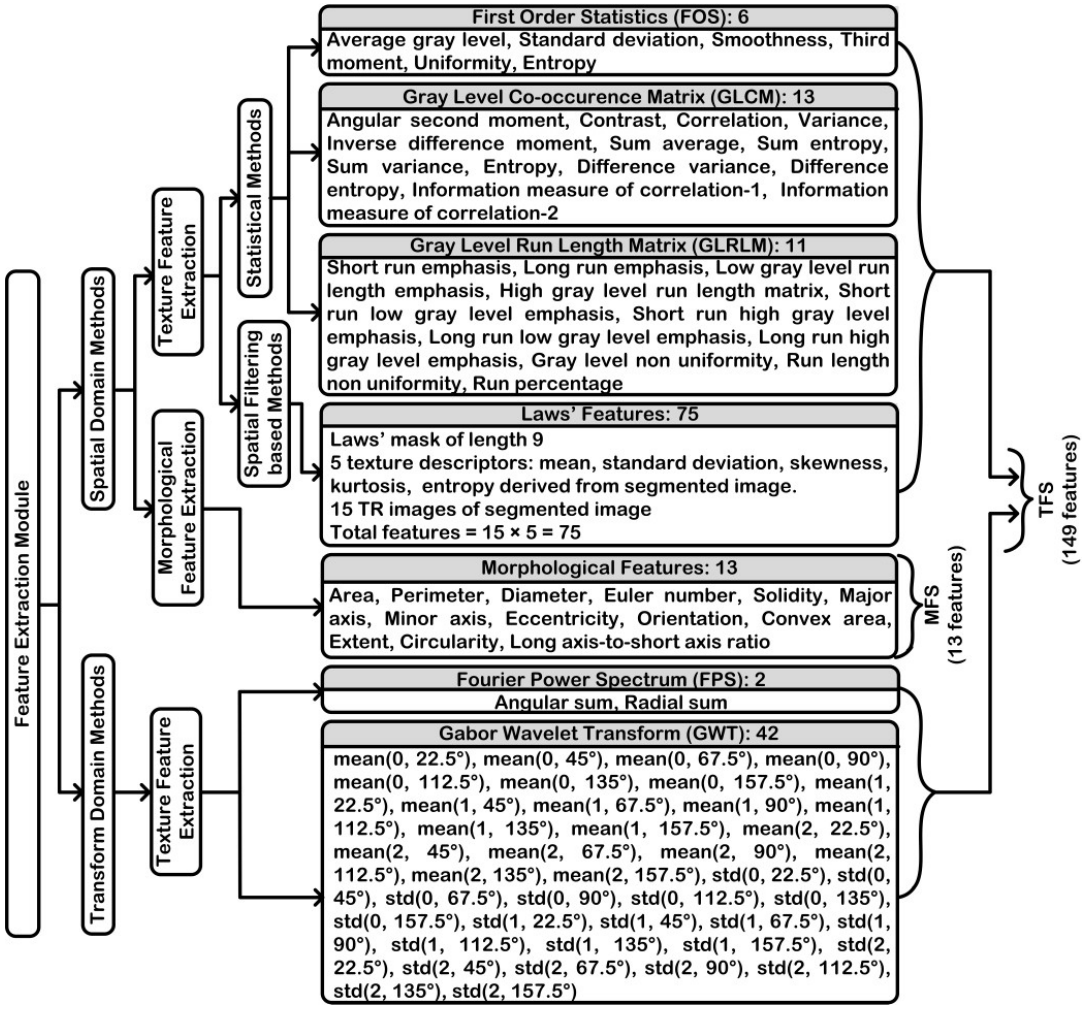

Fig. 5.2 Different features computed in the present work.
Note: TR: Rotation invariant texture image, std: Standard deviation, TFS: Texture feature set, MFS: Morphological feature set.

5.2.4.1. Texture feature extraction

The statistics of the gray level distributions in an image are quantified using texture features. Generally, the methods for texture feature extraction are categorised as statistical methods, spatial filtering based methods and transform domain based methods. In statistical methods, the gray level intensities of the pixels are used to compute the texture features. In spatial filtering based methods, the images are first convolved with some filters to enhance particular properties and then the statistics of the gray level distribution are computed. In transform domain methods, the image is first transformed to frequency domain at different scales and orientations and then the texture information at these scales and orientations is computed. A brief description of different texture features computed in the present work is given here.

(*a*) *Statistical methods of feature extraction*

(*i*) First order statistics (FOS): In this method the texture features are computed from the intensity histogram of the image [81, 158,186, 194, 209, 259, 264, 273, 301]. A total of 06 FOS features have been computed from each image.

(*ii*) Gray level co-occurrence matrix (GLCM): In this method, the texture of an image is characterized on the basis of the spatial relationship between two pixels. The co-occurrence matrix is formed by finding the number of occurrences of different combinations of a pair of pixels with a particular gray level for a specified direction (θ), inter-pixel distance (d) and the statistics are computed from the resultant matrix [9, 43, 89, 137, 154, 158, 190-192, 194, 209, 233, 264, 281]. In the present work, the GLCM features have been computed using four different directions (θ = 0°, 45°, 90°, 135°) and inter-pixel distance d = 5. The final texture features are computed by taking the mean of the features computed for all four directions, e.g. let F1 be any feature computed using GLCM then the final mean feature F1 is given as

$$F1_{mean} = \frac{F1_{0^\circ} + F1_{45^\circ} + F1_{90^\circ} + F1_{135^\circ}}{4} \tag{5.1}$$

A total of 13 GLCM features have been computed from each image.

(*iii*) Gray level run length matrix (GLRLM): In this method, the texture characterization is done on the basis of the spatial relationship between more than two pixels. The GLRL matrix is formed by computing the number of consecutive pixels of a particular gray level occurring in a specific direction [158, 209, 233]. In the present work, the GLRLM features have been computed using four different directions (θ = 0°, 45°, 90°, 135°) and the final texture features are computed by taking the mean of the features computed for all four directions. A total of 11 GLRLM features have been computed from each image.

(*b*) *Spatial filtering based methods*

(*i*) Laws' mask analysis: In this spatial filtering based method, 1D filters of different resolutions (i.e. 3, 5, 7 and 9) have been used to enhance the different underlying properties of the images, like level, edges, spots, ripples and waves [58, 140, 251, 253, 254, 273]. These 1D filters are used to form 2D filter masks using convolution operation and the resultant 2D masks are then convolved with the images. The different 1D filters used and corresponding 2D masks formed are given in Fig. 5.3.

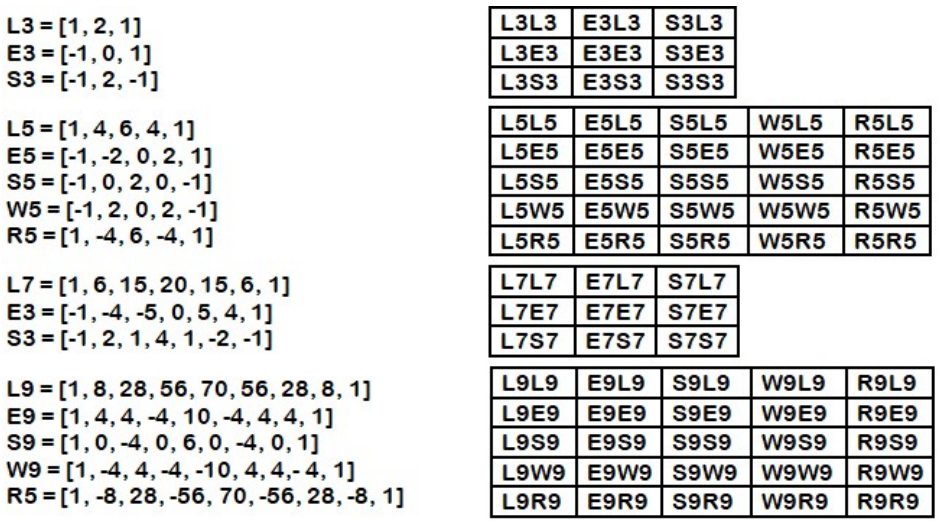

Fig. 5.3 Laws' 1D filters and their corresponding 2D masks.

In the present work, Laws' mask of length 9 has been used for analysis. The steps followed in Laws' mask analysis for the computation of texture features is represented in Fig. 5.4. A total of 75 Laws' texture features (15 TRs × 5 statistical parameters) are computed for each image.

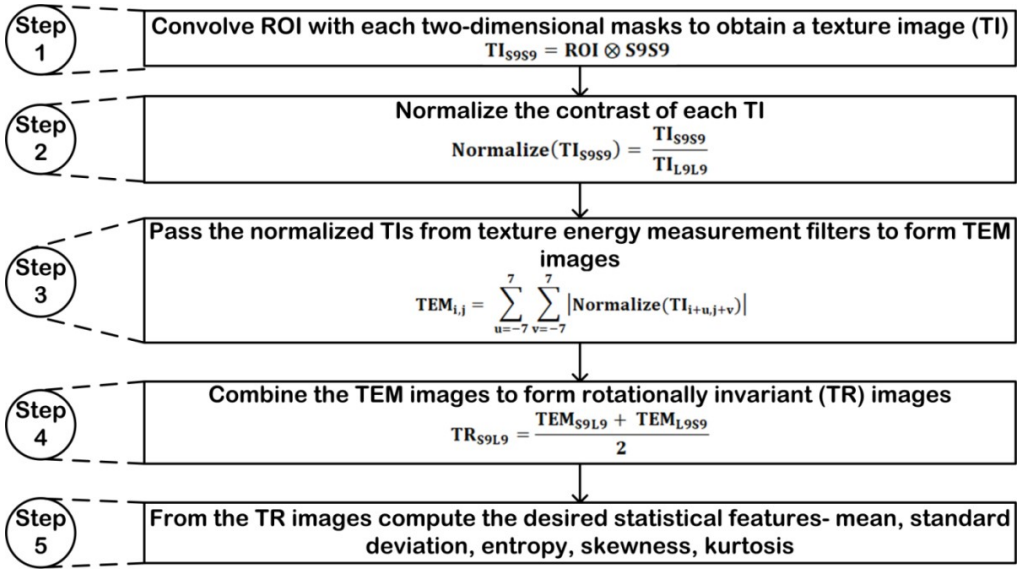

Fig. 5.4 Steps followed in Laws' mask analysis.

(*c*) *Transform domain based methods*

(*i*) Fourier power spectrum (FPS): In this method, the images are first transformed into frequency domain using discrete Fourier transform and then from the transformed images radial sum and angular sum have been computed as features. A total of 02 FPS features have been computed from each image.

(*ii*) 2D-Gabor wavelet transform (2D-GWT): In this method, Gabor functions are used to process the images. The Gabor functions are formed by performing dilation and shifting operations on the mother wavelet. As a result of application of 2D-GWT, a set of filters are obtained that are frequency and orientation selective [199, 226]. The images are convolved with these filters resulting in the formation of feature images. In the present work, 3 scales (0, 1, 2) and seven orientations (22.5^o, 45^o, 67.5^o, 90^o, 112.5^o, 135^o and 157.5^o) have been used to obtain 21 different Gabor filters. The real part of the 21 wavelets resulting from a 13 × 13 convolution mask with 3 scales and 7 orientations as shown in Fig 5.5.

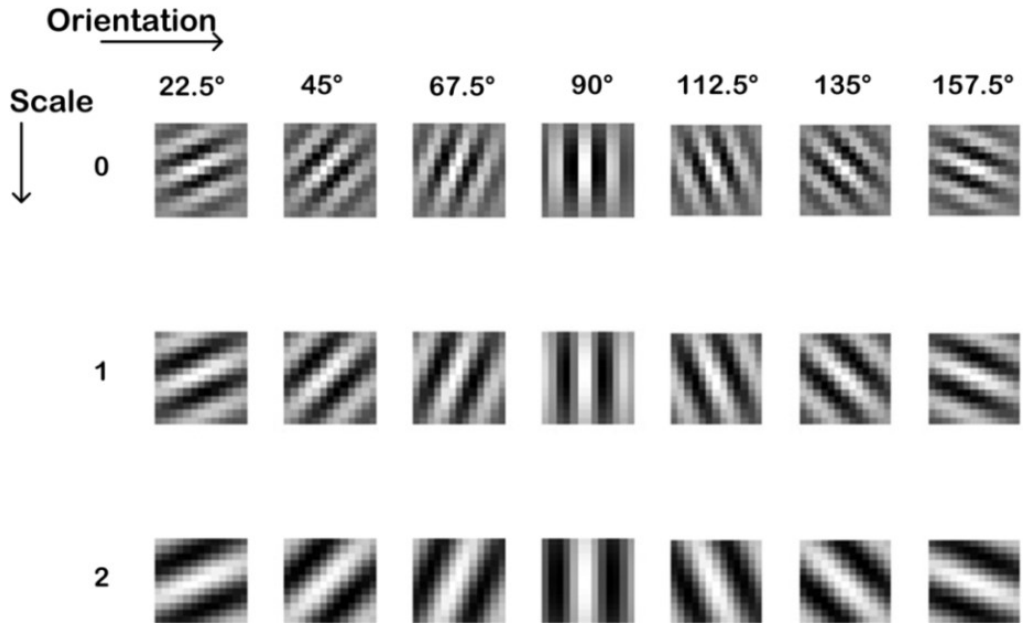

Fig. 5.5 Real part of the 21 wavelets with 3 scales and 7 orientations.

These filters are then convolved with the segmented images to obtain 21 feature images for each segmented image. From these 21 feature images, two texture descriptors namely mean and standard deviation have been computed. A total of 42 Gabor based features have been computed from each image.

5.2.4.2.Computation of texture feature set

By combining the above 149 texture features (6 FOS + 13 GLCM + 11 GLRLM + 75 Laws' + 2 FPS + 42 GWT), a texture feature set (TFS) is computed using all the images.

5.2.4.3. Morphological feature extraction

The morphological features represent the shape and margin characteristics of the tumor. It has been well established that shape and margin information plays a significant role in differentiation of breast tumors [40] *i.e.* benign tumors have a smooth and well-defined margin while malignant tumors have an ill-defined margin. Accordingly, different morphological features have been computed in the present work.

A brief description of the computed morphological features is given here.

(*a*) Area: The number of pixels in the tumor region [12, 62, 253], given as:

$$Area = \sum Pixels_{tumor} \tag{5.2}$$

(*b*) Perimeter: The distance of the tumor boundary [12, 62, 253], given as:

$$Perimenter = \sum Pixels_{tumor\ contour} \tag{5.3}$$

(*c*) Equivalent diameter: The diameter of the circle having equivalent area as that of the tumor [21, 226].

(*d*) Convex area: The number of pixels present in the convex hull of the tumor [62, 218, 286, 287, 310], given as:

$$Convex\ area = \sum Pixels_{tumor\ convex-hull} \tag{5.4}$$

Here, the convex hull represents a set of pixels included in the smallest convex polygon surrounding the white pixels in a binary image.

(*e*) Euler number: The number of objects in a region minus the holes in that object [21].

(*f*) Solidity: The ratio of tumor area to convex hull area [62, 218, 286, 287, 310], given as:

$$Solidity = \frac{Area}{Convex\ area} \tag{5.5}$$

(*g*) Major axis: The length of the major axis of the ellipse i.e. number of pixels in the longest axis [12, 21].

(*h*) Minor axis: The length of the minor axis of the ellipse i.e. number of pixels in the shortest axis [12, 21].

(*i*) Eccentricity: The ratio of the distance between center of ellipse and its focus to the length of its major axis [43], given as:

$$Eccentricity = \frac{Distance\ from\ center\ of\ ellipse\ and\ focus}{Length_{major\ axis}} \tag{5.6}$$

(*j*) Orientation: The angle between horizontal axis and the major axis of ellipse [21].

(*k*) Extent: The ratio of tumor area to the area of the bounding rectangle of the tumor [154, 285, 286], given as:

$$Extent = \frac{Area}{Bounding\ rectangle} \tag{5.7}$$

(*l*) Circularity: The ratio of square of perimeter to area of the tumor [12, 21, 218, 253], given as:

$$Circularity = \frac{Perimeter^2}{Area} \tag{5.8}$$

(*m*) Long axis-to-short axis ratio (LS_{ratio}): The ratio of length of major axis to length of minor axis [12, 161], given as:

$$LS_{ratio} = \frac{Length_{major\ axis}}{Length_{minor\ axis}} \tag{5.9}$$

The sample image showing the convex hull (used for calculating convex area and solidity), bounding rectangle (used for calculating extent) and ellipse (used for computing lengths of major axis and minor axis, eccentricity, long-axis-to-short axis ratio) of the tumor along with tumor boundary is given in Fig. 5.6.

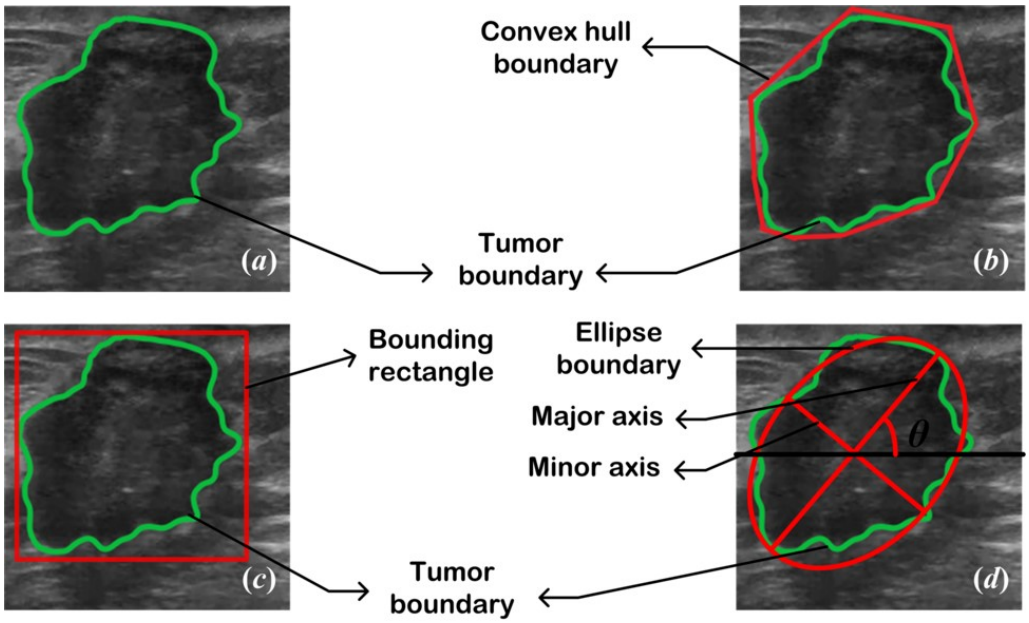

Fig. 5.6 Sample tumor image with (*a*) Convex hull boundary and tumor boundary marked, (*b*) Bounding rectangle and tumor boundary marked, (*c*) Ellipse boundary, axis and tumor boundary marked.

5.2.4.4. Computation of morphological feature set

By combining the above 13 morphological features a morphological feature set (MFS) is computed using all the images.

5.2.5. Feature fusion module

In feature fusion, different feature sets can be combined together to obtain a single feature set. The feature fusion techniques used can either be serial fusion, parallel fusion or weighted

fusion. In serial feature fusion the features of different features sets are simply concatenated one after the other (union operation) to obtain a combined feature set (CFS) [7]. In case of parallel feature fusion, different feature sets are combined to obtain a single feature set with the help of a complex vector [7]. In case of weighted some features which are diagnostically more important than other features are assigned a weight and then fused using serial or parallel fusion techniques. The diagnostically important features can be short listed from a set of features based on the input from experienced radiologists. In the present work, the computed texture and morphological feature sets have been combined to obtain a CFS using serial feature fusion. Let there be three individual feature sets FS_1 (l_1), FS_2 (l_2), FS_3 (l_3). Here, FS is the feature set and l is the length of feature vector. The combined feature set formed using serial fusion is given as CFS (l) = [FS_1 FS_2 FS_3] ($l_1 + l_2 + l_3$) with the length of CFS being $l = l_1 + l_2 + l_3$. The process of serial feature fusion is represented in Fig. 5.7.

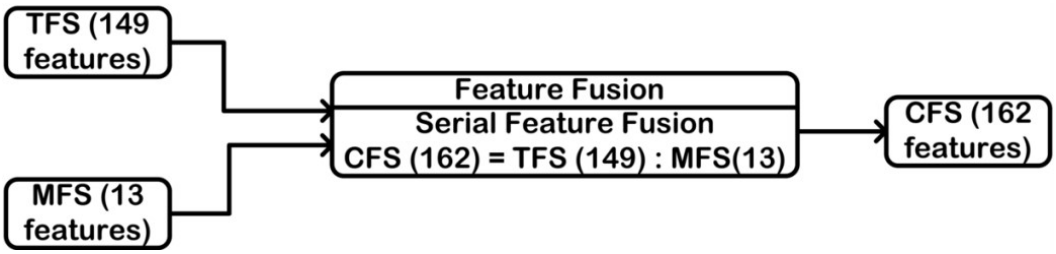

Fig. 5.7 Serial feature fusion.
Note: TFS: Texture feature set, MFS: Morphological feature set, CFS: Combined feature set.

5.2.6. Feature space dimensionality reduction module

After the process of feature extraction the resultant feature set may contain some features that are correlated to each other. These features are redundant and do not provide any useful information for differentiation between the benign and malignant tumors. In the present work, principal component analysis (PCA) has been used to reduce the dimensionality of the input feature space thus finding the optimal principal components (PCs) useful for classification task [12, 140, 198, 274, 282]. The steps followed in PCA algorithm are represented in Fig. 5.8.

The optimal number of PCs to be retained for classification task is determined empirically by carrying out recurrent experimentation and stepping through first few PCs $\in$ {2, 3, …,15} to build the classification model [139].

The steps followed for building the final SVM model using PCA-SVM algorithm are given in Fig. 5.9.

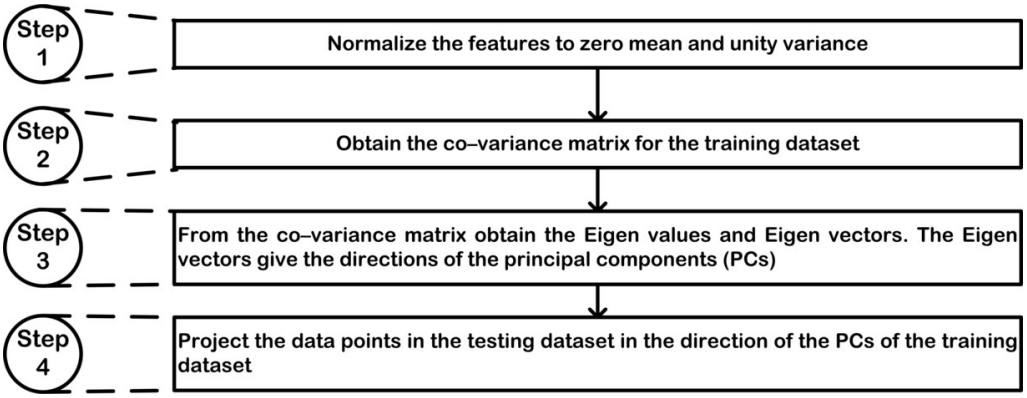

Fig. 5.8 Steps followed in PCA algorithm.

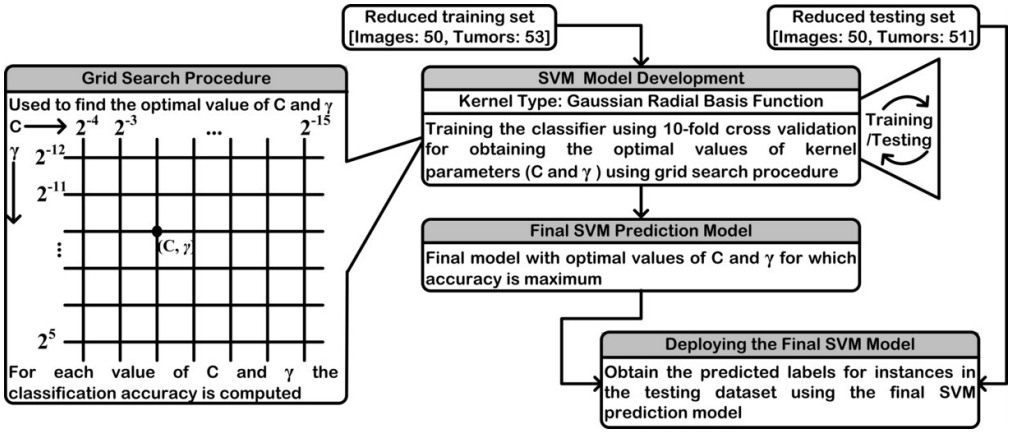

Fig. 5.9 The steps followed for building the final SVM model using PCA-SVM algorithm.

5.2.7. Classification module

The support vector machine (SVM) is a kernel based classifier used popularly for machine learning tasks involving classification specifically in case of breast ultrasound images [32, 62, 111, 113, 115, 133, 137, 154, 186, 198, 209, 218, 236, 237, 248, 273, 285-287, 298, 301, 310, 321]. Accordingly, in the present work SVM classifier has extensively been used to develop various classification models. In this classifier, the instances are separated into disjoint classes in feature space using a hyper-plane that maximises the margin between two classes. The SVM classifier has been implemented using LibSVM library [38]. The non-linear data has been mapped to the higher dimensionality feature space using Gaussian radial basis function (GRBF) kernel.

5.3. Experiments and Results

For developing an efficient CAD system for classification of breast tumors, exhaustive experiments have been conducted in the present work using both existing and hybrid approaches of CAD system designs. The conducted experiments are described in Table 5.1.

Table 5.1 Description of experiments for the design of PCA-SVM based CAD systems.

Experiment 1	Design of PCA-SVM based CAD system using texture and morphological features computed from original images (Existing approach-1).
Experiment 2	Design of PCA-SVM based CAD system using texture features and morphological features computed from despeckled images (Existing approach-2).
Experiment 3	Design of PCA-SVM based CAD system using texture features computed from original images and morphological features computed from despeckled images (Hybrid approach-1).
Experiment 4	Design of PCA-SVM based CAD system using texture features computed from despeckled images and morphological features computed from original images (Hybrid approach-2).

5.3.1. Experiment 1: Existing approach-1: Design PCA-SVM based CAD system using texture and morphological features computed from original images

For carrying out this experiment, different texture features and morphological features have been computed from original images. These features have been combined to form CFS_{OO} that has then been used for classification of breast tumors using PCA-SVM algorithm. The results of the classification for Experiment-1 are shown in Table 5.2.

Table 5.2 Classification results of PCA-SVM based CAD system using texture and morphological features computed from original images (Existing approach-1).

CAD system (FS: *l*)	**CM**			**Accuracy (%)**	**ICA_B (%)**	**ICA_M (%)**
PCA-SVM based CAD system (RFS_{OO}: 10)		B	M	94.1	90.4	96.6
	B	19	2			
	M	1	29			

Note: FS: Features set, *l*: No. of optimal PCs, PCA: Principal component analysis, RFS: Reduced feature set, SVM: Support vector machine, O: Original image, CM: Confusion matrix, ICA: Individual class accuracy, B: Benign class, M: Malignant class.

From Table 5.2, it has been noted that using the feature set RFS_{OO} obtained by applying PCA-SVM to CFS_{OO} containing texture and morphological features computed from original images, a classification accuracy of 94.1 % has been achieved. The individual class accuracy (ICA) values obtained for the benign and malignant classes are 90.4 % and 96.6 %, respectively. Out of 51 testing instances, 3 instances have been classified incorrectly.

5.3.2. Experiment 2: Existing approach-2: Design of PCA-SVM based CAD system using texture and morphological features computed from despeckled images

For carrying out this experiment, *06 best performing despeckle filtering algorithms* have been used. Different texture features and morphological features have been computed from despeckled images. These features have been combined to form CFS_{DD} for each filter that has then been used for classification of breast tumors using PCA-SVM algorithm. The results of the classification for Experiment-2 are shown in Table 5.3.

Table 5.3 Classification results of PCA-SVM based CAD system using texture and morphological features computed from despeckled images (Existing approach-2).

CAD system (FS: *l*)	**CM**			**Accuracy (%)**	**ICA_B (%)**	**ICA_M (%)**
PCA-SVM based CAD system ($RFS_{DD(Lee\ sigma)}$: 6)		B	M	60.7	61.9	60.0
	B	13	8			
	M	12	18			

PCA-SVM based CAD system ($RFS_{DD(BayesShrink)}$: 9)	B	12	9	64.7	57.1	73.3
	M	8	22			
PCA-SVM based CAD system ($RFS_{DD(DPAD)}$: 9)	B	11	10	64.7	52.3	73.3
	M	8	22			
PCA-SVM based CAD system ($RFS_{DD(FI)}$: 5)	B	14	7	66.6	66.6	66.6
	M	10	20			
PCA-SVM based CAD system ($RFS_{DD(FB)}$: 4)	B	10	11	66.6	47.6	80.0
	M	6	24			
PCA-SVM based CAD system $RFS_{DD(HFB)}$: 8)	B	11	10	62.7	52.3	70.0
	M	9	21			

Note: FS: Feature set, *l*: No. of optimal PCs, PCA: Principal component analysis, RFS: Reduced feature set, SVM: Support vector machine, D: Despeckled image, CM: Confusion matrix, ICA: Individual class accuracy, B: Benign class, M: Malignant class, DPAD: Detail preserving anisotropic diffusion, FI: Fourier ideal, FB: Fourier ideal, HFB: Homomorphic Fourier Butterworth.

From Table 5.3 it has been noted that using the feature set $RFS_{DD(FB)}$ obtained by applying PCA to $CFS_{DD(FB)}$ containing texture and morphological features computed from images despeckled using FB filter, a classification accuracy of 66.6 % has been achieved. The ICA values obtained for the benign and malignant classes are 47.6 % and 80.0 %, respectively. Out of 51 testing instances, 17 instances have been classified incorrectly. It is worth noting that same accuracy of 66.6 % has also been achieved using the feature set $RFS_{DD(FI)}$ obtained by applying PCA to $CFS_{DD(FI)}$ containing texture and morphological features computed from images despeckled using FI filter but the ICA value for the malignant class is less in comparison to the feature set $RFS_{DD(FB)}$ and any CAD system developed for medical images should be able to correctly classify the maximum number of malignant instances.

5.3.3. Experiment 3: Hybrid approach-1: Design of PCA-SVM based CAD system using texture features computed from original images and morphological features computed from despeckled images

For carrying out this experiment, *06 best performing despeckle filtering algorithms* have been used. Different texture features have been computed from original images and morphological features have been computed from despeckled images. These features have been combined to form a CFS_{OD} for each filter that has then been used for classification of breast tumors using PCA-SVM algorithm. The results of the classification for Experiment-3 are shown in Table 5.4.

Table 5.4 Classification results of PCA-SVM based CAD system using texture features computed from original images and morphological features computed from despeckled images (Hybrid approach-1).

CAD system (FS: *l*)		**CM**		**Accuracy (%)**	**ICA_B (%)**	**ICA_M (%)**
		B	M			
PCA-SVM based CAD system ($RFS_{OD(Lee\ sigma)}$:10)	B	19	2	92.1	90.4	93.3
	M	2	28			
PCA-SVM based CAD system ($RFS_{OD(BayesShrink)}$: 10)	B	18	3	92.1	85.7	96.6
	M	1	29			
PCA-SVM based CAD system ($RFS_{OD(DPAD)}$:	B	20	1	96.0	95.2	96.6

11)	M	1	29			
PCA-SVM based CAD system ($RFS_{OD(FI)}$: 10)	B	19	2	92.1	90.4	93.3
	M	2	28			
PCA-SVM based CAD system ($RFS_{OD(FB)}$: 11)	B	19	2	94.1	90.4	96.6
	M	1	29			
PCA-SVM based CAD system ($RFS_{OD(HFB)}$: 13)	B	19	2	94.1	90.4	96.6
	M	1	29			

Note: FS: Feature set, *l*: No. of optimal PCs, PCA: Principal component analysis, RFS: Reduced feature set, SVM: Support vector machine, O: Original image, D: Despeckled image, CM: Confusion matrix, ICA: Individual class accuracy, B: Benign class, M: Malignant class, DPAD: Detail preserving anisotropic diffusion, FI: Fourier ideal, FB: Fourier ideal, HFB: Homomorphic Fourier Butterworth.

From Table 5.4 it has been noted that using the feature set $RFS_{OD(DPAD)}$ obtained by applying PCA to $CFS_{OD(DPAD)}$ containing texture and morphological features computed from images despeckled using DPAD filter, a classification accuracy of 96.0 % has been achieved. The ICA values obtained for the benign and malignant classes are 95.2 % and 96.6 %, respectively. Out of 51 testing instances, 2 instances have been classified incorrectly.

5.3.4. Experiment 4: Hybrid approach-2: Design of PCA-SVM based CAD system using texture features computed from despeckled images and morphological features computed from original images

For carrying out this experiment, *06 best performing despeckle filtering algorithms* have been used. Different texture features have been computed from despeckled images and morphological features have been computed from original images. These features have been combined to form a CFS_{DO} for each filter that has then been used for classification of breast tumors using PCA-SVM algorithm. The results of the classification for Experiment-4 are shown in Table 5.5.

Table 5.5 Classification results of PCA-SVM based CAD system using texture features computed from despeckled images and morphological features computed from original images (Hybrid approach-2).

CAD system (FS: *l*)	**CM**			**Accuracy (%)**	**ICA_B (%)**	**ICA_M (%)**
		B	M			
PCA-SVM based CAD system ($RFS_{DO\ (Lee\ sigma)}$: 3)	B	13	8	68.6	61.9	73.3
	M	8	22			
PCA-SVM based CAD system ($RFS_{DO\ (BayesShrink)}$: 5)	B	8	13	60.7	38.0	76.6
	M	7	23			
PCA-SVM based CAD system ($RFS_{DO\ (DPAD)}$: 9)	B	10	11	66.6	47.6	80.0
	M	6	24			
PCA-SVM based CAD system ($RFS_{DO\ (FI)}$: 5)	B	14	7	66.6	66.6	66.6
	M	10	20			
PCA-SVM based CAD system ($RFS_{DO\ (FB)}$: 5)	B	15	6	66.6	71.4	63.3
	M	11	19			
PCA-SVM based CAD system ($RFS_{DO\ (HFB)}$: 5)	B	10	11	66.6	47.6	80.0
	M	6	24			

Note: FS: Feature set, *l*: No. of optimal PCs, PCA: Principal component analysis, RFS: Reduced feature set, SVM: Support vector machine, D: Despeckled image, O: Original image, CM: Confusion matrix, ICA: Individual class accuracy, B: Benign class, M: Malignant class, DPAD: Detail preserving anisotropic diffusion, FI: Fourier ideal, FB: Fourier ideal, HFB: Homomorphic Fourier Butterworth.

From Table 5.5 it has been noted that using the feature set $RFS_{DO(Lee\ sigma)}$ obtained by applying PCA to $CFS_{DO(Lee\ sigma)}$ containing texture features computed from images despeckled by Lee Sigma filter and morphological features computed from original images, a classification accuracy of 68.6 % has been achieved. The ICA values obtained for the benign and malignant classes are 61.9 % and 73.3 %, respectively. Out of 51 testing instances, 16 instances have been classified incorrectly.

After conducting exhaustive experiments with existing and hybrid approaches it was observed that the underlying textural features are better preserved in original images where as the morphological features are better preserved in despeckled images. However in the hybrid approach 2, texture features were computed from despeckled images and morphological features were computed from original images. The distorted underlying texture information in the despeckled images is a significant factor due to which lower classification accuracy is obtained in this case. The reason for the gap between the accuracy values can be attributed to the fact that there are significant differences between morphological features of benign and malignant breast tumors.

5.3.5. Results: Individual texture feature sets computed from original and despeckled images and individual morphological feature sets computed from original and despeckled images

For classification of breast tumors using ultrasound images, initially PCA-SVM algorithm has been applied to individual texture feature sets and individual morphological feature sets computed from original as well as despeckled images. The results obtained by individual texture feature sets and morphological features sets computed from original as well as despeckled images are shown in Table 5.6.

Table 5.6 Results obtained by individual texture feature sets and individual morphological features sets computed from original as well as despeckled images.

CAD system	Accuracy (%) (*l*)	CAD system	Accuracy (%) (*l*)
PCA-SVM (TFS_O)	90.1 (10)	PCA-SVM (MFS_O)	62.7 (5)
PCA-SVM ($TFS_{D\ (Lee\ sigma)}$)	70.6 (2)	PCA-SVM ($MFS_{D\ (Lee\ sigma)}$)	66.6 (2)
PCA-SVM ($TFS_{D\ (BayesShrink)}$)	62.7 (6)	PCA-SVM ($MFS_{D\ (BayesShrink)}$)	68.5 (8)
PCA-SVM ($TFS_{D\ (DPAD)}$)	64.7 (5)	PCA-SVM ($MFS_{D\ (DPAD)}$)	70.5 (6)
PCA-SVM ($TFS_{D\ (FI)}$)	60.7 (2)	PCA-SVM ($MFS_{D\ (FI)}$)	68.5 (6)
PCA-SVM ($TFS_{D\ (FB)}$)	64.7 (5)	PCA-SVM ($MFS_{D\ (FB)}$)	66.6 (4)
PCA-SVM ($TFS_{D\ (HFB)}$)	68.6 (2)	PCA-SVM ($MFS_{D\ (HFB)}$)	64.7 (6)

Note: PCA: Principal component analysis, SVM: Support vector machine, O: Original image, D: Despeckled image, TFS: Texture feature set, MFS: Morphological feature set, *l*: No. of optimal PCs, DPAD: Detail preserving anisotropic diffusion, FI: Fourier ideal, FB: Fourier Butterworth, HFB: Homomorphic Fourier Butterworth.

From Table 5.6, it can be observed that (*a*) texture information is not effectively preserved in the despeckled images as is evident from the fact that maximum classification accuracy of 90.1 % is achieved using original texture features in comparison with the

maximum classification accuracy of 70.6 % achieved using despeckled texture features (Lee sigma). (*b*) The shape/margin characteristics of the tumors are enhanced in the despeckled images as compared to the original images as is evident from the fact that the despeckled morphological features yielded higher accuracy in all cases in comparison with the original morphological features. It can be noted that the maximum classification accuracy of 70.5 % has been obtained by using despeckled morphological features (DPAD).

5.3.6. Comparative analysis of PCA-SVM based CAD system designs implemented in the present work using existing approaches and hybrid approaches

A comparative analysis of the results obtained for PCA-SVM based CAD system designs implemented in the present work using existing approaches and hybrid approaches is shown in Table 5.7.

Table 5.7 Comparative analysis of the results of PCA-SVM based CAD system designs implemented in the present work using existing approaches and hybrid approaches.

CAD system (FS: *l*)		CM		Accuracy (%)	ICA_B (%)	ICA_M (%)
		B	M			
Existing approach-1: PCA-SVM based CAD system (RFS_{OO} : 10)	B	19	2	94.1	90.4	96.6
	M	1	29			
Existing approach-2: PCA-SVM based CAD system ($RFS_{DD(FB)}$: 4)	B	10	11	66.6	47.6	80.0
	M	6	24			
Hybrid approach-1: PCA-SVM based CAD system ($RFS_{OD(DPAD)}$: 11)	B	20	1	96.0	95.2	96.6
	M	1	29			
Hybrid approach-2: PCA-SVM based CAD system ($RFS_{DO\ (Lee\ sigma)}$: 3)	B	13	8	68.6	61.9	73.3
	M	8	22			

Note: FS: Feature set, *l*: Length of feature set, PCA: Principal component analysis, RFS: Reduced feature set, SVM: Support vector machine, B: Benign class, M: Malignant class, O: Original image, D: Despeckled image, CM: Confusion matrix, ICA: Individual class accuracy.

The shaded grey region indicates the optimal PCA-SVM based CAD system using texture features computed from original images and morphological features computed from images despeckled using DPAD filter.

It can be noted from Table 5.7, that the feature set $RFS_{OD(DPAD)}$ obtained by applying PCA-SVM algorithm to $CFS_{OD(DPAD)}$ consisting of texture features computed from original images and morphological features computed from images despeckled by DPAD filter achieved maximum accuracy of 96.0 % for classification of breast tumors using ultrasound images. The ICA values obtained for the benign and malignant classes are 95.2 % and 96.6 %, respectively. Out of 51 testing instances, only 2 instances have been misclassified. It can also be noted that in case of experiments where texture information has been computed from the images after the application of despeckle filtering algorithms, the classification performance has degraded in comparison to the experiments where the texture information has been computed from the original images. An increase of 1.9 % is noted in the accuracy when texture information is computed from original images and the shape information is computed from images despeckled by DPAD filter in comparison to the experiment when both the texture and

shape features are computed from original images. It can also be noted that the sensitivity of malignant cases remains same for both the experiments and an increase of 4.8 % is noted in the ICA value of benign cases when texture information is computed from original images and the morphological information is computed from images despeckled by DPAD filter.

The existing approach-2 uses both texture and morphological features computed from despeckled images, however after conducting the exhaustive experiments it was observed that the underlying textural features are better preserved in original images where as the morphological features better preserved in despeckled images. The authors feel that this is the reason for disparity in existing approach-2 which attributed to significantly lower values of accuracy obtained using this approach.

The performance of the PCA-SVM based CAD system designs implemented in the present work can be represented pictorially in terms of ROC curves along with their AUC values as given in Fig. 5.10. The ROC analysis has been carried out using ROCR library of the R package [219].

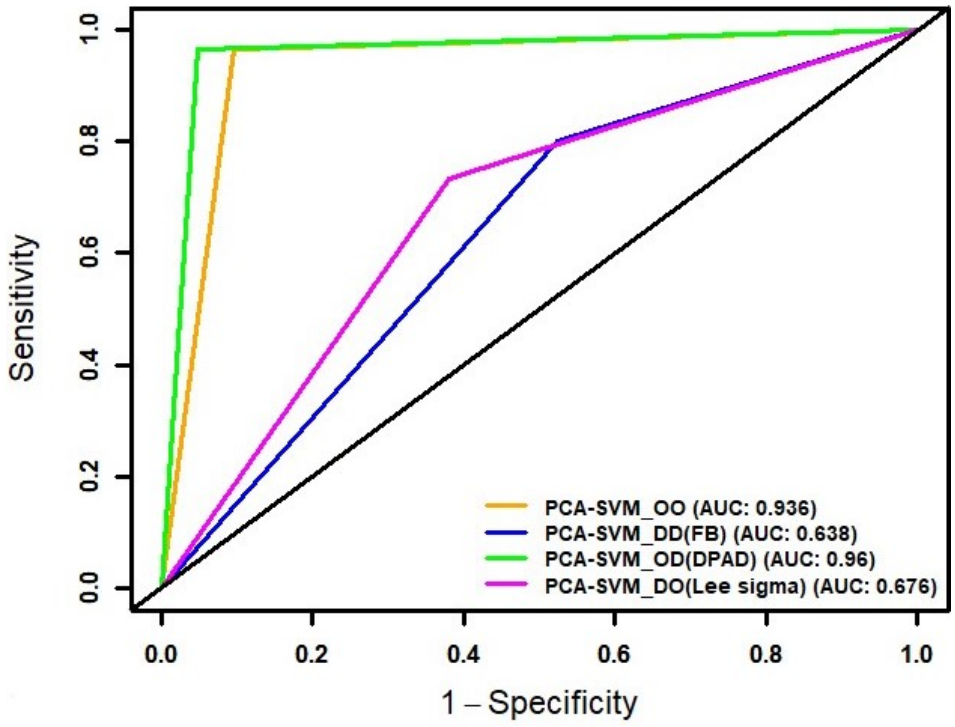

Fig. 5.10 ROC curves for PCA-SVM based CAD system designs implemented in the present work along with their AUC values.

The optimal PCA-SVM based CAD system design for classification of breast tumors is given in Fig. 5.11.

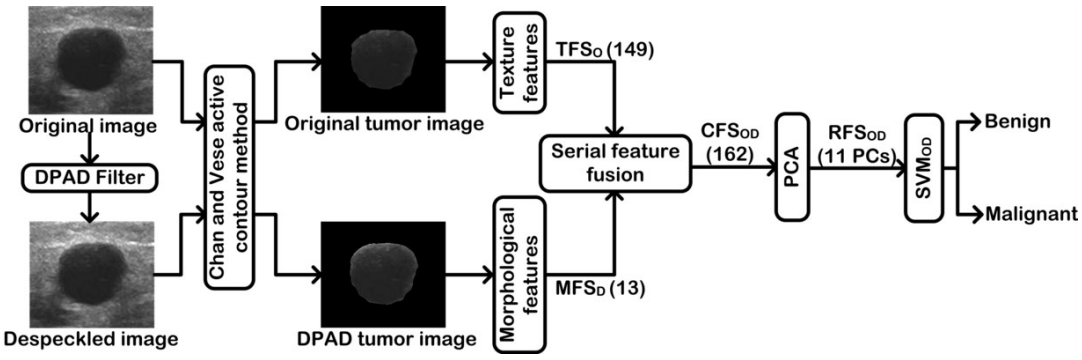

Fig. 5.11 Optimal PCA-SVM based CAD system design for classification of breast tumors.
Note: DPAD: Detail preserving anisotropic diffusion, O: Original image, D: Despeckled image, TFS: texture feature set, MFS: Morphological feature set, CFS: Combined feature set, PCA: Principal component analysis, RFS: Reduced feature set, SVM: Support vector machine.

5.4. Concluding Remarks

From the results of the exhaustive experiments conducted in the present work, following points have been concluded: (*a*) For differential diagnosis between benign and malignant breast tumors using ultrasound images, the texture of the region inside the tumor as well as the shape/margin characteristics of the tumor are important. (*b*) By the application of despeckle filtering algorithms, the texture information in the region inside the tumor is not preserved resulting in poor accuracy when texture information is extracted. (*c*) The features representing the shape/margin characteristics of the tumor are better exhibited by the application of DPAD despeckle filtering algorithms. Thus based on the points above, maximum accuracy for differential diagnosis between breast tumors is obtained when texture information is computed from original images and shape/margin characteristics are derived from the images after the application of DPAD despeckle filtering algorithm.

The exhaustive experimentation carried out in the present work to design an efficient PCA-SVM based CAD system for differential diagnosis between benign and malignant breast ultrasound tumors indicate that texture features computed from original images combined with morphological features computed from images despeckled by DPAD filter yield best results. *Therefore, for further experimentation original images have been used to compute texture features while images despeckled by DPAD filter have been used to compute morphological features.*

Also based on the exhaustive review of literature, it has been observed that local binary pattern (LBP) based texture descriptors have been used widely for texture quantification in medical images [53, 94, 119, 134, 146, 152, 196, 210, 256, 265, 266]. For classification of breast tumors using ultrasound images the LBP based texture features have been used for

texture quantification [2, 32, 185, 198] and subsequent classification. However, the performance of LBP based texture features combined with morphological features for breast tumor classification has not been tested yet. *Accordingly in the next chapter, experiments have been conducted exhaustively to design an efficient CAD system by computing texture features from original images and morphological features computed from images despeckled using DPAD filter.*

Chapter 6

LBP based CAD System Designs for Classification of Breast Tumors

6.1. Introduction

For diagnosing breast abnormalities using ultrasound images, many attempts have been made by the researchers in the past to design efficient computer-aided diagnostic (CAD) systems in order to enhance the diagnostic potential of B-mode ultrasound imaging modality for the diagnosis of breast tumors [58, 62, 90, 162, 218, 253, 273, 285, 298, 310].

From the comprehensive review of the literature carried out for differential diagnosis between breast abnormalities, it has been observed that these CAD systems have been designed using features extracted from either original ultrasound images only, or pre-processed ultrasound images only. Among these studies it has been noted that for the computation of texture features, most of the studies have employed statistical methods of texture feature extraction, followed by transform domain based methods. However another set of features namely local binary patter (LBP) based texture descriptors have also become a popular choice for texture quantification for different medical images [53, 94, 119, 134, 152, 162, 196, 256, 265, 266].

Han et al. [94] proposed an automatic system for the analysis of digital mammograms taken from Digital database of screening mammography (DDSM). The suspicious region has been segmented by using an isocontour map algorithm. From the segmented region, LBP based texture descriptors and conventional morphological features have been computed and combined. On the resultant feature set correlation based feature selection has been employed and a cost-sensitive neural network has been used to classify the region to be mass or non-mass.

Laroussi et al. [152] reported the use of different texture and morphological features for classification of mammographic masses using images taken form DDSM database. The authors used LBP based features for the quantification of texture and Zernike moments for the quantification of morphological features. The combined feature set containing both texture and morphological features has been fed to the artificial neural network (ANN) classifier.

Plissti et al. [210] in their study proposed an automated method for nuclei detection in pap smear images. The nuclei segmentation has been carried out by using watershed transform.

From the segmented images different intensity based features, LBP based texture features and morphological features have been computed and classified using different classifiers.

Kumar et al. [146] attempted to automatically classify the ovarian abnormalities by using a probabilistic neural network (PNN) classifier and computing a set of shape, invariant moments, gray level co-occurrence matrix (GLCM), LBP based texture and Gabor wavelet transform (2D-GWT) based features.

Theodorakopoulos et al. [266] used a combination of morphological and uniform LBP based texture features for classification of human epithelial cell line (HEp-2) images using support vector machine (SVM) classifier.

Tashk et al. [265] combined LBP based texture features with stiffness matrix for geometric, morphometric and shape-based features to detect mitosis in histopathology images of breast cancer using SVM classifier.

The studies reported in [2, 32, 185, 198] make use of LBP based features for the quantification of texture and subsequent classification of breast tumors. However, it is worth mentioning that the performance of LBP based texture features combined with the morphological features has not been tested for classification of breast tumors using ultrasound images which have otherwise yielded good results in case of other medical images [94, 146, 152, 210, 266].

Accordingly, in the present work attempt has been made to design an efficient CAD system that utilizes LBP based texture features computed from original tumor images combined with morphological features computed from images despeckled by the DPAD filter for classification of breast tumors.

6.2. Experimental Workflow : LBP based CAD System Designs for Classification of Breast Tumors

The experimental workflow followed for the design of LBP based CAD systems for classification of breast tumors is given in Fig. 6.1.

6.2.1. Dataset description

For carrying out the experiments in the present work, dataset described in section 3.2.1 of Chapter 3 has been used as presented in Fig. 3.2. The entire image dataset was stored on a 64-bit windows 10 PC with Intel (R) Core (TM) i3-5005U, 2.00 GHz processor and 4.00 GB RAM and the experiments have been conducted using MATLABR2015b and MATLABR2018b.

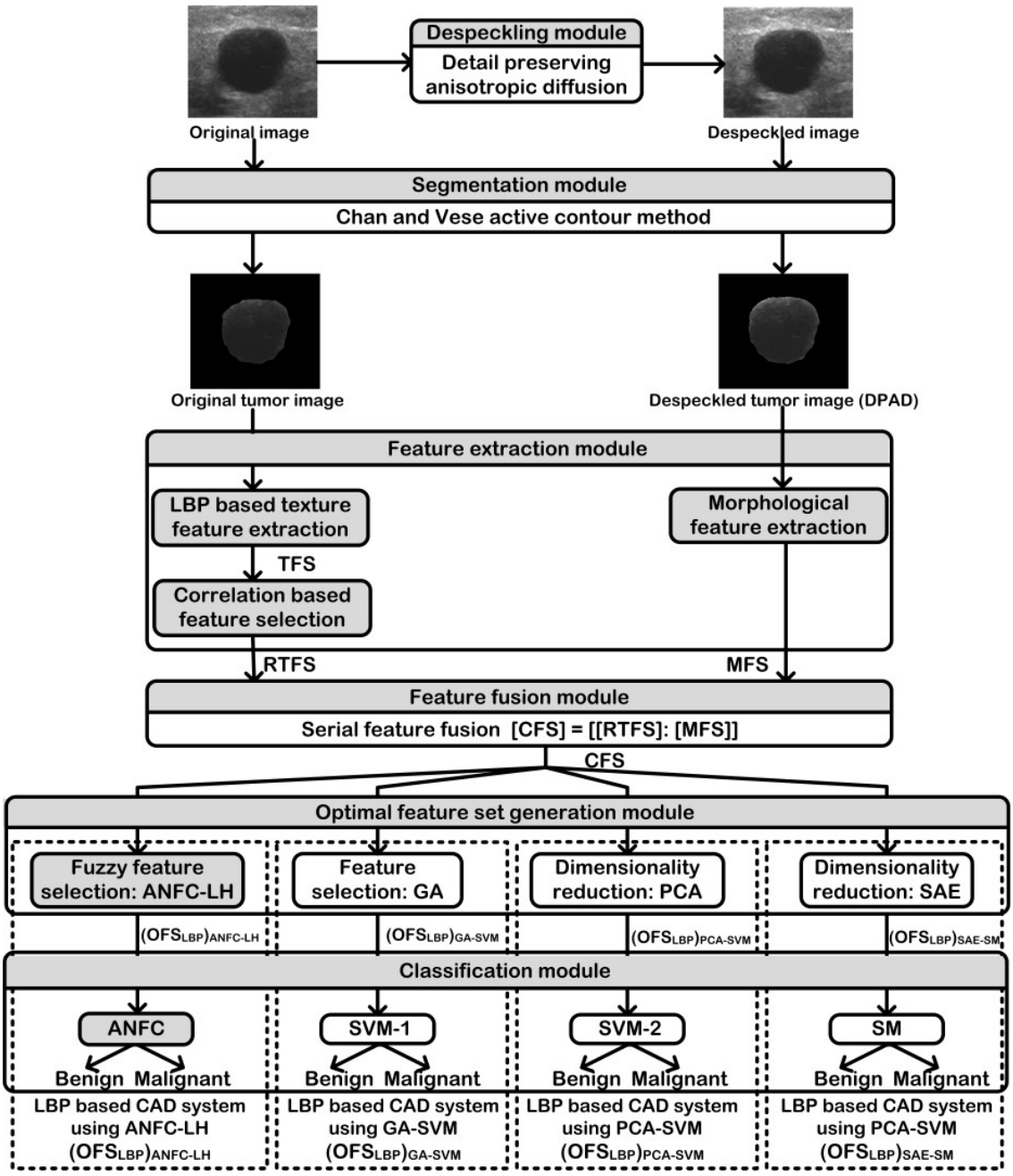

Fig. 6.1 Experimental workflow followed for the design of LBP based CAD systems for classification of breast tumors. The shaded grey region indicates the optimal LBP based CAD system design for classification of breast tumors.

Note: TFS: Texture feature set, MFS: Morphological feature set, RTFS: Reduced texture feature set, LBP: Local binary patterns, CFS: Combined feature set, OFS: Optimal feature set, ANFC-LH: Adaptive neuro-fuzzy classifier using linguistic hedges, GA: Genetic algorithm, PCA: Principal component analysis, SAE: Stacked autoencoder, SVM: Support vector machine, SM: Softmax.

6.2.2. Despeckling module

Based on the exhaustive experiments carried out in *Chapter-5* for obtaining an optimal despeckle filtering algorithm with respect to edge/feature/structure preservation, it has been

established that morphological features are better exhibited by images despeckled by the DPAD filter. Accordingly, DPAD filtered images have been considered for the extraction of morphological feature set.

6.2.3. Segmentation module

In the present work, to segment the breast tumors from original and despeckled images, the Chan and Vese active contour method [37] has been used as described in *Chapter-4*

6.2.4. Feature extraction module

Feature extraction converts the perceptible information of an image into mathematical descriptors based on intensity distribution of the image or on shape of the tumor or on the colour features [7, 9, 11, 17, 21, 43, 130, 226, 253]. In the present work to compute the texture features, LBP method of feature extraction has been used forming a texture feature set (TFS) while morphological features have been extracted from images despeckled by DPAD filter to form a morphological feature set (MFS). The process of combined feature set generation is given in Fig. 6.2.

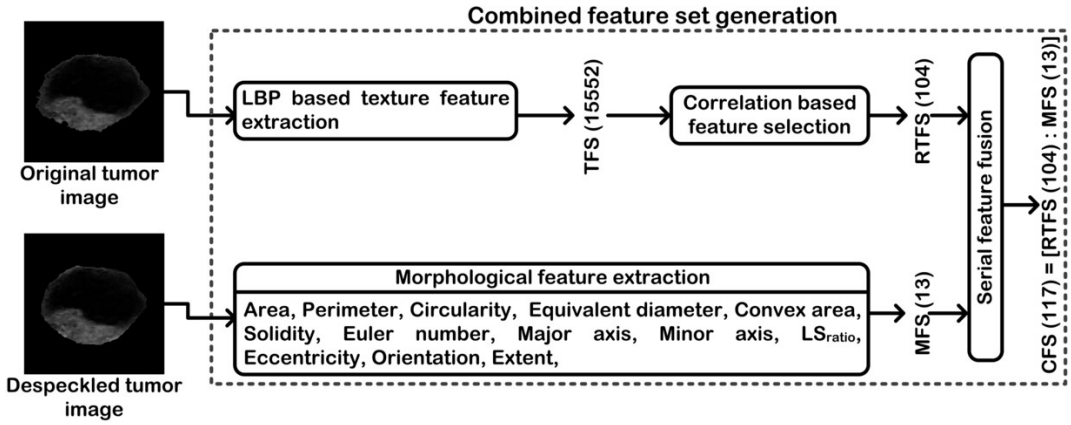

Fig. 6.2 Combined feature set generation using selected LBP based texture features extracted from original images and morphological features extracted from images despeckled by DPAD filter.
Note: LBP: Local binary pattern, TFS: Texture feature set, MFS: Morphological feature set, RTFS: Reduced texture feature set, CFS: Combined feature set, LS_{ratio}: Ratio of length of major axis to length of minor axis

The texture feature set obtained by using LBP algorithm contains a large number of features which may be redundant. In order to remove these redundant features, correlation based feature selection (CrFS) has been used resulting in the formation of a reduced texture feature set (RTFS). Finally RTFS and MFS have been fused serially forming a combined feature set (CFS).

6.2.4.1. LBP based texture feature extraction

The texture features are used to quantify gray level distribution statistics in an image. The LBP based method of feature extraction has been used by many researchers for analysis of

various medical images [53, 94, 119, 134, 152, 161, 196, 256, 265, 266]. Ojala et al. [203] introduced LBP for image texture quantification of local neighbourhood. In LBP algorithm, the pixels of an image are labelled using a threshold value for each pixel neighbourhood and the final result is considered as a binary number. The steps followed for computing the LBP based texture features are given in Fig. 6.3.

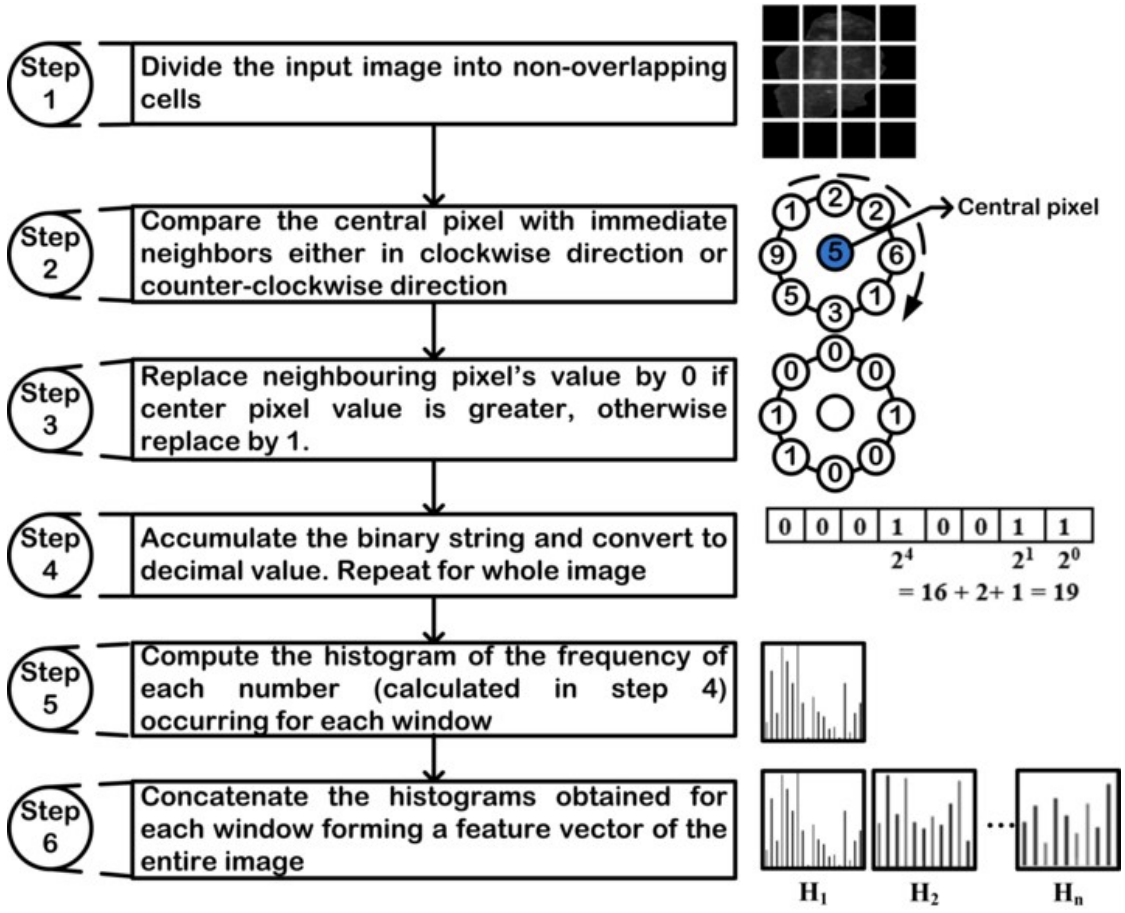

Fig. 6.3 Steps followed for the implementation of LBP algorithm.
Note: H_1: Histogram of 1st window, H_n: Histogram of n^{th} window

The length of the final LBP feature vector is given as:

$$NumCells = prod\left(floor\left(\frac{Image\ size}{C}\right)\right) = prod\left(\frac{512}{64}\right) = 8 \times 8 = 64 \tag{6.1}$$

$$B: No.of\ bins\ of\ histogram = N \times (N-1) + 3 = 16 \times (16-1) + 3 = 243 \tag{6.2}$$

$$LBP\ (l) = NumCells\ \times B = 243 \times 64 = 15552 \tag{6.3}$$

Here, C: Cell size, N: Number of neighbors, l: length of feature vector.

From the original tumor images, a texture feature set (TFS) is formed containing 15552 LBP features computed at radius (R) = 1, N = 16, C = 64.

6.2.4.2. Correlation based feature selection

The texture feature set computed from the original tumor images containing LBP based texture features may have some redundant features and can negatively affect the classification performance of the CAD systems. Thus, the selection of relevant features is a pre-requisite for the design of efficient CAD systems. The advantages of feature selection are: faster training time, reduced complexity of classification model and reduced overfitting. In CrFS the best subset of features is selected based on the value of correlation coefficient. The section criterion is based on the fact that the features are uncorrelated to each other but are highly correlated to the class [188]. The computed score used as a threshold to select the optimal feature subset is given as:

$$S = \frac{k \times \overline{r_{cf}}}{\sqrt{k + k(k-1)\overline{r_{ff}}}} \tag{6.4}$$

Here, k: number of features, $\overline{r_{ff}}$: mean inter-correlation between features, $\overline{r_{cf}}$: mean correlation between feature and class.

In the present work the TFS having a length of 15552 is subjected to CrFS yielding a reduced texture feature set (RTFS) having length 104.

6.2.4.3. Morphological feature extraction

The morphological features represent the shape characteristics of the tumor. It has been well established that the benign and malignant breast tumors can be differentiated based on their shape e.g. benign tumors have a regular shape (round or oval) while malignant tumors are irregularly shaped [82, 83]. The different morphological features computed for the breast tumor characterization are: area, perimeter, circularity, equivalent diameter, convex area, solidity, Euler number, length of major axis, length of minor axis, LS_{ratio}, orientation, eccentricity and extent of the tumor region. By combining these 13 morphological features a morphological feature set (MFS) is computed for all breast tumor images.

6.2.4.4. Serial feature fusion

In feature fusion, a single feature set is formed by aggregating multiple feature sets. In serial feature fusion, a combined feature set is formed by simply concatenating different features one after the other (union operation) [7]. In the present work, the selected texture and morphological feature sets have been combined serially to obtain a feature set CFS, i.e. RTFS (104), MFS (13), are combined serially as: CFS (117) = [RTFS : MFS] (104 + 13).

The feature fusion step has been used to combine the texture features and morphological features as both of these features play an important role in the classification of breast abnormalities. The step of feature reduction has been performed to remove the redundant

features from the combined feature pool so as to train the classifier with the optimal (textural and morphological) selected features.

6.2.5. Optimal feature set generation module

The combined feature set has been further subjected to two feature selection and two feature space dimensionality reduction methods to obtain optimal feature sets (OFS). The different methods employed for the generation of an OFS are given in Fig. 6.4.

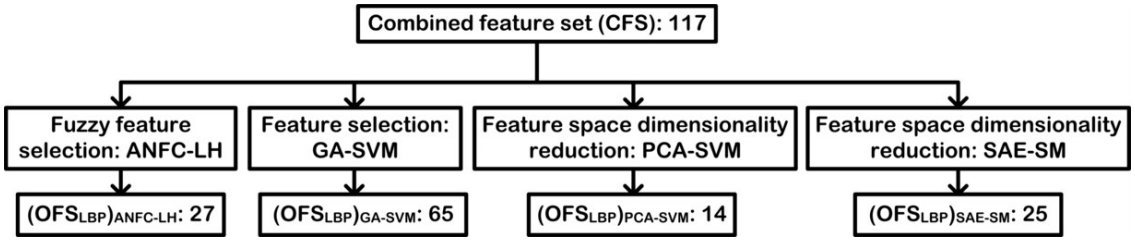

Fig. 6.4 Different methods employed for the generation of an OFS.
Note: ANFC-LH: Adaptive neuro-fuzzy classifier, GA: Genetic algorithm, SVM: Support vector machine, PCA: Principal component analysis, SAE: Stacked autoencoder, SM: Softmax, OFS: Optimal feature set, LBP: Local binary pattern.

6.2.5.1. Feature selection using ANFC-LH algorithm

In the present work a fuzzy feature selection using technique adaptive neuro-fuzzy classifier using linguistic hedges (ANFC-LH) has been used to find an optimal feature set from the CFS consisting of a total of 117 features (104 texture and 13 morphological features).

The linguistic hedges (LHs) are used to introduce the importance of fuzzy rules. The LH values are tuned in such a way so as to improve the flexibility of fuzzy sets, thus removing the ambiguity of the overlapped classes. The LHs are defined as the linguistic terms that can be used to modify other linguistic terms [309]. Suppose L is a continuous linguistic term for an input variable x having a membership function $\mu_L(x)$. The modified linguistic term can be defined as:

$$L^S: \{(x, (\mu_L(x))^P) | x \in X\} \tag{6.5}$$

Here, p indicates the linguistic hedge value of the linguistic term L.

A conventional simple fuzzy rule having two inputs (a_1, a_2) and one output (b) is given as: IF a_1 is X_1 AND a_2 is X_2 THEN b is Y.

When LHs are associated with a fuzzy rule, new fuzzy rule can be redefined as:

IF a_1 is X_1 with hedge value p_1 AND a_2 is X_2 with hedge value p_2 THEN b is Y.

In the present work, ANFC using linguistic hedges has been used for selecting the optimal features from the obtained CFS.

For an ANFC using linguistic hedges, a fuzzy classification rule for two inputs and one output with LHs is defined as:

IF a_1 is X_1 with hedge value p_1 AND a_2 is X_2 with hedge value p_2 THEN b is C_1.

Here, X_1 and X_2 denote linguistic terms on A_1 and A_2 feature space,

p_1, p_2 are the linguistic hedges and C_1 is the class label of an output b.

The general fuzzy rules can be written as:

Rule1: IF a_1 is X_1 with hedge value $p_1 = 1$ AND a_2 is X_2 with hedge value $p_2 = 0$ THEN b is F_1

Rule2: IF a_1 is X_1 with hedge value $p_1 = 0$ AND a_2 is X_2 with hedge value $p_2 = 1$ THEN b is F_2

The corresponding reduced set of rules can be re-written as:

Rule1: IF a_1 is X_1 with hedge value $p_1 = 1$ THEN b is F_1

Rule2: IF a_2 is X_2 with hedge value $p_2 = 1$ THEN b is F_2

The reduced rules represent the selected features only. For the selection of the features, LH values are used. It can be interpreted that if the LH value of fuzzy set for particular feature is 1, then that feature is considered to be important.

The general architecture of ANFC-LH is given in Fig. 6.5 having two inputs in the feature space to be separated into two classes with each input being described by two linguistic variables, thus giving a total of four fuzzy rules.

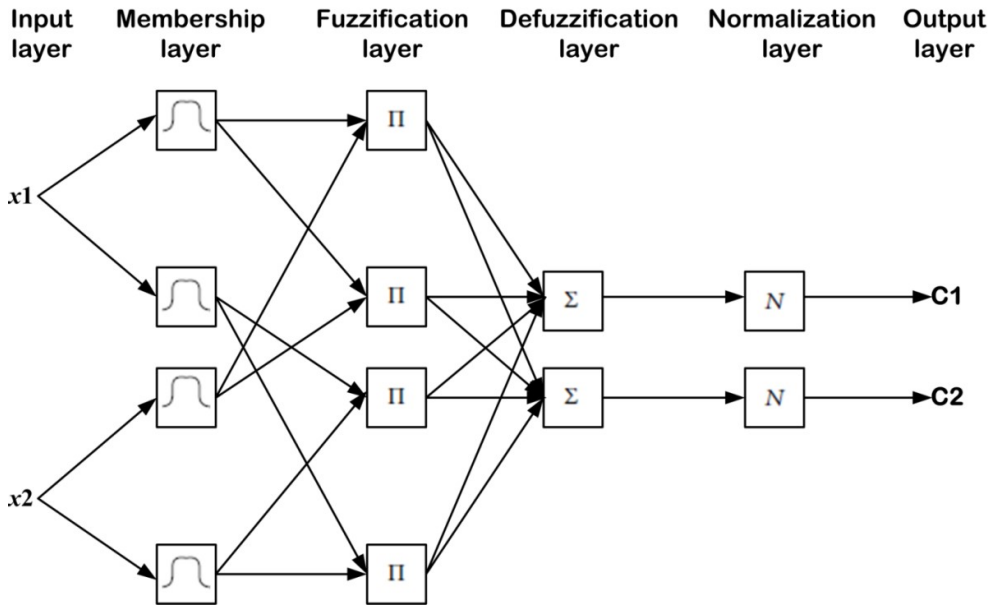

Fig. 6.5 General layer architecture of ANFC-LH.

The description of each layer is given here:

(*i*) Membership layer: In this layer the membership function of each input variable is defined. The most commonly used membership function is Gaussian as it has less parameters and smoother partial derivatives. The Gaussian membership function is given as:

$$\mu_{ij}(x_{sj}) = e^{-0.5\frac{(x_{sj}-c_{ij})^2}{\sigma_{ij}^2}} \quad (6.6)$$

Here, μ_{ij} (x_{sj}): membership grade for i^{th} rule and j^{th} feature, x_{sj}: s^{th} input sample and j^{th} feature, c_{ij}: Center of the Gaussian function, σ_{ij}: Width of Gaussian function

(*ii*) Power layer: In this layer the secondary meanings of the fuzzy sets are calculated along with the linguistic hedges.

$$\alpha_{ijs} = [\mu_{ij}(x_{sj})]^{p_{ij}} \quad (6.7)$$

Here, α_{ijs}: modified membership grade, p_{ij}: linguistic hedge value of i^{th} rule and j^{th} feature.

(*iii*) Fuzzification layer: In this layer, a signal corresponding to the degree of fulfilment of the fuzzy rule for sample x_s is generated at each node. This is called the firing strength of the fuzzy rule. For an i^{th} rule, the firing strength is given as:

$$\beta_{is} = \prod_{j=1}^{D} \alpha_{ijs} \quad (6.8)$$

Here, β_{is}: Firing strength of i^{th} rule, D: No. of features.

(*iv*) Defuzzification layer: In this layer, the weighted output of an input sample belonging to a particular class is computed. Class weights are large if a rule controls a specific class region. The weighted output for a sample *s* belonging class *k* is calculated as:

$$o_{sk} = \sum_{i=1}^{M} \beta_{is} w_{ik} \quad (6.9)$$

Where, w_{ik}: degree of belongingness to class *k* controlled by i^{th} rule, M: No. of rule.

(*v*) Normalization layer: Used to normalize the outputs of the network such that the summation of weights does not exceed 1. The value of normalized output is given as:

$$h_{sk} = \frac{o_{sk}}{\sum_{l=1}^{K} o_{sl}} \quad (6.10)$$

Where, h_{sk}: normalized value of s^{th} sample, belonging to k^{th} class, K: No. of classes.

From the CFS having 117 features, on the basis of linguistic hedge values, a total of 27 optimal features have been selected, thus forming an optimal feature set $(OFS_{LBP})_{ANFC\text{-}LH}$. The relationship between input features and their respective power of LH value is given in Fig. 6.6.

6.2.5.2. Feature selection using GA-SVM algorithm

Genetic algorithm (GA) is an evolutionary search procedure inspired by the biological evolution model. In GA, the features are represented as binary vectors and the feature search space is considered to be an *n*-dimensional Boolean space. The GA selects a random set of individuals from the given population and works towards producing the off-springs for the next

generation. Three main operators used in GA are selection, crossover and mutation to create the successive generation using current population on the basis of a fitness function. This process of fitness dependent selection is repeated multiple times till an optimal solution is found [285].

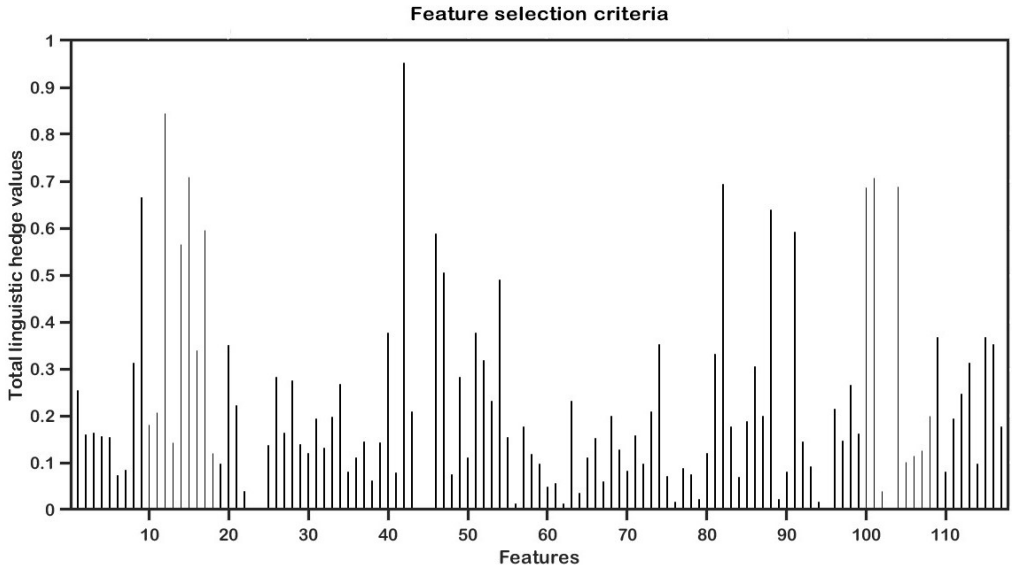

Fig. 6.6 The relationship between input features and their respective power of LH value.

The computed features have been normalized in the range [0, 1] by using min-max normalization in order to avoid any bias caused by unbalanced feature values. Firstly, the min-max normalization procedure has been applied to the feature values in the training set and then the same settings have been applied to normalize the feature values in the testing set.

In the present work, the initial population is defined as a set of 117-bit binary coded chromosomes. The fitness of a chromosome is evaluated on the basis of the classification accuracy obtained by the SVM classifier. The general schematic of GA-SVM algorithm applied to CFS to generate optimal feature set is given in Fig. 6.7.

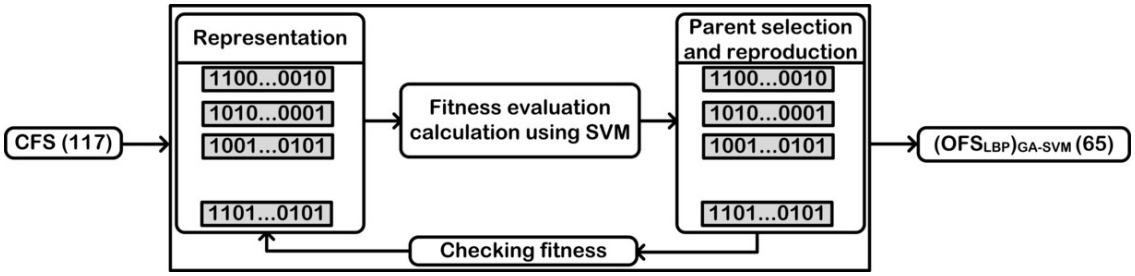

Fig. 6.7 General schematic for implementation of GA-SVM algorithm.
Note: CFS: Combined feature set, OFS: Optimal feature set obtained, LBP: Local binary pattern, GA: Genetic algorithm, SVM: Support vector machine.

The different parameters used during the run of GA are Number of variables: 117, Population size: 200, Scaling function: Rank, Selection function: Roulette, Crossover function:

Single point, Crossover fraction: 0.7, Mutation rate: 0.01. The algorithm terminates when the maximum iteration count is reached or no improvement is witnessed in the fitness value. The steps followed in GA are given in Fig. 6.8.

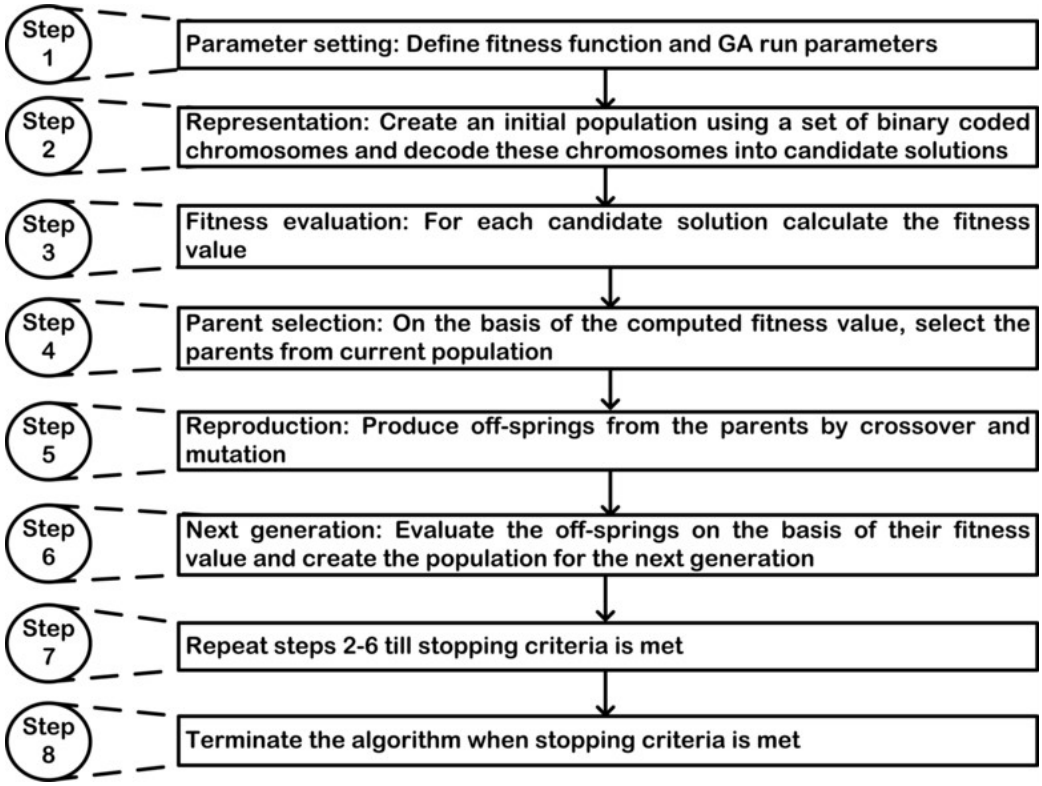

Fig. 6.8 Steps followed in the formation of optimal feature set using genetic algorithm.

The general schematic indicating the steps followed for building the final SVM model using GA-SVM algorithm is given in Fig. 6.9.

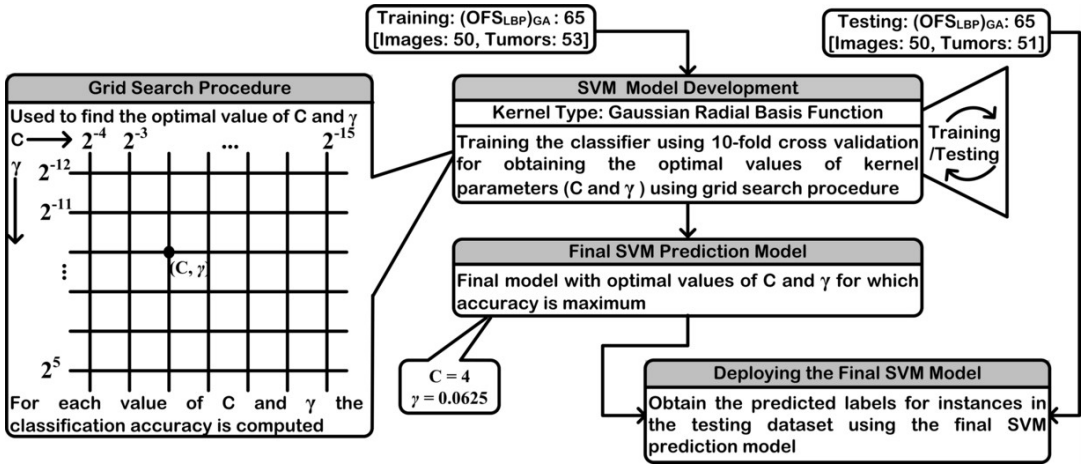

Fig. 6.9 The general schematic indicating the steps followed for building the final SVM model using GA-SVM algorithm.

Note: SVM: Support vector machine, OFS: Optimal feature set, GA: Genetic algorithm, LBP: Local binary pattern.

6.2.5.3. Feature space dimensionality reduction using PCA-SVM algorithm

The principal component analysis-support vector machine (PCA-SVM) algorithm is algorithm is used to find optimal number of principal components (PCs) for designing efficient CAD systems for classification [12, 140, 198, 274, 282]. In the present work, the redundant features present in CFS, do not provide any significant information for discriminating between the breast tumors. Therefore, to remove this redundancy, the features in the CFS are converted to optimal attributes using PCA-SVM algorithm. The optimal number of PCs to be retained has been decided empirically by conducting recurrent experiments and stepping through first few PCs $\in$ {2, 3, …,15} to build the classification model [140]. The computed features have been normalized in the range [0, 1] by using Z-score normalization in order avoid any bias caused by unbalanced feature values. Firstly, the Z-score normalization procedure has been applied to the features in the training set and then the same settings have been applied to normalize the features in the testing set. The general schematic indicating the steps followed for building the final SVM model using PCA-SVM algorithm is given in Fig. 6.10.

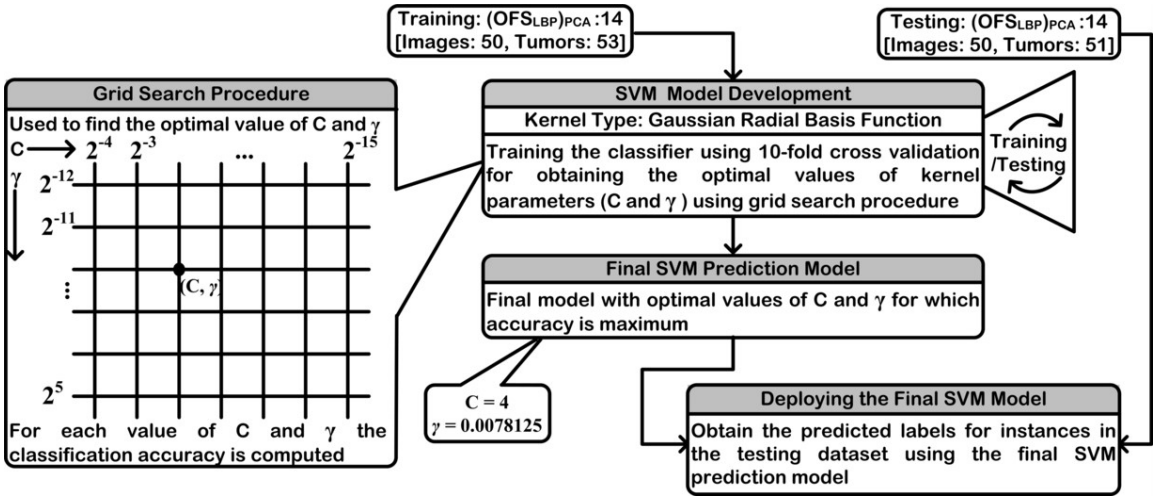

Fig. 6.10 The general schematic indicating the steps followed for building the final SVM model using PCA-SVM algorithm.
Note: SVM: Support vector machine, OFS: Optimal feature set, PCA: Principal component algorithm, LBP: Local binary pattern.

6.2.5.4. Feature space dimensionality reduction using SAE-SM algorithm

The stacked autoencoder with softmax classifier (SAE-SM) is a popular feature space dimensionality reduction technique used to find optimal attributes for designing efficient CAD systems for classification of medical images [48, 97, 99]. Autoencoders (AE) come under the class of generative deep models useful for unsupervised learning. The output of the AE is same as the input.

Firstly, the AEs compress the input data into a latent space representation and then try to reconstruct the output from this representation. Thus an AE can be viewed to have two parts: (*i*) Encoder function, (*ii*) Decoder function. The general architecture of an AE is given in Fig. 6.11.

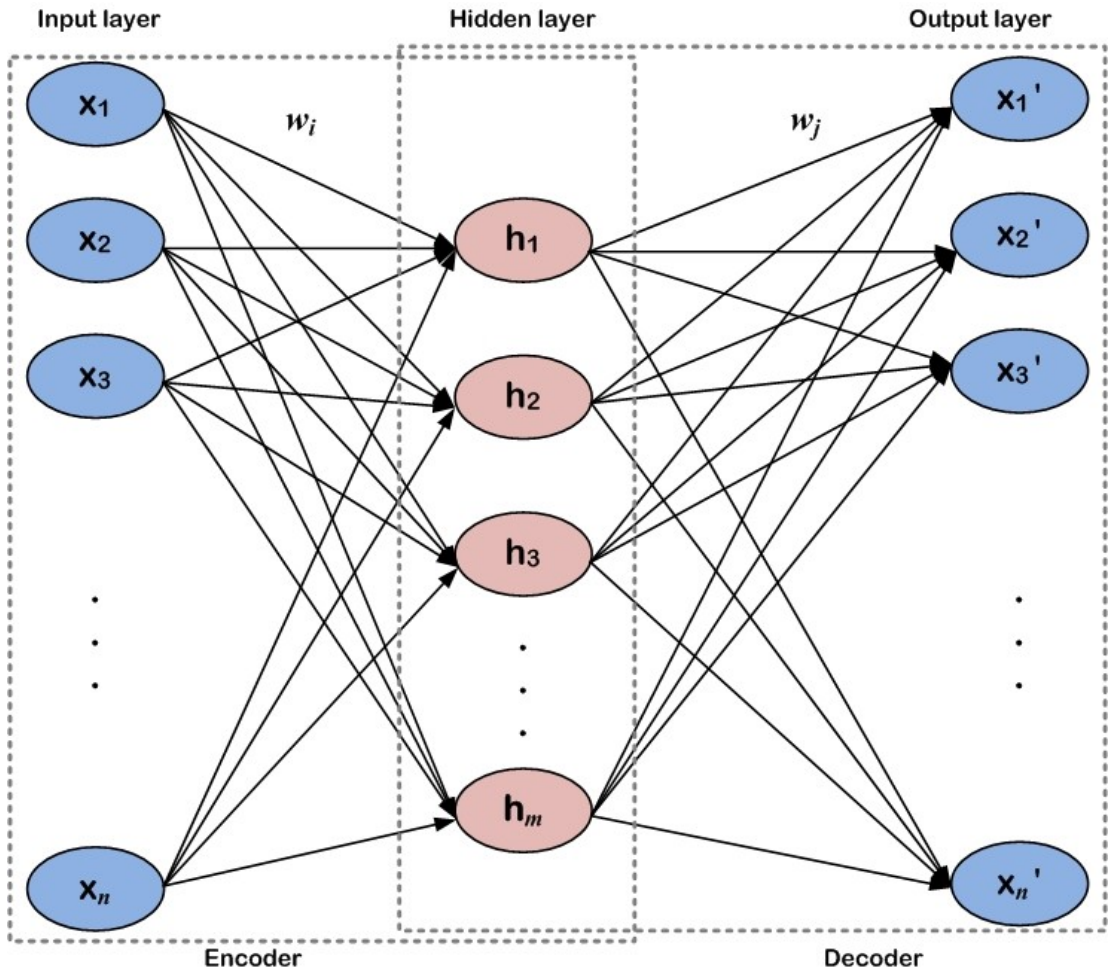

Fig. 6.11 General architecture of an autoencoder.

The encoder maps the input vector x to another vector y using a transfer function h as

$$y = h(w_i x + b_i) \tag{6.11}$$

Here, w_i: weight matrix at encoder side and b_i: bias vector.

The function of the decoder is to reconstruct the vector y to estimate the original input vector

$$x' = h'(w_j y + b_j) \tag{6.12}$$

Here, w_j: weight matrix at decoder side and b_j: bias vector.

When the encoding layer's output is connected to another encoding layer's input, then the resultant architecture is called a stacked autoencoder (SAE), allowing for several layers of abstraction. The general architecture of a SAE is given in Fig. 6.12.

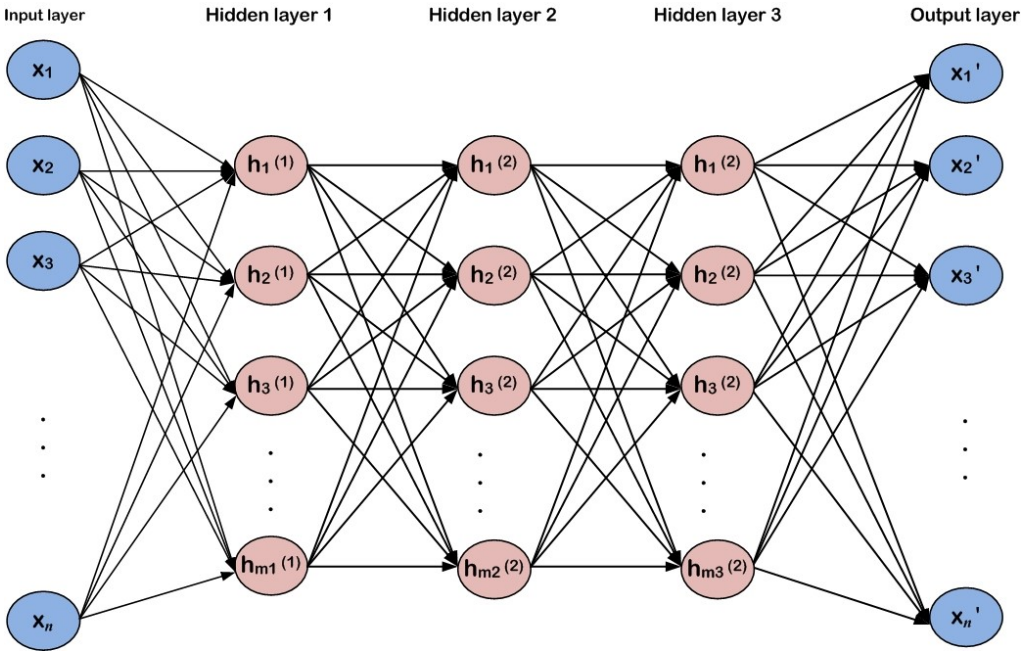

Fig. 6.12 General architecture of a stacked autoencoder.

When multiple hidden layers are used, a greedy layer-wise approach is used for initializing the hidden layers. This process is called pre-training, wherein the input training data trains the first hidden layer. The output from the first hidden layer is then used for training the second hidden layer and so on, till all the hidden layers of the network have been trained.

The hyperparameters of a SAE are the weights and bias of the network, number of hidden layers and number of hidden units present in each layer. For getting the final network structure used in the present work, a random search was exhaustively used to select the parameters that produced the best performance [48, 97, 99].

6.2.6. Classification module

Classification is a learning approach wherein a computer program learns the underlying properties of the input data fed to it and on the basis of the gained knowledge, tries to classify the new data instances into discrete classes. It has been established that SVM is widely accepted for the classification of medical images and mostly performs well in various classification tasks. In the present work however, the performance of wide variety of classifiers has been studied for comparison purposes.

6.2.6.1. Adaptive neuro-fuzzy classifier

A neuro-fuzzy classifier (NFC) is a combination of neural network classifier and fuzzy inference system. The fuzzy inference system uses a set of fuzzy IF-THEN rules that can approximate non-linear functions to deal with imprecise problems. The problem with fuzzy systems is that they cannot learn from their environment and thus cannot adjust themselves

adaptively. This problem is overcome in the neural network which has the capability to self-organize and learn adaptively from its environment. Thus in the combination of neural network and fuzzy inference system, their respective advantages are integrated. Hence the neuro-fuzzy classifier has a powerful description capability of fuzzy inference system combined with the learning capabilities of neural networks such that the feature space can be easily partitioned into classes. The network contains multiple nodes connected to each other by directional links. The output of the nodes is dependent on the parameters of the nodes which can be changed during network training to reduce the error, hence the network is said to be adaptive and named as adaptive neuro-fuzzy classifier (ANFC) [226]. The layer architecture of ANFC used in the present work is given in Fig. 6.13.

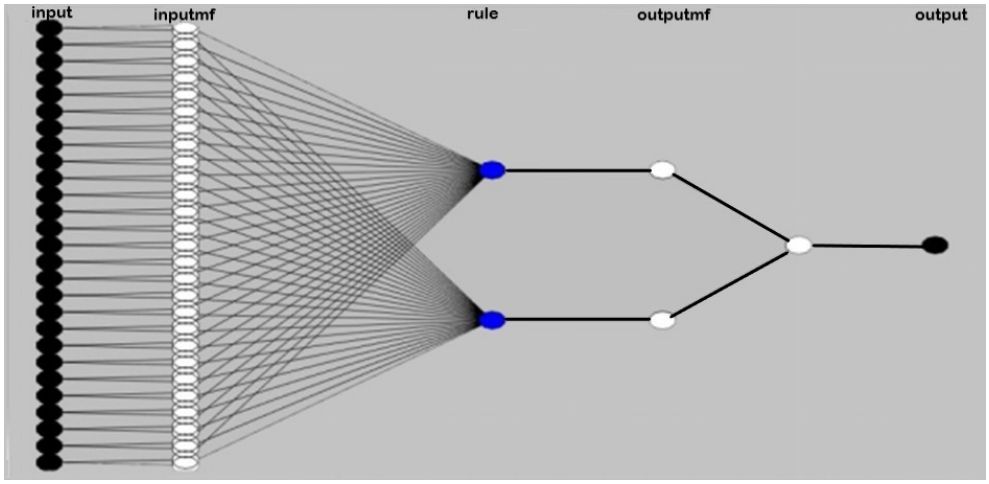

Fig. 6.13 The layer architecture of ANFC used in the present work.

During the training of ANFC the center and width values of the Gaussian membership function, power value of LHs and weights of the connections between fuzzification and defuzzification layer need to be optimized for finding the optimum fuzzy region. In order to form the fuzzy IF-THEN rules, the initial parameters are obtained using *k*-means clustering. For the parameter optimization, the scaled conjugate gradient (SCG) algorithm has been used as it has shown to produce lowest error rate for the optimization. The computed features have been normalized in the range [0, 1] by using min-max normalization in order to avoid any bias caused by unbalanced feature values. Firstly, the min-max normalization procedure has been applied to the features in the training set and the same settings have then been applied to normalize the features in the testing set.

6.2.6.2. Support vector machine classifier

The SVM classifier uses a kernel-based approach to separate the instances into disjoint classes using a hyper-plane that maximises the margin between two classes and is less prone to

overfitting. In the present work, SVM with GRBF kernel has been utilized that maps the non-linear data from input feature space to a higher dimensionality feature space [16, 21, 32, 62, 111, 113, 115, 154, 198, 209, 218, 248, 285-287, 297, 298, 321]. For the implementation of the SVM algorithm, LibSVM library has been used [38].

6.2.6.3. Softmax classifier

The softmax classifier is stacked on top of the trained SAE network to represent the class labels of the input data [48, 97, 99]. The number of units in the softmax layer equals the number of classes in the classification problem. The final network thus formed consists of a stack of all the hidden layers and the softmax layer as given in Fig. 6.14.

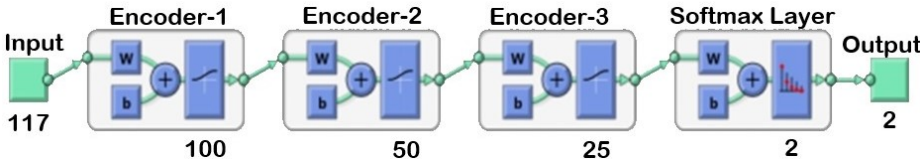

Fig. 6.14 Architecture of final network made up of SAE with softmax classifier.
Note: *w*: weights, *b*: bias.

As seen from Fig. 6.14, a SAE with three hidden layers stacked with a softmax classifier has been used for classification of breast tumors. The input layer consists of 117 units representing the size of the input feature set. The three hidden layers have 100, 50 and 25 nodes respectively and the softmax layer consists of 2 units corresponding to the benign and malignant classes. The hidden layers and softmax layer was trained for 2000 epochs each. This final network is then trained as a whole in a supervised manner to achieve the final classification performance. To fine-tune the network and update the parameters, error back-propagation and scaled conjugate gradient have been used. The computed features have been normalized in the range [0, 1] by using min-max normalization in order to avoid any bias caused by unbalanced feature values.

6.3. Experiments and Results

For evaluating the performance of the CAD system designs for classification of breast tumors, exhaustive experiments have been conducted. The description of experiments is shown in Table 6.1.

Table 6.1 Description of experiments for the design of LBP based CAD systems.

Experiment 1	Design of LBP based CAD system using ANFC-LH for classification of breast tumors.
Experiment 2	Design of LBP based CAD system using GA-SVM for classification of breast tumors.
Experiment 3	Design of LBP based CAD system using PCA-SVM for classification of breast tumors.
Experiment 4	Design of LBP based CAD system using SAE-SM for classification of breast tumors.

Note: LBP: Local binary pattern, ANFC-LH: Adaptive neuro-fuzzy classifier using linguistic hedges, GA: Genetic algorithm, SVM: Support vector machine, PCA: Principal component analysis, SAE: Stacked autoencoder, SM: Softmax.

6.3.1. Experiment 1: Design of LBP based CAD system using ANFC-LH algorithm for classification of breast tumors

In this experiment, the CFS (117) containing both texture and morphological features is subjected to a feature selection method using ANFC-LH algorithm, generating an optimal feature set $(OFS_{LBP})_{ANFC\text{-}LH}$ (27) that is further fed to the ANFC for differentiating between the benign and malignant breast tumor types. The classification results obtained for LBP based CAD system using ANFC-LH algorithm are shown in Table 6.2.

Table 6.2 Classification results obtained for LBP based CAD system using ANFC-LH algorithm.

CAD system (FS: *l*)	CM			Accuracy (%)	ICA_B (%)	ICA_M (%)
		B	M			
LBP based CAD system using ANFC-LH	B	19	2	96.0	90.4	100
$((OFS_{LBP})_{ANFC\text{-}LH}$: 27)	M	0	30			

Note: FS: Feature set, *l*: Length of feature vector in OFS, OFS: Optimal feature set, LBP: Local binary pattern, ANFC-LH: Adaptive neuro-fuzzy classifier using linguistic hedges, CM: Confusion matrix, ICA: Individual class accuracy, B: Benign class, M: Malignant class.

From Table 6.2 it can be noted that using OFS consisting of 27 optimal features obtained by applying ANFC-LH to CFS consisting of 104 selected LBP based texture features and 13 morphological features yielded an accuracy of 96.0 %. The individual class accuracy (ICA) value for the benign class is 90.4 % while for malignant class the ICA value is 100 %. It is worth noting that out of 51 instances in the testing set, only 2 benign instances have been incorrectly classified while all the malignant cases have been classified correctly.

6.3.2. Experiment 2: Design of LBP based CAD system using GA-SVM algorithm for classification of breast tumors

In this experiment, the CFS (117) containing both texture and morphological features is subjected to a feature selection method using GA-SVM algorithm, generating an optimal feature set $(OFS_{LBP})_{GA\text{-}SVM}$ (65) that is fed to the SVM classifier for differentiating between the benign and malignant breast tumor types. The classification results obtained for LBP based CAD system using GA-SVM algorithm are shown in Table 6.3.

Table 6.3 Classification results obtained for LBP based CAD system using GA-SVM algorithm.

CAD system (FS: *l*)	CM			Accuracy (%)	ICA_B (%)	ICA_M (%)
		B	M			
LBP based CAD system using GA-SVM	B	19	2	92.2	90.4	93.3
$((OFS_{LBP})_{GA\text{-}SVM}$: 65)	M	2	28			

Note: FS: Feature set, *l*: Length of feature vector in OFS, OFS: Optimal feature set, LBP: Local binary pattern, GA: Genetic algorithm, SVM: Support vector machine, CM: Confusion matrix, ICA: Individual class accuracy, B: Benign class, M: Malignant class,

From Table 6.3, it can be noted that using OFS consisting of 65 optimal features obtained by applying GA-SVM to CFS consisting of 104 selected LBP based texture features and 13 morphological features yielded an accuracy of 92.2 %. The ICA value for benign class is

90.4 % while for the malignant class the ICA value is 93.3 %. Out of 51 instances in the testing dataset, 4 instances have been incorrectly classified.

6.3.3. Experiment 3: Design of LBP based CAD system using PCA-SVM algorithm for classification of breast tumors

In this experiment, the CFS (117) containing both texture and morphological features is subjected to a feature space dimensionality reduction method by using PCA-SVM algorithm, generating an optimal feature set $(OFS_{LBP})_{PCA\text{-}SVM}$ (14). The obtained optimal PCs are then further used to train an SVM classifier for differentiating between the benign and malignant breast tumor types. The classification results obtained for LBP based CAD system using PCA-SVM algorithm are shown in Table 6.4.

Table 6.4 Classification results obtained for LBP based CAD system using PCA-SVM algorithm.

CAD system (FS: *l*)	CM			Accuracy (%)	ICA_B (%)	ICA_M (%)
LBP based CAD system using PCA-SVM ($(OFS_{LBP})_{PCA\text{-}SVM}$: 14)		B	M	94.1	90.4	96.6
	B	19	2			
	M	1	29			

Note: FS: Feature set, *l*: No. of optimal PCs, OFS: Optimal feature set, LBP: Local binary pattern, CM: Confusion matrix, ICA: Individual class accuracy, PCA: Principal component analysis, SVM: Support vector machine, B: Benign class, M: Malignant class.

From Table 6.4 it can be observed that using OFS consisting of 14 optimal PCs obtained by applying PCA-SVM to CFS consisting of 104 selected LBP based texture features and 13 morphological features yielded an accuracy of 94.1 %. The ICA value for benign class is 90.4 % while for the malignant class the ICA value is 96.6 %. Out of 51 instances in the testing set, 3 instances have been incorrectly classified.

6.3.4. Experiment 4: Design of LBP based CAD system using SAE-SM algorithm for classification of breast tumors

In this experiment, the CFS (117) containing both texture and morphological features is subjected to a feature space dimensionality reduction method using SAE-SM algorithm, generating an optimal feature set $(OFS_{LBP})_{SAE\text{-}SM}$ (25) that is used to train a softmax classifier for differentiating between the benign and malignant breast tumor types. The classification results obtained for LBP based CAD system using SAE-SM algorithm are shown in Table 6.5.

Table 6.5 Classification results obtained for LBP based CAD system using SAE-SM algorithm.

CAD system (FS: *l*)	CM			Accuracy (%)	ICA_B (%)	ICA_M (%)
LBP based CAD system using SAE-SM ($(OFS_{LBP})_{SAE\text{-}SM}$: 25)		B	M	92.2	80.9	100
	B	17	4			
	M	0	30			

Note: FS: Feature set, *l*: No. of optimal attributes, OFS: Optimal feature set, LBP: Local binary pattern, CM: Confusion matrix, ICA: Individual class accuracy, SAE: Stacked autoencoder, SM: Softmax, B: Benign class, M: Malignant class.

From Table 6.5 it can be observed that using OFS consisting of 22 optimal attributes obtained by applying SAE-SM to CFS consisting of 104 selected LBP based texture features and 13 morphological features yielded an accuracy of 92.2 %. The ICA value for the benign class is 80.9 % while for malignant class the ICA value is 100 %. Out of 51 instances in the testing set, 4 benign instances have been incorrectly classified while all the malignant cases have been classified correctly.

6.3.5. Comparative analysis of the results obtained by LBP based CAD system designs for classification of breast tumors

In the present work, the performance of four different LBP based CAD systems using (*a*) ANFC-LH algorithm, (*b*) GA-SVM algorithm, (*c*) PCA-SVM algorithm and (*d*) SAE-SM algorithm has been compared for classification of breast tumors. The comparative analysis of results obtained by LBP based CAD system designs for classification of breast tumors is given in Table 6.6.

Table 6.6 Comparative analysis of results obtained by LBP based CAD system designs for classification of breast tumors.

CAD system (FS: *l*)		CM		Accuracy (%)	ICA_B (%)	ICA_M (%)
		B	M			
LBP based CAD system using ANFC-LH ($(OFS_{LBP})_{ANFC-LH}$: 27)	B	19	2	96.0	90.4	100
	M	0	30			
LBP based CAD system using GA-SVM ($(OFS_{LBP})_{GA-SVM}$: 65)	B	19	2	92.2	90.4	93.3
	M	2	28			
LBP based CAD system using PCA-SVM ($(OFS_{LBP})_{PCA-SVM}$: 14)	B	19	2	94.1	90.4	96.6
	M	1	29			
LBP based CAD system using SAE-SM ($(OFS_{LBP})_{SAE-SM}$: 25)	B	17	4	92.2	80.9	100
	M	0	30			

Note: FS: Feature set, *l*: Length of feature vectors in OFS, OFS: Optimal feature set, LBP: Local binary pattern, ANFC-LH: Adaptive neuro-fuzzy classifier using linguistic hedges, GA: Genetic algorithm, SVM: Support vector machine, PCA: Principal component analysis, SAE: Stacked autoencoder, SM: Softmax, B: Benign class, M: Malignant class, CM: Confusion matrix, ICA: Individual class accuracy.

The shaded grey region indicates the optimal LBP based CAD system using ANFC-LH algorithm for classification of breast tumors

From the comparative analysis of the results presented in Table 6.6, it can be noted that highest accuracy of 96.0 % has been achieved by LBP based CAD system using ANFC-LH algorithm for classification of breast tumors with the ICA values of benign and malignant classes being 90.4 % and 100%, respectively. The next highest accuracy of 94.1 % has been achieved by LBP based CAD system using PCA-SVM algorithm. Comparable classification accuracy of 92.2 % has been obtained for the other two LBP based CAD system designs with the difference being in the ICA values for benign and malignant classes.

The performance of LBP based CAD system designs implemented in the present work has been represented pictorially in terms of ROC curves along with their AUC values as given in Fig. 6.15.

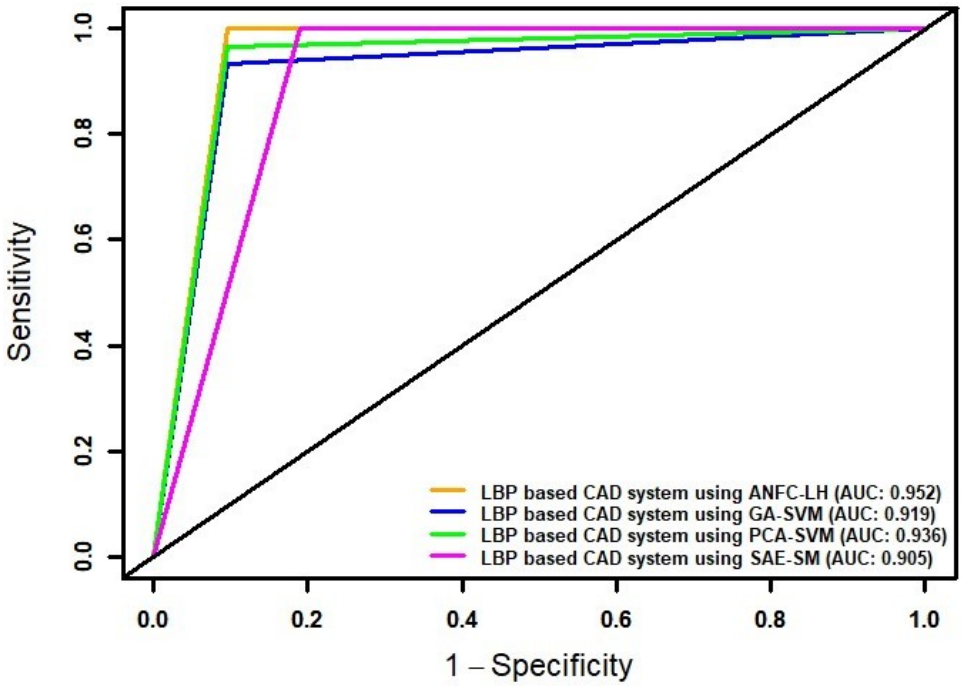

Fig. 6.15 ROC curves for LBP based CAD system designs implemented in the preset work along with their AUC values.

The optimal LBP based CAD system design for classification of breast tumors is given in Fig. 6.16.

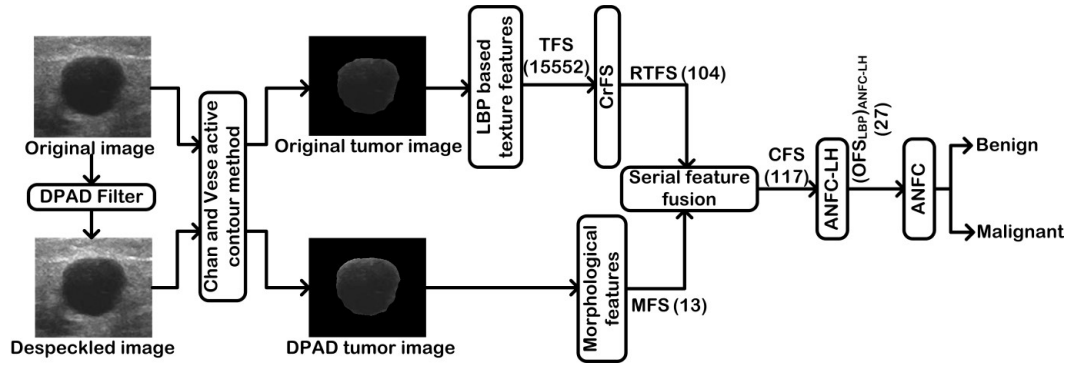

Fig. 6.16 Optimal LBP based CAD system design for classification of breast tumors.
Note: DPAD: Detail preserving anisotropic diffusion, LBP: Local binary pattern, TFS: Texture feature set, MFS: Morphological feature set, CrFS: Correlation based feature selection, RTFS: Reduced texture feature set, CFS: Combined feature set, ANFC-LH: Adaptive neuro-fuzzy classifier, OFS: Optimal feature set.

6.4. Concluding Remarks

From the results of the experiments conducted for designing an efficient LBP based CAD system for classification of breast tumors, it is noted that CAD system based on ANFC-LH

algorithm utilizing LBP based texture features extracted from original ultrasound images and morphological features extracted from images despeckled by DPAD filter yielded the highest accuracy of 96.0 % with an ICA value of 100 % for malignant class. The present CAD system design is different from the other related studies as: The LBP based texture features have found extensive use in medical images for the efficient texture description however for the analysis of breast ultrasound images, the potential of a combination of these LBP based texture features with morphological features remains to be tested. Therefore, in the present work CAD systems based on different optimal feature sets that are composed of the LBP based texture features combined with the morphological features have been experimented.

The overall performance of the conventional CAD system designs heavily depends upon feature engineering stage to compute effective features for obtaining satisfactory results. The inputs from medical fraternity are desired in order to decide upon the set of optimal features which should be extracted from the images for differential diagnosis between abnormalities. These hand-crafted features are not robust to the variations in shape, size and orientation of the tumors resulting in lower sensitivity. Thus deep feature extraction and classification of breast ultrasound images have recently gained attention from research community. In order to explore the potential of different deep learning algorithms for classification of breast tumors, different convolutional neural network (CNN) based CAD systems have been designed and discussed in Chapter-7.

Chapter 7

Convolutional Neural Network based CAD System Designs for Classification of Breast Tumors

7.1. Introduction

For timely detection of breast cancer, different conventional computer-aided diagnostic (CAD) system designs based on machine learning techniques have been developed which involve the steps of feature extraction, feature selection and classification [57, 68, 74, 90, 191, 199, 319]. The deep networks come with an advantage of directly learning the representative features from the images. Convolutional neural networks (CNNs) have been widely used for analysing medical images (detection, segmentation and classification of abnormalities) because of the associated advantage of automatic learning and computing underlying global/local texture and shape features from the medical images, through series of convolution and pooling layers thus eliminating the need of feature engineering stage [4, 178, 225, 243]. However, these networks are difficult to train from scratch if the representative training data is small in size. Therefore transfer learning approach for classification of medical images has been used [31, 34, 49, 75, 92, 93, 207, 234].

Han et al. used pre-trained GoogLeNet CNN model for classification of a total of 7408 breast tumor ultrasound images. In [92] the authors used full images as input to the network achieving an accuracy of 91.0 % while in [93] manually extracted ROIs were used as inputs to the network achieving an accuracy of 90.4 %.

Xiao et al. [294] reported the use of pre-trained InceptionV3 CNN model, self-designed CNN model, and a hybrid method where features computed from ResNet-50, Xception and Inceptionv3 models were fed to neural network (NN) classifier for classification of benign and malignant breast tumors.

Fujioka et al. [75] also attempted to classify 120 breast tumors using a pre-trained GoogLeNet CNN model.

Byra et al. [29] computed a deep feature set from VGG-19 CNN model for classification of 882 breast ultrasound images using support vector machine (SVM) classifier.

Zhang et al. [312] used stacked convolutional autoencoder (SCAE) model for classification 295 breast ultrasound images pre-processed using distance transformation coupled Gaussian filter (DTGF) and segmented using watershed transform.

Most of the studies using deep learning models have been carried out either on full size images or manually extracted ROIs while very few studies have reported the use of segmented tumor images for classification of breast tumors. It is also worth noting that the studies have either been carried out on original images only or pre-processed images only. In the present work, for the segmentation of tumor images both original images and images despeckled by detail preserving anisotropic diffusion (DPAD) filter have been used such that the shape characteristics of tumor are taken from the despeckled images while texture information has been retained by using the original images [144].

7.2. Dataset Generation

The workflow adopted for generation of dataset for CNN based CAD system designs used for classification of breast tumors is given in Fig. 7.1.

7.2.1. Pre-processing Module

7.2.1.1. Pre-processing stage-1: Despeckle filtering

The quality of the ultrasound image is deteriorated because of the presence of speckle noise and low contrast because of which the computer-assisted segmentation becomes a little difficult as the edges of the tumor are sometimes not clearly indicated and masked thus making the margin of the tumor unclear. As validated in *Chapter 3* and *Chapter 4*, the morphological characteristics of breast tumors are better exhibited by images filtered by DPAD despeckle filtering algorithm resulting in adequate segmentation of tumor contour for both benign and malignant tumors. Accordingly, in the present work DPAD filter has been used to pre-process the breast ultrasound images.

7.2.1.2. Pre-processing stage-2: Tumor segmentation

For obtaining the tumor boundary/contour the images despeckled by DPAD filter have been used, as the shape characteristics of the tumor are better represented in despeckled images than in original images. The despeckled images have been subjected to Chan and Vese active contour method. The output of the segmentation algorithm is a binary image with the desired tumor region indicated in white (tumor mask). This tumor mask thus obtained from the DPAD filtered images is superimposed on the original images to retain the original texture resulting in the formation of segmented tumor image.

7.2.1.3. Pre-processing stage-3: Image resizing

The deep learning architectures accept images of a fixed pre-defined size, therefore before feeding the images to the deep learning network for analysis, the images are resized to the appropriate size matching the input layer of the deep network. It is also noteworthy that for

the characterization of breast tumors, the shape of the tumor is also considered to be an important diagnostic criteria and directly resizing the image without maintaining the aspect ratio to match the desired network size sometimes distorts the shape of the tumor compared to original image.

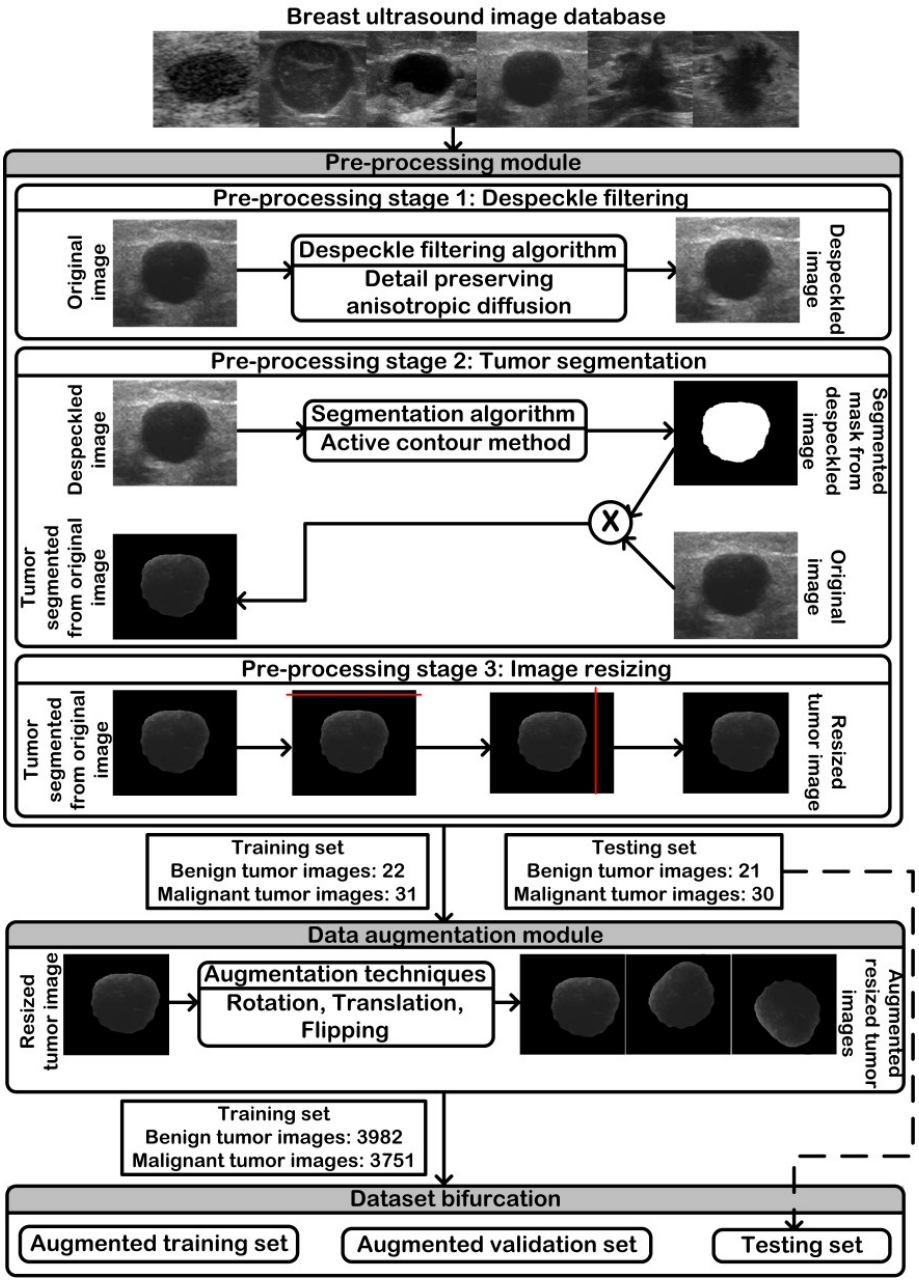

Fig. 7.1 The workflow followed for generation of dataset for CNN based CAD system designs used for classification of breast tumors.

Therefore, in the present work segmented tumor images have been resized to match the input size of the network architecture by preserving their aspect ratio. The procedure followed for the image resizing is given in Fig. 7.2.

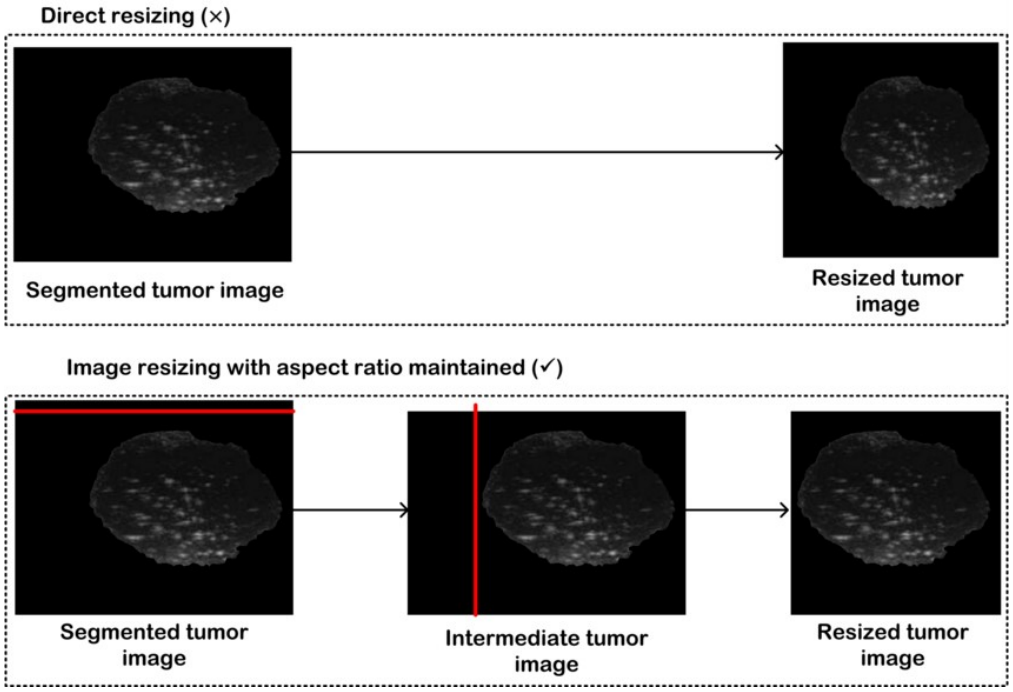

Fig. 7.2 Image resizing.
Note: L_A: Actual length, B_A: Actual breadth, L_D: Desired length, B_D: Desired breadth.

For generating square shaped resized tumor images while maintaining the aspect ratio, the first step is to scale the smaller side of the original image to desired size thereby obtaining an intermediate image. Then from this intermediate image crop of desired size from longer side is taken. Let original image has size $L_A \times B_A$, with $L_A > B_A$, then in the first step, the breadth of the image is scaled to the desired size B_D, resulting in the formation of an intermediate image having size $L_A \times B_D$. Then from this intermediate image, the length L_A can be cropped to desired size L_D, thus generating the resized square image having size $L_D \times B_D$, with $L_D = B_D$.

7.2.2. Data augmentation module

The size of the dataset affects the performance of deep learning algorithm. In case there is limited amount of data, various data augmentation techniques can be applied for increasing the number of representative images [79, 189, 278]. Data augmentation is a technique used for virtually increasing the number of samples present in the dataset by using the existing data. A variety of techniques can be applied to the images for augmentation purposes e.g. geometrical transformations, random cropping, changing the contrast of image, adding noise to the image, and colour jittering etc. The advantages of data augmentation are: (*i*) Generation of new data from the existing data without changing its label information. (*ii*) Overfitting in deep learning occurs when a model achieves a good accuracy on training data however performs poorly for the new unseen data. Overfitting can be reduced by increasing the amount of training data

provided to the model. Thus data augmentation contributes to reduce overfitting. (*iii*) Provides implicit regularization. (*iv*) During data augmentation, the existing image data is transformed using different geometric and photometric transformation methods. This makes the network invariant to the applied transformations (i.e. translations, size of object, illumination, orientation etc.) thus increasing the robustness of the deep learning model. (*v*) In case of imbalanced dataset, data augmentation can be used to balance the data.

Depending upon the type of tissue to be examined, the underlying features of the abnormal region i.e. either only texture or texture and shape or texture, shape and colour information are considered clinically significant for the diagnosis. For the augmentation of breast ultrasound images, geometric transformations have been widely used [29, 30, 92, 93, 294, 311]. However, these transformations should be carefully selected such that both texture and shape information is preserved. Accordingly, in the present work, rotation, translation and flipping have been selected for augmenting the images as by the application of these techniques the texture as well as shape of the tumor remains preserved. The sample benign and malignant tumor images selected from the dataset along with their augmented versions are given in Fig. 7.3 and Fig. 7.4, respectively.

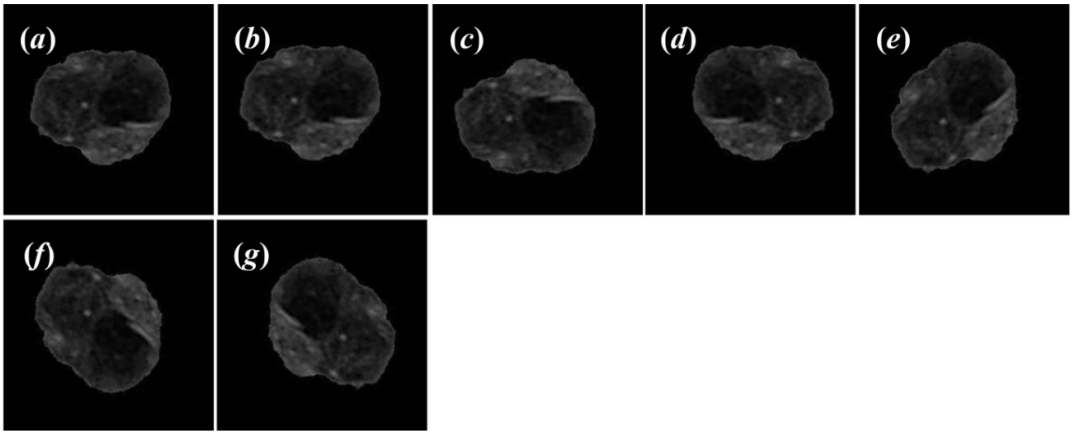

Fig. 7.3 Sample benign images indicating (*a*) Segmented tumor image, (*b*) Translated tumor image, (*c*) Translated tumor image flipped vertically, (*d*) Translated tumor image flipped horizontally, (*e*) Rotated tumor image, (*f*) Rotated tumor image flipped vertically, (*g*) Rotated tumor image flipped horizontally.

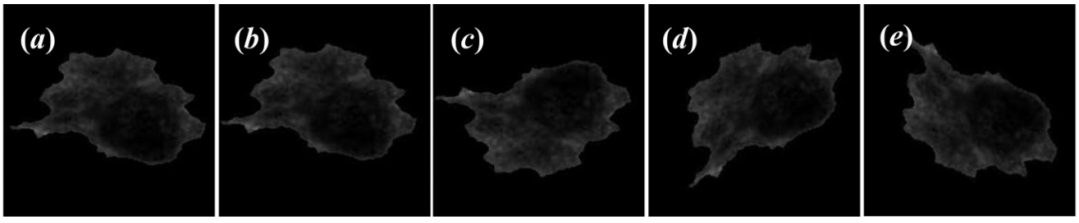

Fig. 7.4 Sample malignant images indicating (*a*) Segmented tumor image, (*b*) Translated tumor image, (*c*) Translated tumor image flipped vertically, (*d*) Rotated tumor image, (*e*) Rotated tumor image flipped vertically.

The augmentation techniques have been differently applied to benign and malignant tumors for balancing the dataset. The augmentation scheme applied to benign and malignant tumor images is given in Fig. 7.5.

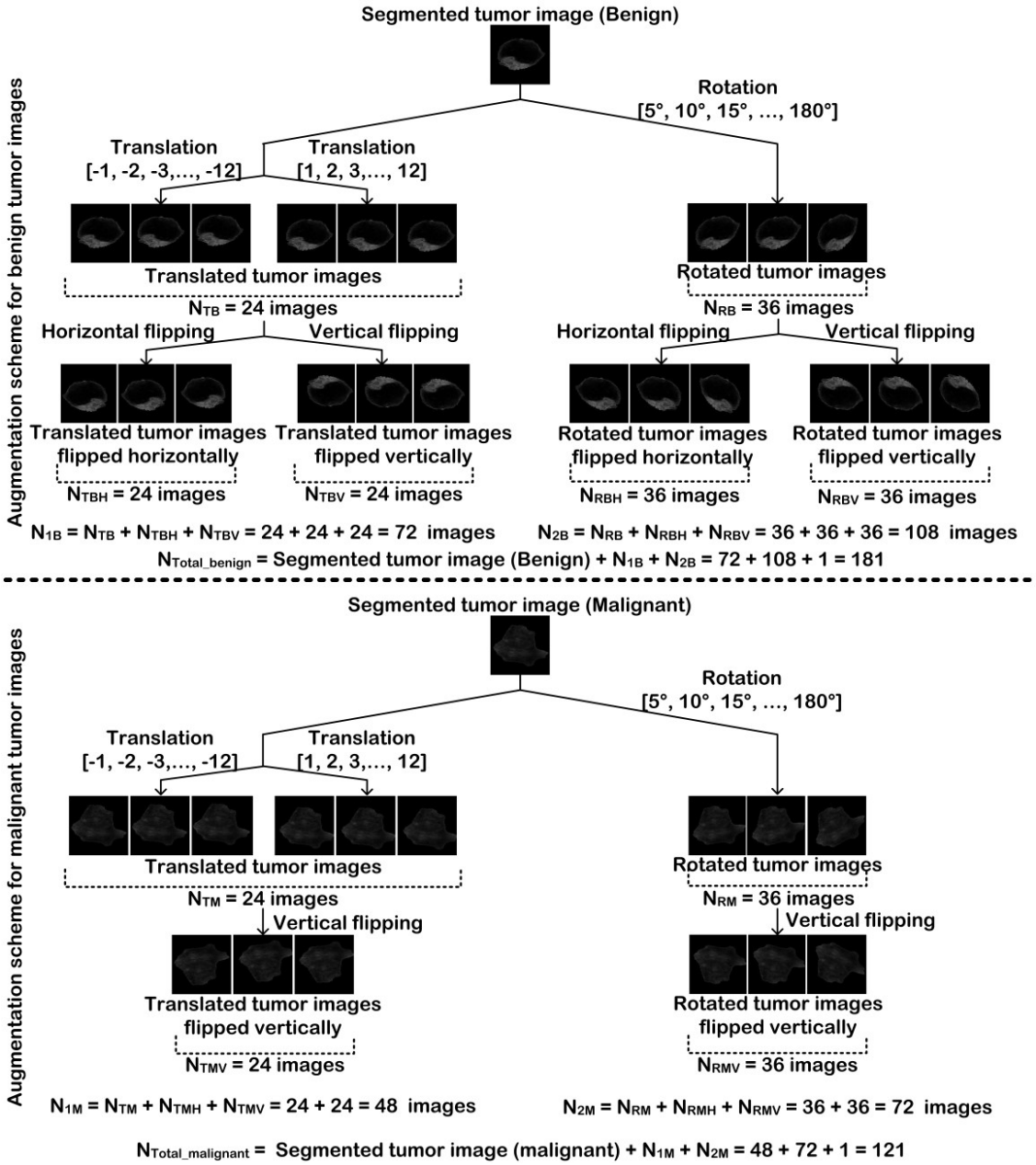

Fig. 7.5 Augmentation scheme applied to benign and malignant tumor images.

Note: N_{TB}: Number of translated benign tumor images, N_{TBH}: Number of translated benign tumor images flipped horizontally, N_{TBV}: Number of translated benign tumor images flipped vertically, N_{RB}: Number of rotated benign tumor images, N_{RBH}: Number of rotated benign tumor images flipped horizontally, N_{RBV}: Number of benign rotated tumor images flipped vertically, N_{TM}: Number of translated malignant tumor images, N_{TMH}: Number of translated malignant tumor images flipped horizontally, N_{TMV}: Number of translated malignant tumor images flipped vertically, N_{RM}: Number of rotated malignant tumor images, N_{RMH}: Number of rotated malignant tumor images flipped horizontally, N_{RMV}: Number of malignant rotated tumor images flipped vertically.

7.2.3. Dataset bifurcation

For carrying out the present work, the dataset has been bifurcated into three subsets i.e. training, validation and testing. The schematic diagram indicating the dataset bifurcation is given in Fig. 7.6.

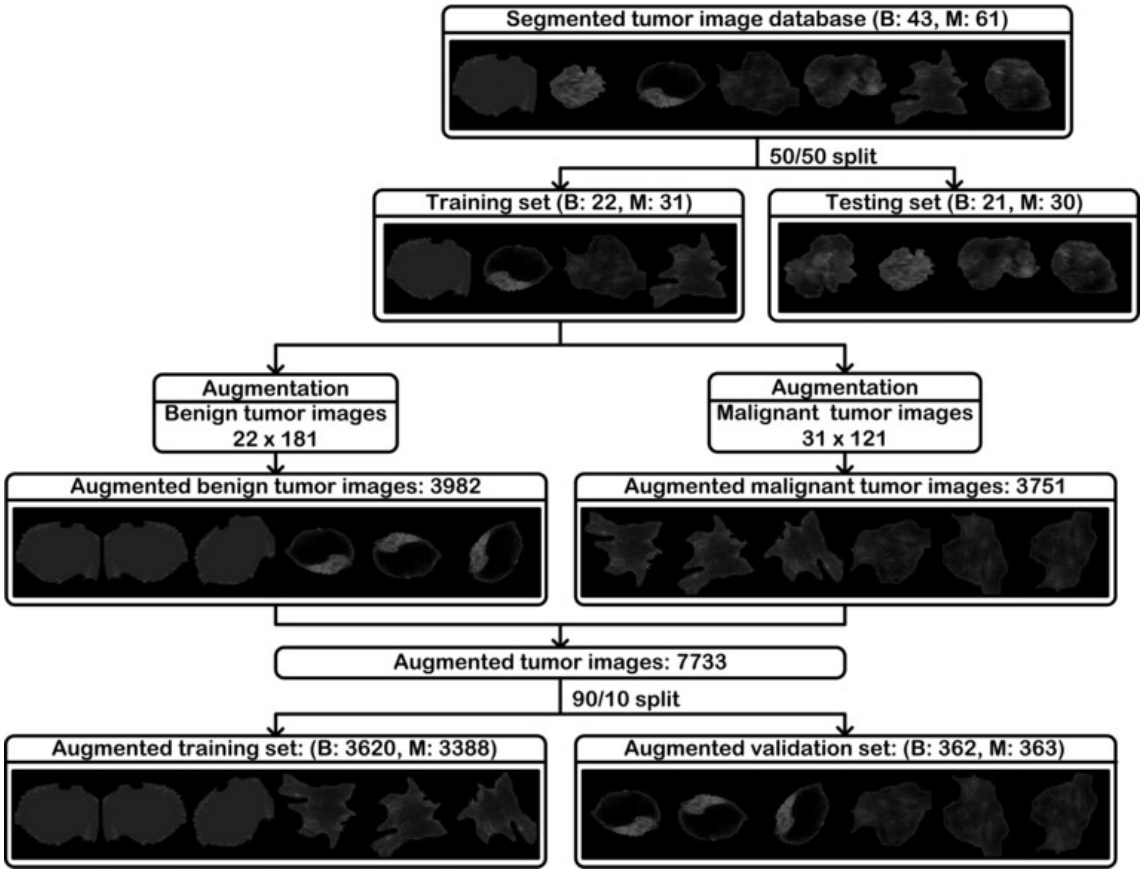

Fig. 7.6 Schematic diagram indicating the dataset bifurcation.
Note: B: Benign, M: Malignant.

Initially whole dataset has been bifurcated into training and testing sets using a 50/50 split. Data augmentation techniques have been applied to the images in the training set in order to increase the number of representative cases as well as balance the number of images in both the classes. From the augmented dataset, 10 % of the data is selected for validation purposes.

7.3. Convolutional Neural Network based CAD System Designs

Over the years, CNN based CAD system designs have been used for classification of medical images [4, 31, 49, 100, 178, 207, 234, 243, 258, 260, 278, 284]. For classification of breast ultrasound images, various attempts have been made by using either pre-trained CNN models or self-designed CNN models as end-to-end networks [56, 92, 93, 294] or as feature extractors [29, 294].

The CNNs have a layered architecture to represent high level abstraction in data. The different CNN layers are (*a*) convolution, (*b*) activation, (*c*) pooling, (*d*) fully connected and (*e*) softmax. The CNNs are able to recognize the underlying visual patterns of an input image by learning the local and global image features through training. Transfer learning and fine-tuning approaches are more prevalently used for the analysis and classification of medical images [145, 225, 262, 284, 307, 322]. Transfer learning is a training strategy wherein, a network developed and trained for one task is reused for another task i.e. a source network is trained on a source dataset for a task and the learned weights are then transferred to a second network to be trained on a target dataset for a target task [225, 284, 307]. In case of fine-tuning, the new dataset is used to adjust the parameters of the pre-trained network considering that the new dataset is similar to the original dataset [145, 262, 322]. The diagram illustrating the transfer learning approach is indicated in Fig. 7.7.

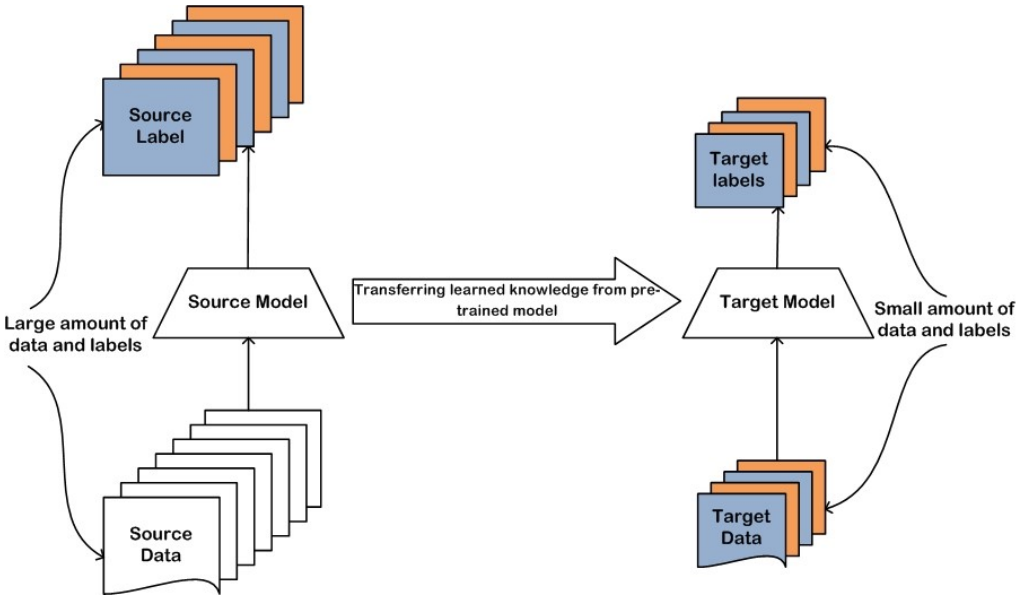

Fig. 7.7 Transfer learning approach.

The basic layers of a convolution neural network are described as follows:

(*a*) Convolution layer: These layers are the feature extractors as they learn feature representations from the input images. The inputs are convolved with the learnable weights of the convolution layer to form an output feature map. The output of the neurons is computed using the dot product between weights and a small region in the input image to which they are connected. An example indicating the convolution operation is given in Fig. 7.8.

(*b*) Activation layer: These layers are used to apply the non-linearity to the input so that it can learn and perform complex tasks. The activation function decides whether a particular neuron should be activated or not. The most commonly used activation functions used in the deep

learning models are sigmoid, *tanh*, rectified linear unit (ReLU) and its variants like leaky ReLU (LReLU), parametric ReLU (PReLU) and exponential linear unit (ELU). The different activation functions used are given in Fig. 7.9.

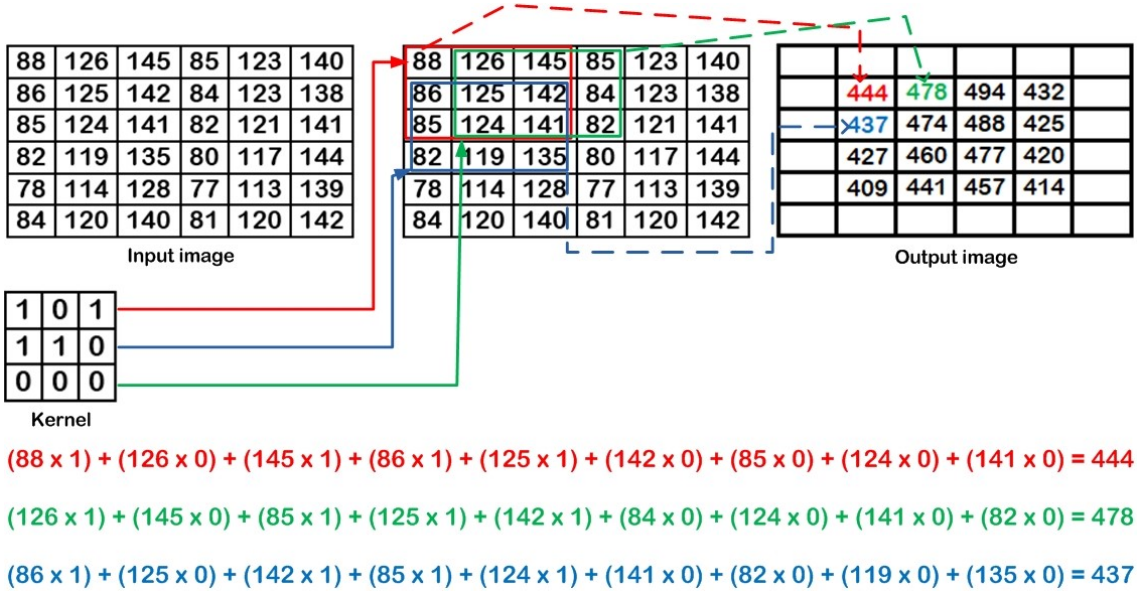

Fig. 7.8 Convolution operation.

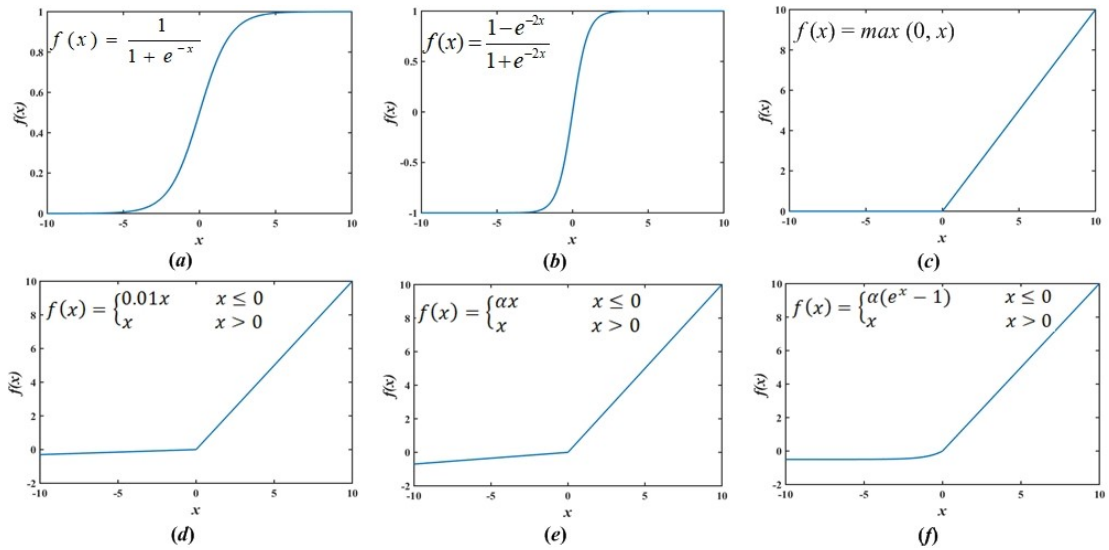

Fig. 7.9 Activation functions used in deep learning. (*a*) Sigmoid, (*b*) *tanh*, (*c*) ReLU, (*d*) LReLU, (*e*) PReLU, (*f*) ELU.

(*c*) Pooling layer: These layers are used to reduce the spatial dimension of the input so as to reduce the number of network parameters and computations to be performed. Also due to the reduced spatial resolution, the pooling layers are able to achieve spatial invariance to translations and input distortions. The most common pooling operations are average pooling and maximum pooling. An example indicating the pooling operation is given in Fig. 7.10.

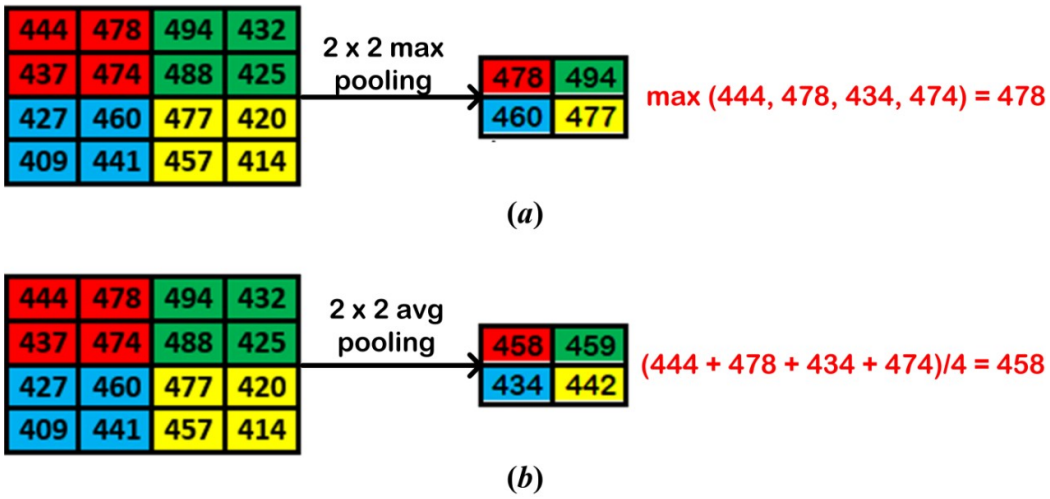

Fig. 7.10 Pooling operation. (*a*) Maximum pooling, (*b*) Average pooling.
Note: max: maximum, avg: average.

(*d*) Fully connected layer: These layers are used to flatten and aggregate all the information from the previous layers to a 1D vector. The fully connected layers interpret the feature representations extracted by the convolution and pooling layers. The 1D data then acts as the input to the neuron of the last fully connected layer which performs a dot product of this input data and the neuron's weights to produce a single number as output.

(*e*) Softmax layer: This layer is the last layer of the deep learning network yielding the actual probability scores of each class.

In the present work the popularly used CNN models namely GoogLeNet, VGG-19 and ResNet-18 have been used on the basis of comprehensive literature survey while their performance has also been compared to a compressed network SqueezeNet which is said to use lesser parameters.

7.4. Experimental Workflow : CNN based CAD System Designs for Classification of Breast Tumors

The experimental workflow followed in the present work for the design of CNN based CAD systems for classification of breast tumors is given in Fig. 7.11.

From Fig 7.11 it can be observed that to design an efficient CNN based CAD system for classification of breast tumors exhaustive experiments have been carried out in the present work. These experiments are described as: (*a*) Design of CNN based CAD system using GoogLeNet model, (*b*) Design of CNN based CAD system using VGG-19 model, (*c*) Design of CNN based CAD system using ResNet-18 model, (*d*) Design of CNN based CAD system using SqueezeNet model and (*e*) Design of CNN based CAD system using GoogLeNet model as feature extractor and ANFC classifier.

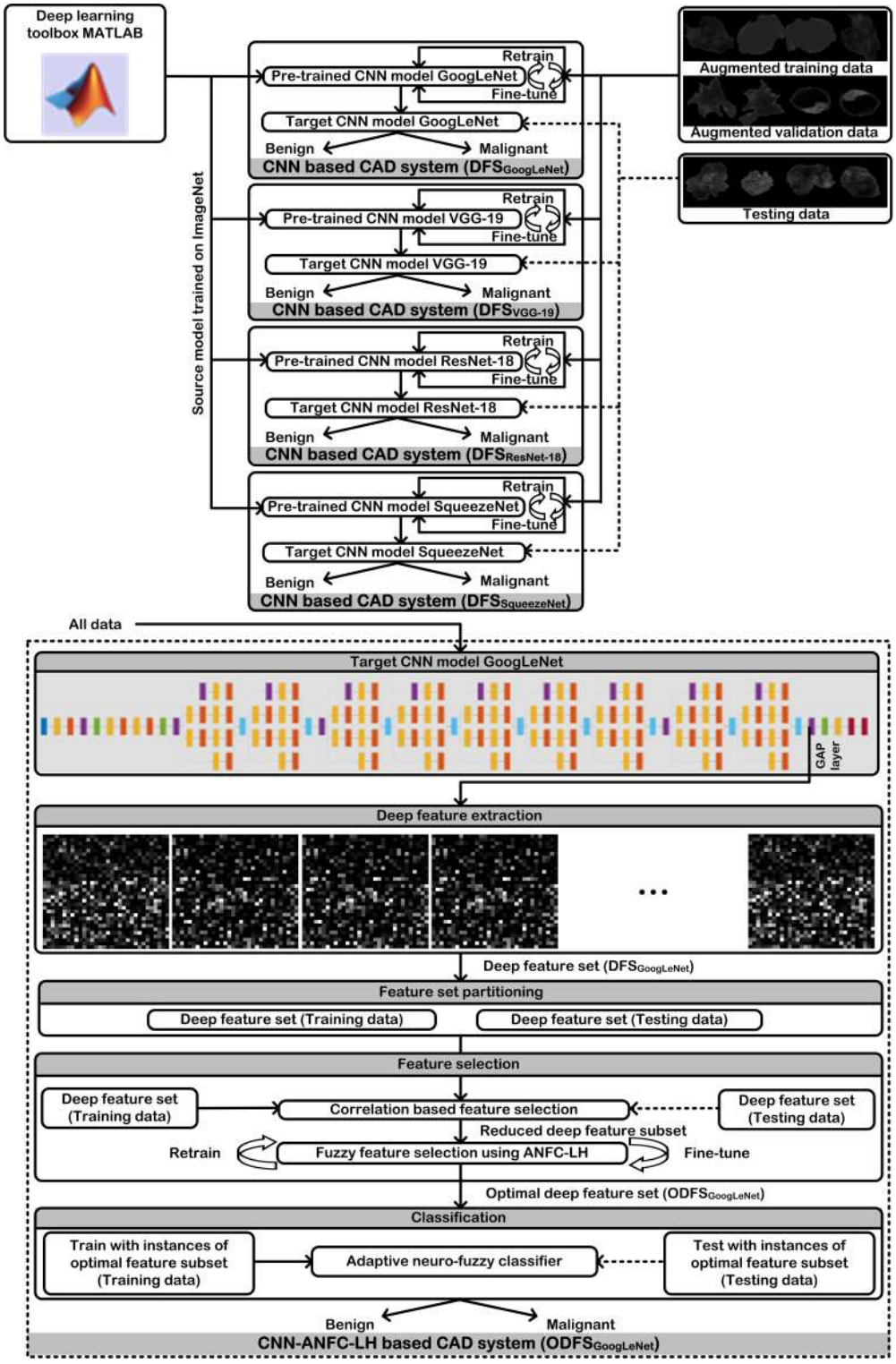

Fig. 7.11 Experimental workflow followed for the design of CNN based CAD systems for classification of breast tumors. ■ The shaded grey region indicates the optimal CNN based CAD system for classification of breast tumors.

Note: CNN: Convolutional neural network, GAP: Global average pooling, $ODFS_{GoogLeNet}$: Optimal deep feature set obtained by applying correlation based feature selection followed by ANFC-LH algorithm to $DFS_{GoogLeNet}$, ANFC-LH: Adaptive neuro-fuzzy classifier using linguistic hedges.

7.4.1. Design of CNN based CAD system using GoogLeNet model

The GoogLeNet architecture was proposed by Szegedy et al. [261] and the winner of ILSVRC 2014. The GoogLeNet CNN model has been used in the analysis of medical images [100, 160, 260, 277] particularly for breast ultrasound images [75, 92, 93]. In the present work, source GoogLeNet CNN model trained on ImageNet data has been retrained and fine-tuned using the augmented training and validation datasets consisting of segmented breast ultrasound tumor images to obtain the target GoogLeNet CNN model. The architecture of GoogLeNet CNN model and configuration of an inception module is given in Fig. 7.12.

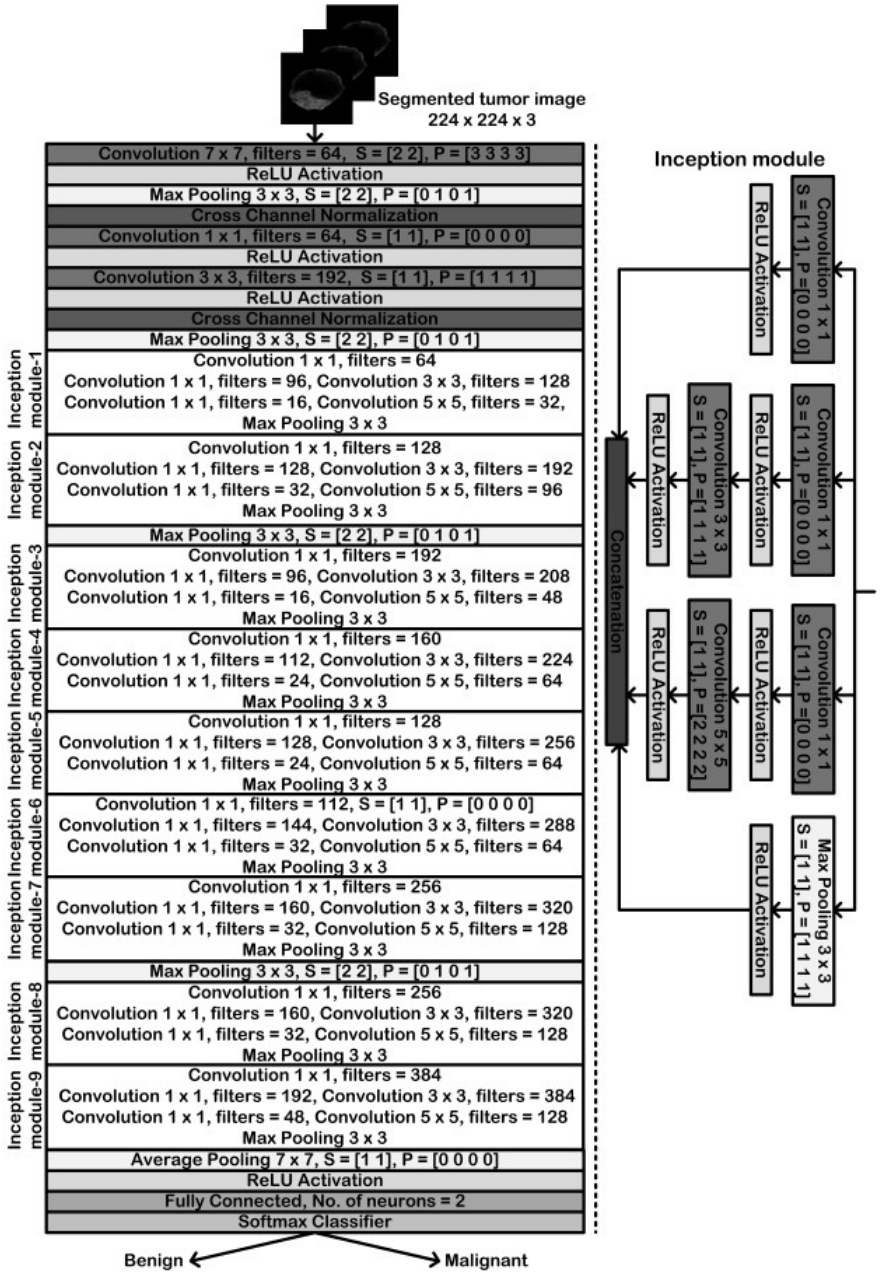

Fig. 7.12 Architecture of GoogLeNet CNN model and configuration of an inception module.

GoogLeNet CNN model introduces the concept of 1 × 1 convolutions, global average pooling (GAP) and inception module. In this network, 1 × 1 convolution is used for dimension reduction to reduce computational bottlenecks. The GAP layer is used instead of fully connected layers to reduce the computation cost of the network as there are no trainable weights in a GAP layer. Nine inception modules have been used in the middle of the network. The inception network is a combination of all the convolutions (1 × 1, 3 × 3, 5 × 5) with the final output being the concatenation of the result of each convolution. The inception modules were introduced to overcome the variation in the location information of an object in the image which requires the selection of right kernel size.

7.4.2. Design of CNN based CAD system using VGG-19 model

The VGGNet CNN model was developed by the visual geometry group of the University of Oxford and the runner-up of ILSVRC 2014 [250]. The VGGNet CNN model and its variants have been used in the analysis of medical images [4, 49, 260, 277, 284, 307] particularly for breast ultrasound images [28-30].

In the present work, source VGG-19 CNN model trained on ImageNet data has been retrained and fine-tuned using the augmented training and validation datasets consisting of segmented breast ultrasound tumor images to obtain the target VGG-19 CNN model. The architecture of VGG-19 CNN model is given in Fig. 7.13.

The model is built entirely upon the use of 3 × 3 convolutional filters instead of large size filters used in AlexNet or GoogLeNet. It has been shown that by replacing larger filters with a group of 3 × 3 filters results in the same receptive field being covered by the larger filter size however, the number of parameters required has been reduced which in turn results in faster convergence and reduced overfitting [250].

7.4.3. Design of CNN based CAD system using ResNet-18 model

The residual networks were introduced by He et al. in the year 2015 [98]. The ResNet CNN model and its variants have been used in the analysis of medical images [260, 277, 284, 307] particularly for breast ultrasound images [294, 295].

In the present work, source ResNet-18 CNN model trained on ImageNet data has been retrained and fine-tuned using the augmented training and validation datasets consisting of segmented breast ultrasound tumor images to obtain the target ResNet-18 CNN model. The architecture of ResNet-18 CNN model and configuration of residual blocks is given in Fig. 7.14.

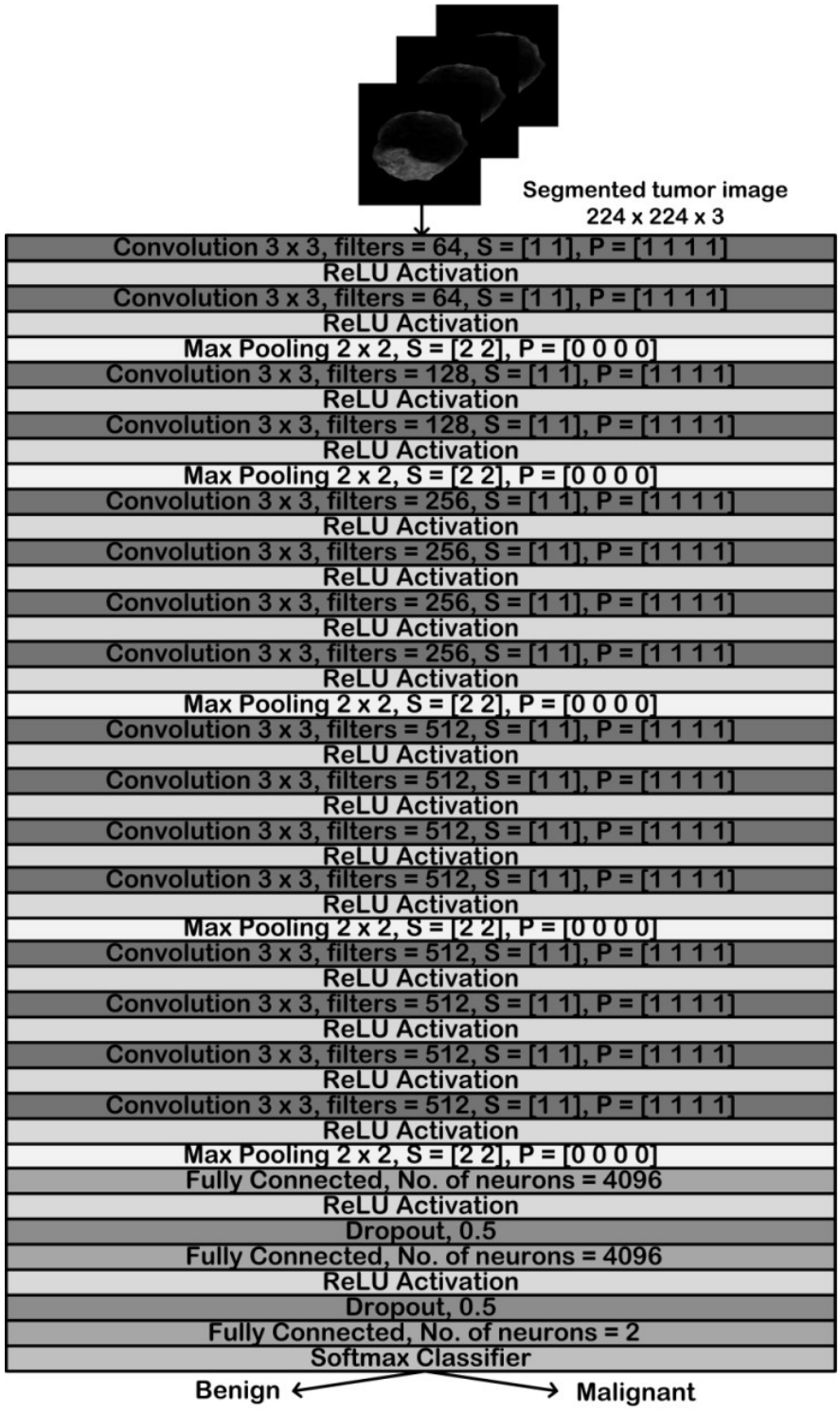

Fig. 7.13 Architecture of VGG-19 CNN model.

The main idea behind ResNet CNN model is the introduction of identity shortcut connections by jumping over one or more layers. These shortcut connections were introduced in order to overcome the problem of vanishing gradient in deep networks by reusing the previous layer activations.

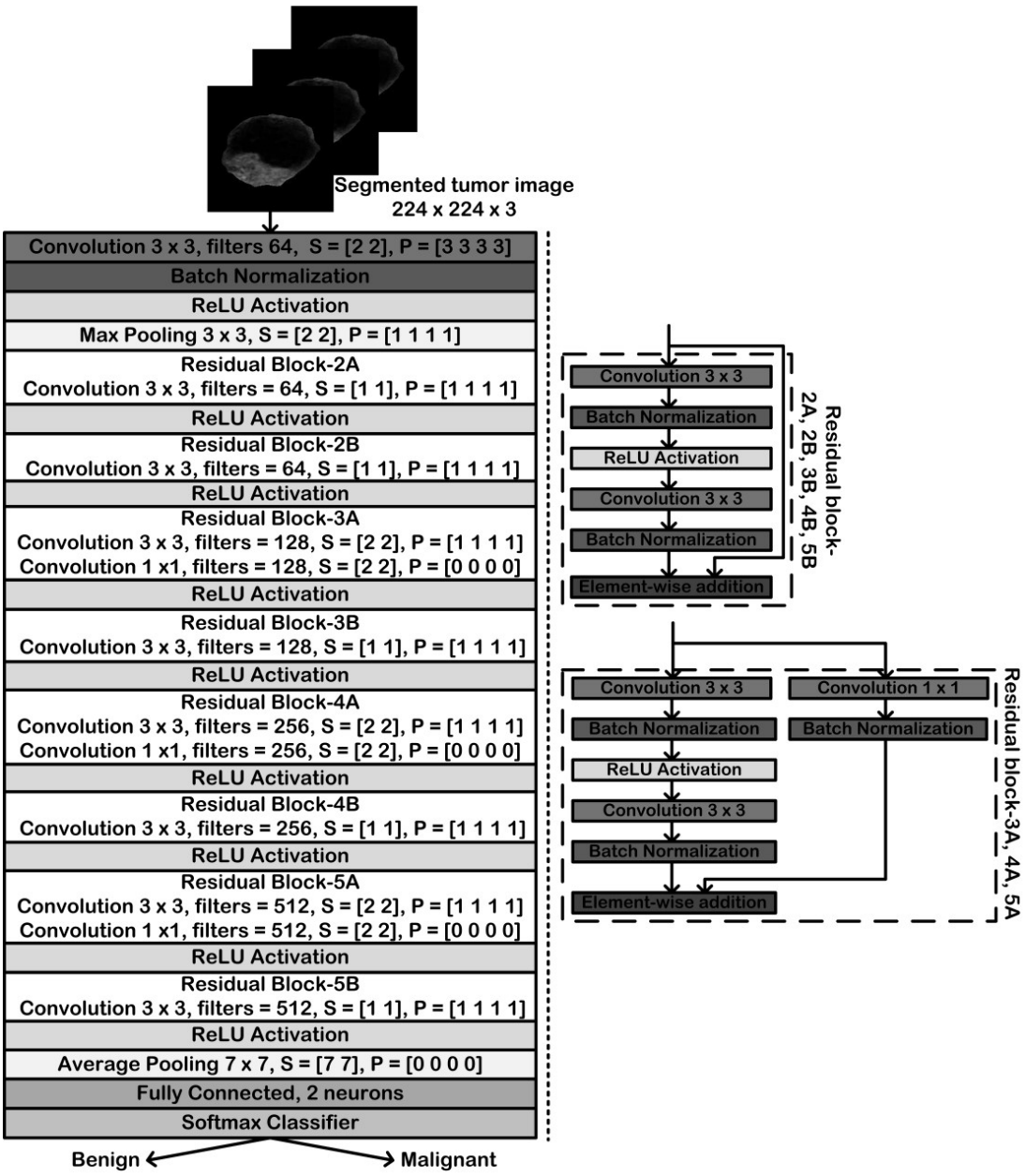

Fig. 7.14 Architecture of ResNet-18 CNN model and configuration of residual blocks.

7.4.4. Design of CNN based CAD system using SqueezeNet model

The network was introduced in 2016 by the researchers at DeepScale, University of California, Berkeley and Stanford [116]. It was designed with an aim to create networks with lesser parameters thus requiring less storage space and transmission bandwidth. The SqueezeNet CNN model has been used in the analysis of medical images [222, 227, 275]. In the present work, source SqueezeNet CNN model trained on ImageNet data has been retrained and fine-tuned using the augmented training and validation datasets consisting of segmented

breast ultrasound tumor images to obtain the target SqueezeNet CNN model. The architecture of SqueezeNet CNN model and configuration of fire module is given in Fig. 7.15.

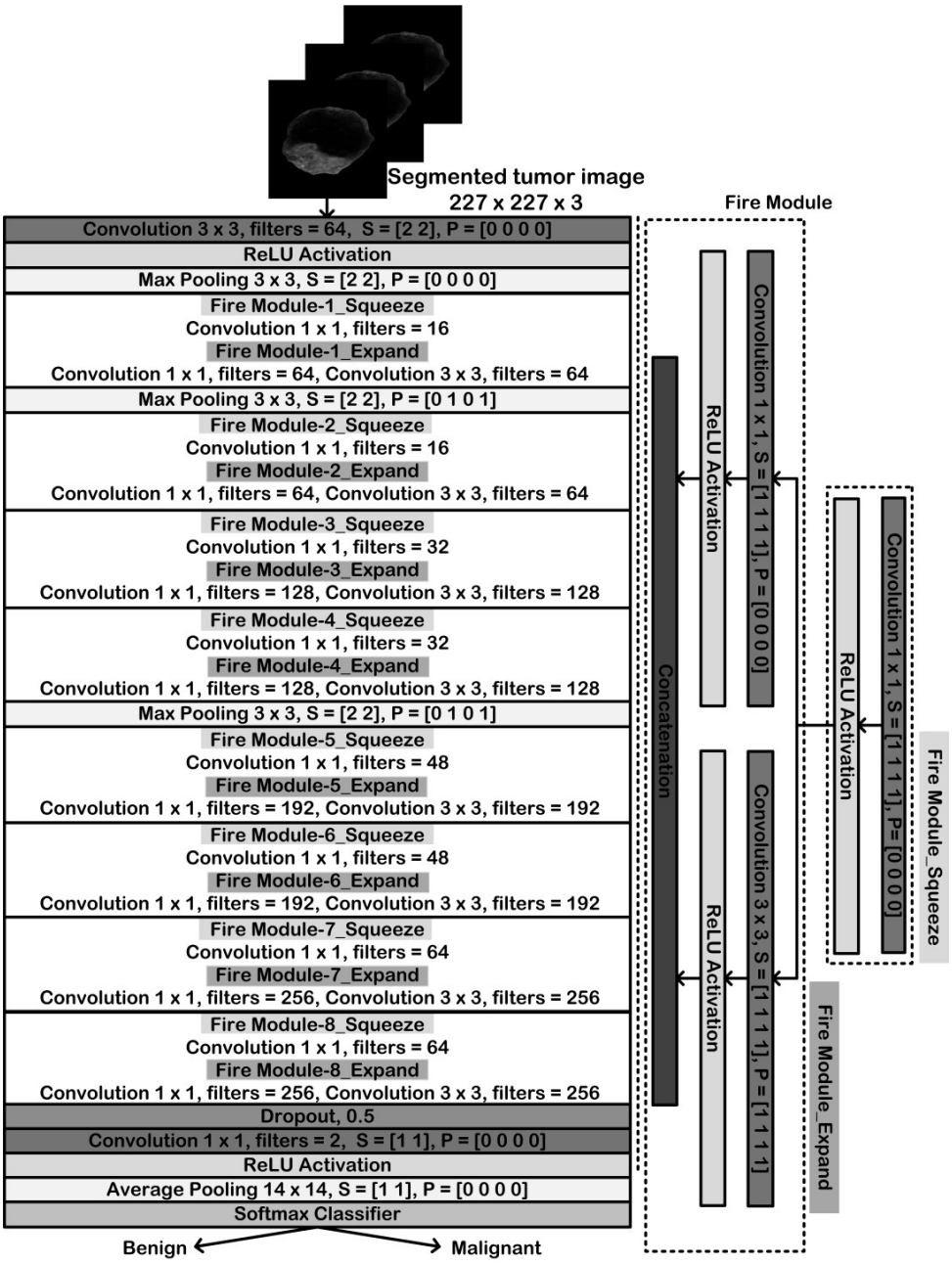

Fig. 7.15 Architecture of SqueezeNet CNN model and configuration of fire module.

The SqueezeNet CNN model is composed of fire modules which consists of a squeeze layer and an expand layer. The squeeze layer is entirely made up of 1 × 1 convolutions while the expand layer is made up of a combination of 1 × 1 and 3 × 3 convolutions. A total of 8 fire modules are used in the SqueezeNet architecture. It has been validated that SqueezeNet CNN model achieved same accuracy as that of AlexNet CNN model with lesser parameters and faster training time.

7.4.5. Design of CNN based CAD system using GoogLeNet model as feature extractor and ANFC classifier

In this experiment the performance of target GoogLeNet CNN model has been evaluated as feature extractor and the computed deep feature set has been fed to an adaptive neuro-fuzzy classifier (ANFC) for classification of breast tumors.

7.4.5.1. Deep feature extraction and feature set partitioning

For extracting the deep features to be used for classification of breast tumors, the GAP layer of target GoogLeNet CNN model has been used. The breast ultrasound tumor image dataset has been fed to the target GoogLeNet CNN model and for each image a deep feature vector consisting of 1024 features has been computed. All these deep feature vectors have been combined to form a deep feature set (DFS). This DFS has then been partitioned into training and testing set used further for classification of breast tumors.

7.4.5.2. Feature selection

The computed feature set sometimes contains a large number of features which may be redundant and can negatively affect the classification performance of the CAD systems. Thus, the selection of relevant features is a pre-requisite for the design of efficient CAD systems. For this experiment a 2-stage feature selection process has been followed. In the 1st stage, correlation based feature selection (CrFS) has been applied to the computed deep feature set to remove the correlated features thus generating a reduced deep feature set (RDFS). This reduced feature set has further been subjected to a fuzzy feature selection technique, adaptive neuro-fuzzy classifier using linguistic hedges (ANFC-LH) for finding out an optimal deep feature set (ODFS).

(*a*) *Correlation based feature selection*: In correlation based feature selection, best subset of features is selected based on the value of correlation coefficient. The selection criterion is based on the fact that the features are uncorrelated to each other but are highly correlated to the class [184]. From the DFS having 1024 features, after the application of CrFS a total of 60 features have been selected forming the RDFS.

(*b*) *Feature selection using ANFC-LH algorithm*: In the present work, a fuzzy feature selection method based on the linguistic hedges (LHs) has been implemented for breast tumor characterization using ultrasound images [226, 309]. From the RDFS having 60 features, on the basis of linguistic hedge values, after the application of ANFC-LH algorithm a total of 22 optimal features have been selected forming an ODFS. The relationship between input features and their respective power of LH value is represented in Fig. 7.16.

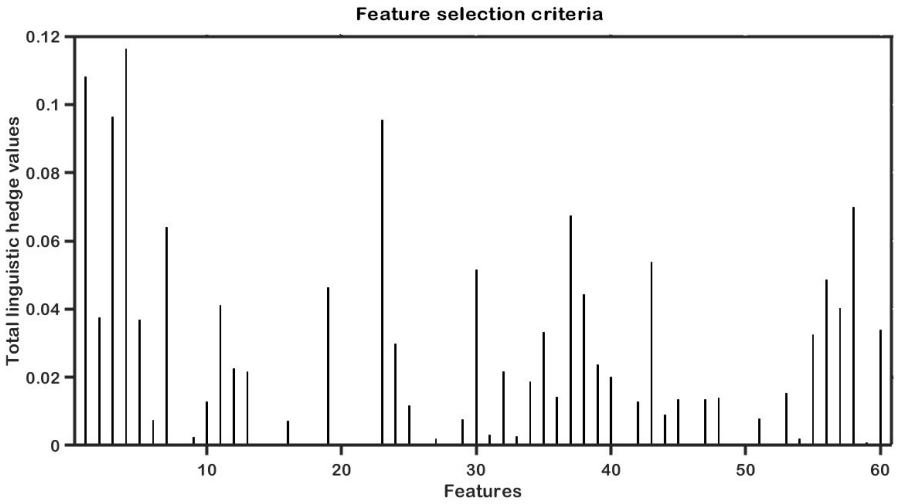

Fig. 7.16 The relationship between input features and their respective power of LH value.

7.4.5.3. Adaptive neuro-fuzzy classifier

For classification of breast tumors, the computed ODFS has been fed to the ANFC classifier. The computed features have been normalized in the range [0, 1] by using min-max normalization in order to avoid any bias caused by unbalanced feature values. Firstly, the min-max normalization procedure has been applied to the features in the training set and the same settings have then been applied to normalize the features in the testing set. The layer architecture of ANFC used in the present work is given in Fig. 7.17.

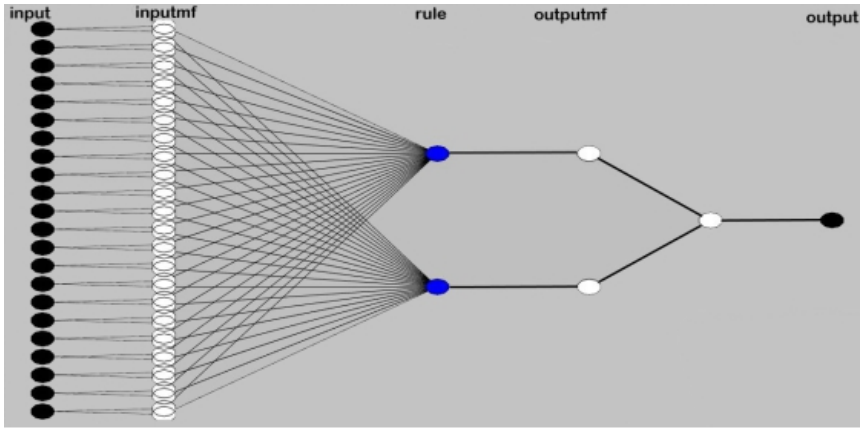

Fig. 7.17 The layer architecture of ANFC used in the present work.

7.4.6. Implementation details

In the present work the deep network training was implemented using pre-trained deep learning models available in the Deep learning toolbox of MATLAB R2018b. The entire image dataset was stored on a 64-bit windows 10 PC with Intel (R) Core (TM) i7-4790 CPU@3.6 GHz processor and NVIDIA 1650TI GPU with 890 CUDA cores. The pre-trained networks were

retrained and fine-tuned on augmented training and validation sets consisting of segmented breast ultrasound tumor images. The networks were trained using Adam as the optimizer at learning rates varying in the range $\{10^{-3}, 10^{-4}, 10^{-5}, 10^{-6}\}$ and a mini-batch size of 48. The size of mini-batch was selected with care such that it evenly divides the number of images in the augmented training data such that whole dataset was to be passed through the network every epoch during training and no data is discarded. To avoid the discarding of same data, the option for data shuffling to be specified in the training options was set to 'every-epoch' in case the mini-batch size does not evenly divide the training and validation datasets. The networks were trained for 100 epochs. To avoid overfitting, an early stopping criterion was used in case the performance of the model starts degrading on the validation set (i.e. validation loss begins to increase or accuracy begins to decrease).

As studied from the exhaustive literature review of the related studies the best network and the activation function varies in different classification tasks. For the present classification task, i.e. classification of segmented breast ultrasound images, transfer learning approach has been used thus the base GoogLeNet model with ReLU as activation function has been used to extract the deep features. Also exhaustive experiments were carried out to find an ideal optimizer to train the deep network and it was found that the deep features computed using the GoogLeNet model trained with Adam optimizer when fed to ANFC-LH classifier, yielded best classification performance.

7.5. Experiments and Results

For evaluating the performance of CAD systems designed for classification of breast tumors, exhaustive experiments have been conducted as described in Table 7.1.

Table 7.1 Description of the experiments for the design of CNN based CAD systems.

Experiment 1	Design of CNN based CAD system using GoogLeNet model for classification of breast tumors.
Experiment 2	Design of CNN based CAD system using VGG-19 model for classification of breast tumors.
Experiment 3	Design of CNN based CAD system using ResNet-18 model for classification of breast tumors.
Experiment 4	Design of CNN based CAD system using SqueezeNet model for classification of breast tumors.
Experiment 5	Design of CNN based CAD system using GoogLeNet model as feature extractor and ANFC classifier for classification of breast tumors.

Note: CNN: Convolutional neural network, CAD: Computer aided diagnostic, ANFC: Adaptive neuro-fuzzy classifier.

7.5.1. Experiment 1: Design of CNN based CAD system using GoogLeNet model for classification of breast tumors

In this experiment, a pre-trained GoogLeNet CNN model has been retrained and fine-tuned on breast ultrasound images using the augmented training and validation sets to obtain a

target GoogLeNet CNN model. The results obtained by projecting the testing set to this target GoogLeNet CNN model are represented in Table 7.2.

Table 7.2 Classification results of CNN based CAD system using GoogLeNet model for classification of breast tumors.

CAD system (DFS : *l*)	CM			Accuracy (%)	ICA_B (%)	ICA_M (%)
CNN based CAD system ($DFS_{GoogLeNet}$: 1024)		B	M	94.1	90.4	96.6
	B	19	2			
	M	1	29			

Note: DFS: Deep feature set, *l*: Length of feature vector in DFS, CNN: Convolutional neural network, CM: Confusion matrix, ICA: Individual class accuracy, B: Benign, M: Malignant.

From the results shown in Table 7.2, it can be noted that the target GoogLeNet CNN model yielded an accuracy of 94.1 % for differentiating between benign and malignant tumor types. The individual class accuracy (ICA) value of benign class is 90.4 % and the ICA value obtained for malignant class is 96.6 %. Out of the total 51 instances in the testing set, 3 instances have been incorrectly classified out of which 2 instances belong to benign class and 1 instance belongs to the malignant class.

7.5.2. Experiment 2: Design of CNN based CAD system using VGG-19 model for classification of breast tumors

In this experiment, a pre-trained VGG-19 CNN model has been retrained and fine-tuned on breast ultrasound images using the augmented training and validation sets to obtain a target VGG-19 CNN model. The results obtained by projecting the testing set to this target VGG-19 CNN model are represented in Table 7.3.

Table 7.3 Classification results of CNN based CAD system using VGG-19 model for classification of breast tumors.

CAD system (DFS : *l*)	CM			Accuracy (%)	ICA_B (%)	ICA_M (%)
CNN based CAD system (DFS_{VGG-19} : 2048)		B	M	90.2	85.7	93.3
	B	18	3			
	M	2	28			

Note: DFS: Deep feature set, *l*: Length of feature vectors in DFS, CNN: Convolutional neural network, CM: Confusion matrix, ICA: Individual class accuracy, B: Benign, M: Malignant.

From the results shown in Table 7.3, it can be noted that the target VGG-19 CNN model yielded an accuracy of 90.2 % for differentiating between benign and malignant tumor types. The ICA value of benign class is 85.7 % and the ICA value obtained for malignant class is 93.3 %. Out of the total 51 instances in the testing set, 5 instances have been incorrectly classified out of which 3 instances belong to benign class and 2 instance belongs to the malignant class.

7.5.3. Experiment 3: Design of CNN based CAD system using ResNet-18 model for classification of breast tumors

In this experiment a pre-trained ResNet-18 CNN model has been retrained and fine-tuned on breast ultrasound images using the augmented training and validation sets to obtain a target ResNet-18 CNN model. The results obtained by projecting the testing set to this target ResNet-18 CNN model are represented in Table 7.4.

Table 7.4 Classification results of CNN based CAD system using ResNet-18 model for classification of breast tumors.

CAD system (DFS : *l*)		CM		Accuracy (%)	ICA_B (%)	ICA_M (%)
		B	M			
CNN based CAD system ($DFS_{ResNet\text{-}18}$: 512)	B	18	3	88.2	85.7	90.0
	M	3	27			

Note: DFS: Deep feature set, *l*: Length of feature vectors in DFS, CNN: Convolutional neural network, CM: Confusion matrix, ICA: Individual class accuracy, B: Benign, M: Malignant.

From the results shown in Table 7.4, it can be noted that the target ResNet-18 CNN model yielded an accuracy of 88.2 % for differentiating between benign and malignant tumor types. The ICA value of benign class is 85.7 % and the ICA value obtained for malignant class is 90.0 %. Out of the total 51 instances in the testing set, 6 instances have been incorrectly classified out of which 3 instances belong to benign class and 3 instances belong to the malignant class.

7.5.4. Experiment 4: Design of CNN based CAD system using target SqueezeNet model for classification of breast tumors

In this experiment, a pre-trained SqueezeNet CNN model has been retrained and fine-tuned on breast ultrasound images using the augmented training and validation sets to obtain a target SqueezeNet CNN model. The results obtained by projecting the testing set to this target SqueezeNet CNN model are represented in Table 7.5.

Table 7.5 Classification results of CNN based CAD system using SqueezeNet model for classification of breast tumors.

CAD system (DFS : *l*)		CM		Accuracy (%)	ICA_B (%)	ICA_M (%)
		B	M			
CNN based CAD system ($DFS_{SqueezeNet}$: 392)	B	19	2	90.2	90.4	90.0
	M	3	27			

Note: DFS: Deep feature set, *l*: Length of feature vectors in DFS, CNN: Convolutional neural network, CM: Confusion matrix, ICA: Individual class accuracy, B: Benign, M: Malignant.

From the results shown in Table 7.5, it can be noted that the target SqueezeNet CNN model yielded an accuracy of 90.2 % for differentiating between benign and malignant tumor types. The ICA value of benign class is 90.4 % and the ICA value obtained for malignant class is 90.0 %. Out of the total 51 instances in the testing set, 5 instances have been incorrectly classified out of which 2 instances belong to benign class and 3 instances belong to the malignant class.

7.5.5. Experiment 5: Design of CNN based CAD system using GoogLeNet model as feature extractor and ANFC classifier for classification of breast tumors

From the results of the experiments 1-4 as seen from Tables 7.2-7.5, it is noted that the target GoogLeNet CNN model yielded highest classification accuracy of 94.1 % therefore, for this experiment; the features from the GAP layer of target GoogLeNet model have been extracted. As a result of the application of CrFS, the deep feature set containing 1024 features is reduced to a feature set containing 60 uncorrelated features which are further fed to a fuzzy feature selection method employing ANFC-LH algorithm resulting in the generation of an optimal feature set containing 22 features. These optimal features are further fed to an ANFC classifier for classification of breast tumors. The classification results obtained for this experiment are shown in Table 7.6.

Table 7.6 Classification results of CNN based CAD system using GoogLeNet model as feature extractor and ANFC as classifier for classification of breast tumors.

CAD system (DFS : *l*)		CM		Accuracy (%)	ICA_B (%)	ICA_M (%)
		B	M			
CNN-ANFC-LH based CAD system ($ODFS_{GoogLeNet}$: 22)	B	21	0	98.0	100	96.6
	M	1	29			

Note: DFS: Deep feature set, *l*: Length of feature vectors in DFS, CNN: Convolutional neural network, $ODFS_{GoogLeNet}$: Optimal deep feature set obtained by applying correlation based feature selection followed by ANFC-LH algorithm to $DFS_{GoogLeNet}$, ANFC: Adaptive neuro-fuzzy classifier using linguistic hedges, CM: Confusion matrix, ICA: Individual class accuracy, B: Benign, M: Malignant

From the results shown in Table 7.6, it can be noted that the optimal features extracted from the target GoogLeNet CNN model yield an accuracy of 98.0 % with ANFC classifier for differentiating between benign and malignant tumor types. The ICA value of benign class is 100 % and the ICA value obtained for the malignant class is 96.6 %. Out of the total 51 instances in the testing set, only 1 instance has been incorrectly classified which belongs to the malignant class.

7.5.6. Comparative analysis of CNN based CAD system designs for classification of breast tumors

A comparative analysis of results of the CNN based CAD system designs for classification of breast tumors is shown in Table 7.7.

Table 7.7 Comparative analysis of results of the CNN based CAD system designs for classification of breast tumors.

CAD system (DFS : *l*)		CM		Accuracy (%)	ICA_B (%)	ICA_M (%)
		B	M			
CNN based CAD system ($DFS_{GoogLeNet}$: 1024)	B	19	2	94.1	90.4	96.6
	M	1	29			
CNN based CAD system (DFS_{VGG-19} : 2048)	B	18	3	90.2	85.7	93.3
	M	2	28			
CNN based CAD system ($DFS_{ResNet-18}$: 512)	B	18	3	88.2	85.7	90.0
	M	3	27			

CNN based CAD system ($DFS_{SqueezeNet}$: 392)	B	19	2	90.2	90.4	90.0
	M	3	27			
CNN-ANFC-LH based CAD system ($ODFS_{GoogLeNet}$: 22)	B	21	0	98.0	100	96.6
	M	1	29			

Note: DFS: Deep feature set, *l*: Length of feature vectors in DFS,, CNN: Convolutional neural network, ODFS: Optimal deep feature set obtained, ANFC: Adaptive neuro-fuzzy classifier using linguistic hedges, B: Benign class, M: Malignant class, CM: Confusion matrix, ICA: Individual class accuracy.

The shaded gray region indicates the optimal CNN based CAD system for classification of breast tumors.

From Table 7.7 it can be noted that for the diagnosis of breast tumor types CNN based CAD system design using GoogLeNet model yielded the highest classification accuracy of 94.1 %, indicating that the GoogLeNet CNN model efficiently captures the underlying features of the ultrasound images responsible for the differential diagnosis between benign and malignant breast tumors. Based on this observation, the target GoogLeNet CNN model has been used for the extraction of deep features the optimal features extracted from the segmented breast ultrasound images. Using the target GoogLeNet CNN model and fuzzy feature selection by ANFC-LH yielded the highest classification accuracy of 98.0 % with ANFC classifier. The ICA value for benign and malignant class is 100 % and 96.6 % respectively.

The ROC curves along with the corresponding area under the curve (AUC) values for the CNN based CAD system designs implemented in the present work for classification of breast tumors are given in Fig. 7.18.

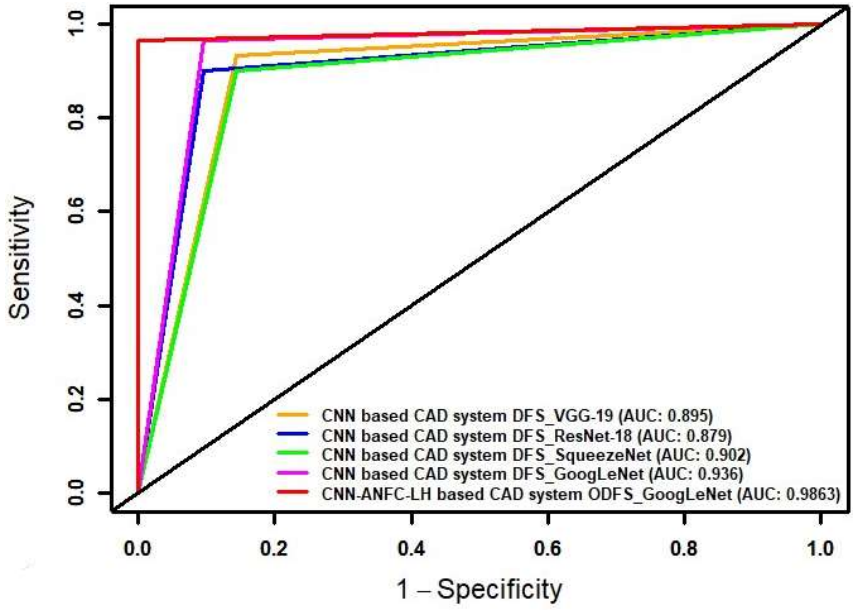

Fig. 7.18 The ROC curves and corresponding AUC values for CNN based CAD system designs implemented in the present work for classification of breast tumors.

The optimal CNN based CAD system design for classification of breast tumors is presented in Fig. 7.19.

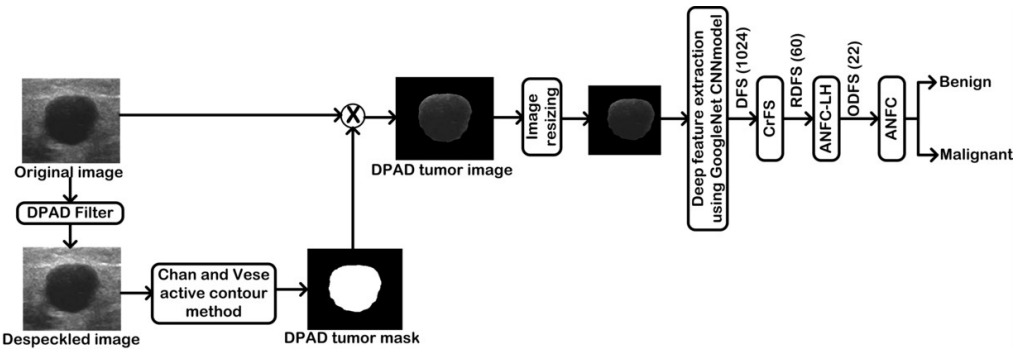

Fig. 7.19 Optimal CNN based CAD system design for classification of breast tumors.
Note: DPAD: Detail preserving anisotropic diffusion, DFS: Deep feature set, CrFS: Correlation based feature selection, RDFS: Reduced texture feature set, ANFC-LH: Adaptive neuro-fuzzy classifier, ODFS: Optimal deep feature set.

7.6. Concluding Remarks

The performance of different CNN based CAD system designs using pre-trained GoogLeNet, VGG-19, ResNet-18 and SqueezeNet models have been compared for classification of breast tumors in the present work. On the basis of the obtained results, it has been noted that CNN based CAD system design using GoogLeNet model yielded the highest classification accuracy of 94.1 % which implies that the GoogLeNet CNN model has been able to efficiently capture the underlying features of the ultrasound images responsible for the differential diagnosis between benign and malignant breast tumors. Based on this observation, the target GoogLeNet CNN model has been used for the extraction of deep features which were further subjected to CrFS for retaining the uncorrelated features. This reduced feature vector was then subjected to a fuzzy feature selection algorithm; ANFC-LH for obtaining an optimal feature set. This optimal feature set has been subjected to ANFC classifier for the differential diagnosis between the breast tumor types, achieving an accuracy of 98.0 % along with an AUC value of 0.983.

The present study differs from other related studies considering the following facts: (*a*) Most of the previous related studies have used either full images or manually extracted ROIs as the input to deep networks for classification of breast tumors however, in the present study segmented tumor images have been used for carrying out the exhaustive experiments for the design of efficient CNN based CAD system for classification of breast tumors. (*b*) For obtaining the tumor boundary/contour the images despeckled using the DPAD filter have been used as shape characteristics of tumor are better represented in despeckled images in comparison to the original images. The tumor mask thus obtained from the DPAD filtered image as a result of segmentation has been superimposed onto the original images to retain the original texture.

Chapter 8

Conclusions and Future Scope

8.1. Introduction

The main aim of the present study, "*Analysis and Classification of Breast Abnormalities Using Ultrasound Images*" is to enhance the diagnostic potential of conventional B-mode ultrasound imaging modality for differential diagnosis between benign and malignant tumors. To achieve this, exhaustive experimentation has been carried out in the present work to (*a*) Analyze the effect of despeckle filtering algorithms on breast ultrasound images, (*b*) Analyze the effect of despeckle filtering algorithms on segmentation of breast tumors, (*c*) Analyze the effect of despeckle filtering algorithms on classification of breast tumors, (*d*) Design LBP based CAD system designs for classification of breast tumors and (*e*) Design convolutional neural network based CAD system designs for classification of breast tumors. The conclusions drawn from the exhaustive experiments carried out in the present research work are depicted below:

8.2. Conclusions- Effect of Despeckle Filtering Algorithms on Breast Ultrasound Images

From the results of the experiments undertaken for analysing the effect of despeckle filtering algorithms on breast ultrasound images, it can be concluded that the DPAD filter produces more clinically acceptable images.

8.3. Conclusions- Effect of Despeckle Filtering Algorithms on Segmentation of Breast Tumors

From the results of the experiments undertaken for analysing the effect of filtering algorithms on segmentation of breast tumors, it has been concluded that images filtered by DPAD filter yields controlled despeckling thereby preserving the margins of the tumor resulting in better segmentation of tumors.

8.4. Conclusions- Effect of Despeckle Filtering Algorithms on Classification of Breast Tumors

From the results of the experiments undertaken for analysing the effect of filtering algorithms on classification of breast tumors following points can be concluded (*i*) Texture information is not effectively preserved in the despeckled images as is evident from the results of individual feature vectors, the maximum classification accuracy of 90.1 % is achieved using

original texture features in comparison with the maximum classification accuracy of 70.6 % achieved using despeckled texture features (Lee sigma). (*ii*) The shape/margin characteristics of the tumors are enhanced in the despeckled images as compared to the original images as is evident from the fact that the despeckled morphological features yielded higher accuracy in all cases in comparison with the original morphological features. It can be noted that the maximum classification accuracy of 70.5 % has been obtained by using despeckled morphological features (DPAD). (*iii*) For differential diagnosis between benign and malignant breast tumors using ultrasound images, the texture of the region inside the tumor as well as the shape/margin characteristics of the tumor are important.(*iv*) The feature set containing texture features computed from original images and morphological features computed from images despeckled by DPAD filter yield highest classification accuracy indicating that DPAD filter efficiently captures the morphological information for classifying breast ultrasound images.

8.5. Conclusions-LBP based CAD System Designs for Classification of Breast Tumors

Exhaustive experiments have been carried out for designing an efficient LBP based CAD system for classification of breast tumors, based on the results of the experiments, it can be concluded that the LBP based CAD system using ANFC-LH classifier has been considered optimal with LBP based texture features computed from original images and morphological features computed from images despeckled by DPAD filter.

8.6. Conclusions- Convolutional Neural Network based CAD System Designs for Classification of Breast Tumors

Exhaustive experiments have been carried out for designing efficient CNN based CAD system design for classification of breast tumors, on the basis of the obtained results, it has been observed that CAD system design with deep feature extraction by target GoogLeNet CNN model and ANFC-LH classifier can be considered optimal for the present classification task.

8.7. Comparison of CAD System Designs Implemented in the Present Research Work for Classification of Breast Tumors

A comparative analysis of the results of different CAD system designs implemented in the present research work for classification of breast tumors is shown in Table 8.1.

Optimal CAD system design based on machine learning: From the results presented in Table 8.1, it can be noted that using machine learning approaches, both PCA-SVM ($RFS_{OD(DPAD)}$) based CAD system and LBP based CAD system using ANFC-LH ($(OFS_{LH})_{ANFC\text{-}LH}$) yield same accuracy of 96.6 %. However, higher ICA value is yielded by

LBP based CAD system using ANFC-LH and is hence considered optimal machine learning based CAD system design for classification of breast tumors.

Table 8.1 A comparative analysis of the results of different CAD system designs implemented in the present research work for classification of breast tumors.

S. No.	Machine leaning based CAD system (FS: *l*)	Accuracy (%)	ICA_B (%)	ICA_M (%)
1.	PCA-SVM based CAD system ($RFS_{OD(DPAD)}$: 11)	96.0	95.2	96.6
2.	LBP based CAD system using ANFC-LH ($(OFS_{LBP})_{ANFC-LH}$: 27)	96.0	90.4	100
3.	LBP based CAD system using GA-SVM ($(OFS_{LBP})_{GA-SVM}$: 65)	92.2	90.4	93.3
4.	LBP based CAD system using PCA-SVM ($(OFS_{LBP})_{PCA-SVM}$: 14)	94.1	90.4	96.6
5.	LBP based CAD system using SAE-SM ($(OFS_{LBP})_{SAE-SM}$: 25)	92.2	80.9	100
S. No.	**CNN based CAD system (FS: *l*)**	**Accuracy (%)**	**ICA_B (%)**	**ICA_M (%)**
6.	CNN based CAD system ($DFS_{GoogLeNet}$: 1024)	94.1	90.4	96.6
7.	CNN based CAD system (DFS_{VGG-19}: 2048)	90.2	85.7	93.3
8.	CNN based CAD system ($DFS_{ResNet-18}$: 512)	88.2	85.7	90.0
9.	CNN based CAD system ($DFS_{SqueezeNet}$: 392)	90.2	90.4	90.0
10.	CNN-ANFC-LH based CAD system ($ODFS_{GoogLeNet}$: 22)	98.0	100	96.6

Note: FS: Feature set, *l*: Length of feature vector in FS, PCA: Principal component analysis, SVM: Support vector machine, RFS: Reduced feature set, O: Original image, D: Despeckled image, DPAD: Detail preserving anisotropic diffusion, OFS: Optimal feature set, LBP: Local binary pattern, ANFC-LH: Adaptive neuro-fuzzy classifier using linguistic hedges, GA: Genetic algorithm, SAE: Stacked autoencoder, SM: Softmax, CNN: Convolutional neural network, DFS: Deep feature set, ODFS: Optimal deep feature set, ICA: Individual class accuracy, B: Benign, M: Malignant.

Optimal CNN based CAD system design: The results shown in Table 9.1 also indicate that CNN-ANFC-LH based CAD system ($ODFS_{GoogLeNet}$) designed using optimal deep features computed for target GoogLeNet CNN model yielded highest classification accuracy of 98.0 % and is thus considered optimal CNN based CAD system design for classification of breast tumors.

The obtained results indicate the usefulness of the proposed CAD system design to (*a*) assist the radiologists in their assessment by providing second opinion in case of overlapping sonographic appearances of breast abnormalities, (*b*) act as training tool to aid the radiology students in identifying the sonographic changes being exhibited by different breast tumor types.

The main conclusion of the present research work is that texture features computed from original ultrasound images and morphological features computed from images despeckled using DPAD filter collectively enhance the performance of the CAD system for classification of breast tumors.

8.8. Limitations and Future Scope

8.8.1. Limitations

The present work has been carried out on a *standard benchmark database* consisting of representative images from each subclass of both benign and malignant tumors. Although the database contains information about the ground truth with respect to the tumor sub-classes at the same time, the information about tumor boundary is not specified. Accordingly, in the present work considerable amount of time was invested in getting the tumor boundaries marked by the experienced participating radiologist with the help of *ImageJ* software. For overcoming the effect of intra-observer variability, the display settings have been kept same for viewing all the images. For inter-observer variability, inputs from more than two (generally three) experienced radiologist are required. However, in the present work the number of processed images as well as the parameters required to be analysed for each image were quite large, so the processed images could be evaluated by only one participating radiologist having rich experience for analysing breast ultrasound images.

8.8.2. Future scope

The recommendations of the future work for the present research work are as follows: (*i*) The performance of the designed CAD systems needs to be tested on a dataset containing ground-truth marked images captured using multiple scanners at different resolution settings. (*ii*) For the pre-processing of breast ultrasound images, in order to improve the visual quality of the images, various despeckling and enhancement methods are available. The present work focuses on despeckling methods in future the effect of different enhancement methods and a combination of both despeckling and enhancement methods on the classification performance can be tested. (*iii*) For the segmentation of tumor region from the breast ultrasound images, the initial mask is provided by the radiologist thus preventing the CAD system design from being fully automatic. Thus, to make the CAD system designs user-independent, automatic methods of lesion detection followed by segmentation should be utilized to extract the desired tumor region. (*iv*) The present work has been carried out for the binary classification of breast ultrasound images into benign and malignant classes. A new benchmark database has been very recently made available in December 2019 for research purposes [6]. Using this benchmark database, researchers can design CAD systems for (*a*) binary classification between normal and abnormal classes, (*b*) multi-class classification between normal, benign and malignant classes, (*c*) hierarchical classification between normal and abnormal classes in the first stage and subsequent classification of images belonging to abnormal class into benign and malignant classes in the second stage.

References

[1] Abdelrahman A, Hamid O (2011, February). Lesion boundary detection in ultrasound breast images. In Proceedings of *1st Middle East Conference on Biomedical Engineering* (pp. 320-323), IEEE.

[2] Acharya UR, Meiburger KM, Koh JEW, Ciaccio EJ, Arunkumar N, See MH, Taib NAM, Vijayananthan A, Rahmat K, Fadzli F, Leong SS, Westerhout CJ, Astaiza AC, Gonzalez GR (2019). A novel algorithm for breast lesion detection using textons and local configuration pattern features with ultrasound imagery. *IEEE Access*, 7, 22829-22842.

[3] Aja-Fernández S, AlberolaLópez C (2006). On the estimation of the coefficient of variation for anisotropic diffusion speckle filtering. *IEEE Transactions on Image Processing*, 15 (9), 2694-2701.

[4] Akilan T, Wu QJ, Zhang H (2018). Effect of fusing features from multiple DCNN architectures in image classification. *IET Image Processing*, 12 (7), 1102-1110.

[5] Al-Dhabyani W, Fahmy A, Gomma M, Khaled H (2019). Deep learning approaches for data augmentation and classification of breast masses using ultrasound images. *International Journal of Advanced Computer Science and Applications*, 10 (5), 618-627.

[6] Al-Dhabyani W, Gomaa M, Khaled H, Fahmy A (2020). Dataset of breast ultrasound images. *Data in Brief*, 28, 104863, doi: https://doi.org/10.1016/j.dib.2019.104863.

[7] Alivar A, Danyali H, Helfroush MS (2016). Hierarchical classification of normal, fatty and heterogeneous liver diseases from ultrasound images using serial and parallel feature fusion. *Biocybernetics and Biomedical Engineering*. 36 (4), 697-707.

[8] Almajalid R, Shan J, Du Y, Zhang M (2018, December). Development of deep-learning-based method for breast ultrasound image segmentation. In Proceedings of *17th IEEE International Conference on Machine Learning and Applications*, (pp. 1103-1108), IEEE.

[9] Alvarenga AV, Infantosi AFC, Pereira WCA, Azevedo CM (2012). Assessing the combined performance of texture and morphological parameters in distinguishing breast tumors in ultrasound images. *Medical Analysis*, 39 (12), 7350-7358.

[10] Alvarenga AV, Infantosi AFC, Pereira WCA, Azevedo CM (2010). Assessing the performance of morphological parameters in distinguishing breast tumors on ultrasound images. *Medical Engineering and Physics*, 32 (1), 49-56.

[11] Alvarenga AV, Pereira WCA, Infantosi AFC, de Azevedo CM (2005, September). Classification of breast tumors on ultrasound images using morphometric parameters. In Proceedings of *2005 IEEE International Workshop on Intelligent Signal Processing* (pp. 206-210), IEEE.

[12] Amin KM, Shahin AI, Guo Y (2016). A novel breast tumor classification algorithm using neutrosophic score features. *Measurement*, 81, 210-220.

[13] Anderson BO, Braun S, Lim S, Smith RA, Taplin S, Thomas DB (2003). Early detection of breast cancer in countries with limited resources. *The Breast Journal*, 9, S51-S59.

[14] Antropova N, Huynh BQ, Giger ML (2017). A deep feature fusion methodology for breast cancer diagnosis demonstrated on three imaging modality datasets. *Medical Physics*, 44 (10), 5162-5171.

[15] Ardakani AA, Gharbali A, Mohammadi A (2015). Classification of breast tumors using sonographic texture analysis. *Journal of Ultrasound in Medicine*, 34 (2), 225-231.

[16] Bazzocchi M, Mazzarella F, Del Frate C, Girometti F, Zuiani C (2007). CAD systems for mammography: a real opportunity? A review of the literature. *La Radiologica Medica*, 112 (3), 329-353.

[17] Behnam H, Zakeri FS, Ahmadinejad N (2010). Breast mass classification on sonographic images on the basis of shape analysis. *Journal of Medical Ultrasonics*, 37 (4), 181-186.

[18] Berg WA, Blume JD, Cormack JB, Mendelson EB, Lehrer D, Bohm-Velez M, Pisano ED, Jong RA, Evans WP, Morton MJ, Mahoney MC, Larsen LH, Barr RG, Farria DM, Marques HS, Boparai K (2008). Combined screening with ultrasound and mammography vs mammography alone in women at elevated risk of breast cancer. *Journal of American Medical Association*, 299 (18), 2151-2163.

[19] Bhateja V, Misra M, Urooj S, Lay-Ekuakille A (2014, September). Bilateral despeckling filter in homogeneity domain for breast ultrasound images. In: Proceedings of *2014 International Conference on Advances in Computing, Communications and Informatics* (pp. 1027-1032), IEEE.

[20] Bhatia A, Srivastava S, Agarwal A (2010, November). Face detection using fuzzy logic and skin color segmentation in images. In Proceedings of *3rd International Conference on Emerging Trends in Engineering and Technology* (pp. 225-228), IEEE.

[21] Bhusri S, Jain S, Virmani J (2016). Breast lesion classification using the amalgamation of morphological and texture features. *International Journal of Pharma and Bio Sciences*, 7 (2), 617-624.

[22] Bhusri S, Jain S, Virmani J (2016). Classification of breast lesions using the difference of statistical features. *Research Journal of Pharmaceutical, Biological and Chemical Sciences*, 7 (4), 1365-1372.

[23] Biradar N, Dewal ML, Rohit MK (2015). Speckle noise reduction in B-mode echocardiographic images: a comparison. *IETE Technical Review*, 32 (6), 435-453.

[24] Biradar N, Dewal ML, Rohit MK (2016). Blind source parameters for performance evaluation of despeckling filters. *International Journal of Biomedical Imaging*, 2016, 1-12.

[25] Bochhi L, Rogai F (2011). Segmentation of ultrasound breast images: optimization of algorithm parameters. In: Di Chio C et al. (eds.), *Applications of Evolutionary Computation*, vol. 6624, pp. 163-172, Springer, Berlin.

[26] Boukerroui D, Basset O, Guerin N, Baskurt A (1998). Multiresolution texture based adaptive clustering algorithm for breast lesion segmentation. *European Journal of Ultrasound*, 8 (2), 135-144.

[27] Burckhardt CB (1978). Speckle in ultrasound B-mode scans. *IEEE Transactions on Sonics and Ultrasonics*, SU-25 (1), 1-6.

[28] Burgess MD, O'Neal EL (2019). Breast ultrasound for the evaluation of benign breast disease. *Current Radiology Reports*, 7 (3), 9, doi: https://doi.org/10.1007/s40134-019-0316-x.

[29] Byra M (2018). Discriminant analysis of neural style representations for breast lesion classification in ultrasound. *Biocybernetics and Biomedical Engineering*, 38 (3), 684-690.

[30] Byra M, Galperin M, Ojeda-Fournier H, Olson L, O'Boyle M, Comstock C, Andre M (2019). Breast mass classification in sonography with transfer learning using a deep convolutional neural network and color conversion. *Medical Physics*, 46 (2), 746-755.

[31] Byra M, Styczynski G, Szmigielski C, Kalinowski P, Michalowski L, Paluszkiewicz R, Wroblewska BZ, Zieniewicz K, Sobieraj P, Nowicki A (2018). Transfer learning with deep convolutional neural network for liver steatosis assessment in ultrasound images. *International Journal of Computer Assisted Radiology and Surgery*, 13 (12), 1895-1903.

[32] Cai L, Wang X, Wang Y, Guo Y, Yu J, Wang Y (2015). Robust phase-based texture descriptor for classification of breast ultrasound images. *BioMedical Engineering OnLine*, 14 (1), 26-46.

[33] Cai L, Wang Y (2013, December). A phase-based active contour model for segmentation of breast ultrasound images. In Proceedings of *2013 6th International Conference on Biomedical Engineering and Informatics* (pp. 91-95), IEEE.

[34] Cao Z, Duan L, Yang G, Yue T, Chen Q (2019). An experimental study on breast lesion detection and classification from ultrasound images using deep learning architectures. *BMC Medical Imaging*, 19 (1), 51, doi: https://doi.org/10.1186/s12880-019-0349-x.

[35] Cengiz M, Senturk S, Cetin B, Bayrak AH, Bilek SU (2014). Sonographic assessment of fatty liver: intraobserver and interobserver variability. *International Journal of Clinical and Experimental Medicine*, 7 (12), 5453-5460.

[36] Chamberlain J, Rogers P, Price JL, Ginks S. Nathan BE, Burn I (1975). Validity of clinical examination and mammography as screening tests for breast cancer. *The Lancet*, 306 (7943), 1026-1030.

[37] Chan TF, Vese LA (2001). Active contours without edges. *IEEE Transactions on Image Processing*, 10 (2), 266-277.

[38] Chang CC, Lin CJ. LIBSVM, A library for support vector machines. Software available at http://www.csie.ntu.edu.tw/~cjlin/libsvm. Accessed October 2014.

[39] Chang RF, Wu WJ, Moon WK, Chen DR (2003). Improvement in breast tumor discrimination by support vector machines and speckle emphasis texture analysis. *Ultrasound in Medicine and Biology*, 29 (5), 679-686.

[40] Chang RF, Wu WJ, Moon WK, Chen DR (2005). Automatic ultrasound segmentation and morphology based diagnosis of solid breast tumors. *Breast Cancer Research and Treatment*, 89 (2), 179-185.

[41] Chang RF, Wu WJ, Moon WK, Chou YH, Chen DR (2003). Support vector machines for diagnosis of breast tumors on US images. *Academic Radiology*, 10 (2), 189-197.

[42] Chang SG, Yu B, Vettereli M (2009). Adaptive wavelet thresholding for image denoising and compression. *IEEE Transactions on Image Processing*, 9 (9), 1532-1546.

[43] Chen CY, Chiou HJ, Chou SY, Chiou SY, Wang HK, Chou YH, Chiang HK (2009). Computer-aided diagnosis of soft-tissue tumors using sonographic morphologic and texture features. *Academic Radiology*, 16 (12), 1531-1538.

[44] Chen DR, Chang RF, Chen CJ, Ho MF, Kuo SJ, Chen ST, Hung SJ, Moon WK (2005). Classification of breast ultrasound images using fractal feature. *Journal of Clinical Imaging*, 29 (4), 235-245.

[45] Chen DR, Chang RF, Huang YL (1999). Computer-aided diagnosis applied to US of solid breast nodules by using neural networks. *Radiology*, 213 (2), 407-412.

[46] Chen DR, Chang RF, Kuo WJ, Chen MC, Huang YL (2002). Diagnosis of breast tumors with sonographic texture analysis using wavelet transform and neural networks. *Ultrasound in Medicine and Biology*, 28 (10), 1301-1310.

[47] Cheng HD, Hu L, Tian J, Sun L (2005). A novel Markov random field segmentation algorithm and its application to breast ultrasound image analysis. In *Proceedings of 6th International Conference on Computer Vision, Pattern Recognition and Image Processing*, (pp. 1-4).

[48] Cheng JZ, Ni D, Chou YH, Qin J, Tiu CM, Chang YC, Huang CS, Shen D, Chen CM (2016). Computer-aided diagnosis with deep learning architecture: applications to breast lesions in US images and pulmonary nodules in CT. *Scientific Reports*, 6 (1), 1-13, doi: 10.1038/srep24454.

[49] Cheng PM, Malhi HS (2017). Transfer learning with convolutional neural networks for classification of abdominal ultrasound images. *Journal of Digital Imaging*, 30 (2), 234-243.

[50] Chiang HH, Cheng JZ, Hung PK, Liu CY, Chung CH, Chen CM (2010, April). Cell-based graph cut for segmentation of 2D/3D sonographic breast images. In Proceedings of *2010 IEEE International Conference on Biomedical Imaging: from Nano to Micro* (pp. 177-180), IEEE.

[51] Chiao JY, Chen KY. Liao KYK, Hsieh PH, Zhang G, Huang TC (2019). Detection and classification the breast tumors using mask R-CNN on sonograms. *Medicine*, 98 (19), doi: http://dx.doi.org/10.1097/MD.0000000000015200.

[52] Cho BH, Seong YK, Kim J, Liu Z, Hao Z, Ko EY, Woo KG (2014). Ultrasound breast lesion segmentation using adaptive parameters. In: Aylward S, Hadjiiski LM (eds.), *Medical Imaging 2014: Computer-Aided Diagnosis*, vol. 9035, doi: 10.1117/12.2041893, SPIE.

[53] Christiyana CC, Rajamani V (2012). Comparison of local binary pattern variants for ultrasound kidney image retrieval. *International Journal of Advanced Research in Computer Science and Software Engineering*. 2 (10), 224-228.

[54] Chucherd S, Makhanov SS (2011). Sparse phase portrait analysis for pre-processing and segmentation of ultrasound images of breast cancer. *International Journal of Computer Science*, 38 (2), 1-14.

[55] Chucherd S, Makhanov SS (2011, March). Multiresolution phase portrait analysis for segmentation of ultrasound images for detection of breast cancer. In Proceedings of *World Congress on Engineering* (pp. 460-465), International Association of Engineers.

[56] Ciritsis A, Rossi C, Eberhard M,Marcon M Becker, AS, Boss A (2019). Automatic classification of ultrasound breast lesions using a deep convolutional neural network. *European Radiology*, 29 (10), 5458-5468.

[57] Cristerna AR, Gomez-Flores W, Pereira WCA (2018). A computer-aided diagnosis for breast ultrasound based on weighted BI-RADS classes. *Computer Methods and Programs in Biomedicine*, 153, 33-40.

[58] Cristerna AR, Guerrero-Cedillo CP, Donati-Olvera GA, Gomez-Flores W, Pereira WCA (2017, October). Study of the impact of image processing approaches on segmentation and classification of breast lesions on ultrasound. In Proceedings of *14th International Conference on Electrical Engineering, Computer Science and Automatic Control* (pp. 299-317). IEEE

[59] Cui J, Sahiner B, Chan HP, Nees A, Paramagul C, Hadjiiski LM, Zhou C, Shi J (2009). A new automated method for the segmentation and characterization of breast masses on ultrasound images. *Medical Physics*, 36 (5), 1553-1565.

[60] Cui J, Sahiner B, Chan HP, Shi J, Nees A, Paramagul C, Hadjiiski LM (2009). A computer-aided diagnosis system for prediction of the probability of malignancy of breast masses on ultrasound images. In: Karssemeijer N, Giger ML (eds.) *Medical Imaging 2009: Computer-Aided Diagnosis*, vol. 7260, doi: 0.1117/12.813722.

[61] Daoud MI, Baba MM, Awwad F, Al-Najjar M, Tarawneh ES (2012, November). Accurate segmentation of breast tumors in ultrasound images using a custom-made active contour model and signal-to-noise variations. In Proceedings of *8th International Conference on Signal Image Technology and Internet Based Systems* (pp. 137-141), IEEE.

[62] Daoud MI, Bdair TM, Al-Najar M, Alazral R (2016). A fusion based approach for breast ultrasound image classification using multiple-ROI texture and morphological analyses. *Computational and Mathematical Methods in Medicine*, 2016, 1-12.

[63] Drukker K, Edwards DC, Giger ML, Nishikawa RM, Metz CE (2004). Computerized detection and 3-way classification of breast lesions on ultrasound images. In: Fitzpatrick JM et al. (eds.), *Medical Imaging 2004: Image Processing*, vol. 5370, pp. 1034-1041, International Society for Optics and Photonics.

[64] Drukker K, Giger ML, Horsch K, Kupinski MA, Vyborny CJ (2002). Computerized lesion detection on breast ultrasound. *Medical Physics*, 29 (7), 1438-1446.

[65] Drukker K, Giger ML, Vyborny CJ, Schmidt RA, Mendelson EB, Stern M (2003). Computerized detection and classification of lesions on breast ultrasound, In: Sonka M, Fitzpatrick JM (eds.), *Medical Imaging 2003: Image Processing*, vol. 5032, pp. 106-110.

[66] Drukker K, Gruszauskas NP, Sennett CA, Giger ML (2008). Breast US computer-aided diagnosis workstation: performance with a large clinical diagnostic population. *Radiology*, 248 (2), 392-397.

[67] Drukker K, Sennett CA, Giger ML (2009). Automated method for improving system performance of computer-aided diagnosis in breast ultrasound. *IEEE Transactions on Medical Imaging*, 28 (1), 122-128.

[68] Drukker K, Gruszauskas NP, Giger ML (2009). Principal component analysis, classifier complexity and robustness of sonographic breast lesion classification. In: Karssemeijer N, Giger ML (eds.), *Medical Imaging 2009: Computer-Aided Diagnosis*, vol. 7260, doi: 10.1117/12.811341.

[69] Elawady M, Sadek I, Shabayek AR, Pons G, Ganau S (2016). Automatic nonlinear filtering and segmentation of breast ultrasound images. In: Campilho A, Karray F (eds.), *Image Analysis and Recognition*, pp. 206-213, Springer, Switzerland.

[70] Feng X, Guo X, Huang Q (2017). Systematic evaluation on speckle suppression methods in examination of ultrasound breast images. *Applied Sciences*, 7 (1), 37, doi: https://doi.org/10.3390/app7010037.

[71] Feng Y, Dong F, Xia X, Hu CH, Fan Q, Hu Y, Gao M, Mutic S (2017). An adaptive fuzzy c-means method utilizing neighbouring information for breast tumor segmentation in ultrasound. *Medical Physics*, 44 (7), 3752-3760.

[72] Finn S, Glavin M, Jones E (2011). Echocardiographic speckle reduction comparison. *IEEE Transactions on Ultrasonics, Ferroelectrics and Frequency Control*, 58 (1), 82-101.

[73] Flores MA, Alvarez L, Caselles V (2007). Texture-oriented anisotropic filtering and geodesic active contours in breast tumor ultrasound segmentation. *Journal of Mathematical Imaging and Vision*, 28 (1), 81-97.

[74] Flores WG, Pereira WCA, Infantosi AFC (2015). Improving classification performance of breast lesions on ultrasonography. *Pattern Recognition*, 48 (4), 1125-1136.

[75] Fujioka T, Kubota K, Mori M, Kikuchi Y, Katsuta L, Kasahara M, Oda G, Ishiba T, Nakagawa T, Tateishi U (2019). Distinction between benign and malignant breast masses at breast ultrasound using deep learning method with convolutional neural network. *Japanese Journal of Radiology*, 37 (6), 466-472.

[76] Ganesan K, Acharya UR, Chua CK, Min LC, Abraham TK, Ng KH (2013). Computer-aided breast cancer detection using mammograms: a review. *IEEE Reviews in Biomedical Engineering*, 6, 77-98.

[77] Gao L, Liu X, Chen W (2012). Phase- and GFV-based level set segmentation of ultrasonic breast tumors. *Journal of Applied Mathematics*, 2012, doi: 10.1155/2012 /810805.

[78] Gao L, Yang W, Liao Z, Liu X, Feng Q, Chen W (2012). Segmentation of ultrasonic breast tumors based on homogeneous patch. *Medical Physics*, 39 (6), 3299-3318.

[79] Garcia AH, Konig P (2018). Further advantages of data augmentation on convolutional neural networks. In: Kurkova V et al. (eds.), *Artificial Neural Networks and Machine Learning*, vol. 11139, pp. 95-103, Springer, Cham.

[80] Gardezi SJS, Elazab A, Lei B, Wang T (2019). Breast cancer detection and diagnosis using mammographic data: systematic review. *Journal of Medical Internet Research*, 21 (7), e14464.

[81] Ghosh S, Chaudhary KN (2016). On fast bilateral filtering using Fourier kernels. *IEEE Signal Processing Letters*, 23 (5), 570-573.

[82] Gokhale S (2009). Ultrasound characterization of breast masses. *Indian Journal of Radiological Imaging*, 19 (3), 242-247.

[83] Golub RM, Parsons RE, Sigel B, Feleppa EJ, Justin J, Zaren HA, Rorke M, Sokil-Melgar J, Kimitsuki H (1993). Differentiation of breast tumors by ultrasonic tissue characterization. *Journal of Ultrasound in Medicine*, 12 (10), 601-608.

[84] Gomez W, Infantosi AFC, Leija L, Pereira WCA (2010). Active contour without edges applied to breast lesions in ultrasound. In Proceedings of *XII Mediterranean Conference on Medical and Biological Engineering and Computing*, (pp. 292-295), Springer.

[85] Gomez W, Leija L, Alvarenga AV, Infantosi AFC, Pereira WCA (2010). Computerized lesion segmentation of breast ultrasound based on marker-controlled watershed transformation. *Medical Physics*, 37 (1), 82-95.

[86] Gomez W, Leija L, Pereira WCA, Infantosi AFC (2009, March). Morphological operators on the segmentation of breast ultrasound images. In: Proceedings of *2009 Pan American Health Care Exchanges-PAHCE Conferences, Workshops and Exhibits* (pp. 67-71), IEEE.

[87] Gomez W, Leija L, Pereira WCA, Infantosi AFC (2010). Segmentation of breast nodules on ultrasonographic images based on marke d-controlled watershed transform. *Computacion y Sistemas*, 14 (2), 165-174.

[88] Gomez W, Pereira WCA, Infantosi AFC (2012). Analysis of co-occurrence texture statistics as a function of gray level quantization for classifying breast ultrasound. *IEEE Transactions on Medical Imaging*, 31 (10), 1889-1899.

[89] Gomez W, Pereira WCA, Infantosi AFC (2016). Evolutionary pulse coupled neural network for segmenting breast lesions on ultrasonography. *Neurocomputing*, 175, 877-887.

[90] Gruszauskas NP, Drukker K, Giger ML, Sennett CA, Pesce LL (2008). Performance of breast ultrasound computer-aided diagnosis dependence on image selection. *Academic Radiology*, 15 (10), 1234-1245.

[91] Guo Y, Sengur A, Tian JW (2016). A novel breast ultrasound image segmentation algorithm based on neutrosophic similarity score and level set. *Computer Methods and Programs in Biomedicine*, 123, 43-53.

[92] Han S, Kang HK, Jeong JY, Park MH, Kim W, Bang WC, Seong YK (2017). A deep learning framework for supporting the classification of breast lesions in ultrasound images. *Physics in Medicine and Biology*, 62 (19), 7714-7728.

[93] Han S, Lee S, Lee JR (2019). A practical implementation of deep learning method for supporting the classification of breast lesions in ultrasound images. *International Journal of Advanced Smart Convergence*, 8 (1), 24-34.

[94] Han W, Dong J, Guo Y, Zhang M, Wang J (2011, November). Identification of masses in digital mammogram using optimal set of features. In Proceedings of *2011 10th International Conference on Trust, Security and Privacy in Computing and Communications* (pp. 1763-1768), IEEE.

[95] Hao Z, Wang Q, Ren H, Xu K, Seong YK, Kim J (2012, September). Multiscale superpixel classification for tumor segmentation in breast ultrasound images. In Proceedings of *19th IEEE International Conference on Image Processing*, (pp. 2817-2820), IEEE.

[96] Hao Z, Wang Q, Seong YK, Lee JH, Ren H, Kim J (2012). Combining CRF and multi-hypothesis detection for accurate lesion segmentation in breast sonograms. In: Ayache N et al. (eds.), *Medical Image Computing and Computer Assisted Intervention*, vol. 7510, pp. 504-511, Springer, Berlin.

[97] Hassen TM, Elmogy M, Sallam ES (2017). Diagnosis of focal liver diseases based on deep learning technique for ultrasound images. *Arabian Journal for Science and Engineering*. 42 (8), 3127-3140.

[98] He K, Zhang X, Ren S, Sun J (2016). Deep residual learning for image recognition. In Proceedings of *IEEE Conference on Computer Vision and Pattern Recognition* (pp. 770-778), IEEE.

[99] Hegde RB, Prasad K, Hebbar H, Singh BMK (2019). Comparison of traditional image processing and deep learning approaches for classification of white blood cells in peripheral blood smear images. *Biocybernetics and Biomedical Engineering*. 39 (2), 382-392.

[100] Hooda R, Mittal A, Sofat S (2019). Automated TB classification using ensemble of deep architectures. *Multimedia Tools and Applications*, 78 (22), 31515-31532.

[101] Horsch K, Giger ML, Venta LA, Vyborny CJ (2001). Automatic segmentation of breast lesions on ultrasound. *Medical Physics*, 28 (8), 1652-1659.

[102] Horsch K, Giger ML, Venta LA, Vyborny CJ (2002). Computerized diagnosis of breast lesions on ultrasound. *Medical Physics*, 29 (2), 157-164.

[103] http://ultrasoundcases.info/category.aspx?cat=67, Accessed December 2016.

[104] Hu Y, Guo Y, Wang Y, Yu J, Li J, Zhou S, Chang C (2018). Automatic tumor segmentation in breast ultrasound images using a dilated fully convolutional network combined with an active contour model. *Medical Physics*, 46 (1), 215-228.

[105] Huang K, Chen HD, Zhang Y, Zhang B, Xing P, Ning C (2018, August). Medical knowledge constrained semantic breast ultrasound image segmentation. In Proceedings of *24th International Conference on Pattern Recognition*, (pp. 1193-1198), IEEE.

[106] Huang Q, Bai X, Li Y, Jin L, Li X (2014). Optimized graph-based segmentation for ultrasound images. *Neurocomputing*, 129, 216-224.

[107] Huang Q, Yang F, Liu L, Li X (2015). Automatic segmentation of breast lesions for interaction in ultrasonic computer-aided diagnosis. *Information Sciences*, 314, 293-310.

[108] Huang QH, Lee SY, Liu LZ, Lu MH, Jin LW, Li H (2012). A robust graph-based segmentation method for breast tumors in ultrasound images. *Ultrasonics*, 52 (2), 266-275.

[109] Huang Y, Han L, Dou H, Luo H, Yuan Z, Liu Q, Zhang J, Fin G (2019). Two-stage CNNs for computerized BI-RADS categorization in breast ultrasound images. *BioMedical Engineering OnLine*, 18 (1), 1-18.

[110] Huang YL, Chen DR (2004). Watershed segmentation for breast tumor in 2-D sonography. *Ultrasound in Medicine and Biology*, 30 (5), 625-632.

[111] Huang YL, Chen DR (2005). Support vector machines in sonography application to decision making in the diagnosis of breast cancer. *Clinical Imaging*, 29 (3), 179-184.

[112] Huang YL, Chen DR (2005, January). Automatic contouring for breast tumors in 2D sonography. In Proceedings of *27th Annual Conference on Engineering in Medicine and Biology* (pp. 3225-3228), IEEE.

[113] Huang YL, Chen DR, Jiang YR, Kuo SJ, Wu HK, Moon WK (2008). Computer-aided diagnosis using morphological features for classifying breast lesions on ultrasound. *Ultrasound in Obstetrics and Gynecology*, 32 (4), 565-572.

[114] Huang YL, Jiang YR, Chen DR, Moon WK (2007). Level set contouring for breast tumor in sonography. *Journal of Digital Imaging*, 20 (3), 238-247.

[115] Huang YL, Wang KL, Chen DR (2006). Diagnosis of breast tumors with ultrasonic texture analysis using support vector machines. *Neural Computing and Applications*, 15 (2), 164-169.

[116] Iandola FN, Han S, Moskewicz MW, Ashraf K, Dally WJ, Keutzer K (2016). SqueezeNet: AlexNet-level accuracy with 50× fewer parameters and < 0.5 MB model size. *arXiv:1602.07360*.

[117] Image Processing and Analysis in JAVA, Image J 1.49 version 1.6.024 http://imagej.nih.gov/ij/download/win32/ij149-jre6-64.zip.

[118] Jackson VP (1990). The role of ultrasound in breast imaging. *Radiology*, 177 (2), 305-311.

[119] Jani KK, Srivastava S, Srivastava R (2019). Computer-aided diagnosis system for ulcer detection in capsule endoscopy images using optimized feature set. *Journal of Intelligent & Fuzzy Systems*, 37 (1), 1491-1498.

[120] Jiang P, Peng J, Zhang G, Cheng E, Megallooikonomou V, Ling H (2012, May). Learning-based automatic breast tumor detection and segmentation in ultrasound images. In Proceedings of *9th IEEE International Symposium on Biomedical Imaging* (pp. 1587-1590), IEEE.

[121] Jiao J, Wang Y (2011, May). Automatic boundary detection in breast ultrasound images based on improved pulse coupled neural network and active contour model. In Proceedings of *5th International Conference on Bioinformatics and Biomedical Engineering* (pp. 1-4), IEEE.

[122] Jia-Wei T, Chun-Ping N, Yan-Hui G, Heng-Da C, Xiang-Long T (2012). Effect of novel segmentation algorithm on radiologists' diagnosis of breast masses using ultrasound imaging. *Ultrasound in Medicine and Biology*, 38 (1), 119-127.

[123] Jinyao Y, Boling Z, Qiong Z, Minfen S (2011, August). Novel method of segmenting breast lesion in ultrasound images using grouping bandlets. In Proceedings of *10th International Conference on Electronic Measurement and Instruments*, (pp. 289-293), IEEE.

[124] Joo S, Moon WK, Kim HC (2004, September). Computer-aided diagnosis of solid breast nodules on ultrasound with digital image processing and artificial neural network. In Proceedings of the *26th Annual International Conference of the IEEE EMBS*, (pp.1397-1400).

[125] Joo S, Yang YS, Moon WK, Kim HC (2004). Computer-aided diagnosis of solid breast nodules: use of an artificial neural network based on multiple sonographic features. *IEEE Transactions on Medical Imaging*. 23 (10), 1292-1300.

[126] Jumaat AK, Rehman WEZWA, Ibrahim A, Mahmud R (2010). Segmentation of masses from breast ultrasound images using parametric active contour algorithm. *Procedia-Social and Behavioral Sciences*, 8, 640-647.

[127] Jumaat AK, Rehman WEZWA, Ibrahim A, Mahmud R (2010, May). Comparison of balloon snake and GVF snake in segmenting masses from breast ultrasound images. In Proceedings of *2nd International Conference on Computer Research and Development* (pp. 505-509), IEEE.

[128] Jumaat AK, Rehman WEZWA, Ibrahim A, Mahmud R (2011, November). Segmentation and characterization of masses in breast ultrasound images using active contour. In Proceedings of *IEEE International Conference on Signal and Image Processing Applications*, (pp. 404-409), IEEE.

[129] Jung IS, Thapa D, Wang GN (2005). Automatic segmentation and diagnosis of breast lesions using morphology method based on ultrasound. In: Wang L, Jin Y (eds.), *Fuzzy Systems and Knowledge Discovery*, vol. 3614, pp. 1079-1088, Springer, Berlin.

[130] Kadah YM, Farag AA, Zurada JM, Badawi AM, Youssef ABM (1996). Classification algorithms for quantitative tissue characterization of diffuse liver disease from ultrasound, *IEEE Transactions on Medical Imaging*, 15 (4), 466-478.

[131] Kameswari SSD, VijayakumarV (2019). A CNN based breast tumor classifier using Mendeley BUS dataset. *International Journal of Innovative Technology and Exploring Engineering*, 8 (6), 1340-1343.

[132] Karimi B, Krzyzak A (2013). A novel approach for automatic detection and classification of suspicious lesions in breast ultrasound images. *Journal of Artificial Intelligence and Soft Computing Research*, 3 (4), 265-276.

[133] Karimi B, Krzyzak A (2014). Computer-aided system for automatic classification of suspicious lesions in breast ultrasound images. In: Rutkowski L et al. (eds.), *Artificial Intelligence and Soft Computing*. *ICAISC 2014*, vol. 8468, pp. 131-142, Springer.

[134] Keramidas EG, Iakovidis DK, Maroulis D, Karkanis S (2007). Efficient and effective ultrasound image analysis scheme for thyroid nodule detection. In: Kamel M, Campilho A (eds.), *Image Analysis and Recognition*, *ICIAR*, vol. 4633, pp. 1052-1060, Springer, Heidelberg.

[135] Key TJ, Verkasalo PK, Banks E (2001). Epidemiology of breast cancer. *The Lancet Oncology*, 2 (3), 133-140.

[136] Khusna DA, Nugroho HA, Seosanti A (2015, October). Performance analysis of edge and detailed preserved speckle noise reduction filters for breast ultrasound images. In Proceedings of *2nd International Conference on Information Technology, Computer and Electrical Engineering* (pp. 76-80), IEEE.

[137] Kim K, Song MK, Kim EK, Yoon JH (2017). Clinical application of S-detect to breast masses on ultrasonography: a study evaluating the diagnostic performance and agreement with a dedicated breast radiologist. *Ultrasonography*, 36 (1), 3-9.

[138] Kirimasthong K, Rodtook A, Chaumrattanakul U, Makhanov SS (2017). Phase portrait analysis for automatic initialization of multiple snakes for segmentation of ultrasound images of breast cancer. *Pattern Analysis and Applications*, 20 (1), 239-251.

[139] Kocer HE, Cevik KK, Sivri M, Koplay M (2016). Measuring the effect of filters on segmentation of developmental dysplasia of the hip. *Iranian Journal of Radiology*, 13 (3), e25491.

[140] Kriti, Virmani J, Agarwal R (2017). Characterization of breast tumors using selected Laws' mask texture features, In Proceedings of *4th International Conference on Image Information Processing (ICIIP-2017)*, (pp. 373-378), IEEE.

[141] Kriti, Virmani J, Agarwal R (2019). Assessment of despeckle filtering algorithms for segmentation of breast tumors from ultrasound images. *Biocybernetics and Biomedical Engineering*, 39 (1), 100-121.

[142] Kriti, Virmani J, Agarwal R (2019). Effect of despeckle filtering on classification of breast tumors using ultrasound images. *Biocybernetics and Biomedical Engineering*, 39 (2), 563-560.

[143] Kriti, Virmani J, Agarwal R (2020). A review of segmentation algorithms applied to B-mode breast ultrasound images: A characterization approach. *Archives of Computational Methods in Engineering*, doi: 10.1007/s11831-020-09469-3.

[144] Kriti, Virmani J, Agarwal R (2020). Deep feature extraction and classification of breast ultrasound images. *Multimedia Tools and Applications*, doi: https://doi.org/10.1007/s11042-020-09337-z.

[145] Kumar A, Kim J, Lyndon D, Fulham M, Feng D (2016). An ensemble of fine-tuned convolutional neural networks for medical image classification. *IEEE Journal of Biomedical and Health Informatics*, 21 (1), 31-40.

[146] Kumar HP, Srinivasan S (2014). Classification of ovary abnormality using the probabilistic neural network (PNN). *Technology and Health Care*, 22 (6), 857-865.

[147] Kumar V, Webb JM, Gregory A, Denis M, Meixner DD, Bayat M, Whaley DH, Fatemi M, Alizad A (2018). Automated and real-time segmentation of suspicious breast masses using convolutional neural network. *PLoS ONE*, 15 (3), e0195816, https://doi.org/10.1371/ journal.pone.0195816.

[148] Kwan HK (2003). Fuzzy filters for noise reduction in images. In: Nachtegael M, Van der Weken D, Kerre EE, Van De Ville D. (eds.) F*uzzy Filters for Image Processing*, pp. 25-53. Springer-Verlag, Berlin.

[149] Lal M, Kaur L, Gupta S (2016). Speckle reduction with edge preservation in B-scan breast ultrasound images. *International Journal of Image Graphics and Signal Processing*, 8 (9), 60-68.

[150] Lal M, Kaur L, Gupta S (2018). Automatic segmentation of tumors in B-mode ultrasound images using information gain based neutrosophic clustering. *Journal of X-Ray Science and Technology*, 26 (2), 209-225.

[151] Lal M, Kaur L, Gupta S (2018). Modified spatial neutrosophic clustering technique for boundary extraction of tumours in B-mode BUS images. *IET Image Processing*, 12 (8), 1338-1344.

[152] Laroussi MG, Ayed NGB, Masmoudi AD, Masmoudi DS (2013, June). Diagnosis of masses in mammographic images based on Zernike moments and local binary attributes. In Proceedings of *World Congress on Computer and Information Technology* (pp. 1-6), IEEE.

[153] Lee CY, Chen GL, Zhang ZX, Chou YH, Hsu CC (2018). Is intensity inhomogeneity correction useful for classification of breast cancer in sonograms using deep neural network ? *Journal of Healthcare Engineering*, 2018, 1-10.

[154] Lee JH, Seong YK, Chang CH, Ko EY, Cho BH, Ku J, Woo KG (2013). Computer aided lesion diagnosis in B-mode ultrasound by border irregularity and multiple sonographic features. In: Novak CL, Aylward S (eds.), *Medical Imaging 2013: Computer-Aided Diagnosis*, vol. 8670, pp. 86701O-1-86701O-7.

[155] Lee JS (1983). Digital image smoothing and sigma filter. *Computer Vision, Graphics and Image Processing*, 24 (2), 255-269.

[156] Lee M, Chen Y, Kim S, Kim K (2011, August). Geometric active model for lesion segmentation on breast ultrasound images. In Proceedings of *11th IEEE Conference on Computer and Information Technology* (pp. 150-157), IEEE.

[157] Lee S, Huang Q, Jin L, Lu M, Wang T (2010, June). A graph-based segmentation method for breast tumors in ultrasound images. In Proceedings of *4th International Conference on Bioinformatics and Biomedical Engineering* (pp. 1-4), IEEE.

[158] Lefebvre F, Meunier M, Thibault F, Laugier P, Berger G (2000). Computerized ultrasound B-scan characterization of breast nodules. *Ultrasound in Medicine and Biology*, 26 (9), 1421-1428.

[159] Lestari DP, Madenda S, Ernastuti E, Wibowo EP (2017). Comparison of three segmentation methods for breast ultrasound images based on level set and morphological operations. *International Journal of Electrical and Computer Engineering*, 7 (1), 383-391.

[160] Levy D, Jain A (2016). Breast mass classification from mammograms using deep convolutional neural networks. *arXiv: 1612.00542.*

[161] Liao R, Wan T, Qin Z (2011, August). Classification of benign and malignant breast tumors in ultrasound images based on multiple sonographic and textural features. In Proceedings of *3rd International Conference on Intelligent Human-Machine Systems and Cybernetics* (pp. 71-74), IEEE.

[162] Lin CM, Hou YL, Chen TY, Chen KH (2014). Breast nodules computer-aided diagnostic system design using fuzzy cerebellar model neural networks. *IEEE Transactions on Fuzzy Systems*, 22 (3), 693-699.

[163] Lin QZ, Liu S, Paarajuly SS, Deng Y, Boroczky, Fu S, Wu Y, Pen Y (2013, July). Ultrasound lesion segmentation using clinical knowledge-driven constrained level set. In Proceedings *of 35th Annual International Conference of the IEEE Engineering in Medicine and Biology Society* (pp. 6067-6070), IEEE.

[164] Liu B, Cheng HD, Huang J, Tian J, Liu J, Tang X (2009). Automated segmentation of ultrasonic breast lesions using statistical texture classification and active contour based on probability distance. *Ultrasound in Medicine and Biology*, 35 (8), 1309-1324.

[165] Liu B, Cheng HD, Huang J, Tian J, Tang X, Liu J (2010). Probability density difference based active contour for ultrasound image segmentation. *Pattern Recognition*, 43 (6), 2028-2042.

[166] Liu L, Li K, Qin W, Wen T, Li L, Wu J, Gu J (2018). Automated breast tumor detection and segmentation with a novel computational framework of whole ultrasound images. *Medical and Biological Engineering and Computing*, 56, 183-199.

[167] Liu L, Qin W, Yang R, Yu C, Li L, Wen T, Gu J (2015, November). Segmentation of breast ultrasound image using graph cuts and level set. In Proceedings of *IET International Conference on Biomedical Image and Signal Processing*, doi: 10.1049/cp.2015.0773.

[168] Liu X, Huo Z, Zhang J (2005, January). Automated segmentation of breast lesions in ultrasound images. In Proceedings of *27th IEEE Annual Conference on Engineering in Medicine and Biology*, (pp. 7433-7435), IEEE.

[169] Liu Y, Chen Y, Han B, Zhang Y, Zhang X, Su Y (2018). Fully automatic breast ultrasound image segmentation based on fuzzy cellular automata framework. *Biomedical Signal Processing and Control*, 40, 433-442.

[170] Liu Y, Cheng HD, Huang J, Zhang V, Tang X (2012). An effective approach of lesion segmentation within breast ultrasound image based on the cellular automata principle. *Journal of Digital Imaging*, 25 (5), 580-590.

[171] Liu Z, Zhang L, Ren H, Kim JY (2013). A robust region-based active contour model with point classification for ultrasound breast lesion segmentation. In Novak CL, Aylward S (eds.), *Medical Imaging 2013: Computer-Aided Diagnosis*, vol. 8670, doi: 10.1117/12.2006164, SPIE.

[172] Loizou CP, Pattichis CS (2008). Despeckle filtering algorithms and software for ultrasound imaging. Morgan and Claypool Publishers, USA.

[173] Loizou CP, Theofanous C, Pantziaris M, Kasparis T (2014). Despeckle filtering software toolbox for ultrasound imaging of common carotid artery. *Computer Methods and Programs in Biomedicine*, 114 (1), 109-124.

[174] Lotfollahi M, Gity M, Ye JY, Far AM (2018). Segmentation of breast ultrasound images based on active contours using neutrosophic theory. *Journal of Medical Ultrasonics*, 45 (2), 205-212.

[175] Luisier F, Blu T (2007). A new SURE approach to image denoising: Interscale orthonormal wavelet thresholding. *IEEE Transactions on Image Processing*, 16 (3), 593-606.

[176] Madabhushi A, Metaxas D (2002, July). Automatic boundary extraction of ultrasonic breast lesions. In Proceedings of *IEEE International Symposium on Biomedical Imaging*, (pp. 601-604), IEEE.

[177] Madabhushi A, Metaxas DN (2003). Combining low-, high-level and empirical domain knowledge for automatic segmentation of ultrasonic breast lesions. *IEEE Transactions on Medical Imaging*, 22 (2), 155-169.

[178] Malik J, Kiranyaz S, Kunhoth S, Ince T, Al-Madeed S, Hamila R, Gabbouj M (2019). Colorectal cancer diagnosis form histology images: a comparative study. *arXiv: 1903.11210.*

[179] Marcomini KD, Caneiro AAO, Schiabel H (2014). Development of a computer tool to detect and classify nodule in ultrasound breast images. In: Aylward S, Hadjiiski LM (eds.), *Medical Imaging 2014: Computer-Aided Diagnosis*, vol. 9035, pp. 90351O-1-90351O-9, SPIE.

[180] Marcomini KD, Carneiro AAO, Schiabel H (2016). Application of artificial neural network models in segmentation and classification of nodules in breast ultrasound digital images. *International Journal of Biomedical Imaging*, 2016, doi: http://dx.doi.org/ 10.1155/2016/7987212.

[181] Marcomini KD, Schiabel H (2012). Nodules segmentation in breast ultrasound using the artificial neural network self-organizing map. In Proceedings of *World Congress on Engineering* (pp. 4-7).

[182] Marcomini KD, Schiabel H, Caneiro AAO (2013). Quantitative evaluation of automatic methods for lesions detection in breast ultrasound images. In: Novak CL, Aylward S (eds.), *Medical Imaging 2013: Computer-Aided Diagnosis*, vol. 8670, doi: 10.1117/12.2008056, SPIE

[183] Massich J, Meriaudeau F, Perez E, Marti R, Oliver A, Marti J (2010). Lesion segmentation in breast sonography. In: Marti J et al. (eds.), *IWDM 2010: Digital Mammography*, vol. 6136, pp. 39-45, Springer, Berlin.

[184] Mateo JL, Fernandez-Caballero A (2009). Finding out general tendencies in speckle noise reduction in ultrasound images. *Expert Systems with Applications*, 36 (4), 7786-7797.

[185] Matsumoto MM, Sehgal CM, Udupa JK (2012). Local binary pattern texture-based classification of solid masses in ultrasound breast images. In Bosch JG et al. (eds.), *Medical Imaging 2012: Ultrasonic Imaging, Tomography and Therapy*, vol. 8320, doi: 0.1117/12.911653, SPIE.

[186] Menon RV, Raha P, Kothari S, Chakraborty S (2015, December). Automated detection and classification of mass from breast ultrasound images. In Proceedings of *5th National Conference on Computer Vision, Pattern Recognition, Image Processing and Graphics*, (pp. 1-4), IEEE.

[187] Michailovich OV, Tannenbaum A (2006). Despeckling of medical ultrasound images. *IEEE Transactions on Ultrasonics, Ferroelectrics and Frequency Control*, 53 (1), 64-78.

[188] Michalak K, Kwasnicka H (2006). Correlation-based feature selection strategy in classification problems. *International Journal of Applied Mathematics and Computer Science*. 16, 503-511.

[189] Mikolajczyk A, Grochowski M (2018, May). Data augmentation for improving deep learning in image classification problem. In *International Interdisciplinary PhD Workshop* (pp. 117-122), IEEE.

[190] Moon WK, Chen IL, Yi A, Bae MS, Shin SU, Chang RF (2018). Computer-aided prediction model for axillary lymph node metastasis in breast cancer using tumor morphological and textural features on ultrasound. *Computer Methods and Programs in Biomedicine*, 162, 129-137.

[191] Moon WK, Huang YS, Lo CM, Huang CS, Bae MS, Kim WH, Chen JH, Chang RF (2015). Computer-aided diagnosis for distinguishing between triple-negative breast cancer and fibroadenomas based on ultrasound texture features. *Medical Physics*, 42 (6), pp. 3024-3035.

[192] Moon WK, Lo CM, Chang JM, Huang CS, Chen JH, Chang RF (2013). Quantitative ultrasound analysis for classification of BI-RADS category 3 breast masses. *Journal of Digital Imaging*, 26 (6), 1091-1098.

[193] Moon WK, Lo CM, Cho N, Chang JM, Huang CS, Chen JH, Chang RF (2013). Computer-aided diagnosis of breast masses using quantified BI-RADS findings. *Computer Methods and Programs in Biomedicine*, 111 (1), 84-92.

[194] Moon WK, Lo CM, Huang CS, Chen JH, Chang RF (2012). Computer-aided diagnosis based on speckle patterns in ultrasound images. *Ultrasound in Medicine and Biology*, 38 (7), 1251-1261.

[195] Moraru L, Moldovanu S, Biswas A (2014). Optimization of breast lesion segmentation in texture feature space approach. *Medical Engineering and Physics*, 36 (1), 129-135.

[196] Nanni L, Lumini A, Brahnam S (2010). Local binary patterns variants as texture descriptors for medical image analysis. *Artificial Intelligence in Medicine*. 49 (2), 117-125.

[197] Narayanan SK, Wahidabanu RSD (2009). A view on despeckling in ultrasound imaging. *International Journal of Signal Processing, Image Processing and Pattern Recognition*, 2 (3), 85-98.

[198] Nasser MA, Melendez J, Moreno A, Omer OA, Puig D (2017). Breast tumor classification in ultrasound images using texture analysis and super-resolution methods. *Engineering Applications of Artificial Intelligence*, 59, 84-92.

[199] Nemat H, Fehri H, Ahmadinejad N, Frangi AF, Gooya A (2018). Classification of breast lesions in ultrasonography using sparse logistic regression and morphology-based texture features. *Medical Physics*, 45 (9), 4112-4124.

[200] Nugroho A, Nugroho HA, Choridah L (2015, October). Active contour bilateral filter for breast lesions segmentation on ultrasound images. In Proceedings of *International Conference on Science in Information Technology* (pp. 36-40), IEEE.

[201] Nugroho HA, Triyani Y, Rahmawaty M, Ardiyanto I (2017, October). Breast ultrasound image segmentation based on neutrosophic set and watershed method for classifying margin characteristics. In Proceedings of *7th IEEE International Conference on System Engineering and Technology*, (pp. 43-47), IEEE.

[202] Nugroho HA, Triyani Y, Rahmawaty M, Ardiyanto I, Choridah L (2016, September). Performance analysis of filtering techniques for speckle reduction on breast ultrasound images. In Proceedings of *International Electronics Symposium* (pp. 450-454), IEEE.

[203] Ojala T, Pietikainen M, Maenepaa M (2002). Multiresolution gray-scale and rotation invariant texture classification with local binary patterns. *IEEE Transactions on Pattern Analysis and Machine Intelligence*, 24 (7), 971-987.

[204] Olsen O, Gotzsche PC (2001). Cochrane review on screening for breast cancer with mammography. *The Lancet*, 358 (9290), 1340-1342.

[205] Osman FM, Yap MH (2018). The effect of filtering algorithms for breast ultrasound lesions segmentation. *Informatics in Medicine Unlocked*, 12, 14-20.

[206] Othman AA, Tizhoosh HR (2011). Segmentation of breast ultrasound images using neural networks. In: Iliadis I, Jayne C (eds.), *Engineering Applications of Neural Networks*, vol. 363, pp. 260-269, Springer, Berlin.

[207] Pang S, Yu Z, Orgun MA (2017). A novel end-to-end classifier using domain transferred deep convolutional neural networks for biomedical images. *Computer Methods and Programs in Biomedicine*, 140, 283-293.

[208] Panigrahi L, Verma K, Singh BK (2019). Ultrasound image segmentation using a novel multi-scale Gaussian kernel fuzzy clustering and multi-scale vector field convolution. *Expert Systems with Applications*, 115, 486-498.

[209] Piliouras N, Kalatzis I, Dimitropolous N, Cavouras D (2004). Development of the cubic least squares mapping linear-kernel support vector machine classifier for improving the

characterization of breast lesions on ultrasound. *Computerized Medical Imaging and Graphics*, 28 (5), 247-255.

[210] Plissiti ME, Nikou C, Charchanti A (2011). Combining shape, texture and intensity features for cell nuclei extraction in pap smear images. *Pattern Recognition Letters*, 32 (6), 838-853.

[211] Pons G, Marti J, Marti R, Ganau S, Vilanova JC, Noble JA (2013). Evaluating lesion segmentation on breast sonography as related to lesion type. *Journal of Ultrasound in Medicine*, 32 (9), 1659-1670.

[212] Pons G, Marti J, Marti R, Noble JA (2011). Simultaneous lesion segmentation and bias correction in breast ultrasound images. In: Vitria J et al. (eds.), *Pattern Recognition and Image Analysis* vol. 6669, pp. 692-699, Springer, Berlin.

[213] Prabhakar T, Poonguzhali S (2014). Feature based active contour method for automatic detection of breast lesions in ultrasound images. *Applied Mechanics and Materials*, 573, 471-476.

[214] Prabhakar T, Poonguzhali S (2016). Denoising and automatic detection of breast tumor in ultrasound images. *Asian Journal of Information Technology*, 15 (18), 3506-3512.

[215] Prabhakar T, Poonguzhali S (2017). Analysis of level set methods for lesion segmentation of breast ultrasound images. *International Journal of Pure and Applied Mathematics*, 114 (10), 119-132.

[216] Prabusankarlal KM, Manavalan R, Sivaranjani R (2017). An optimized non local means filter using automated clustering based preclassification through gap statistics for speckle reduction in breast ultrasound images. *Applied Computing and Informatics*, 14 (1), 48-54.

[217] Prabusankarlal KM, Thirumoorthy P, Manavalan R (2014). Combining clustering, morphology and metaheuristic optimization technique for segmentation of breast ultrasound images to detect tumors. *International Journal of Computer Applications*, 86 (14), 28-34.

[218] Prabusankarlal KM, Thirumoorthy P, Manavalan R (2015). Assessment of combined textural and morphological features for diagnosis of breast masses in ultrasound. *Human-centric Computing and Information Sciences*, 5 (1), 12-28.

[219] Prabusankarlal KM, Thirumoorthy P, Manavalan R (2015). Segmentation of breast lesions in ultrasound images through multiresolution analysis using undecimated discrete wavelet transform. *Ultrasonic Imaging*, 38 (6), 384-402.

[220] Prabusankarlal KM, Thirumoorthy P, Manavalan R (2017). Classification of breast masses in ultrasound images using self-adaptive differential evolution extreme learning

machine and rough set feature selection. *Journal of Medical Imaging*, 4 (2), 024507, doi: 10.1117/1.JMI.4.2.024507.

[221] Qi X, Zhang L, Chen Y, Pi Y, Chen Y, Lv Q, Yi Z (2019). Automated diagnosis of breast ultrasonography images using deep learning neural networks. *Medical Image Analysis*, 52, 185-198.

[222] Qian X, Patton EW, Swaney J, Xing Q, Zeng TH (2018, October). Machine learning on cataracts classification using SqueezeNet. In Proceedings of *4th International Conference on Universal Village* (pp. 1-3), IEEE.

[223] R Core Team. A language and environment for statistical computing. Vienna, Austria: R Foundation for Statistical Computing; 2013, http://w.R-project.org/.

[224] Raha P, Menon RV, Chakrabarti I (2017, March). Fully automated computer aided diagnosis system for classification of breast mass from ultrasound images. In Proceedings of *2017 International Conference on Wireless Communications, Signal Processing and Networking (WiSPNET)*, (pp. 48-51), IEEE.

[225] Ravishankar H, Sudhakar P, Venkataramani R, Thiruvenkadam S, Annangi P, Babu N, Vaidya V (2016). Understanding the mechanisms of deep transfer learning for medical images. In: Carneiro G. et al. (eds.), *Deep Learning and Data Labeling for Medical Applications*, vol. 10008, pp. 188-196, Springer, Cham.

[226] Rawat J, Singh A, Bhadauria HS, Virmani J, Devgun JS (2018). Leukocyte classification using adaptive neuro-fuzzy inference system in microscopic blood images. *Arabian Journal for Science and Engineering*, 43 (12), 7041-7058.

[227] Rehman M, Khan SH, Abbas Z, Rizvi SMD (2019, February). Classification of diabetic retinopathy images based on customized CNN architecture. In Proceedings of *Amity International Conference on Artificial Intelligence* (pp. 244-248), IEEE.

[228] Rodrigues PS, Giraldi GA (2017). Improving the non-extensive medical image segmentation based on Tsallis entropy. *Pattern Analysis and Applications*, 14 (4), 369-379.

[229] Rodrigues R, Braz R, Pereira M, Moutinho J, Pinheiro AMG (2015). A two-step segmentation method for breast ultrasound masses based on multi-resolution analysis. *Ultrasound in Medical and Biology*, 41 (6), 1737-1748.

[230] Rodtook A, Kirimasthong K, Lohitvisate W, Makhanov SS (2018). Automatic initialization of active contours and level set method in ultrasound images of breast abnormalities. *Pattern Recognition*, 79, 172-182.

[231] Rodtook A, Makhanov SS (2013). Multi-feature gradient vector flow snakes for adaptive segmentation of ultrasound images of breast cancer. *Journal of Visual Communication and Image Representation*, 24 (8), 1414-1430.

[232] Rudin LI, Osher S, Fatemi E (1992). Nonlinear total variation based noise removal algorithms. *Physica D: Non-linear Phenomena*, 60 (1-4), 259-268.

[233] Ruggiero C, Bagnoli F, Sacile R, Calabrese M, Rescinito G, Sardanelli F (1998, November). Automatic recognition of malignant lesions in ultrasound images by artificial neural networks. In Proceedings of *20th Annual International Conference of the IEEE Engineering in Medicine and Biology Society*, (pp. 872-875), IEEE.

[234] Samala RK, Chan HP, Hadjiiski L, Helvie MA, Wei J, Cha K (2016). Mass detection in digital breast tomosynthesis: Deep convolutional neural network with transfer learning from mammography. *Medical Physics*, 43 (12), 6654-6666.

[235] Samundeeswari ES, Saranya PK, Manavalan R (2016, March). Segmentation of breast ultrasound image using regularized k-means (ReKM) clustering. In Proceedings of *International Conference on Wireless Communications, Signal Processing and Networking* (pp. 1379-1383), IEEE

[236] Saybani MR, Wah TH, Aghabozorgi SR, Shamshirband S, Kiah MLM, Balas VE (2016). Diagnosing breast cancer with an improved artificial immune recognition system. *Soft Computing*, 20 (10), 4069-4084.

[237] Shan J, Alam SK, Garra B, Zhang Y, Ahmed T (2015). Computer-aided diagnosis for breast ultrasound using computerized BI-RADS features and machine learning methods. *Ultrasound in Medicine and Biology*, 42 (4), 980-988.

[238] Shan J, Cheng HD, Wang Y (2008, December). A completely automatic segmentation method for breast ultrasound images using region growing. In Proceedings of *11th Joint International Conference on Information Sciences*, (pp. 1-6), Atlantis Press.

[239] Shan J, Cheng HD, Wang Y (2008, December). A novel automatic seed point selection algorithm for breast ultrasound images. In Proceedings of *19th International Conference on Pattern Recognition* (pp. 1-4), IEEE.

[240] Shan J, Cheng HD, Wang Y (2012). A novel segmentation method for breast ultrasound images based on neutrosophic l-means clustering. *Medical Physics*, 39 (9), 5669-5682.

[241] Shan J, Cheng HD, Wang Y (2012). Completely automated segmentation approach for breast ultrasound images using multiple domain features. *Ultrasound in Medicine and Biology*, 38 (2), 262-275.

[242] Shao H, Zhang Y, Xian M, Cheng HD, Xu F, Ding J (2015, September). A saliency model for automated tumor detection in breast ultrasound images. In Proceedings of *IEEE International Conference on Image Processing* (pp. 1424-1428), IEEE.

[243] Sharma H, Zerbe N, Klempert I, Hellwich O, Hufnagl P (2017). Deep convolutional neural networks for automatic classification of gastric carcinoma using whole slide images in digital histopathalogy. *Computerized Medical Imaging and Graphics*, 61, 2-13.

[244] Shen J, Wang Y, Yu J, Wang W (2006, August). Boundary extraction of breast ultrasonic images. In Proceedings of *28th Annual International Conference of IEEE Engineering in Medicine and Biology Society* (pp. 3082-3085), IEEE.

[245] Shen WC, Chang RF, Moon WK (2007). Computer aided classification system for breast ultrasound based on breast imaging reporting and data system (BI-RADS). *Ultrasound in Medicine and Biology*, 33 (11), 1688-1698.

[246] Shen WC, Chang RF, Moon WK, Chou YH, Huang CS (2007). Breast ultrasound computer-aided diagnosis using BI-RADS features. *Academic Radiology*, 14 (8), 928-939.

[247] Shi J, Xiao Z, Zhou S (2010, August). Automatic segmentation of breast tumors in ultrasound image with simplified PCNN and improved fuzzy mutual information. In Proceedings of *SPIE 744, Visual Computing and Image Processing*, doi: 10.1117/12.863028.

[248] Shi X, Cheng HD, Hu L, Ju W, Tian J (2010). Detection and classification of masses in breast ultrasound images. *Digital Signal Processing*, 20 (3), 824-836.

[249] Shiji TP, Remya S, Thomas V (2017). Computer aided segmentation of breast ultrasound images using scale invariant feature transform (SIFT) and bag of features. *Procedia Computer Science*, 115, 518-525.

[250] Simonyan K, Zisserman A (2014). Very deep convolutional networks for large-scale image recognition. *arXiv: 1409.1556*.

[251] Singh BK, Verma K, Thoke AS (2015). Adaptive gradient descent backpropagation for classification of breast tumors in ultrasound imaging. *Procedia Computer Science*, 46, 1601-1609.

[252] Singh BK, Verma K, Thoke AS (2015). Objective and optical evaluation of despeckle filters in breast ultrasound images. *IETE Technical Review*, 32 (5), 384-398.

[253] Singh BK, Verma K, Thoke AS (2016). Fuzzy cluster based neural network classifier for classifying breast tumors in ultrasound images. *Expert Systems with Applications*, 66, 114-123.

[254] Singh BK, Verma K, Thoke AS, Suri JS (2017). Risk stratification of 2D ultrasound based breast lesions using hybrid feature selection in machine earning paradigm. *Measurement*, 105, 146-157.

[255] Singh BK, Verma K, Thoke S (2016). Investigations on edge preservation and smoothening of frequency domain filters for speckle removal in breast ultrasound images. *International Journal of Biomedical Engineering and Technology*, 20 (2), 97-115.

[256] Singh VP, Srivastava R (2018). Automated and effective content-based mammogram retrieval using wavelet based CS-LBP features and self-organizing map. *Biocybernetics and Biomedical Engineering*, 38 (1), 90-105.

[257] Song JH, Venkatesh SS, Conant EA, Cary TW, Arger PH, Sehgal CM (2005, April). Artificial neural network to aid differentiation of malignant and benign breast masses by ultrasound imaging. In Proceedings of *Medical Imaging: Ultrasonic Imaging and Signal Processing*, vol. 5750, (pp. 148-152), International Society for Optics and Photonics.

[258] Spampinato C, Palazzo S, Giordano D, Aldinucci M, Leonardi R (2017). Deep learning for automated skeletal bone age assessment in X-ray images. *Medical Image Analysis*, 36, 41-51.

[259] Su Y, Wang Y, Jiao J, Guo Y (2011). Automatic detection and classification of breast tumors in ultrasonic images using texture and morphological features. *The Open Medical Informatics Journal*, 5 (Suppl1-M3): 26-37.

[260] Sun J, Wan C, Cheng J, Yu F, Liu J (2017). Retinal image quality classification using fine-tuned CNN. In: Cardoso M et al. (eds.), *Fetal, Infant and Ophthalmic Medical Image Analysis*, vol. 110554, pp. 126-133, Springer, Cham.

[261] Szegedy C, Liu W, Jia Y, Sermanet P, Reed S, Anguelov D, Erhan D, Vanhoucke V, Rabinovich A (2015). Going deeper with convolutions. In Proceedings of *IEEE Conference on Computer Vision and Pattern Recognition* (pp. 1-9), IEEE.

[262] Tajbaksh N, Shin JY, Gurudu SR, Hurst RT, Kendall CB, Gotway MB, Liang J (2016). Convolutional neural networks for medical image analysis: full training or fine tuning? *IEEE Transactions on Medical Imaging*, 35 (5), 1299-1312.

[263] Takemura A, Shimizu A, Hamamoto K (2010). A cost-sensitive extension of AdaBoost with Markov random field priors for automated segmentation of breast tumors in ultrasonic images. *International Journal of Computer Assisted Radiology and Surgery*, 5 (5), 537-547.

[264] Takemura A, Shimizu A, Hamamoto K (2010). Discrimination of breast tumors in ultrasonic images using an ensemble classifier based on the AdaBoost algorithm with feature selection. *IEEE Transactions on Medical Imaging*, 29 (3), 598-609.

[265] Tashk A, Helfroush MS, Danyali H, Akbarzadeh-Jahromi M (2014, May). A CAD mitosis detection system from breast cancer histology mages based on fused features. In Proceedings of *22nd International Conference on Electrical Engineering*, (pp. 1925-1927), IEEE.

[266] Theodorakopoulos I, Kastaniotis D, Economou G, Fotopoulos S (2012, November). Hep-2 cells classification via fusion of morphological and textural features. In Proceedings of *12th International Conference on Bioinformatics and Bioengineering* (689-694), IEEE.

[267] Tian JW, Sun LT, Guo YH, Cheng HD, Zhang YT (2007). Computerized-aid diagnosis of breast mass using ultrasound images. *Medical Physics*, 34 (8), 3158-3164.

[268] Torbati N, Ayatollahi A, Kermani A (2014). An efficient neural network based method for medical image segmentation. *Computers in Medicine and Biology*, 44, 76-87.

[269] Triyani Y, Nugroho HA, Rahmawaty M, Ardiyanto I, Choridah L (2016, October). Performance analysis of image segmentation for breast ultrasound images. In Proceedings of *8th International Conference on Information Technology and Electrical Engineering*, (pp. 1-6), IEEE.

[270] Uzunhisarcikli E, Goreke V (2018). A novel classifier model for mass classification using BI-RADS category in ultrasound images based on Type-2 fuzzy inference system. *Sadhana*, 43 (9), 138, doi: https://doi.org/10.1007/s12046-018-0915-x.

[271] Vachon CM, van Gills CH, Sellers TA, Ghosh K, Pruthi S, Brandt KR, Pankratz VS (2007). Mammographic density, breast cancer risk and risk prediction. *Breast Cancer Research*, 9 (6), doi: 10.1186/bcr1829.

[272] Velez N, Earnest DE, Staren ED (2000). Diagnostic and interventional ultrasound for breast disease. *American Journal of Surgery*, 180 (4), 284-287.

[273] Verma K, Singh BK, Tripathi P, Thoke AS (2015). Review of feature selection algorithms for breast cancer ultrasound images. In: Barbucha B et al. (eds.), *New Trends in Intelligent Information and Database Systems*, vol. 598, pp. 23-32.

[274] Verma VS, Jha RK, Ojha A (2015). Digital watermark extraction using support vector machine with principal component analysis based feature reduction. *Journal of Visual Communications and Image Representation*, 31, 75-85.

[275] Vianna VP (2018). Study and development of a computer-aided diagnosis system for classification of chest X-ray images using convolutional neural networks pre-trained for ImageNet and data augmentation. *arXiv preprint arXiv: 1806.00839.*

[276] Wahdan P, Saad A, Shoukry A (2014, June). Comparing classification techniques to detect breast tumor. In Proceedings of *International Conference on Biomedical Engineering and Systems*, (pp. 1-6), IEEE.

[277] Wan S, Liang Y, Zhang Y (2018). Deep convolutional neural networks for diabetic retinopathy detection by image classification. *Computers & Electrical Engineering*, 72, 274-282.

[278] Wang J, Perez L (2017). The effectiveness of data augmentation in image classification using deep learning. *arXiv: 1712.04621v1*.

[279] Wang LC, Sullivan M, Du H, Feldman MI, Mendelson EB (2013). US appearance of ductal carcinoma in situ. *Radiographics*, 33 (1), 213-228.

[280] Wang W, Zhu L, Qin J, Chui YP, Li BN, Heng PA (2014). Multiscale geodesic active contours for ultrasound image segmentation using speckle reducing anisotropic diffusion. *Optics and Lasers in Engineering*, 54, 105-116

[281] Wang Y, Shen J, Guo Y, Wang W (2008, June). Computerized classification of breast tumors with morphological and texture features of ultrasonic images. In Proceedings of *IEEE International Symposium on Computer-Based Medical Systems* (pp. 23-28), IEEE.

[282] Wei W, Li Y, Deegan AJ, Wang RK (2018). Mapping and quantitating penetrating vessels in cortical brain using eigen-decomposition of OCT signals and subsequent principal component analysis. *IEEE Journal of Selected Topics in Quantum Electronics*, 25 (1), 1-9.

[283] Weickert J (2003). Coherence-enhancing shock filters. In: Michaelis B, Krell G (eds.) *Pattern Recognition*, pp. 1-8, Springer, Heidelberg.

[284] Weiss N, Kost H, Homeyer A (2018). Towards interactive breast tumor classification using transfer learning. In: Campilho A et al. (eds.), *ICIAR 2018*, vol. 10882, pp. 727-736, Springer.

[285] Wu WJ, Lin SW, Moon WK (2012). Combining support vector machine with genetic algorithm to classify ultrasound breast tumor images. *Computerized Medical Imaging Graphics*, 36 (8), 627-633.

[286] Wu WJ, Lin SW, Moon WK (2015). An artificial immune system-based support vector machine approach for classifying ultrasound breast tumor images. *Journal of Digital Imaging*, 28 (5), 576-585.

[287] Wu WJ, Moon WK (2008). Ultrasound breast tumor image computer-aided diagnosis with texture and morphological features. *Academic Radiology*, 15 (7), 873-880.

[288] Xi X, Shi H, Han L, Wang T, Ding HY, Zhang G, Tang Y, Yin Y (2016). Breast tumor segmentation with prior knowledge learning. *Neurocomputing*, 237, 145-157.

[289] Xian M, Cheng HD, Zhang Y (2014, August). A fully automatic breast ultrasound image segmentation approach based on neutron-connectedness. In Proceedings of *22nd International Conference on Pattern Recognition* (pp. 2495-2500), IEEE.

[290] Xian M, Huang J, Zhang Y, Tang X (2012, September). Multiple-domain knowledge based MRF model for tumor segmentation in breast ultrasound images. In Proceedings of *19th IEEE International Conference on Image Processing* (pp. 2021-2024), IEEE.

[291] Xian M, Zhang Y, Cheng HD (2015). Fully automatic segmentation of breast ultrasound images based on breast characteristics in space and frequency domains. *Pattern Recognition*, 48 (2), 485-497.

[292] Xian M, Zhang Y, Cheng HD, Xu F, Huang K, Zhang B, Ding J, Ning C, Wang Y (2018). A benchmark for breast ultrasound image segmentation (BUSIS), *arXiv:1801.03182v1*.

[293] Xiao G, Brady M, Noble JA, Zhang Y (2002). Segmentation of ultrasound B-mode images with intensity inhomogeneity correction. *IEEE Transactions in Medical Imaging*, 21 (1), 48-57.

[294] Xiao T, Liu L, Li K, Qin W, Yu S, Li Z (2018). Comparison of transferred deep neural networks in ultrasonic breast masses discrimination. *BioMed Research International*, 2018, doi: https://doi.org/10.1155/2018/4605191.

[295] Xie X, Shi F, Niu J, Tang X (2018). Breast ultrasound image classification and segmentation using convolutional neural networks. In: Hong R et al. (eds.), *Advances in Multimedia and Information Processing-PCM 2018*, pp. 200–211, Springer, Cham.

[296] Xing J, Li Z, Wang B, Yu B, Zanjani FG, Zheng A, Duits R, Tan T (2019). Automated segmentation of lesions in ultrasound using semi-pixel-wise cycle generative adversarial nets. *arXiv:1905.01902*.

[297] Xu Y, Nishimura T (2009). Segmentation of breast lesions in ultrasound images using spatial fuzzy clustering and structure tensors. *International Journal of Computer, Electrical, Automation, Control and Information Engineering*, 3 (5), 1355-1359.

[298] Yang MC, Moon WK, Wang YCF, Bae MS, Huang CS, Chen JH, Chang RF (2013). Robust texture analysis using multi-resolution gray-scale invariant features for breast

sonographic tumor diagnosis. *IEEE Transactions on Medical Imaging*, 32 (12), 2262-2273.

[299] Yang Z, Fox MD (2004). Multi-resolution non-homogeneous anisotropic diffusion approach to enhance ultrasound breast tumor image legibility. In: Walker WF, Emelianov SV (eds.), *Medical Imaging 2004: Ultrasonic Imaging and Signal Processing*, vol. 5373, pp. 98-107, SPIE, Bellingham.

[300] Yap MH, Edirisinghe EA, Bez HE (2007). Fully automatic lesion boundary detection in ultrasound breast images. In: Plulm JPW, Reinhardt JM (eds.), *Medical Imaging 2007: Image Processing*, vol. 6512, doi: 10.1117/12.708625.

[301] Yap MH, Edirisinghe EA, Bez HE (2009). A comparative study in ultrasound breast imaging classification. In: Pluim JPW, Dawant BM (eds.), *Medical Imaging 2009: Image Processing*, vol. 7259, doi: https://doi.org/10.1117/12.811208.

[302] Yap MH, Goyal M, Osman F, Marti R, Denton E, Juette A, Zwiggelaar R (2018). Breast ultrasound lesions recognition: end-to-end deep learning approaches. *Journal of Medical Imaging*, 6 (1), doi: 10.1117/1.JMI.6.1.011007.

[303] Yap MH, Yap CH (2016, March). Breast ultrasound lesions classification: a performance evaluation between manual delineation and computer segmentation. In Proceedings of *SPIE, Medical Imaging: Image Perception, Observer Performance and Technology Assessment*, vol. 9787, pp. 978718-1-978718-6.

[304] Yeh CK, Chen YS, Fan WC, Liao YY (2009). A disk expansion segmentation method for ultrasonic breast lesions. *Pattern Recognition*, 42 (5), 596-606.

[305] Yin M, Mackley HB, Drabick JJ, Harvey HA (2016). Primary female breast sarcoma: clinicopathological features, treatment and prognosis. *Scientific Reports*, 6 (1), 1-9.

[306] Yu D, Lee S, Lee JW, Kim S (2011). Automatic lesion detection and segmentation algorithm on 2D breast ultrasound images. In: Summers RM, van Ginneken B (eds.), *Medical Imaging 2011: Computer-Aided Diagnosis*, vol. 7963, doi: 10.1117/12.876351, SPIE.

[307] Yu Y, Lin H, Meng J, Wei X, Guo H, Zhao Z (2017). Deep transfer learning for modality classification of medical images. *Information*, 8 (3), 91.

[308] Yu Y, Xiao Y, Cheng J, Chiu B (2018). Breast lesion classification based on supersonic shear-wave elastography and automated lesion segmentation from B-mode ultrasound images. *Computers in Biology and Medicine*, 93, 31-46.

[309] Zadeh LA (1975). The concept of a linguistic variable and its application to approximate reasoning-I. *Information Sciences*. 8 (3), 199-249.

[310] Zakeri FS, Behnam H, Ahmadinejad N (2012). Classification of benign and malignant breast masses based on shape and texture features in sonography images. *Journal of Medical Systems*, 36 (3), 1621-1627.

[311] Zeimarani B, Costa MGF, Nyrani NZ, Filho CFFC (2019). A novel breast tumor classification in ultrasound images, using deep convolutional neural network. In: Costa RF, Machado J, Alvarenga A (eds.), *XXVI Brazilian Congress on Biomedical Engineering*, vol. 70/2, pp. 89-94, Springer, Singapore.

[312] Zhang E, Seiler S, Chen M, Lu W, Gu X (2019). BIRADS features oriented semi-supervised deep learning for breast ultrasound computer-aided diagnosis. *Physics in Medicine and Biology*, 65 (12), 125005, doi: https://doi.org/10.1088/1361-6560/ab7e7d

[313] Zhang J, Lin G, Wu L, Cheng Y (2016). Speckle filtering of medical ultrasonic images using wavelet and guided filter. *Ultrasonics*, 65, 177-193.

[314] Zhang J, Wang C, Chang Y (2015). Comparison of despeckled filters for breast ultrasound images. *Circuits, Systems and Signal Processing*, 34 (1), 185-208.

[315] Zhang J, Zhou SK, Brunke S, Lowery C, Comaniciu D (2010, March). Database-guided breast tumor detection and segmentation in 2D ultrasound images. In Proceedings of *SPIE Medical Imaging 2010: Computer Aided Diagnosis*, vol. 7624, doi: https://doi.org /10.1117/12.844558.

[316] Zhang L, Ren Y, Huang C, Liu F (2011, July). A novel automatic tumor detection for breast cancer ultrasound images. In Proceedings of *8th International Conference on Fuzzy Systems and Knowledge Discovery*, (pp. 401-404), IEEE.

[317] Zhang L, Zhang M (2011). A fully automatic image segmentation using an extended fuzzy set. In: Yu Y, Yu Z, Zhao J (eds.), *Computer Science for Environmental Engineering and Ecoinformatics*, vol.159, pp. 412-417, Springer, Berlin.

[318] Zhang M, Zhang L, Cheng HD (2010). Segmentation of ultrasound breast images based on a neutrosophic method. *Optical Engineering*, 49 (11), doi: https://doi.org/10.1117/1 .3505854.

[319] Zhang Q, Chang H, Liu L, Li A, Huang Q (2014). A computer aided system for classification of breast tumors in ultrasound images via biclustering learning. In: Wang X et al. (eds.), *Machine Learning and Cybernetics, ICMLCI*, pp. 24-32, Springer, Berlin.

[320] Zhou D, Shen X (2008, May). Image denoising using block thresholding. In Proceedings of *Congress on Image and Signal Processing* (pp. 335-338), IEEE.

[321] Zhou S, Shi J, Zhu J, Cai Y, Wang R (2013). Shearlet-based texture feature extraction for classification of breast tumor in ultrasound image. *Biomedical Signal Processing and Control*, 8 (6), 688-696.

[322] Zhou Z, Shin J, Zhang L, Gurudu S, Gotway M, Liang J (2017). Fine-tuning convolutional neural networks for biomedical image analysis: actively and incrementally. In Proceedings of *IEEE Conference on Computer Vision and Pattern Recognition* (pp. 7340-7351), IEEE.

[323] Zhou Z, Wu W, Wu S, Tsui PH, Lin CC, Zhang L, Wang T (2014). Semi-automatic breast ultrasound image segmentation based on mean shift and graph cuts. *Ultrasonic Imaging*, 36 (4), 256-276.

[324] Zhuang Z, Li N, Joseph ANR, Mahesh VGV, Qui S (2019). An RDAU-NET model for lesion segmentation on breast ultrasound images. *PLoSOne*, 14 (8), e0221535.

Publications from the Present Work

[1] **Kriti**, Jitendra Virmani and Ravinder Agarwal, "Assessment of despeckle filtering algorithms for segmentation of breast tumors from ultrasound images", *Biocybernetics and Biomedical Engineering*, vol. 39, pp. 100-121, 2019. [**Status: Published.** Publisher: Elsevier, IF: 2.537] DOI: https://doi.org/10.1016/j.bbe.2018.10.002.

[2] **Kriti**, Jitendra Virmani and Ravinder Agarwal, "Effect of despeckle filtering on classification of breast tumors using ultrasound images", *Biocybernetics and Biomedical Engineering*, vol. 39, pp. 563-560, 2019. [**Status: Published.** Publisher: Elsevier, IF: 2.537] DOI: https://doi.org/10.1016/j.bbe.2019.02.004

[3] **Kriti**, Jitendra Virmani and Ravinder Agarwal, "Deep feature extraction and classification of breast ultrasound images", *Multimedia Tools and Applications*, DOI: https://doi.org/10.1007/s11042-020-09337-z, 2020. [**Status: Published.** Publisher: Springer, IF: 2.313]

[4] **Kriti**, Jitendra Virmani and Ravinder Agarwal, "A review of segmentation algorithms applied to B-mode breast ultrasound images: A characterization approach", *Archives of Computational Methods in Engineering*, DOI: 10.1007/s11831-020-09469-3, 2020. [**Status: Published**. Publisher: Springer, IF: 6.730]

[5] **Kriti**, Jitendra Virmani and Ravinder Agarwal, "LBP based CAD system designs for breast tumor characterization", *Expert Systems with Applications*. [**Status: Communicated.** Publisher: Elsevier, IF: 5.452]

[6] **Kriti**, Jitendra Virmani and Ravinder Agarwal, "A review of CAD system designs for breast tumor classification using B-mode ultrasound images: A characterization approach", *Archives of Computational Methods in Engineering*. [**Status: Communicated.** Publisher: Springer, IF: 6.730]